Towards practical pressure-based leakage characterisation of water distribution pipes with a novel pipe condition assessment device

Prepared by:

Craig Tinashe Tanyanyiwa

Supervisor:

Prof. H. Beushausen

Co-Supervisor:

Prof. J.E. van Zyl

In partial fulfilment of the requirements for:
Master of Science in Civil Engineering

Submission Date: 01 October 2019
Institution: University of Cape Town
Faculty: Engineering and the Built Environment
Department: Civil Engineering

PLAGIARISM DECLARATION

I know the meaning of plagiarism and declare that all the work in the document, save for that which is properly acknowledged, is my own. This thesis/dissertation has been submitted to the Turnitin module and I confirm that my supervisor has seen my report and any concerns revealed by such have been resolved with my supervisor.

Student number: TNYCRA001 Name: Craig Tinashe Tanyanyiwa

Date: 01 October 2019 Signature: Signed by candidate

ABSTRACT

Leakage detection and management have been proposed as effective ways of mitigating and managing water losses in an age where water scarcity has become prevalent. To this end, several methods have been developed and suggested with different benefits and drawbacks

The presently available leakage detection methods, however, fail to identify and characterise the leakage while simultaneously assessing the condition of the water distribution network (WDN). This function is imperative for understanding and addressing leakage. WDN assessments are also important as knowledge of the network parameters helps in reducing water losses through planned infrastructure maintenance programmes.

A pipe condition assessment device (PCAD) was thus developed which can detect, characterise leakage and assess the condition of the WDN. However, the efficacy and reliability of this device had not yet been established. In this study, the device was used to characterise leakage and assess system conditions in water networks.

Initially, laboratory tests on six known leak types were conducted on a standardised laboratory setup. The leakage characteristics of these pipes were found through regression analysis. The results from the tests established that to 95% level of confidence; the standardised setup can produce repeatable and comparable results to previous studies.

The accuracy of the PCAD instrumentation was verified and the device calibrated, the same pipes were then tested on the standardised setup using the PCAD. An overlap of the results from the laboratory experiments and the PCAD revealed that to 95% level of confidence, the device could adequately characterise leakage in pipes. A low variance of less than 4% of the mean parameter, across all tests conducted using the PCAD, informed that the results obtained through using the PCAD are repeatable and reliable. Field tests in the Kensington DMA were done and revealed the limitations of the device, such as its inability to characterise leakage in pipe sections that cannot be successfully isolated. However, in pipelines that were successfully isolated, the PCAD was able to detect and identify leakage characteristics in water networks and aid in conducting maintenance runs.

Consequently, this study contributed to the body of knowledge by statistically establishing that the PCAD could adequately, and reliability characterise leakage in real water distribution networks.

ACKNOWLEDGEMENTS

I want to express my gratitude to all the people who assisted and supported me in carrying out this work. While I cannot mention everyone by name, please know that your input was invaluable.

Firstly, I give thanks to God, who continues to be a present aid and source of strength.

A very special and heartfelt thank you to Professor Kobus van Zyl, for the opportunity you presented to me and the support you gave me along this research journey. I would not have been able to complete this research without your guidance, understanding and dedication. Every interaction, comment and meeting made me a better researcher.

To Professor Hans Beushausen thank you for stepping in and assisting in various concrete ways.

I would also like to thank Ms Lunita Laura Lopez, whom I worked closely with on this project. I appreciate the amount of work you put in to make my interaction with the PCAD easier. I will forever be grateful for that and gaining a friend from this whole exercise. I hope we get to work together again in the future.

To my colleagues who became friends, Rene, Asaph, Tsitsi and Obiora, thank you for the patience, for the advice, and for reassuring me during the times I had to fight the imposter syndrome.

To Gill Vester and everyone from the UCT Department of Civil Engineering who made my research journey infinitely more comfortable, I sincerely thank you.

Finally, I wish to thank my friends and family for supporting me on this MSc journey. For encouraging me and for the love you gave me, freely.

LIST OF SYMBOLS AND ABBREVIATIONS

σ_l:	Longitudinal stress
A:	Area
A_0':	Effective Area
C_d:	Coefficient of discharge
D, d:	Diameter
E:	Young's modulus
g:	Acceleration due to gravity
H, h:	Pressure head
L, l:	Length
L_c:	Length of crack
m:	Head-Area slope
m':	Effective Head-Area slope
N1:	Leakage exponent
p:	Probability value
Q, q:	Discharge
Re:	Reynolds's number
t:	Pipe wall thickness
v:	Poisson's ratio
V:	Velocity
W_c:	Width of the crack

AC:	Asbestos Cement
CL:	Cement lined
DMA:	District Metered Area

FAVAD:	Fixed Area/Variable Area Discharge
FEA:	Finite Element Analysis
FEM:	Finite Element Method
HDPE:	High Density Polyethylene
IWA:	International Water Association
MOE:	Modified Orifice Equation
PCAD:	Pipe Condition Assessment Device
PVC:	Polyvinylchloride
WDN:	Water Distribution Network
WDS:	Water Distribution System

TABLE OF CONTENTS

LIST OF FIGURES

LIST OF TABLES

1 INTRODUCTION

1.1 Background of Study

Water losses have, unfortunately, become a common feature in water distribution networks. Concurrently, with increased water scarcity and projected population growth (Hedden and Cilliers, 2014), the water sector has become more astute with the way they supply and use water (Mukuhlani and Nyamupingidza, 2014). Water scarcity has thus led to an increased awareness of water losses. Water losses are categorised as real (physical) losses and apparent losses (Kanakoudis and Muhammetoglu, 2014). Farley, (2001), categorised real losses as leaks, bursts and overflows. Van Zyl et al., (2013) further classified real losses specific to water distribution networks as bursts (reported and unreported) and background leakage.

Unfortunately, even in this context water utilities often face real loss events which range from 10% in well-maintained systems to over 50% in poorly maintained systems, of the system input volume (Alkasseh et al., 2015).

Four components of real water loss management exist namely, pressure management, infrastructure management, speed and quality of repair, and active leakage control to locate unreported leaks (Lambert, 2002). For each management component, various tools and strategies have been developed and are broadly classified into hardware-based and software-based methods (Li et al., 2015). Each class of methods has associated advantages and disadvantages. Software-based techniques employ software linked techniques such as transient analysis while hardware-based methods utilise specialised hardware such as acoustic devices and real-time monitoring (Puust et al., 2010b).

While reported bursts are often quickly addressed, unreported bursts and background leakage can contribute to substantial volumes of water losses if they remain undetected and unaddressed. Thus, most water loss reduction methods have focused on the detection and management of the leakage component of water losses, which is harder to find as it is often not visible.

The now obvious need to reduce water losses and in this case, leakage in water networks have then meant that both academia and industry have been involved in the improvement and developments of principled methods to detect and manage leakage in water networks.

One particular research field resulted in the understanding that leakage (leak flow rate) is pressure-dependent (Ogura, 1979). Early research suggested that leakage should obey the

orifice equation and the leak flow rate would be proportional to the square root of pressure, however, this was found not to be so in practice (Lambert, 2002). The reason for this deviation was explained by Cassa et al., (2010); Cassa and Van Zyl, (2014); Van Zyl and Malde, (2017); Nsanzubuhoro, Van Zyl, et al., (2017), who established experimentally and by finite element analysis (FEM), that the leak area of an orifice linearly varies with the pressure head of the fluid flowing through the orifice. It was this varying behaviour of the leak area that resulted in leakage not behaving as predicted by the orifice equation. Another outcome of this research field was the assertion that the rate at which the leak area varies, called the head-area slope, is distinct for each leak type (Van Zyl, 2017).

Knowledge of how the leak area varies with pressure and the different rates of leak expansion, referred to as leak characterisation, was then used to develop a pipe condition assessment device (PCAD). The device seeks to detect leakage and identify leakage while conducting pipe condition assessments in water distribution networks as a means of effectively managing water losses in water distribution networks (Lopez and Van Zyl, 2019).

This study will evaluate the efficacy and reliability of this novel, pressure-based and cloud linked pipe condition assessment device, developed at the University of Cape Town

1.2 Aims and Objectives

This study aims to evaluate the reliability of a novel pipe condition assessment device developed in earlier studies at the University of Cape Town and establish its efficacy in conducting condition assessments in water distribution systems.

To achieve the study's aims, the accuracy of the PCAD instrumentation will be checked and verified, and pipe condition assessments on known leak types and in real water networks will be conducted. These objectives will be fulfilled as follows:

For the verification of the PCAD's instrumentation accuracy and standardising the operation, the following tasks were performed;

- uPVC pipes with individual leaks of varied sizes and types were tested using an experimental but standardised method.
- The leakage parameters and characteristics thereof were analysed and statistically compared with pre-established results.
- The device's instrumentation was verified and tested against pre-calibrated standard instrumentation.

- The pipes that were tested using the standardised experimental setup were then further tested on the same setup but using the PCAD.
- The leakage parameters were statistically compared to the parameters obtained from the experimental standardised method.

To establish the efficacy of the device in conducting condition assessments in WDS required conducting a field test on pipes in an actual water distribution system in Cape Town.

1.3 Scope and Limitations of the Study

Initially, the experimental setups tested one set of uPVC pipes wherein a set consisted of one 12 mm round hole, one 100 mm longitudinal crack and one 100 mm circumferential crack. The experimental standardised setup was only used to investigate the repeatability of past experiments and to set up a baseline for tests conducted with the PCAD.

Due to the PCAD's pump characteristics, the tests conducted by the PCAD were on a new set of uPVC pipes wherein a set consisted of one 6 mm round hole, one 60 mm longitudinal crack and one 60 mm circumferential crack. This set was first tested using the standardised experimental setup to establish a baseline.

Field tests were only conducted on five pipe sections in the Kensington DMA's water distribution network.

1.4 Dissertation Layout

This dissertation consists of 9 chapters, a list of references, and two appendices. The structure of the dissertation is as follows:

Chapter 1 contains the background of the study and presents the aims and objectives of the study.

Chapter 2 provides a review of current literature on the field of water losses, including the current understanding of leak behaviour. Existing technologies for characterising and detecting leakage in water distribution networks are also investigated. The chapter concludes with a review of the methods currently employed for leak management.

Chapter 3 describes the research methodology employed to fulfil the aims and objectives of this study. A brief overview of the PCAD is given in this chapter, including its development and functionality.

Chapter 4 presents the method used in characterising leakage on six different pipe samples using a standardised laboratory-based method at standard pressure ranges and the results thereof.

Chapter 5 shows additional leakage characterisation tests conducted on three pipe samples at lower pressure ranges. The chapter also contains an evaluation of the effect of different pressure ranges on leak parameters.

Chapter 6 contains the method employed to characterise leakage of the three pipe samples used in the previous chapter, albeit with the the PCAD. A comparison of the results obtained, with the results obtained in chapter 5 is made.

Chapter 7 describes the field tests conducted in a residential area in Cape Town and contains a discussion of the results derived from those tests.

Chapter 8 contains an overall discussion of the whole study and summates the key findings and arguments presented in this dissertation.

Chapter 9 then concludes and highlights the critical contributions of the study. It also provides recommendations for future work based on this study's findings.

2 LITERATURE REVIEW

To fully understand the various concepts involved in this study, it is essential to review the literature that is currently available. This literature review explored the history of leakage, including more recent modern-day findings, both in the academic sphere and in practice.

The review began with an overview of leakage in water distribution systems, discussing how work in the field began, its progression, and where it currently is. The various concepts relating to leakage that have been developed were discussed and where required, adopted in the study. The scientific principles behind leakage characterisation and detection were explored. After said concepts had been discussed, this review then sought to investigate the various methods that exist, to detect leakage and to characterise leakage. Finally, an assessment of the efficacy and accessibility of those methods was done.

2.1 Water Distribution Systems

Every great civilisation has been characterised by some planned infrastructure. As early as circa 700 BC the Persians had a network of roads and some form of water reticulation for agriculture. At its simplest form, a water reticulation system can be imagined as a system that transports water from one point to the other, source to the user. With this definition, it can be said that nearly every organised society has had a reticulation system, even if that system consisted of individuals transporting the water in containers and not conduits. The Greeks developed a system of water networks that transported water to public baths and away from baths, reminiscent of a modern-day water and sewer network. This system was further improved by the Romans who built aqueducts around 312 BC, the remains of which can still be seen now. Not only did these systems have open channel flow, but they also had pipes mostly made out of hollowed-out logs or drilled stone, but a few were made of clay and lead as well (Tata & Howard, 2015). From the evidence gathered, it is now believed that the Romans also had advanced knowledge of water hydraulics (Hodge, 2002).

After the fall of the Roman Empire, the world entered what is now known as the Dark Ages. Most of the advancements made by the Romans were lost, including water reticulation systems. At the height of this Dark Age, there were increases in deaths related to the unsanitary conditions in towns and cities. Walski, (2006), reports that during the 13th century, a 5.5-kilometre lead pipeline was installed in the United Kingdom. However, the first recorded significant pipeline project was carried out in France in 1664. This pipeline was a 25-kilometre cast-iron pipeline that transported water to the Versailles. It is interesting to note from these

two examples, how the pipelines or water conveyance systems served the nobles more than the commoners. The same case is observed with the Romans, although they had public baths and public water collection points for the rest of the population whilst the nobles had direct connections to their residencies.

After about a hundred years, London had its own pipe network of over 50 kilometres which consisted of pipes made from wood, cast iron and lead. The smaller pipes diameters were made from hollowed-out logs, which remained operational as long as they were filled with water (Sanks, 2005). Tata & Howard, (2015), report that around the same time, circa 1652, Boston also had its own water reticulation network made up of conduits from hollowed-out wood. The challenge was that uneven grades and the water impeded the flow and thus the water had a woody taste.

Figure 2-1 - A section of wooden pipe originally part of the Seattle distribution system (Walski, 2006)

Furthermore, the wooden pipes would split due to excess pressures from pumping as the network grew. This led to an adoption of alternative pipe materials such as cast iron and lead. Older networks in America and in Europe were composed of cast-iron pipes. The bell and spigot made from poured lead were eventually phased out and replaced by push-in joints. Cement lined pipes were first used in 1922 and lining cast iron pipes with cement lining became a common practice to reduce corrosion of pipes. Polyethene encasement of pipes introduced in 1951 represents one of the first uses of PCV based networks (Walski, 2006).

Moving on to more modern times, every major centre with human dwelling has a well-developed water reticulation system. This system often consists of a supply dam or river, a water treatment plant, and a water reticulation system. Additionally, standards have been developed to ensure the standardisation of the processes involved while practices such as integrated urban water management have been proposed to aid in the conservation of our water supplies and systems.

The evolution of material science, water distribution design and maintenance has resulted in continuous development in the field, and this has resulted in more sophisticated and principles ways of operating WDS.

2.1.1 Operation and Maintenance

Adequate operation and maintenance of water distribution systems are imperative for the sustainable provision of water services (Van Zyl, 2014). The absence of such practices means that new WDS tend to decline to a point where the service provision is compromised. The effect of this includes increases in water losses, financial losses, and potential health risks.

Furthermore, if operation and maintenance are neglected for long enough, it may be necessary to replace the entire system or significant sections thereof. This results in the need for more capital to finance this activity when that capital could have been used in other sectors. Consequently, the proper and planned maintenance of WDS presents more benefits financially and health-wise while ensuring the system's sustainability.

Van Zyl, (2014) mentions how the activities mentioned above seek to protect the integrity of the system, which means protecting the system's physical, hydraulic and water quality integrity.

With respect to water distribution systems, system maintenance relates to the process of ensuring that the system performs optimally and efficiently. The process may entail assessing the efficiency of pumps, valves, and the water distribution network. The assessment of the water distribution network involves conducting water audits that help to find the physical and hydraulic efficiency of the system. Another maintenance practice may be the assessment of the fixtures, i.e. valves, pumps, and the water pipes. The assessment allows for prompt repairs and reduces the likelihood of catastrophic events. Knowledge of the system is of importance if the system is to be maintained. This requires knowledge of the pipe materials used and other alternatives that exist.

2.1.2 Pipe Materials

Water distribution systems have evolved in various ways, but the materials used are similar. This is because some of the pipes laid 50 years back are still in use, and while their replacement has been underway, the cost of the exercise means the process is often lethargic. The selection of the appropriate pipe material is hinged on a number of factors. Kayombo (1981) states that the following factors determine the choice of pipe materials used in a water system:

- The strength of the pipe which is characterised by the pipe's ability to withstand internal and external pressure
- Safety of use and cost of the pipe
- The ease of transportation and
- the availability of related resources

The availability of materials that are used in the manufacture of pipes has been so significant in the choice of pipe types used, and this is seen through the evolution of pipe materials in WDNs. This evolution in material usage is documented by Mora-Rodríguez *et al.*, (2014) who illustrate how initially, cast iron was commonly used in water systems and with the progression of time other pipe materials were adopted. Figure 2-2 shows this progression.

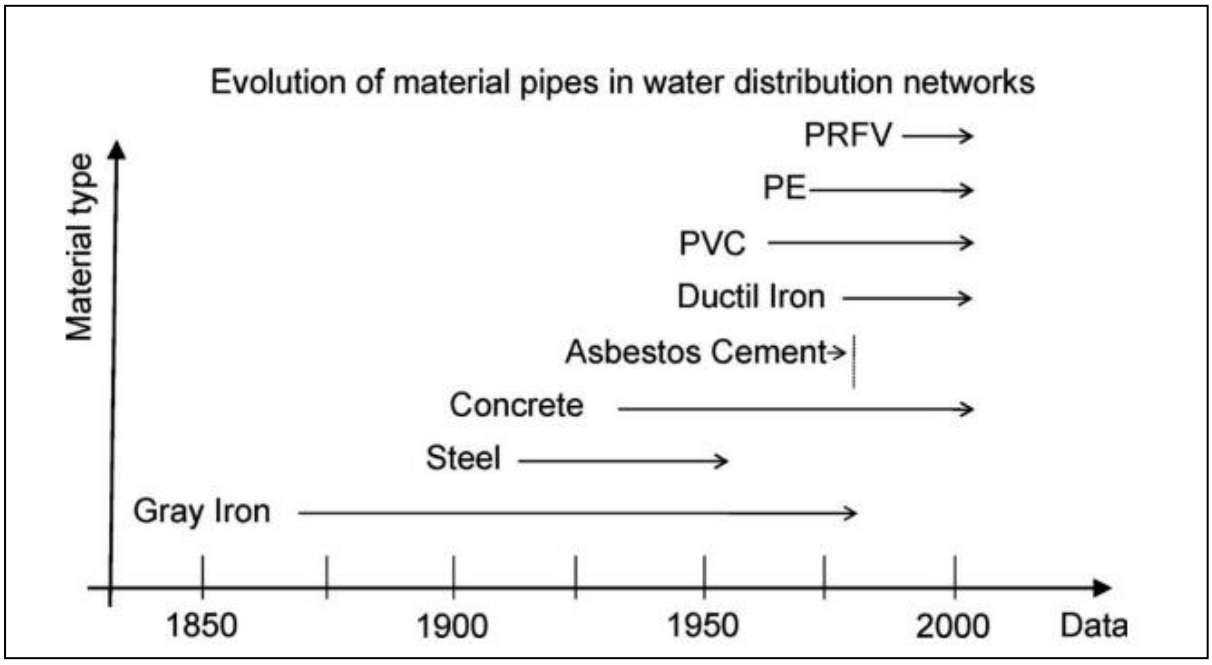

Figure 2-2 - Evolution of pipe materials in WDN (Mora-Rodríguez et al., 2014)

In terms of usage, the most common pipe materials are metal (cast iron and ductile iron), asbestos cement (AC) and plastics (PVC, HDPE) Mora-Rodríguez *et al.*, (2014). Most bulk

lines are steel pipes while distribution lines are now often PVC pipes in its various forms such as uPVC, mPVC and HDPE and more recently polyester reinforced with fibre glass (PRFV). Service lines into households are usually copper pipes (Rajani and Kleiner, 2001).

2.1.2.1 Cast iron and other metal types

Due to the availability of iron deposits and the relative ease of manufacture, cast iron quickly became a popular material for manufacturing pipes (Mora-Rodríguez et al., 2014). Nevertheless, cast iron and other metals are highly susceptible to electrochemical corrosion with the damage manifesting as corrosion pits. These corrosion pits often grow until the pipe eventually breaks. Electrochemical corrosion is accelerated by stray electrical currents, soil characteristics such as chemical composition and moisture content and by two metals connected to each other. Metallic pipes are also subject to tuberculation and crevice erosion, which reduce the effective diameter and present a breeding ground for bacteria. The quality of water transported in these pipes can also result in internal corrosion. Water properties such as pH, dissolved oxygen and free chlorine residuals play a role in the propagation of internal corrosion (Rajani and Kleiner, 2001).

2.1.2.2 Asbestos Cement

Hu and Hubble, (2007) give an account of how asbestos cement (AC) was intensively installed in the United States, United Kingdom and Australia. These installations occurred during the period between 1920 and late 1980. Presently, AC pipes remain a significant component in water networks. However, due to their age in the water network, AC pipes are prone to significant breakage rates.

Inasmuch as the use of AC pipes has been widespread, that has not come without its fair share of controversy. Reports of how the inhaling of dust from the manufacture and use of AC products leads to carcinogenic related diseases, coupled with the discovery of better materials saw a decrease in the usage of AC.

Additionally, AC pipes tend to be bulky, and transportation of these while avoiding breakages presents a challenge to contractors who tend to shun them. Hu and Hubble, (2007) however stated that, because some utilities have a large inventory of these pipes, they tend to use them still to reduce operational costs. This results in AC usage still being around 12% of replaced pipes in the United States (Mora-Rodríguez et al., 2014).

2.1.2.3 PVC Pipes

PVC is formed by the polymerisation of vinyl chloride with or without other vinyl monomers by the free radical initiation which generates polymers/copolymers. These are converted by compounding and eventually fabrication into the types of plastics/PVC products found today (Nass *et al.*, 1986)

Van Zyl (2014) describes how PVC is modified or manufactured to form the different types of PVC classifications. The grains are arranged in such a way that the strength is increased for one orientation o increase the strength of PVC materials in different orientations/directions. The material produced through this is known as oriented PVC (oPVC). For use in pipes and construction, the PV material needed ought to be different. Therefore, for this industry, the PVC used has no plasticisers in it and is referred to as un-plasticized PVC (uPVC). PVC also tends to easily fracture on impact in its original form, to decrease the possibility of fracture the PVC material is modified. The modification also allows for the pipes to have thinner walls and is achieved using additives. The material thus produced is termed modified PVC (mPVC).

Moreover, Van Zyl (2014) points out that while PVC is resistant to corrosion and has high hardness, it is not suitable for use at high temperatures nor should it be exposed to direct sunlight. Therefore, for applications that involve high temperatures, such as the transport of hot water, chlorine is added to the PVC to produce chlorinated PVC (cPVC) that is resistant to high temperatures (Van Zyl, 2014).

PVC and HDPE (another polyethene-based product) are the most commonly used structural materials in water distribution systems. Such that according to Kowalska and Kowalski, (2014), approximately 70% of all newly installed networks have either one of the two materials.

PVC pipes were not as commonly used in water distribution systems until the 1970s (Walski, 2006). Initially, the use PVC on WDS faced opposition from manufacturers of steel and cast-iron pipes who saw it as a threat to their industries. They even had public campaigns against it, citing it as a danger to human health (in reference to the carcinogenic properties of the vinyl chloride monomer gas) (Nass *et al.*, 1986). However, due to the development of many standards by associations such as the American Water Works Association (AWWA), it was gradually accepted in WDS, and because of its desirable properties, PVC became quite popular (AWWA, 2000).

The discovery and progression in development have made PVC the most commonly used pipe material in new water distribution systems (Mora-Rodríguez et al., 2014). PVC's popularity

has been aided by its various desirable properties such as its chemical inertness in WDS, its lightness and affordability.

2.1.3 Pipe Failures

Pipe failures occur when the environmental and operating tensions in and around a pipe diminish the structural integrity of the pipe such that it fails. This weakening can be caused by various factors such as external and internal loading, corrosion, degradation, manufacturing defects etcetera (Mora-Rodríguez et al., 2014).

Mora-Rodríguez *et al.* (2014) go on to classify pipe failures into 4 categories;

1) Circumferential breaks, as depicted in Figure 2-4, are caused by longitudinal tension.
2) Longitudinal breaks as shown in Figure 2-3 that are caused by radial tension
3) Cracks caused by a cross-sectional tension in the pipe.
4) Round holes that are caused by corrosion

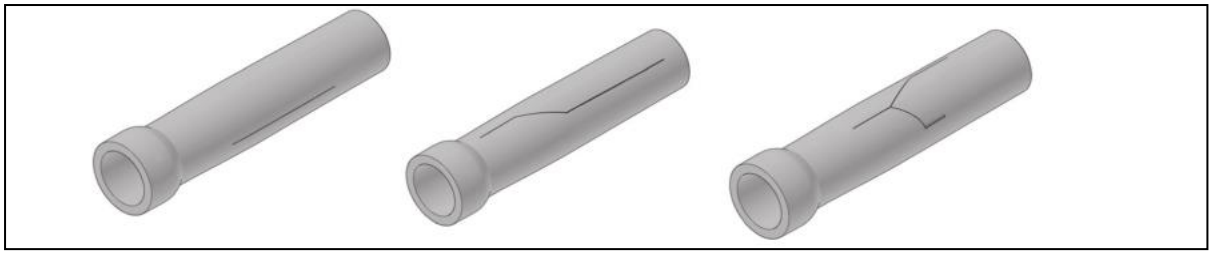

Figure 2-3 - Longitudinal cracks (Rodriguez et al., 2014)

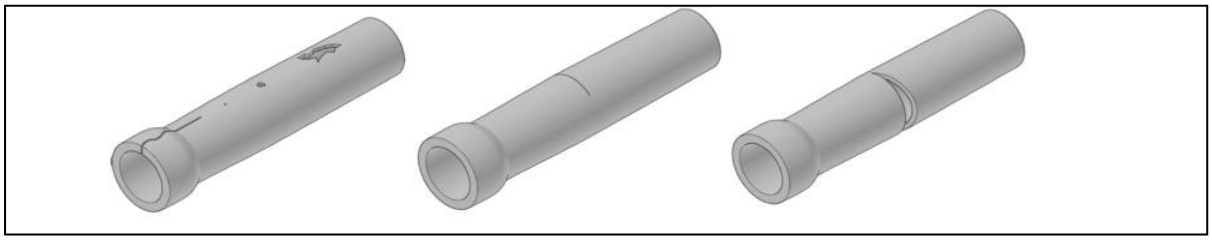

Figure 2-4 – Circumferential cracks and round holes (Rodriguez et al., 2014)

They go on to explain how circumferential breaks due to longitudinal tension arise due to one or more of the following:

i) Thermal contraction
ii) Tension flexion due to the differential in the ground movement in a section with poor ground preparation
iii) Inadequate ditches and supporting beds
iv) Other factors

Internal pressures in pipes contribute to both the longitudinal and circumferential tensions in the pipe with circumferential stresses being double the longitudinal stresses in a pressurised pipe (Hibbeler, 2016). However, most systems have thrust blocks that counteract the longitudinal forces in pipes. As a result, the dominant forces are circumferential stresses.

Correspondingly, Rajani and Kleiner, (2001) in their review of the structural deterioration of water mains, also report that one of the reported causes of pipe failures is corrosion. To back this assertion, they analyse how the pipe life deteriorates in relation to soil resistivity, which shows the level of the corrosiveness of a soil.

In like manner, Srikanth *et al.*, (2005) state that corrosion can occur due to a number of reasons. They highlight how pitting erosion from material inhomogeneities. In the study, they investigated how corrosion pits are formed, and such pits are shown in Figure 2-5. They further suggest other causes of corrosion such as sulphate action, microbial action and tuberculation, which play a significant role in pipe failure.

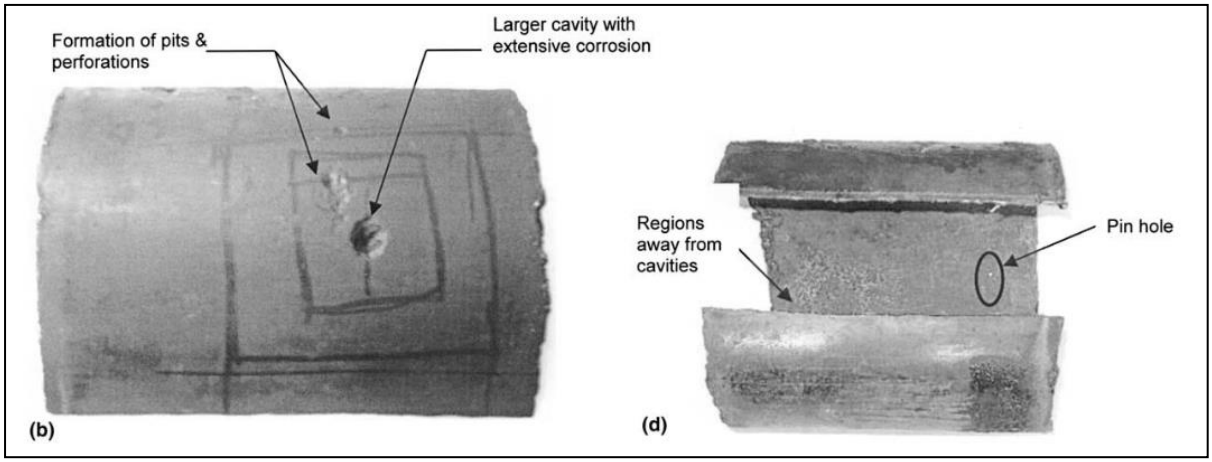

Figure 2-5 - Corrosion pits on a pipeline (Srikanth et al., 2005)

In a later paper which sought to investigate the factors that attributed to AC mains pipe failure, Hu and Hubble, (2007) conducted a water mains breakage analysis in their study area. They identified certain factors that were responsible for AC pipe failure. Amongst these were static factors such as soil type as some soils, e.g. Regina clay, can damage pipe by the expansion and contraction mechanism when the soil gains and loses moisture. Other factors are dynamic influences such as temperature and soil moisture. They also considered the effect of pipe age on pipe failures and found that there was a correlation between the two. This was similar to the findings made by Srikanth *et al.*, (2005).

The immediate impact of pipe failures is usually water losses which tend to be costly in terms of water lost, chemicals wasted, and energy lost from pumping. In a text on the operation and maintenance of water distribution systems Van Zyl, (2014) mentions how a system can be affected by contaminated water that is introduced into the water network through a hole/crack as a result of negative pressures. Thus, pipe failures provide points of intrusion in the event of negative pressures but also provide sources of contamination if the repair operation is not done correctly. As a result of the potential harm due to contamination from intrusion events coupled with the need to conserve water, it then becomes imperative to understand how leakage behaves and the various models available to explain leakage.

2.2 Leakage in Water Distribution Systems

2.2.1 Leakage Behaviour

The quantity of water lost through leakage is related to pressure (Ogura, 1979). In order to appreciate this relationship between pressure and leakage, it is essential to understand leakage behaviour. Correspondingly, to fully comprehend leakage behaviour, it is essential to investigate the mechanisms responsible for the observed leakage behaviour.

Van Zyl and Clayton, (2007) initially proposed that there were four causative factors that might explain the sensitivity of leakage to pressure. Subsequent to their paper, other factors were then found and published. These possible causative factors are discussed below.

2.2.1.1 Leak Hydraulics

The orifice equation describes the conversion of all the potential energy in a fluid in the form of pressure, to kinetic energy. The coefficient of discharge is included to incorporate energy losses and the reduction of the jet diameter downstream.

In an orifice of fixed diameter, this coefficient of discharge is not constant although the exponent is regarded as a fixed 0.5 (Greyvenstein and Van Zyl, 2007). For flow through an orifice, it is observed that a laminar regime develops at Reynolds number (Re) of about 10 and a turbulent flow regime is observed at Reynolds numbers above 4000 – 5000. The intermediary values represent the transitional zone, and the exponent can vary between 0.5 at the transitional-turbulent boundary and 1 at the lamina-transitional boundary. Van Zyl and Clayton (2007) developed equations that relate flow to the Reynolds number. With the equations, they could find the laminar and transitional flow rates of different leak types, at normal operating pressures. The equations are shown below,

For circular leak openings:

$$Q = \frac{\pi v^2 Re^2}{4C_d\sqrt{2gh}} \qquad (1)$$

For a rectangular leak opening:

$$Q = \frac{(n+1)^2 v^2 Re^2}{4nC_d\sqrt{2gh}} \qquad (2)$$

From equations 1 and 2, Van Zyl and Clayton (2007) plotted the velocities and the corresponding heads for maximum laminar and transitional flows. The results are shown in Figure 2-6.

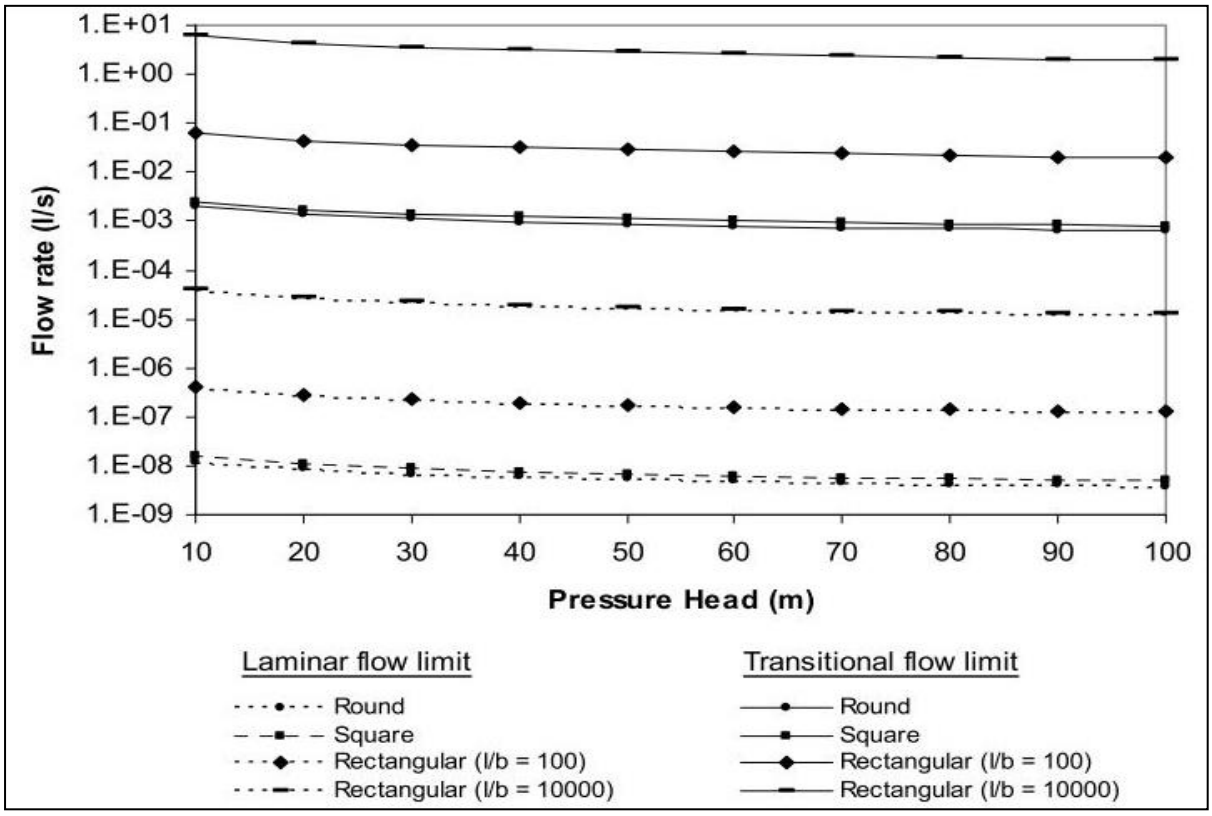

Figure 2-6- Maximum lamina and transitional flow rates for different leak openings (Van Zyl & Clayton, 2007)

Their findings revealed that rectangular cracks could have higher flow rates for both laminar and transitional flows because of having a greater wetted perimeter. Laminar flow rates were found to be small, and as a result, it was believed that full laminar flow would not play a considerable role in leakage.

Their conclusion in this paper then asserts that because of this, transitional flow and by extension, background leakage will contribute to leakage exponents that are greater than 0.5, albeit less than 1.

However, in a later paper Van Zyl (2014), states that observing the leakage flowrate in the lamina and transitional flow regimes, it seems questionable that transitional flow has much of an impact on the leakage exponent of the system.

2.2.1.2 Pipe Material Behaviour

From the structural analysis of pipes in response to internal pressure, the stresses in a pipe under internal pressure are double in the circumferential direction than in the longitudinal direction. While both stresses can exist in the pipe, the presence of thrust blocks in water system means that the longitudinal stresses are minor and circumferential stresses are more dominant stresses in a pipe system.

By considering that the presence of an orifice in a pipe increases the stresses around the orifice, van Zyl and Clayton, (2007), suggested that flow rate through a circular hole can be found by the expression shown in (3).

$$\boldsymbol{Q} = (0.125g)^{0.5}\pi C_d {d_0}^2(h^{0.5} + 2Ch^{1.5} + C^2h^{1.5}) \qquad \boldsymbol{(3)}$$

Where C is a constant, d_0 is the original diameter and q is the flow rate through a circular hole. This equation contains terms with exponents 0.5, 1.5 and 2.5, which seem to suggest that the experimental and field results of the N1 are appropriate. However, calculations done using the above equation go on to show that the 1.5 and 2.5 exponent is negligible under normal circumstances.

Further investigations by Cassa and Van Zyl, (2013), revealed a regression analysis that the elastic modulus of the pipe material had a significant influence on leakage while the Poisson ration did not have much influence. This finding showed that while pipe material properties have an influence on leakage behaviour, the extent of each parameter's influence varied.

2.2.1.3 Soil Hydraulics

A simplified application of seepage as it pertains to geotechnical engineering would suggest that the rate of seepage is proportional to the head of fluid above the point of seepage as described by Darcy's law;

$$q = Fkh \qquad \boldsymbol{(4)}$$

Where F is the soil form factor, k is the coefficient of permeability and *h*, is the head difference. Van Zyl and Clayton, (2007), explain the different implications of this law for leakage. They show how there is an incompatibility between Darcy's law and the orifice equation. To demonstrate this, they analysed the differences in flow under a hydraulic grade of one and the

flow through an orifice, with the former having velocities ranging between 10^{-2} and 10^{-8} m/s while the latter has much higher velocities.

Another aspect worth considering is the limits to which Darcy's law is valid, which only applies to laminar flow through the soil medium. The velocity is a function of the hydraulic gradient, and laminar flow is possible at dh/dl <<1, it can then be concluded that this limit is exceeded at the hydraulic gradient between the pipe and soil can at times exceed 30. The hydraulic gradient usually results in the flow regime becoming turbulent, and at these velocities; darcy's law is invalid, and leakage does not obey the seepage theory at the point of leakage.

2.2.1.4 Water Demand

Van Zyl, Haarhoff and Husselmann (2003), found that the effect of pressure on water demand could be expressed as:

$$Q_{dem} = Ch^{\beta} \qquad (5)$$

Where C is a constant coefficient, and β is the elasticity of water demand with respect to pressure. Although water demand is not strictly classified as leakage (leaking cisterns and taps could be considered as leakage/ water lost), it is challenging to differentiate consumption and leakage in the system even during minimum night flow measurements (Silva et al., 2011).

Initially, Van Zyl *et al.,* (2003) assumed that the elasticity demand ranged between 0.15-0.25. A study conducted at the University of Johannesburg revealed that the indoor elasticity was 0.2 did not exceed 0.5 (Bartlett, 2004). For an extensive distribution system, it is highly likely that the measured minimum night flows will include some component of consumption (Van Zyl and Clayton, 2007).

Therefore, provided that the demand variation is low during minimum night flow conditions (when the system exponent values are recorded), the systems overall leakage exponent would not be affected by the demand as is shown to have exponent values of less than 0.5.

2.2.1.5 Quantity and distribution of leaks

In a later paper, Schwaller and Zyl, (2014) contributed another factor that affects leak behaviour. In the study a statistical model for the distribution of leaks in a network was proposed, through which it was found that a small number of leaks with high individual leakage exponents would increase the overall system's leakage exponent.

2.2.2 The Orifice Equation

The Torricelli equation describes how the velocity of a fluid is related to height, *h*, which is the pressure head from which the flow obtains its energy. This relationship is shown in (6). The equation is based on the conservation of energy and can be derived from Bernoulli's equation with a few assumptions.

$$V = \sqrt{2gh} \tag{6}$$

Where *V* is the velocity of the fluid through the orifice, *h*, is the pressure/head difference between the pressures on either side of the container and *g*, is the acceleration due to gravity.

The flow through the hole/orifice is therefore described as a function of the velocity through the orifice and the area of the orifice, in practice the assumptions made while deriving the Torricelli equation are invalid and as a result a coefficient of discharge, C_d. This gives the orifice equation:

$$Q = C_d A\sqrt{2gh} \tag{7}$$

There *Q* is the flow rate through the orifice, and the other terms are the same as above. What this equation tells us is that the flow through an orifice is proportional to the root of the pressure. As a result, an increase in pressure should result in an increase in flow rate.

2.2.2.1 The Discharge Coefficient

When a fluid flows through an orifice, the area of the jet from the orifice rarely has the same area as the orifice area due to the convergence of fluid streamlines leading to a region called a vena contracta forming as shown Figure 2-7 from Douglas et al., (2006).

As such, a coefficient is used to relate the discrepancy in the two areas/regions and is expressed in the equation below.

$$A_j = C_c A_0$$

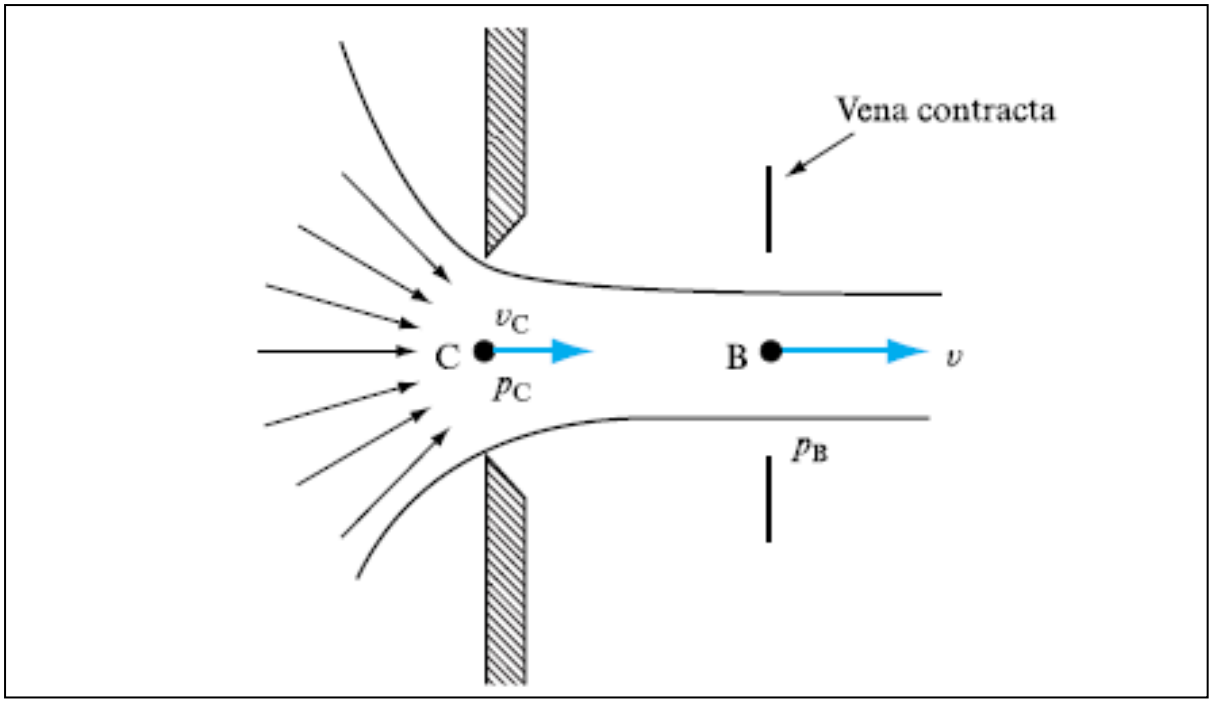

Figure 2-7 - Contraction of a jet from an orifice (Douglas et al., 2006)

where C_c is the coefficient contraction and A_j, is the area of the jet at point B in Figure 2-7, and A_0 is the orifice area at point C. In addition to the contraction of the fluid, there is also a loss in energy, which leads to a loss in velocity. Thus, a coefficient of velocity, which accounts for the difference in velocities, is required and is expressed in the following equation:

$$V_j = C_v V_0$$

Through the comparison and application of the conservation of mass between the points B and C, the equations relating the actual fluid discharge and theoretical discharge is obtained which contain a parameter that describes the coefficient of discharge and is expressed below:

$$Q_{actual} = C_c C_v Q_0$$

With the discharge coefficient described as:

$$C_d = C_c C_v \qquad (8)$$

A more in-depth derivation can be found in most fluid mechanics textbooks such as Douglas et al., (2006) and Chadwick et al., (2013).

The factors that influence the coefficient of discharge have been investigated, and it has been established that some notable factors that influence the coefficient of discharge include:

- **The smoothness of the orifice edge** – In their study which sought to determine the coefficient of discharge from a drained pipe, Hicks and Slaton, (2013), developed an experimental setup that involved investigating the different values of Cd obtained from orifices of different sizes and smoothness. The smoothness of the orifices was provided using grommets that were placed on the round hole orifices while another plate with a similar-sized orifice was just drilled and used as it was. Thus, the presence of a grommet determined the smoothness of an orifice. They then measured the discharge through the uPVC pipe and the orifices on a plate and compared the values to obtain a coefficient of discharge. Their experiments showed that the smoother orifice exhibited and larger valuer of Cd which implied that the flow through the orifice was closer to the theoretical flow rate, while the "rough" orifice exhibited values often quoted in experiments of 0.65 -0.66 apart from the 4mm round hole that had a Cd value of 0.761.
- **The d/D ratio** – Prohaska, (2008) also investigated the various influences that affect the discharge coefficients. While the study focused on orifices usually associated with stormwater rise pipes, the flow model is like other orifice flow models. One of their findings found that the discharge coefficient decreases as the d/D ratio increases. d/D was defined as the ratio between the orifice diameter, d and the riser diameter, D. This meant that on a riser of the same diameter the coefficient of discharge on the orifice found on that riser would increase and as the area of the orifice increases. This is explained by the boundary layer separation theory found in fluid mechanics texts. This theory explains how as the flow into an orifice slows down (in this case as a result of a larger area and smaller d/D ratio) the distorted area at the vena contractor is substantial and the coefficient of contraction increases and therefore, Cd increases. Thus, explaining how a decrease in the d/D ratio will result in an increase in the coefficient of discharge.
- **The pressure head above the orifice** – Another result from Prohaska, (2008) was the finding that the coefficient of discharge was seen to increase as the pressure head decreased. This was explained as being due to the exiting velocity of the fluid reducing as the pressure head reduced, resulting in the flow streamlines of the fluid slowing down. This leads to an increase in the vena contracta and consequently, an increase in the coefficient of contraction C_c. This then means that the coefficient of discharge (C_d) also increases from equation 8.

This then means that the above-mentioned factors have an influence on the flowrate found using the orifice equation (equation 7) as it is dependent on the coefficient discharge.

2.2.3 The N1 Concept

Water practitioners initially attempted to use the orifice equation to try and explain the relationship of pressure with leakage in water distribution systems (A. O. Lambert, 2002). However, because the orifice equation and the different factors that affect it were not user-friendly in practice (Thornton and Lambert, 2005), they simplified the orifice equation to the form:

$$Q = ch^{\alpha} \qquad (9)$$

This is known as the power equation with a power exponent, α, and groups the terms $C_{d,}\ A, \sqrt{2g}$ into one constant, c. From the orifice equation, it is/was expected that the relationship between the flow rate and the pressure would result in an exponent with the value, 0.5. This was what a set of Japanese (Hiki, 1980) experiments on 1 – 5 mm holes drilled in 60 - 80 mm diameter, metal pipes found with the study finding values ranging between 0.36 - 0.7. Van Zyl, (2014), mentioned how the exponent of 0.5 through an orifice was true for turbulent flow. This means that a value of 0.5 from the orifice is still to be expected.

Ogura, (1979), linked the relationship between leakage and pressure with a leak exponent value of 1.15 in Japan and tested 20 small zones of 4.7 km in length and averaged the values of the leakage exponent to attain an exponent 1.15. other practitioners also found exponent values greater than 0.5, and this led to the use of the power exponent rather than the orifice equation. By the time practitioners had started using the exponent in leakage in pressure studies, it had been given an alphanumeric name “the N1” by the water losses taskforce (Thornton and Lambert, 2005). Such that the power equation became;

$$Q = ch^{N1}$$

Interestingly, results from various systems in countries such as Japan, Brazil, Canada, Malaysia, the United Kingdom, Croatia, and Australia (Thornton and Lambert, 2005), showed that the N1 exponent mostly ranged from as 0.5 to 2.5 with some areas showing exponent values of 2.83. Practitioners tried to partially explain this deviation from the expected range of 0.5-1.5 by component analysis of the various leaks and pipes (rigid and flexible).

2.2.4 The Fixed Area/Variable Area Discharge (FAVAD) Concept

Van Zyl, Lambert and Collins, (2017) found that the power equation should only be used within its calibration range. They then recommended that a modified orifice equation be instead used in leakage modelling. This idea of a modified orifice equation had been initially popularised by May, (1994), who in his seminal article stated that high pressure causes a substantive increase in leakage and bursts and as a result pressure control is fundamental to any leakage control policy. This assertion had already been stated by Ogura, (1979) and went on to be proven by researchers such as Thornton and Lambert, (2006); Lambert et al., (2013); Deyi et al., (2014).

May, (1994) also reinstated the idea that the relationship of how leakage flow rate is related to the pressure is a bit more nuanced than initially put across by the orifice equation. This is because a reduction in pressure results in the contraction of individual leakage paths.

Through analysing the data from a pressure-controlled area which had undergone a pressure reduction exercise, he realised that a change in pressure resulted in a change in the system leakage area. Thus, the leakage area is a function of pressure. He then postulated that leakage in any water distribution system could be represented by a two-part equation with the two terms representing the fixed leakage path (such as pipe bursts and undeclared consumers of water) and the variable leakage path which are pressure dependent.

Although the nature of expansion/contraction may be governed by several complex factors such as ground conditions and the type of joint, it was reasonable to assume that the relationship between leakage path area and the pressure was linear (May, 1994).

Finally, May, (1994) asserted that due to the possibilities of this type of leakage path in every pipe joint being subject to the most significant uncertainty, i.e. the human factor, it is perhaps statistically reasonable to expect a uniform behaviour and that the expansion/contraction term applies to the whole system.

As a result, the following equation was suggested which explained leakage flow rate as being fixed area/variable area discharge (FAVAD):

$$Q_L = A_f{}' C_d \sqrt{2g} h^{0.5} + S C_d \sqrt{2g} h^{1.5} \qquad (10)$$

Where: Q_L = Leakage flow rate (m^3/s), C_d = Coefficient of discharge (dimensionless), $A_f{}'$ = Area of fixed leakage paths (m^2), g = acceleration due to gravity (m/s^2), h, is the Average Zone Night Pressure (AZNP) (m), and S is the system expansion coefficient.

S and $A_f{}'$ reflect the system characteristics and were evaluated by making small adjustments to the AZNP and measuring the resulting flow. He also stated that because of the presence of pressure-dependent leakage flow paths, there would be a level of leakage that will be hard to find and uneconomic to repair.

2.2.5 Experimental Work Related to The FAVAD Concept

The work that was done by the scholars discussed above gave an insight as to the possible factors that influence leakage behaviour. However, their conclusions suggested that more work needed to be done to understand the behaviour of various leaks from different pipe materials. This work was done through controlled experimental investigations, and the next section will address the experiments that specifically relate to the FAVAD concept.

2.2.5.1 The Modified Orifice Equation

Cassa and van Zyl, (2006), investigated the behaviour of different pressurised leak openings of different material using finite element analysis. In their study, they assumed that the materials displayed elastic behaviour. The leak openings and parameters were modelled on the ABAQUS standard finite element software and the Solid Works computer-aided design software.

From their study, they found that pipe stresses were significantly affected by leak openings and the local stresses can often exceed the pipe's material yield strength causing permanent deformation and, in some cases, pipe failure. By varying the pressure head and measuring the leak area from the position of the nodes on the finite element model, and the relationship between the leak opening area and the pressure head was found and is represented by (11).

$$A = A_0 + mh \qquad (11)$$

Where A is it leak area at a pressure, h, A_0 is the initial leak area, and m is the slope of the head-area relationship. Replacing A, in the orifice equation, gives the modified orifice equation:

$$Q = C_d\sqrt{2g}(A_0 h^{0.5} + mh^{1.5}) \qquad (12)$$

This equation is similar to equation 10. However, there is a difference in the interpretation. May had hypothesised that in a system there would be leaks that had fixed areas and have a 0.5 exponent, and variable area leaks with 1.5 exponents. The modified orifice equation differs in that it considers all leaks to have a component of the variable area.

They went on to further show how the equation provides a better description than the power equation for the behaviour of a single leak, and they conclude that for a distribution system with many leaks the use of this equation needs further investigation. Another finding on the equation and the N1 exponent was that the modified orifice equation predicts a maximum N1 of 1.5 and as a result, does not explain higher leakage exponents.

2.2.5.2 Predicting the Head-Area Slope

Cassa and Van Zyl, (2013) resumed the research from 2.2.5.1 and sought to predict the head-area slope, *m.* Finite element analysis was used to predict the head-area slope for longitudinal and circumferential cracks. Only the linear elastic material behaviour was considered in the study. To obtain an expression to express the head area slope; the impact of loading, pipe material, section and crack properties were investigated. The internal pressure and external stresses where simulated in the model. It was found that the leak area expands linearly with pressure irrespective of pipe material, leak type or loading state. By altering various pipe and leakage parameters, they managed to obtain the relationship of each parameter with head area slope. Figure 2-8 shows how some of these parameters behaved.

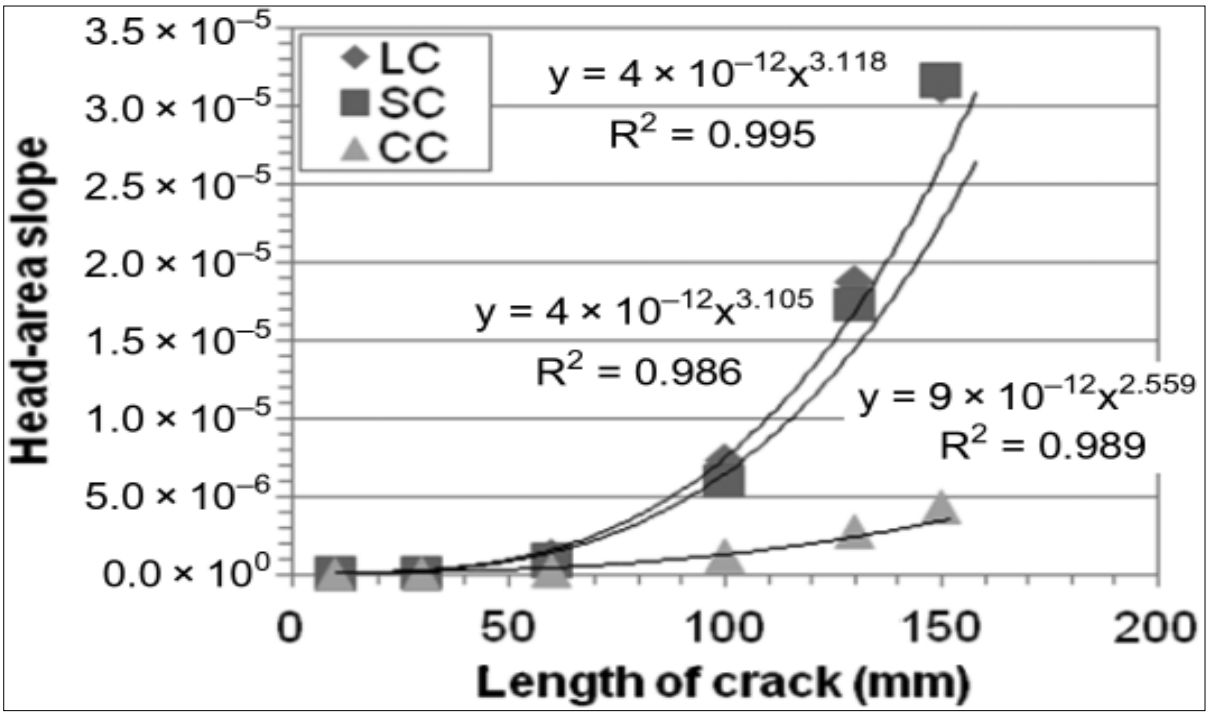

Figure 2-8 - Graph showing the effect crack length has on the head-area slope (Cassa and Van Zyl, 2013)

Other parameters investigated were, pressure (P), Young's modulus (E), Poisson's ratio (ν), longitudinal stress (σ_l), wall thickness (t), internal diameter (ID), length of crack (L_c) and the width of the crack (W_c).

They also found that in the absence of longitudinal stresses, circumferential cracks have a negative head-area slope. This suggests that the crack closes due to circumferential expansion, which results from the dominant circumferential stresses. This finding is supported by previous studies in which exponents with values less than 0.5 were found on pipes with circumferential cracks.

A regression analysis was then used on the data to derive 3 mathematical models describing the head-area slope, m, as a function of the parameters of the pipe and the crack. It was found that the parameters with the most considerable influence on the head-area slope, *m*, were the crack length, wall thickness, Young's modulus, internal diameter and longitudinal stress, although in real systems the longitudinal stresses are negligible as they are countered by thrust blocks.

These three models are shown below with equation 13, 14, and 15 predicting the head area slope for longitudinal, spiral and circumferential cracks, respectively:

$$m = \frac{2.93157.d^{0.3379}.L_c{}^{4.80}.10^{0.5997(log\,L_c)^2}.\rho.g}{E.t^{1.746}} \quad (13)$$

$$m = \frac{3.7714.d^{0.178569}.L_c{}^{6.051}.\sigma_l{}^{0.0928}10^{1.05(log\,L_c)^2}.\rho.g}{E.t^{1.6795}} \quad (14)$$

$$m = \frac{1.64802\ x\ 10^{-5}.L_c{}^{4.87992662}.\sigma_l{}^{1.09182555}10^{0.82763163(log\,L_c)^2}.\rho.g}{E.d^{0.186376316}.t^{0.33824224}} \quad (15)$$

Combining these equations with equation 12 (the modified orifice equation) by substitution allows one to predict the head area slope for any pipe section, material and crack length within the bounds of regression analysis. These predictions are made under the assumption of linear elastic behaviour.

In their conclusion, they reiterate how at the time of publishing only the leakage exponent, N1, has been studied and reported on and not the head-area slope. They also suggest that more work needs to be done to verify the proposed equations. Other authors then expanded on the work done by Cassa and Van Zyl, (2013). Of interest is a study conducted by Nsanzubuhoro, Van Zyl and Zingoni, (2017) that looked at predicting the head area slope of circular holes. This particular orifice type had not been covered by Cassa and Van Zyl, (2013).

In the study by Nsanzubuhoro, Van Zyl and Zingoni, (2017), a finite element analysis was conducted using the ABAQUS software. The aim of the study was to understand the head-area slope of round holes in water distribution pipes through a sensitivity analysis of various parameters that affect the head-area slope. Initially, the pressure-discharge relationship of a

leak on a 110 mm uPVC pipe with a wall thickness of 3 mm was initially investigated. It was found that there was a linear relationship between the leak area and the pressure in the pipe described by equation 11, as observed by Cassa and van Zyl, (2006).

To achieve the aims of the study, the pipe material and leak parameters/variables that were investigated are; elastic modulus, Poisson's ratio, longitudinal stress, internal diameter, wall thickness and hole diameter. The FEA showed that the parameters that affect the head-area slope the most were the wall thickness (t), elastic modulus (E), and internal pipe diameter (d).

By assessing various solid mechanics and mathematical concepts, an expression to predict the head-area slope for round holes was derived as:

$$m = 8.00\left[\left(\frac{A_0 K \rho g r}{tE}\right)(\alpha - v + 1 - v\alpha) - 8x10^{-9}\right] \qquad (16)$$

Where A_0 is the initial hole area, K is the stress concentration factor typically 3, ρ is the fluid density, g is the acceleration due to gravity, r is the internal pipe radius, t is the pipe wall thickness, E is the Elastic modulus, α is the ratio of the longitudinal stress and the circumferential stress, assumed to be 0.5. In a later paper Nsanzubuhoro, van Zyl and Zingoni, (2017) showed that when inputting the known values for K and α and further manipulation, the equation can be reduced to:

$$m_{eq} = \left(\frac{9A_0 \rho g r}{2tE}\right)(1 - v) \qquad (17)$$

They then compared expected head area slopes with experimental data from work done by Malde, (2015), and from the linear relationship between the two datasets, obtained the expression shown below:

$$m = 0.35\left[\left(\frac{9A_0 \rho g r}{2tE}\right)(1 - v)\right] - 0.0076 \qquad (18)$$

They state that the equation requires further verification and calibration due to the limited data used to derive the relationship between the experimental data and predicted values.

2.2.5.3 Laboratory Work to Establish the Head-Area Slope

The finding by Cassa, van Zyl and Laubscher, (2010) were at the time, based on the finite element modelling, which was a controlled simulated setup. While these finding gave an insight as to how leaks in pipes ought to behave when subjected to pressure, there was no substantial evidence that this was practically true.

Ferrante, (2012) then sought to investigate the effect of pipe material on the head-discharge relationship of leaks. The laboratory experiment shown in Figure 2-9, involved four pipes of 1.05 meters in length, each pipe with its own rheology, which was determined by the pipe material and thickness. Two 90 mm longitudinal leaks were then machined on these pipes, and a test rig was set up that allowed a sample pipe to be fitted and removed at will. The flow rate was controlled by a pump and valves with measuring devices upstream and downstream of the pipe sample, which recorded the pressure and the flow rate through the leak.

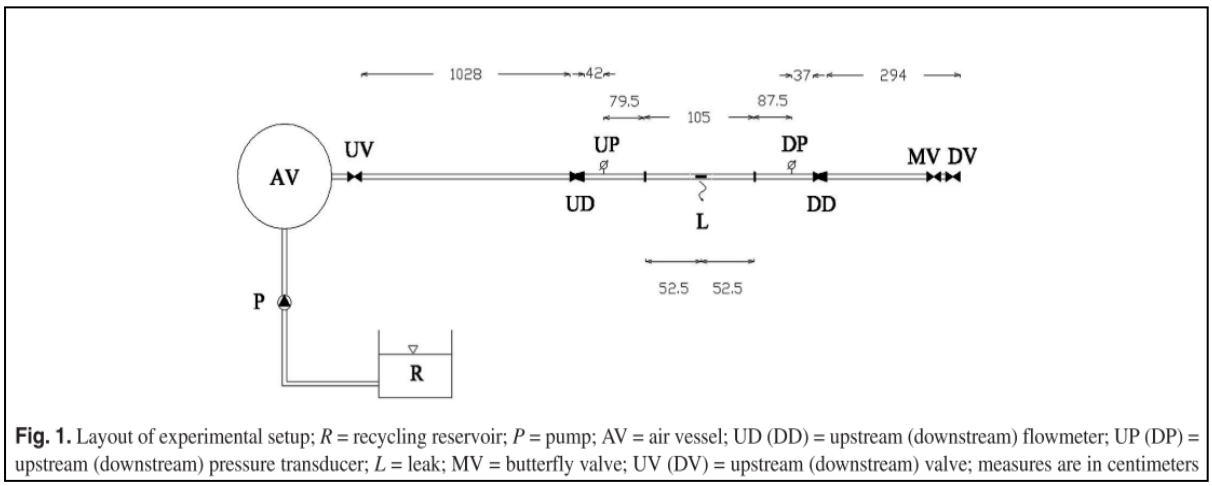

Fig. 1. Layout of experimental setup; *R* = recycling reservoir; *P* = pump; AV = air vessel; UD (DD) = upstream (downstream) flowmeter; UP (DP) = upstream (downstream) pressure transducer; *L* = leak; MV = butterfly valve; UV (DV) = upstream (downstream) valve; measures are in centimeters

Figure 2-9 - Experimental Setup Layout from Ferrante, (2012)

The rheological behaviours investigated were; deformable, elastoplastic, elastic, and viscoelastic behaviour. They interpreted experimental results for leaks in pipes of different material by using different head-discharge relationships. From this, they found that Torricelli's formula cannot interpret all the data from the tests unless a variation in the leak area with pressure was also considered. This finding also agreed with the reasoning by May, (1994) and showed how the power equation might fail to explain some leakage behaviour. To add on to that, they mention how while the power equation can explain the leak discharge relationships, it does not give a physical explanation of the leak area variation with the head.

Ferrante (2012) also found that the leak area deformation depends on the pressure head, the pipe thickness and pipe material. These conditions had been determined as having an effect on

leak areas by Cassa, van Zyl and Laubscher, (2010), using finite element analysis and now were collaborated by laboratory experiments.

They then conclude by proposing an assumption; that if the conditions and dimensions of the fourth sample, i.e. the viscoelastic HDPE pipe are considered as to be representative of real-world systems and the differences in leak flow rate can be up to 20% for the same value of pressure, then the effect of pipe material on the leak-discharge relationship in HDPE could be relevant for practical applications. From this, they call for more tests on HDPE pipes to give better insight into the dependence of leak-discharge relationship on pipe rheology.

Further work on the modified equation this was done through an experimental study of leaks in a laboratory set up by Van Zyl and Malde, (2017). The study involved testing several different leak types on different pipe materials to investigate the leakage characteristics of each sample. The schematic layout of the experiment is shown in Figure 2-10.

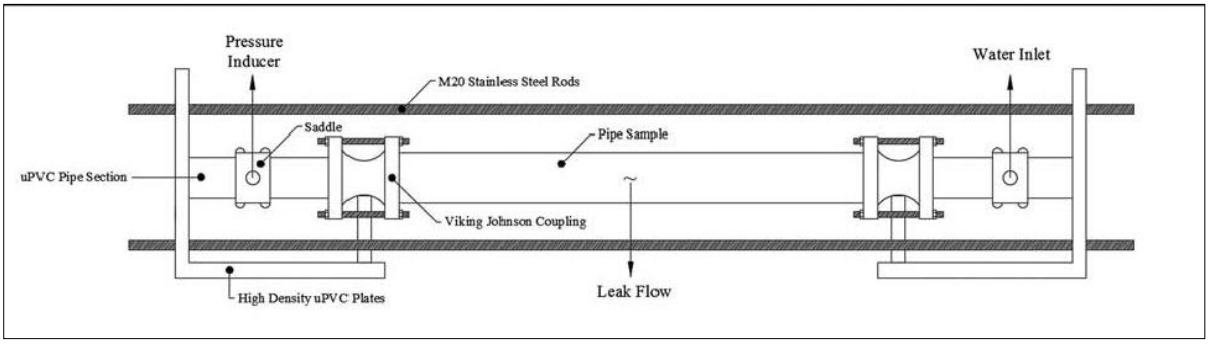

Figure 2-10 - Schematic layout of the main components of the experimental setup (Van Zyl and Malde. 2017)

The setup had two removable end sections mounted on a high-density uPVC plate, as shown in Figure 2-10. The pipe section with the induced failure was fitted to the sections using flexible Viking Johnson couplings. The setup was held together by three 2.5 m long stainless-steel rods of 20 mm diameters that also took up the longitudinal stresses in the pipe and thus acted like thrust blocks in WDS. The pipe sections tested were 800 mm long. One end of the setup was connected to a pumped water supply that delivers water, and the pressure could be varied by varying the speed of the pump.

A calibrated magnetic flow meter was used to measure the flow. The pressure in the system was measured on a transducer that was fitted on the other end of the setup. Care was taken to ensure there was no air in the pipe by allowing water to flow out of the end with the transducer connection point before the transducer was attached. The flow and pressure measurements were recorded on data loggers with data collected every second.

For each of the test sections, the setup was placed horizontally with the leak and the pressure transducer at the same level. The leak discharged into the atmosphere. The flow and pressure were increased and then decreased in five steps with each step lasting at least 30 seconds. This was done 3 times in succession per pipe, and the data was downloaded and analysed (Van Zyl and Malde, 2017). The results obtained were analysed, and the effective head area slope and effective leak area were obtained. As the initial area was known the coefficient of discharge was obtained for all sections tested. The statistical interference theory was used to obtain the confidence intervals of these results. This test represented the first time the modified orifice equation had been tested using a laboratory set up. The results, shown Figure 2-11, were tested against equation 13, and it was found that the equation performs reasonably well in predicting the head area slope in longitudinal cracks.

Pipe material	Length/diameter (mm)	N1	A_0 (mm²)	95% SCI for A_0 (mm)	m' (mm²/m)	95% SCI for m' (mm²/m)	p for m' (%)	C_d
Round holes								
uPVC	12	0.499	68.3	±0.11	−0.00141	±0.00230	12.5	0.603
mPVC	12	0.500	68.3	±0.17	0.00021	±0.00360	87.9	0.604
HDPE	12	0.501	70.3	±0.16	0.00180	±0.00345	4.5	0.621
Steel	12	0.497	67.4	±0.18	−0.00486	±0.00365	0.2	0.596
Longitudinal slits (width = 1 mm)								
uPVC	50	0.886	27.4	±2.08	0.28658	±0.0193	<0.1	0.547
uPVC	100	1.041	52.9	±2.59	2.51200	±0.129	<0.1	0.529
mPVC	50	0.989	37.5	±6.00	0.86711	±0.139	<0.1	0.749
HDPE	73	0.835	62.8	±11.7	0.97499	±0.348	<0.1	0.860
HDPE	100	0.798	94.5	±12.0	2.03031	±0.578	<0.1	0.945
Steel	50	0.500	22.0	±0.22	0.00011	±0.00275	10.3	0.440
Steel	100	0.529	44.7	±0.13	0.02166	±0.00205	<0.1	0.447
Spiral slits (width = 1 mm)								
uPVC	50	0.657	36.6	±0.53	0.10802	±0.00800	<0.1	0.732
uPVC	100	0.797	78.4	±1.31	1.24352	±0.0476	<0.1	0.784
mPVC	50	0.798	43.2	±1.47	0.37375	±0.0288	<0.1	0.865
HDPE	50	0.656	33.0	±3.08	0.09377	±0.0451	<0.1	0.660
HDPE	78	0.703	69.0	±4.68	0.48148	±0.123	<0.1	0.884
Steel	50	0.490	22.8	±0.08	−0.00267	±0.00095	6.4	0.457
Steel	105	0.523	44.2	±0.17	0.01615	±0.00265	1.6	0.421
Circumferential slits (width = 1 mm)								
uPVC	50	0.455	34.8	±0.26	−0.02170	±0.00380	<0.1	0.696
uPVC	100	0.327	50.2	±1.28	−0.11423	±0.0189	<0.1	0.502
mPVC	50	0.433	37.2	±0.27	−0.03403	±0.00380	<0.1	0.743
HDPE	54	0.185	20.6	±1.74	−0.06212	±0.0213	<0.1	0.382
HDPE	80	−0.262	37.4	±5.14	−0.20706	±0.0646	<0.1	0.467
Steel	53	0.499	22.6	±0.37	−0.00008	±0.00485	33.3	0.427

SCI, simultaneous confidence interval.

Figure 2-11 - Summary of experimental results (Van Zyl and Malde, 2017)

The laboratory tests discussed thus far had all been on leaks that discharged into the air. However, more realistic behaviour of leaks in water distribution systems should be obtained from leaks that are buried/underground.

De Paola *et al.*, (2014), recognised the importance of characterisation of the leakage pressure relationship for modelling losses in WDS. They also observed that most experiments, as noted above, had been on pipes that discharged to the atmosphere and as a result, they conducted tests on a pipe buried in the soil. The test was done on a 3.2 m HDPE pipe that was fitted along with a steel pipeline. Downstream an air vessel had a driving pressure of 0 - 10 bar on water obtained from a sump. Pressure and flow were measured downstream of the pipe. The HDPE section was accommodated in a sloping Perspex box that was 2 m long, 0.35 m wide, 0.45 m high. A drainage layer of gravel was laid underneath the pipe with variable thickness. A schematic of the laboratory setup is shown in Figure 2-12.

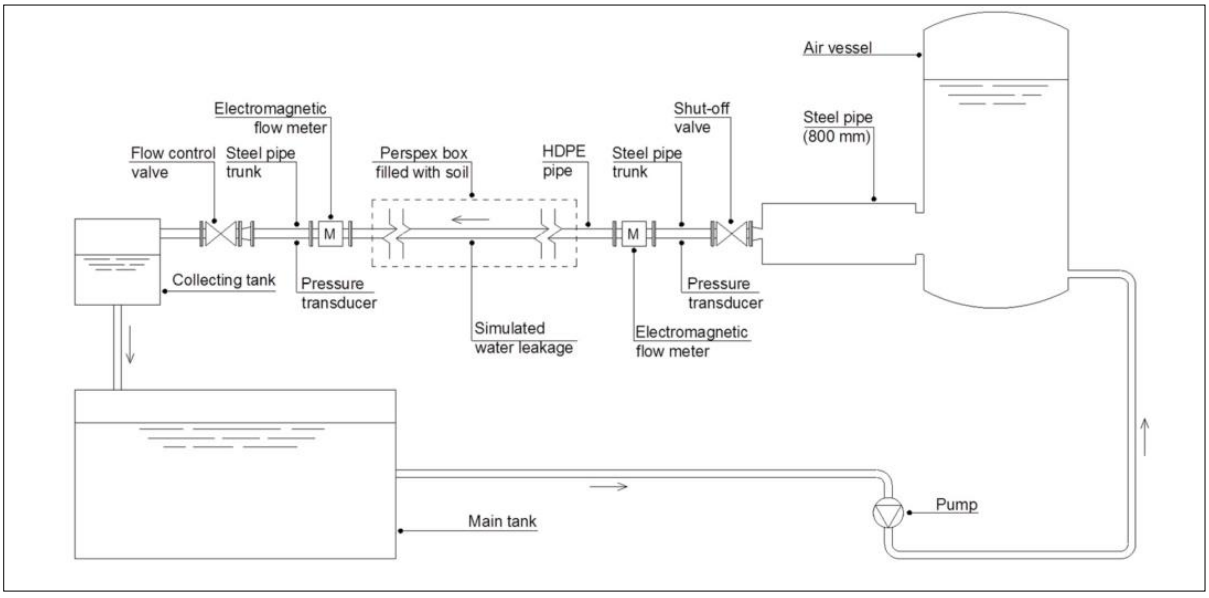

Figure 2-12 - Schematic of the experimental setup (De Paola et al., 2014)

The pipe was then covered in 0.3 meters of volcanic sandy soil and a load, in the form of a mass, was applied on the top of the soil to simulated ground conditions of 450 N/m^2. In the preliminary results, it was observed that an excavation of soil in the proximity of the leak occurred. The magnitude of flow and velocity was also found to vary significantly with pressure. The maximum depth of the excavation profile was governed by the magnitude of pressure while the direction of the leak governed the shape of the excavation. These findings were similar to observed experiments by Van Zyl *et al.*, (2013) who were investigating soil fluidisation outside leaks on pipes.

With respect to hydraulic behaviour, no significant differences were observed in the buried pipe and pipes that discharged to the atmosphere. This was probably due to the negligible presence of soil around the leak, thus reproducing the boundary conditions of free outflow in the air. The results were also compared to the power equation but not with the modified orifice equation. From this experiment, De Paola *et al.*, (2014), obtained similar N1 values for the buried pipe and non-buried pipe.

From the section above, it can be concluded that laboratory work on leakage has been conducted. However, research that looks specifically at the modified orifice equation has thus far been only done by Van Zyl and Malde, (2017).

2.3 Leakage Detection and Quantification in Water Distribution Systems

2.3.1 Detecting Leakage

Leakage assessments are usually carried out to quantify the total losses in a water distribution system. Through these assessments, it is possible to detect whether the system has leakage or not. The nature of leakage means there are various methods used to assess and find leakage which depends on the component of leakage being sought. The 3 main leakage components are shown in Figure 2-13 below.

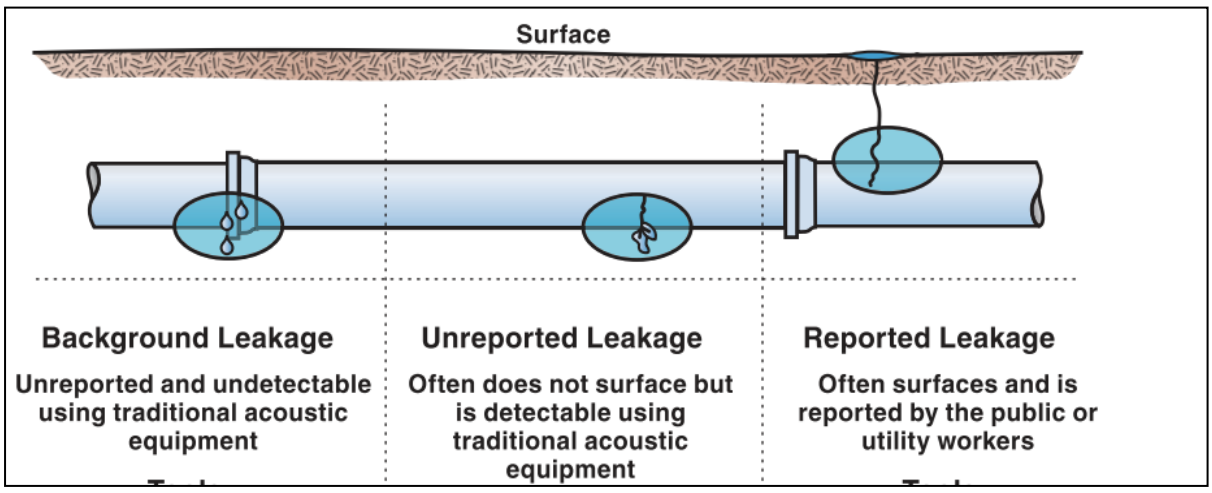

Figure 2-13 - Components of leakage found in water distribution systems (George and Reinhard, 2011)

Literature tends to vary in the definition of detection and awareness (Farley and Trow, 2003; Wu et al., 2011). Puust *et al.*, (2010), in their review of leakage detection methods and models, mention detection of leaks and location in the same phrase, insinuating that detection applies to knowledge of where the leak is. In their definition of leakage awareness, they mention that this term is used to explain the discovery of a leak in a pipe within the water network. However,

this does not give any information about the location of the leak (localisation). Puust *et al.*, (2010a) define leakage localisation as, an activity that identifies and prioritises the area of leakage to make the pinpointing of leakage easier.

The current standard procedure in leakage detection, localisation and repair is described in the following steps by Yang *et al.*, (2011);

- Localising a leak to an area within a DMA through DMA analysis
- Localising the leak to a smaller area of the DMA or to a section of pipe.
- Pinpointing the exact leak position.

The first step indicates how one must initially localise a leak to an area within a district metered area (DMA) through DMA analysis. DMA analysis or zone monitoring involves the installation of flow meters at strategic points throughout a WDS with each flowmeter recording flow into a discrete zone that has a well-defined and permanent boundary (Trow and Farley, 2003). Through monitoring the flow into a DMA, a manager can assess the water losses in the DMA by employing a concept known as the minimum night flow. This concept requires the estimation of leakage when the flow to the DMA is minimum. The standard time at which this occurs is noted to be between 0200 hrs and 0400 hrs. However, some DMAs have different flow profiles, and one should analyse the given DMA before arbitrarily assigning a MNF period. The night flow that is recorded at this period, less the legitimate night consumption is the leakage in the system.

2.3.2 Leak Localisation and Pinpointing Technologies

To date, several methods have been developed that attempt to find the location of the leak in a system. These methods will be briefly discussed below;

Transients or transient waves use wave characteristics such as; frequency and amplitude to pinpoint the position of a leak. The waves are used and analysed in various ways such as the leak reflection method, inverse transient analysis, impulse response analysis (Kim, 2005) and frequency domain analysis (Yang *et al.*, 2011). A pressure wave is generated through various means such as the quick closing of a valve or a quick pump cycle. The pressure wave generation should be done in such a manner that safe network velocities and pressures are maintained (Yang et al., 2011). The generated waves are measured against the reflected wave using methods such as frequency domain response analysis to determine the position of the leak or the defect (Brunone et al., 2000). This method has some limitations to it, as the waves are

affected by the pipe friction and the system architecture (Brunone et al., 2000). Wu *et al.,* (2011), also points out that it is difficult to extract useful information from the transient analysis as various sources of background noise mask it.

Step testing is a leak localising method that progressively isolates sections of a pipe by closing the line valves. A step test is usually conducted at a minimum night flow period to avoid significant disruptions to customers (Pilcher, 2003, 2007). The test should be done in a discrete DMA or a sub-district of a DMA. A step test begins with the operator noting the initial flowrate into the area. The operator then begins the tests by closing pipe furthest from the inlet meter and ends at the pipe section nearest to the meter. The valves are closed for a short period of time, and the flow rate at the inlet meter is noted for each closure action. If the flow rate reduces after a section has been isolated via valve closure, then that reduction represents the leakage plus the night flow in that section. As the test is conducted at minimum night flow periods, a substantial decrease in flow rate or "step" indicates the presence of a leak in the isolated section. Leak pinpointing can then be conducted on the sections identified to have higher than expected flowrates.

Sounding Sticks are an acoustic based method used to locate leakage. Acoustic methods use the sound produced by water as it leaks out a pipe to locate or pinpoint the leakage. The most basic sounding stick is a metal rod placed on a metallic fixture that the user listens to as sound is transmitted up the "stick" (Pilcher, 2003). An experienced operator with good hearing is required to identify the fitting closest to the leak leaks. An electronic stick can also be used which amplifies the sound for the user.

Ground microphones are an acoustic based method that can also be employed for leak pinpointing. A standard ground microphone that has two modes, contact mode or survey mode and employs acoustic technology to locate and pinpoint leaks (Farley, 2008). The contact mode is for sounding on fittings such as valves and hydrants, much like the sounding stick. In survey mode, the hydrophone is placed on the ground along the pipe at set intervals, and the change in sound us noted as the microphone approaches the leak (Farley and Trow, 2003). The loudest leak noise will indicate the location of the leak (Hamilton and Charalambous, 2013). This method requires an experienced and trained user with excellent hearing.

Correlation is an acoustic-based technique used for localising leaks that employs sound logging units to locate the section with leakage. A cluster of data loggers (up to 15) is distributed across the area to be surveyed. The data loggers are attached to the fixtures in the

water system such as valves and hydrants. The loggers can be programmed only to start recording at predetermined times. The usual practice is to allow logging during the minimum night flow period for the area, for 1 - 4 hours. The data is then collected and analysed. The data can be downloaded on-site or through a drive-by, where a truck with a wireless receiver picks up the data as it drives by the logger. Advancement has made it possible to have GSM enabled loggers that send the data to the "cloud" and software is now available that aids with the data analysis. The data for all loggers is analysed in unison, and the comparison of the sound level and sound spread is made. The analysis will reveal if there is a consistent anomaly at the fixture wherein the logger was positioned.

Further logging at the determined locations can be done to zone in on the leaks. Some manufacturers have attempted to develop a database of leak noises to create a "neural network" that learns and will detect leakage easier and faster (Zheng et al., 2011). The loggers can be set on fixed fixtures or moved around the DMA for more active leakage control.

Gas Injection is a less common pinpointing method that is usually used on hard to find leaks and tiny leaks. In this method, a pipe section is initially isolated by shutting the valves. A gas is then injected into a hydrant, and then a tracer device is used to pinpoint the location of the leak (Farley and Trow, 2003). The sensitivity of the tracer/detector allows this method to detect tiny leaks. The most commonly used inert gases are sulphur hexafluoride, industrial hydrogen (95% nitrogen and 5% hydrogen) and helium because of their lightness that allows them to easily flow through tiny cracks (Li et al., 2015). Using an inert gas to trace a leak in more common in non-metallic pipes but is not recommended for large low-pressure mains due to the high volume of gas required (Zheng et al., 2011). Furthermore, this method presently only detects leaks above the pipeline as the gas cannot flow from the bottom of the pipeline to the surface (Li et al., 2015).

Ground Penetrating Radar (GPR) is a leak pinpointing method used to locate leaks that are hard to find. As the name suggests, radar technology which involves transmitting high-frequency electromagnetic waves and receiving the reflected wave back (Li et al., 2015), is used to pinpoint the leaks by observing the disturbed cavities around a pipe (Pilcher, 2007). This is a non-destructive and non-evasive method that produces a cross-sectional profile of the subsurface. The water from the leak increases the dielectric constant of the medium (usually soil) and the image produced by the GPR will show a radar profile with a lower frequency and higher amplitudes which are used to infer the location of the leak and depth of the pipe.

This method is comparatively fast, albeit expensive and convenient with more accuracy (Li et al., 2015). It is, however, inapplicable in cold climates or saturated soils and is prone to interference from abnormalities such as metal objects which can cause a false positive (Puust et al., 2010a).

Automatic Meter Reading (AMR) relies on continuous communication that involves the water supply company with the meter in use/being monitored. Daily or in some cases, continuous monitoring of the water consumption allows for leakage to be detected through pattern recognition. This is done by analysing the water usage and correlating with known or past usage patterns to detect leakage at a DMA level. Also, the AMR technology can be used to detect leakage in a DMA by comparing the sum of the consumption meters and the inlet meter. If the two readings do not collate for the same time interval, then a leak or breach must exist in the DMA. At a single user level, the presence of a leak can be detected by a continuous non-zero meter reading even at times when there is expected to be no flow. A significant increase in consumption can also be indicative of a leak on the property (Hamilton and Charalambous, 2013).

In-Pipe Inspection is an intrusive, leak pinpointing method in which a physical inspection of the pipeline is conducted. Two inline inspection categories exist, namely tethered systems and free-swimming systems (Farley, 2012; Hamilton and Charalambous, 2013). Farley, (2012) describes one tethered inline leak detection method in the form of fibre optics or while Pilcher, (2007) mentions a method that uses a sensor head/probe. In the method described by Pilcher, (2007) a microphone sensor is inserted into a pipe via a tapping point, the sensor travels along the pipe due to the pull of the flowing water on the (parachute) attached to the sensor (Hamilton and Charalambous, 2013). The sounds in the pipe are then recorded. Once a suspected leak has been located, the probe is stopped at the position of the leak. Tethered inline inspection methods work best in relatively straight sections of pipelines. Free swimming inline inspection systems usually consist of a device that is inserted into a pipeline and is driven along the pipeline by the flow of the water. The device has CCTV and may also consist of onboard acoustic sensors, transponders, memory devices and batteries (Hamilton and Charalambous, 2013). The device is retrieved by extracting it from the pipeline or discharging it into an open reservoir. The data is then downloaded, and the leak position determined. This system can navigate bends and though open inline valves. The length of pipeline inspected is mostly limited by the battery life of the device used.

2.3.3 Quantifying Leakage

Quantifying water losses involves finding out how much water is being lost, how it is being lost, and where it is being lost. Real water losses are assessed using three methods:

1. Top-down annual water balance
2. A bottom-up analysis of night flows
3. Component analysis

Leakage quantification through component analysis (formerly known as the BABE analysis) requires assessing the individual components from first principles. Zheng *et al.*, (2011) state that "a component analysis model breaks down the overall volume of water losses into constituent components for each element of the system infrastructure, based on the most influential parameters".

2.3.3.1 Water Audits

To determine the amount of water lost, one needs to assess where it is used in comparison to what is supplied. This entails conducting a water audit. Lambert *et al.*, (2014) define a water audit as "an in-depth record and examination of the distribution system that carries the water, to determine the operational efficiency of the system and identify sources of water loss and revenue loss". A few methods have been formulated, such as the AWWA and IWA water balance, but the frequently used one is the IWA water balance (Farley, 2008; Zheng et al., 2011).

2.3.3.2 The IWA Water Balance

The IWA water balance, shown in Figure 2-14, is a tool used to analyse the various components of water production, storage, and distribution. Before the volume of losses can be established, there are various components that need to be quantified.

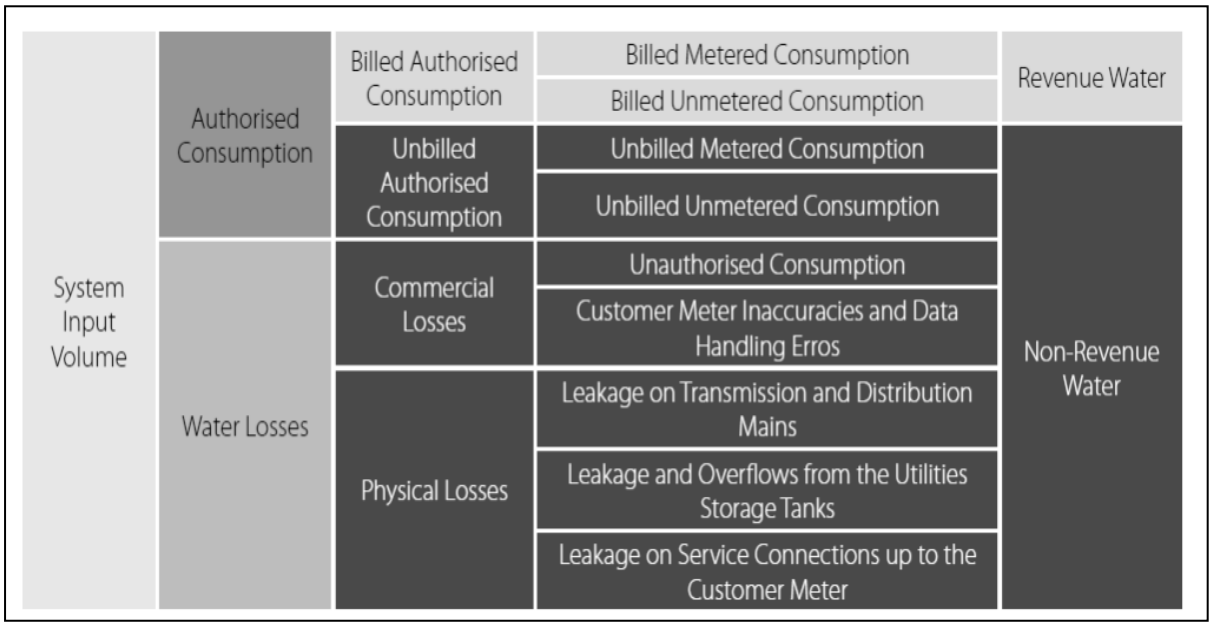

Figure 2-14 - The standard IWA water balance (Farley et al., 2008)

The water balance allows the utility to gain an understanding of the magnitude of the water loss components in the system (Hamilton and Charalambous, 2013). These components are discussed below:

System Input Volume (SIV) – If the entire system input is metered the computation of the SIV is a simple summation of all the meters. However, it is not always that simple as that due to faulty/missing meters or non-discrete boundaries. The SIV volume should also include imported water into the system, and a record of exported water should be kept. Metering inaccuracies can be verified using portable meters. The same meters can be used to help estimate consumption in areas without meters. This entails logging/measuring the supplied for a set period and extrapolating to get the flow rate for the required period, other methods such as the use of pump curves and pumping hours can also be employed to obtain the SIV (Zheng et al., 2011).

Authorised Consumption – consists of Billed Metered Consumption (BMC) and Billed Unmetered Consumption (BUC). The former is obtained from the utility's billing records and depends on the availability of accurate metering systems while the latter is based on estimates. Each of the two components has its uncertainties, which must be considered in the analysis.

Unbilled Metered Consumption – the volume of this component is determined the same way BMC is obtained, albeit this water used is not charged by the utility.

Unbilled Unmetered Consumption – Traditionally, this is the water used by the municipality for operational purposes, and due to the lack of metering, it is often overestimated. In some instances, this overestimation might be an attempt to "reduce" water losses (Wu *et al.*, 2011).

Water losses – Water losses in the system can be determined by subtracting the authorised consumption from the SIV. This water loss component consists of the commercial losses and the real losses

Commercial losses are also referred to as apparent losses are consist of unauthorised consumption and metering inaccuracies.

Physical or real losses are the volume of water lost through leaks, bursts, reservoir overflows and losses on connections (Farley *et al.*, 2008).

It is this figure of real losses that are used to assess the water loss in a system or DMA. From this numerical value, more measures such as leak localisation and pinpointing can be implemented.

2.3.4 Summary of Leak Detection and Quantification Techniques

Table 2-1 contains a summary of the different techniques that were discussed above, with their pros and cons and reveals that none of the reviewed methods presently available can simultaneously detect, locate and characterised leakage in water distribution systems.

Table 2-1 - Summary of leak detection and location methods

Detection Technology/Method	Advantages	Disadvantages	Leak Flow Rate	Leakage Localisation	Leakage Pinpointing	Leakage Characterisation
Automatic Meter Reading (AMR)	Accurate can detect leakage fast with better response times.	Unable to pinpoint the leak in a pipe.	Yes	Yes	No	No
Correlating Noise Loggers	Programmable and relatively accurate	Expensive and requires expertise	No	Yes	Yes	No
Gas Injection	Very accurate and fast	Expensive, not recommended for large pipes	No	No	Yes	No
GPR	Accurate and fast. Effective for small leaks	Inapplicable in saturated soils and is prone to interference from objects underground.	No	Yes	Yes**	No
Hydrophones/Acoustic loggers	Reasonably accurate and easy to use	Requires an experienced and trained user with excellent hearing	No	Yes*	Yes	No

In-Pipe Inspection	Tends to be expensive but accurate.	it requires the user to have expert knowledge	No	No	Yes	No
Transients or transient waves	Can pinpoint the position of the leak.	Requires a straight section of pipe without interference. Can create new leaks & damage pipes	No	No	Yes	No
Water Balance	Easily updated and simple to use	Requires accurate data which is often unavailable	Yes	Yes	No	No

* - *While it is possible to localise leakage using this method, it is a strenuous activity which tends to be difficult and expensive*

** - *This method is rarely used for pinpointing as it requires expertise and a good knowledge of the sub-terrain infrastructure*

3 RESEARCH METHODOLOGY

To successfully assess and evaluate the reliability of the PCAD and establish its efficacy in conducting condition assessments in water distribution systems required a method to be developed that encompassed all activities to be done to fulfil the aims of this study.

A literature review was conducted so as to understand how leakage behaves in water distribution systems and the various factors that influence it. Within that review, an investigation of the technologies that exist which aid in leakage detection and system condition assessments was done. From the literature review, methods and results of processes that identify and characterise leakage were found.

A preferred method was selected and replicated. The results of these replication tasks were compared with the original/published results. An evaluation of the results guided whether any calibration of the methods/ model was required. When the results could be replicated as far as possible, the PCAD instrumentation was calibrated against standard industry calibrated instrumentation.

The PCAD was then used to characterise leakage on pipes using the model that had been chosen for replication. The results of these tests were compared to the replicated tests results. If there were any significant discrepancies, the device was recalibrated, or the reasons for differences were investigated and explained.

An analysis of previously conducted tests on a real water distribution network was done to establish the performance of the PCAD in characterising leakage real water networks. Figure 3-1 outlines the general research path followed to fulfil the aims of this study and summarises the steps explained above.

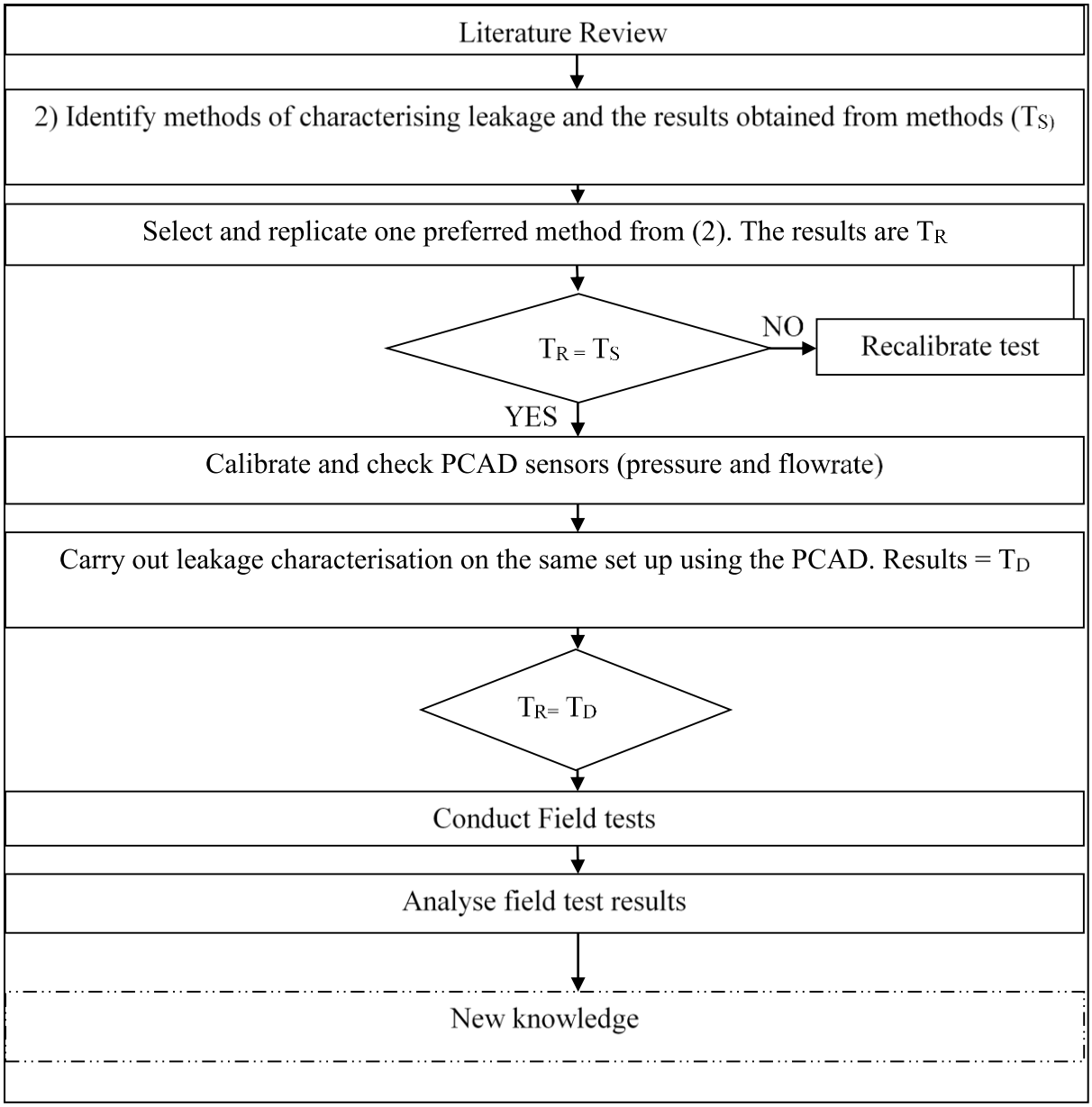

Figure 3-1 - Research Method Flowchart

3.1 Research Methodology

Initially, the FAVAD leakage characteristics of three known leak types on uPVC pipes were found. The leakage characteristics were determined in four distinct ways. Firstly, six sections of uPVC pipes with three known orifices each, namely, 6 and 10 mm round holes, 50 and 100 mm longitudinal cracks and 50 and 100 mm circumferential cracks were tested on a standardised laboratory setup at standard pressure ranges of 30 – 90 m. Initially developed by Malde, (2015), this standardised method was improved on, and these improvements are further explained in section 4.3.1. Three pipe sections with three leak types namely, a 6 mm round hole, a 50 mm longitudinal crack and a 50 mm circumferential crack were then on the same setup using the same method but at a lower pressure range of 6.5 – 30 m. After the leakage

parameters were obtained from the standardised method, the same pipe samples were tested using the Pipe Condition Assessment Device (PCAD). The results obtained from the tests with the laboratory equipment and the PCAD were analysed and statistically compared. The test helped establish the reliability of the device by assessing the repeatability of the results of the tests performed using the device.

Analysis of tests previously conducted in the field was performed to establish the performance of the PCAD in characterising leakage real water networks. To conclude the study, an overall discussion of the tests and results was done.

3.2 Application of the Statistical Inference and Description Theories

Statistical inference is the process of drawing conclusions based on evidence and reasoning. In the experimental work from this study, deductions were made from experimental data supported by statistical analysis.

For this study, descriptive statistics and statistical inference theories were used to analyse the data obtained. More specifically, the relationship between the effective area and pressure head was modelled from the obtained data and evaluated. The data points obtained in the study were used to establish the model parameters at 95% simultaneous confidence intervals. In this section, the statistical theory used in this study will be explained from first principles.

The model that describes the linear relationship of the orifice area and pressure of an orifice with water flowing through it at a set pressure is described as:

$$C_d A_i = C_d A_0 + C_d m_i h_i + \varepsilon_i \qquad (19)$$

This equation then fits the model:

$$y_i = \beta_0 + \beta_i z_i + \varepsilon_i$$

Where y_i is the response, i.e. effective area, and z_i is the predictor parameter representative of pressure head inequation 19. The two parameters hold true for i observations where (i = 1,2, 3..., n). The noise in the model is captured by ε_i. the intercept (initial effective area) and slope (effective head-area) are β_0 and β_i respectively.

Thus, from the available data, β and the error variance σ^2 can be found. Using the method of least squares, a function b, through which is the trial values of β is selected so as to minimise the sum of the squares of the differences and therefore increase the likelihood function.

$$S\,(b) = \sum_{i=1}^{n}\left(y_i - b_0 - b_i z_{i1} - \cdots - b_r z_{jn}\right)^2$$

$$= (y - Zb)'(y - Zb)$$

The coefficients b chosen by the least-squares' criterion are called least squares estimates of the regression parameters β otherwise written as $\hat{\beta}$.

The estimator for the model $\hat{\beta}$ which then maximises the likelihood function is given by:

$$\hat{\beta} = (Z'Z)^{-1}Z'Y$$

Where Z' is the transposed matrix of Z, and Z is given by the matrix function:

$$Z = \begin{bmatrix} 1 & Z_1 \\ 1 & Z_2 \\ 1 & Z_3 \\ : & : \\ 1 & Z_n \end{bmatrix}$$

With Z_1, Z_2, Z_3, …, Z_n being the observed pressure values. $(Z'Z)^{-1}$ is the inverse product matrix of Z' and the Z matrix. Y is the matrix that contains *y* values such that $y_1, y_2, y_3, \ldots, y_n$ are observed C_dA values, this matrix is shown below.

$$Y = \begin{bmatrix} y_1 \\ y_2 \\ y_3 \\ : \\ y_n \end{bmatrix}$$

The coefficients $\hat{\beta}$ are consistent with the data in the sense that they produce estimated (fitted) responses, $\hat{\beta} + \hat{\beta} z_{i1} + \ldots + \hat{\beta} z_{in}$, whose squares of differences from the observed y_1 values are as small as possible. The deviations; $y_1 = \hat{\beta} + \hat{\beta} z_{i1} + \ldots + \hat{\beta} z_{in}$ (i= 1,2, 3…, n) are called residuals. The unknown parameter σ^2 is contained in the vector which describes the error term (residuals) ε, and given by the expression

$$\hat{\varepsilon} = Y - z\hat{\beta}$$

More comprehensive derivations can be found in standard statistics text such as Casella and Berger, (2002); Johnson and Wichern, (2007). The calculation of the above-mentioned parameters can be done with the aid of analytical software such as MATLAB and Microsoft Excel. For this study, Microsoft Excel data analysis tool pack was used to obtain the descriptive

statistics and to carry out the regression analysis that would allow a model which fits the data to be produced.

The descriptive statistics were obtained by the descriptive statistics function in the data analysis tool of the Excel software, the data produced enabled the average values for N1 and C_d with their individual confidence intervals to be obtained for the tests conducted. The same could be done for the effective area, and effective head but a more detailed procedure described below was used due to the nature of the required information. Using the LINEST function of the software, the individual confidence intervals for each calculated parameter, i.e. the effective area and effective slope were obtained. However, as both parameters are often unknown as elaborated by Van Zyl and Malde, (2017) the simultaneous confidence interval (SCI) was more appropriate. These simultaneous confidence intervals are obtained from a regression analysis.

The regression analysis function which produced the SCI for the effective area and effective area-head slope which describes the rate at which a leak area expands with pressure, is an add-on feature in the Excel software. The data was arranged in labelled columns with the observed pressure values and their corresponding calculated effective area for each pressure head step. All the data points for the 10 tests were used (where a data point holds the average pressure and flow rate for each stabilised step). The data in each column was inputted on the analysis pack and the 95% SCI requested. The output data was then used to describe the model fully and to obtain the 95% SCI and p-values (probability values).

3.3 The Pipe Condition Assessment Device

3.3.1 Development

The pipe condition assessment device (PCAD) was developed at the University of Cape Town (UCT) in collaboration with the University of Stellenbosch, Wader Technologies, and other partners. The concept was as an outcome of over 15 years of research led by Professor J.E van Zyl. The first prototype of the system was first developed in collaboration with the University of Stellenbosch by Erwee (2016) who developed and tested the electronic components of the device.

The aim was to develop a system that could utilise pressure-flow relationship and the modified orifice equation (equation 11) to detect, quantify, locate and characterise leakage. Further work on this prototype led to the development of the PCAD by (Lopez and Zyl, 2019). This device, in its current form, is a novel, mobile, self-contained, condition assessment device.

The PCAD is remotely linked to a cloud-based pipe condition assessment system that is used to provide risk analysis models with network state indicators. This is done by evaluating the behaviour of leakage flow rate under the influence of pressure (Lopez and van Zyl, 2019). The metadata and data from these characterisation tests are uploaded to a database, and the data is used to provide the risk assessment models. The risk assessment models are utilised in decision-making processes and assist in establishing which pipes and fixtures to replace first. The PCAD thus also assists in the optimisation of water network maintenance (Lopez and van Zyl, 2019).

3.3.2 Principles

The principle behind the device's function and operation are borrowed from many fields and combined to enable this device to function. As shown in the literature review section of this study, pressure tests have been regularly conducted in water systems. In these tests, a step test was employed to produce a range of pressure and flow values in a system; this was often achieved by manipulating the pressure control device at the inlet point.

It has also been explained how research work is done in the sector by various authors such as May, (1994); Greyvenstein and Van Zyl, (2007); Cassa et al., (2010), had shown that if the flow rate and the pressure values for a test are known, these parameters can be used to characterise leakage in a pipe/system. In the development of the PCAD, the modified orifice equation was used to characterise leakage because of its ability to estimate the physical leakage characteristics through a pressure test (Lopez and van Zyl, 2019).

Combining these two principles allowed researchers to create a mobile device that can carry out pressure step tests, collect the data, store it, and allow for the data to be analysed to characterise leakage in a pipe and assess the overall condition of a system through a series of tests and data analysis.

3.3.3 Operation

Lopez and van Zyl, (2019) remark that the device has six states, namely; idle, waiting for input, filling, isolation, leak test and dumping. Each of these states performs a unique operation that allows the system parameters to be analysed and for leakage to be detected and characterised. The device operations are controlled by the user via the electronic control panel, which is shown in Figure 3-2 as item C.

The test procedure to conduct a pipe condition assessment is as follows:

a) From GIS data and as-built drawings, a test pipe that can be isolated and has a hydrant, or a convenient point of connection, between the isolation valves is identified.

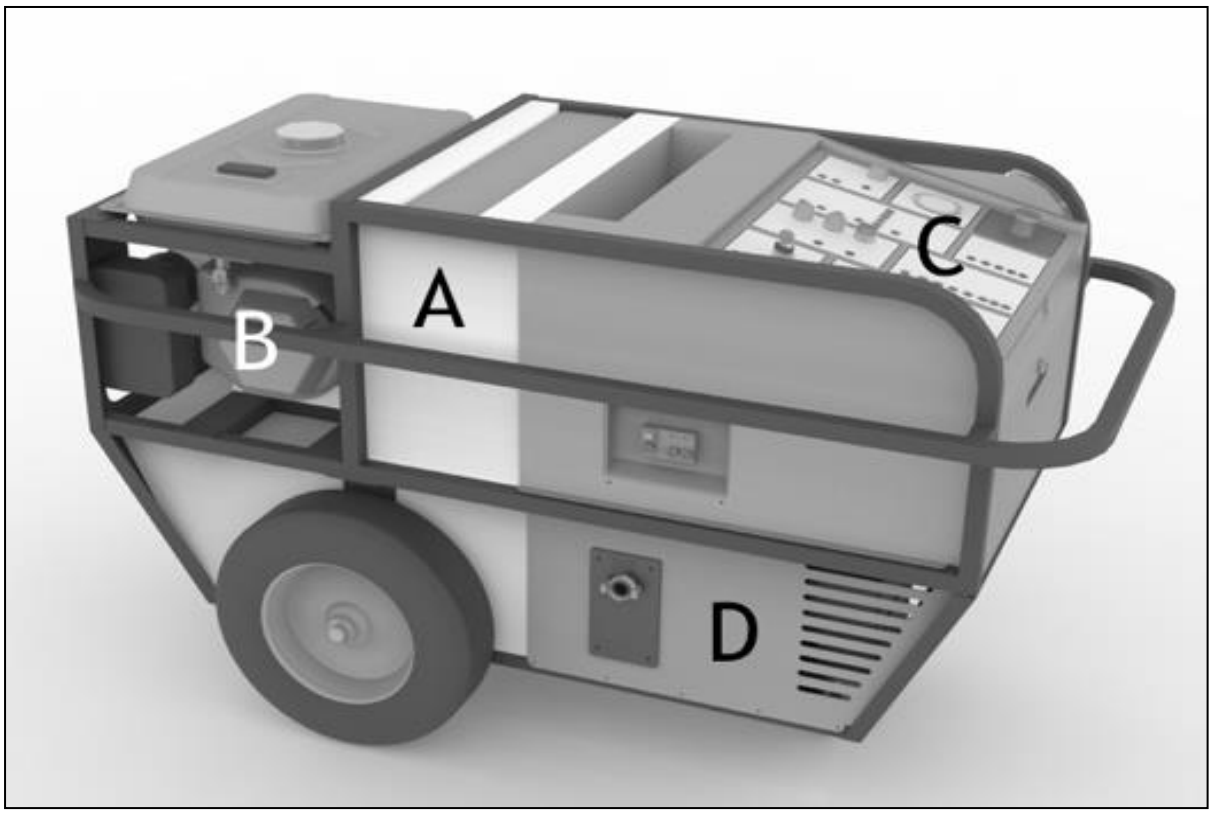

Figure 3-2 - PCAD components (Lopez and van Zyl, 2019)

b) The device is connected to the hydrant, or convenient point of connection using a quick release coupler. The hydrant is briefly flushed, i.e., water is allowed to run from the pipe section identified to clear sediments and stagnant water in the hydrant pipe. This process is called flushing. For the flushing process, water can flow through the device via the inlet connection and is expelled from the outlet point of the device.

   Figure 3-3 shows a schematic of the flushing operation with the device components represented by symbols. Valves are abbreviated as V1, V2 e.tc, the two flowmeters are labelled F1 and F2, and the tank level sensors are labelled L1 and L2 for the empty and full sensors respectively. The flushing procedure shown in Figure 3-3, shows how water flows past the flow meter (F2) and through the open outlet valve (V3) to allow water to flow out through the outlet point. Valves V1 and V2 remain closed to prevent the potentially dirty water from flowing into the devices' tank.

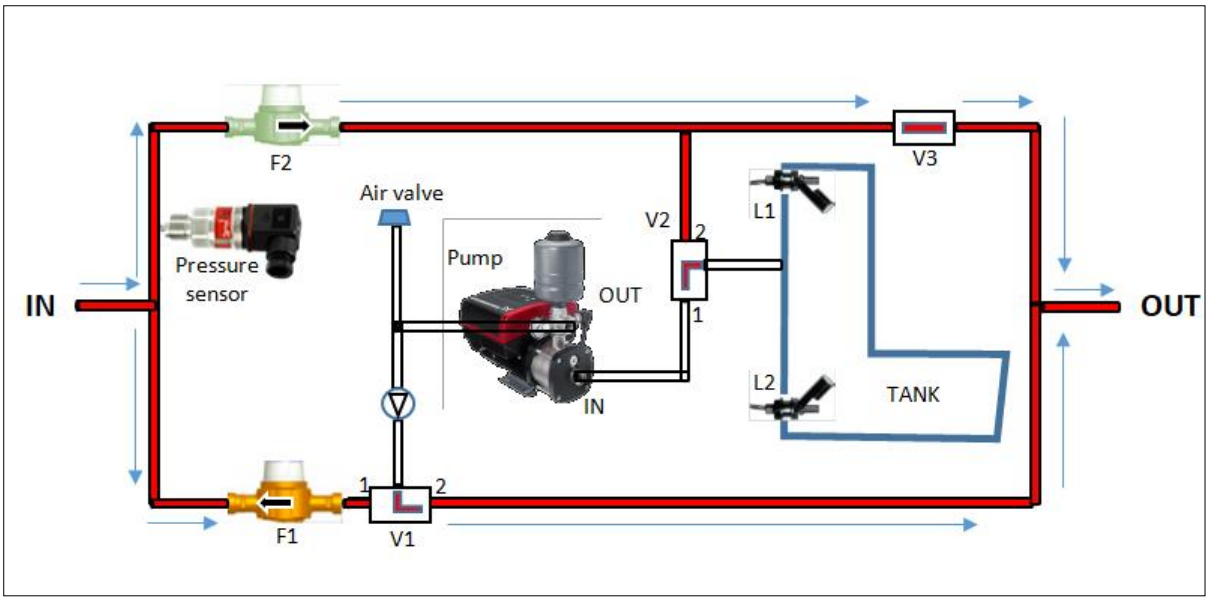

Figure 3-3 - Device operation (hydrant flushing) (Weiss, n.d)

c) The next step entails filling the water tank until it has reached the maximum water level. In the filling procedure, water flows past the pressure transducer, which measures the system pressure, through the flowmeter F2 and valve V2 into the tank. The tank inlet valve (V2) will automatically close due to the presence and action of the L1 sensor. This procedure is shown in Figure 3-4

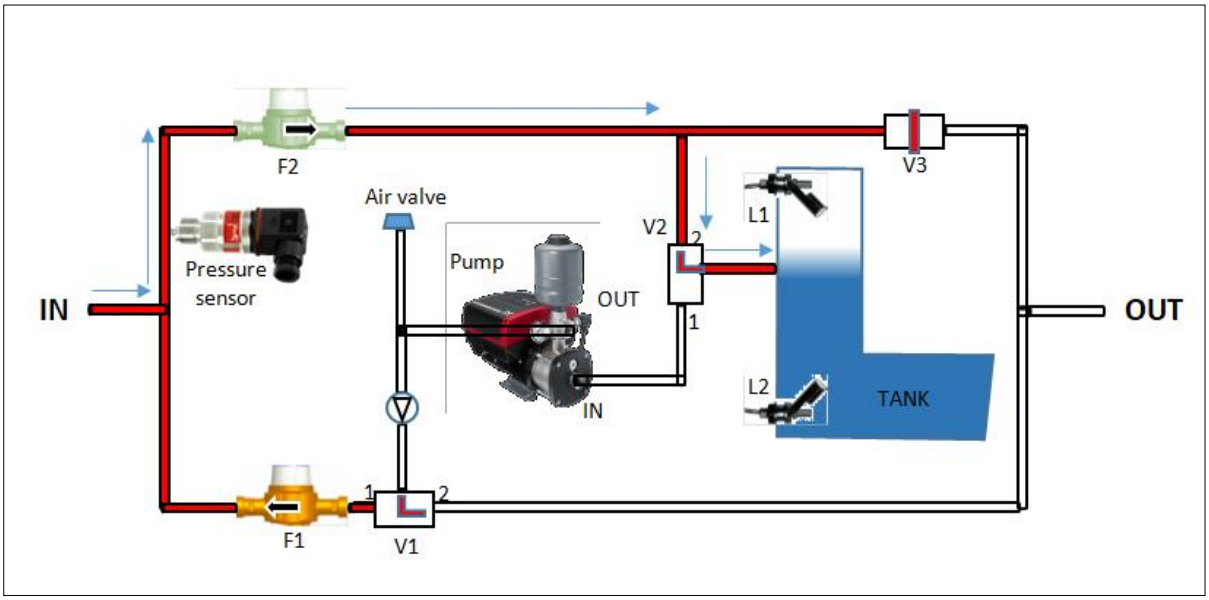

Figure 3-4 - Device operation (tank filling) (Weiss, n.d)

d) Next, shut the upstream and downstream isolation valves on the pipeline and all user connections, to isolate the test pipe.

To verify if the pipe section has been isolated, an isolation test procedure is done. As shown in Figure 3-5, for the isolation test, the device valve V3 is opened while the other valves (V1 and V2) remained closed. If the line is not isolated and one of the system's valves is leaking, the water flows from the pipeline and through the flowmeter, and a flowrate is observed. The duration of the test can be altered by the user to verify that the flow is not just the pipe emptying and due to a leaking/malfunctioning valve. If the device system controller detects no flow, it will automatically stop the isolation test and close the outlet valve (V3). However, if a stable flow is detected, one will have established that one or both valves on the pipeline are not fully functional.

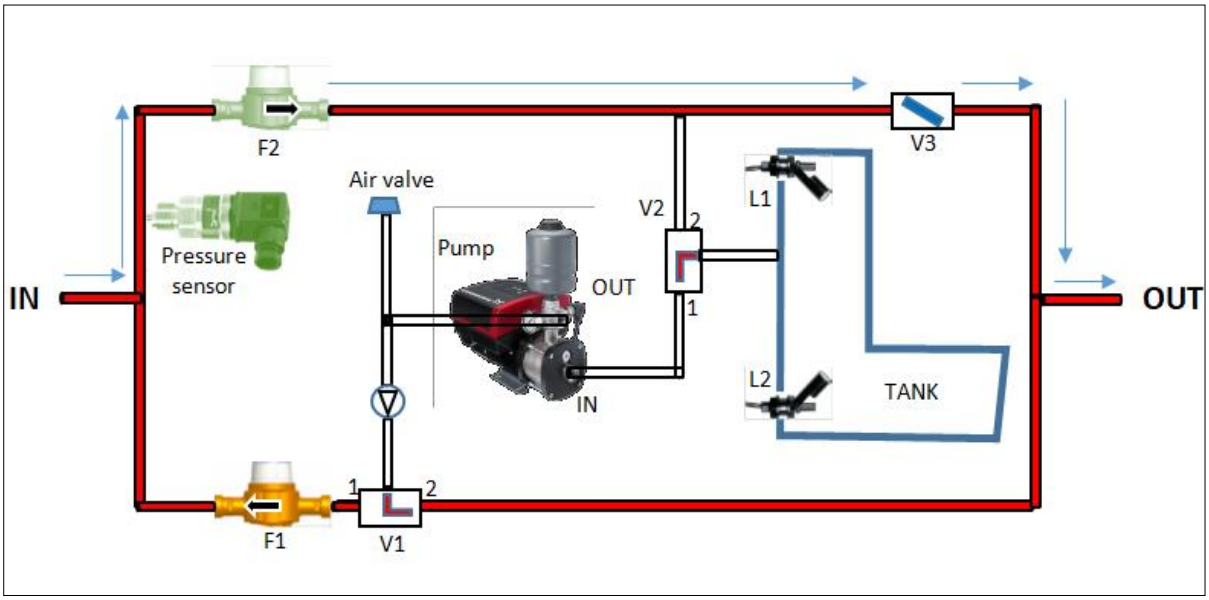

Figure 3-5 - Device operation (isolation test) (Weiss, n.d)

e) Once the pipe has been successfully isolated, the next step is the leak test function. The pipe tests entail pressurising the pipe by pumping the water in the device's tank back into the pipe. For the test, the valve from the tank (V2) and the valve to the device inlet (V1) are open. The valve to the outlet end (V3) remains closed for the duration of the tests. This permits water to be pumped from the tank and to flow through the flow meter (F1) shown in Figure 3-6, and the pressure transducer that records the pressure.

If a leak exists on an isolated pipe, the water will only escape through the leak. The detected flowrate informs the device operator that there is a leak on the pipe. The pressure is varied through altering the different pump speeds on the variable speed pump.

The different pump speeds are called pressure steps, and the pressure steps up of down with and increases or decreases, respectively, in the pump speed. User-defined pressure steps are carried out. The device is programmed to hold a steady pressure for each step until the pressure for that pressure step stabilises. Measurements of the flow rates at each pressure step are recorded by the device. The data is uploaded to an online database for real-time analysis.

-

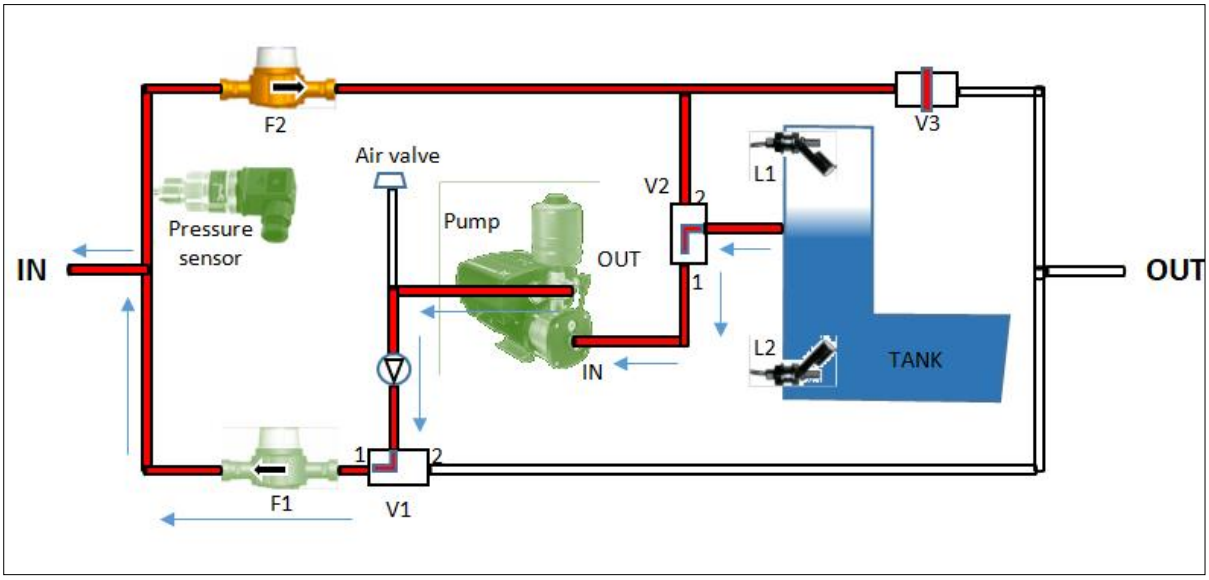

Figure 3-6 - Device operation (pressuring the pipe) (Weiss, n.d)

f) If no flow rate is recorded, then it means that there is no detectable leak on the pipe and the test is stopped. It is possible to find a leak whose flow rate is less than the device's meter's minimum flow rate (25 L/h or 0.42 L/min), this type of leak is identified by the device recording a pressure drop if the pipe is pressurised and the pump switched off afterwards. However, if a flow is recorded as water is pumped into the pipe at each pressure step, then there is a detectable leak in the test pipe.

g) Once the leak test is complete, the machine is disconnected from the connection point. The isolation valves and any user connections that may have been closed are opened so that the distribution network can operate as before.

Operators can move on to the next pipe that will be tested, and the same operating procedure described above is followed. At the end of the testing period, if there is still water in the tank, it can be emptied by using the dumping function. The dumping function involved opening the tank valve (V2) and the outlet valve (V1) and then

pumping the water from the tank and expelling it via the outlet connection as shown in Figure 3-7.

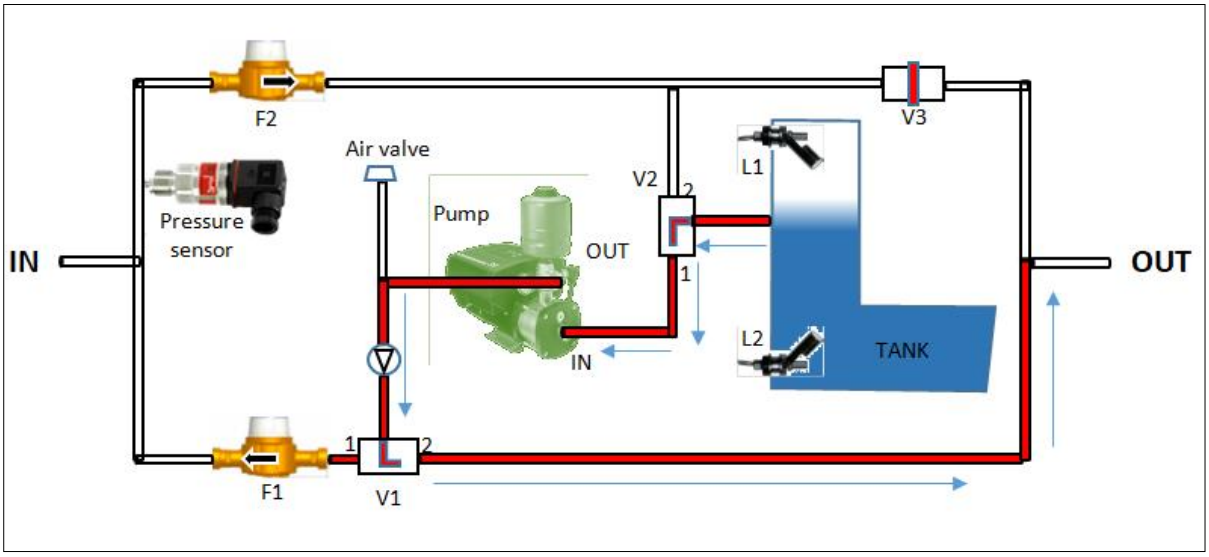

Figure 3-7 - Device operation (emptying the tank) (Weiss, n.d)

However, before the device can be used in a water network, it needs to be calibrated and its efficacy and reliability established. One experimental setup will be used to achieve the aforementioned aims. A minimum of 90 tests on pipes with manufactured leaks will be conducted on these setups using standard laboratory equipment and then using the PCAD. A statistical analysis of the results obtained from these tests will help determine if the device is reliable and can effectively carry out pipe condition assessments.

3.4 Experimental Setups

The study was conducted at the University of Cape Town's hydraulics laboratory. The lab environment consists of a water reticulating system that conveys water from a sump through a system of brass pipes and to two outlets that are metered. The submersible pump is controlled by an inverter unit that has a speed drive which varies the speed of the pump and by extension, the flow through the system. There are also several valves that are used to control the flow of water. Used water is conveyed through channels on the floor back to an underground tank, and thus the water is recycled. This was important considering the geographical location of the university and the water crisis the city was facing. A more in-depth description of the flow meters used in the study is found in chapter 4.

3.4.1 Standardised Leakage Characterisation Setup

Malde, (2015) developed a standardised method for determining the FAVAD leakage characteristics in pipe sections of various pipe materials. This part of the study sought to replicate and utilise the method developed and assemble the setup used in the experimental procedure as described in section 2.2.5.3.

However, due to the need to use the setup for testing with the PCAD, it meant that the original setup had to be modified. Two plastic stands with a glued on 110 mm PVC section and Viking Johnson couples were used to secure pipe samples. The PVC ends were drilled with 12mm holes and clamps used to connect the various fixtures needed. The standard external pipe diameter that can be used on the setup is 110 mm.

The new setup then consisted of two connection points shown in Figure 3-8, which were attached to a clamp. The connection points had quick-release brass couplings which allowed the setup to be pressurised by either the PCAD or laboratory setup. The quick-release couplings aided in the swift change of connection pipes. Ball valves were also included in the setup, as shown below.

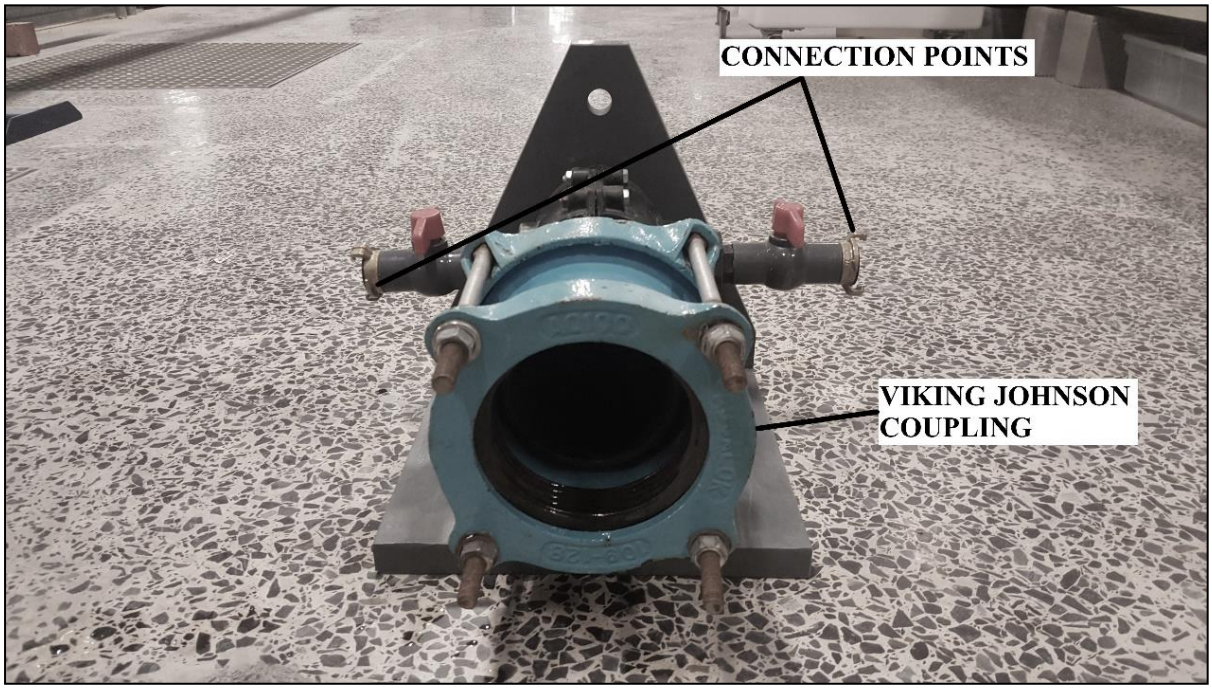

Figure 3-8 - One end of the setup showing the connection points and Viking Johnson Coupling

Similar Viking Johnson couples were used to secure the pipe samples. The Viking Johnson couplings were tightly secured to ensure that water did not leak through the couple, even at

high pressures. Provision for a pressure transducer was also made. To that end, a quick-release clamp installed that could be used to connect the PrimeLogger data logger.

A downstream air valve was used to expel any trapped air the pipe sample. This meant the setup did not need to be lifted to expel trapped air. Furthermore, the pressure logger had stainless steel quick-release coupling connections that allowed the user to expel any air that might distort the pressure reading. This was done by swiftly pushing in the transducer quick release clamp and releasing it, thus expelling water through the connection point. The pipe sample was then secured with 20 mm stainless steel rods whose purpose was to take up the longitudinal stresses exerted by water pressure and thus ensure that no longitudinal stresses were induced in the sample pipe. The assembled modified setup is shown below.

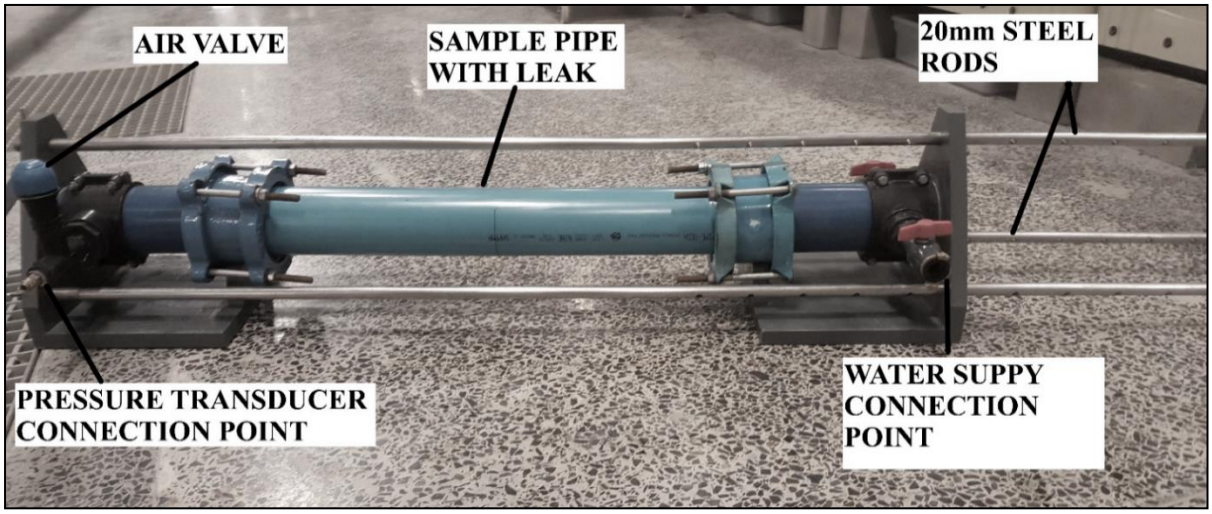

Figure 3-9 - Modified Standardised Leakage Characterisation Setup

The pipe was changed by removing the steel roads and releasing the pipe sample from the Viking Johnson coupling.

4 LEAKAGE CHARACTERISATION WITH STANDARDISED METHOD

4.1 Methodology

This chapter describes the experimental work involved in conducting the tests on the pipe samples using laboratory instrumentation. The experiments were conducted at "standard/typical" pressure range of 30 – 90 meters. Results of the experiments conducted are then presented and discussed.

Malde, (2015) developed a standardised setup that could be used to characterise leakage in pipe sections. In this study, the laboratory setup of the test explained in Chapter 5.2.5.3 was initially assembled. Pipe samples were tested on the setup using laboratory equipment before the same samples were tested using the PCAD. This was done to standardise and calibrate while establishing the repeatability of the tests conducted using the pipe condition assessment device.

However, before the leakage characterisation tests could be conducted with the laboratory setup, the flow and pressure instrumentation had to be calibrated. That process is explained below.

4.1.1 Understanding the Magnetic Flow Meter and Data Loggers

As elaborated by Malde (2015), the UCT hydraulics laboratory has a set of Flowmetrix SAFMAG electromagnetic flowmeters. The meters are connected to a network of copper pipes, lined against a wall (this network will be referred to as the wall unit henceforth). A submersible pump reticulates water which flows through either the DN 15 meter or the DN 25 meter. The choice thereof is dependent on the maximum flow rate required, with the former having a maximum flow rate of 1.77 L/s and the latter, 5 L/s. The two flow meters have a repeatability of 0.1% of the rate.

Additionally, the meters have a display and frequency output accuracy of +/- 0.5% of the flow rate at velocities higher than 0.5 m/s and +/- 0.025% for velocities less than 0.5 m/s. The analogue output has an additional error of +/- 0.008 mA. In the pulse function, the pulse width can be adjusted from 10 ms to 500 ms for each emitted pulse. A light-emitting diode also shows the pulses by flashing each time a pulse is emitted. The meters had already been calibrated, and the calibration certificate is attached in Appendix A.

The flow meters do not possess the ability to store/log the outputs, i.e. the flow rates. However, they do allow external logging, i.e. the collection of outputs via two output channels. The meter data can be collected via an analogue output of either 0-20 mA or 4-20 mA or a pulse output

whose pulse values can be toggled as required. The Sensus Cosmos 1U data logger was used to collect the flow data. This type of logger can record both analogue and pulse datasets. The use of this logger requires the use of the Sensus software to programme the logger functions.

In its analogue function, the upper and lower values of the measured parameter are programmed onto the logger, for instance, for the DN25 meter the lower and upper values would be 0 L/s and 5 L/s respectively. The analogue units, i.e. the parameter units are also programmed, as is the desired logging interval.

Programming for the pulse function is different in that the user can input the initial counter reading. This is used to compare the value the logger collects with the value the meter reads. The units of flow are also adjustable, and the pulse value is also adjustable as needed. A pre-divider also exist which instructs the logger on how to save pulses. Thus, giving the user a choice to either save every pulse emitted or to save after a set number of pulses have elapsed. The latter helps to save internal logger memory.

The collected data on both functions are retrieved via the software and can be exported as text, pdf, or excel files. The resolution of the recorded data can also be toggled such that the user can extract all the data or just the data at set intervals.

For this study, the analogue channel was initially chosen to be used for collecting the flow rate data. The logger was thus programmed as explained above and connected to the electromagnetic flow meter. This was what Malde (2015) had done in his study. Malde had already pointed out that when comparing the flow rate on the electromagnetic meter display and the logger, it was observed that there were discrepancies. A few reasons for this were suggested, such as the length of the cable used to collect the data. In this study, the same challenge was initially faced, however, unlike Malde, (2015) who could at least observe constant figures to then compare with, in this study the logger display did not initially stabilise to a point at which data could be noted down. Consequently, the use of the pulse function was explored.

The base units on the electromagnetic flowmeter had to be programmed to litres to make use of the pulse function. This was due to the way the meter assigned pulse values, which is, it had to be programmed for pulses/unit, and one could only toggle between 0.01, 0.1 and 1.00 pulses per unit. This meant that assigning the base unit to cubic meters (m^3) resulted in the meter emitting one pulse after every 1000 L at best, which was not appropriate for this study. The flow units were set to L/s and the pulse width, after some trials, was set to 50 milliseconds.

This pulse width was believed to be long enough to allow the saving of a pulse but not too long as to allow an overlap of pulses. These settings were then saved.

The calibration was then done by connecting the logger to the electromagnetic flow meter and starting the pump. The valve was slowly opened to avoid transient, and the flow rate on the electromagnetic meter and logger displays were noted down and recorded for different flow rates, a minimum of 10 readings ranging from the minimum flow rate to the maximum flow rate was taken. After the calibration exercise, the data was downloaded from the logger. The resolution used was one that displayed every event observed, i.e. all the data was downloaded. This data was initially saved as a text file which was then converted to an excel sheet to preserve all the data including the time in milliseconds, saving the data directly as an Excel sheet resulted in a time that did not display milliseconds.

The first check was comparing the total volume that the electromagnetic meter had recorded versus the total volume (both in litres) the logger had recorded for the test period. If the volumes matched, the number of pulses recorded by the meter was then compared with the number of pulses the logger recorded (observed as data points on the Excel sheet). If all pulses were collected and none were missing, then the sum of all the pulses should equal the volume observed above as each pulse represented 1 litre. After this check, the flow rates at the time stamps recorded above were compared with the flow rates observed on the electromagnetic flow meter and plotted on a graph.

The volume check was done, and it was observed that, while the volumes recorded by the logger matched the electromagnetic flow rates, the logger was missing pulses. Initially, it was attributed as a logger problem due to the perceived long pulse width of 50 ms. It was suspected that because of the pulse width, some pulses were overlapping and hence the missing pulses. However, even after using the smallest pulse width of 10 ms, there were still some missing pulses. It could be that even a 10 ms pulse width is a long duration at higher flows.

Furthermore, at flow rates above 0.9 L/s the logger, and electromagnetic flow meter display stopped matching with the logger displaying constant values of 1.56 L/s and then oscillating between 1.56 L/s and 3.12 L/s as the flow rate increased.

The electromagnetic flowmeter casing was opened to observe the pulses shown by a flashing LED to verify if this problem was indeed a logger problem, and this was recorded with a camera. From this exercise, it was noted that even at stable flows, the pulses emitted did not display the constant pattern expected, and therefore the problem was because of the

electromagnetic meter's pulse system. As the readings from the pulse unit could not be used with much confidence, it was decided to revert to the analogue channel. That exercise is documented below.

4.1.2 Analogue Flow Channel Verification

As explained earlier on, the electromagnetic flowmeter has an analogue output that uses the 4-20 mA loop to transmit the flow rate signal. This function uses the linear relationship between the parameter to be logged and the 4-20 mA loop. On this function, 4 mA would represent the lower value of the parameter, in this case, 0 L/s and the 20 mA would represent the max flow rate (5 L/s for the DN25 meter)

Initially, the logger was programmed on the analogue channel, but the readings did not stabilise to allow values to be compared. The signal outputs of the entire system were, therefore investigated. For this, a digital ammeter was used. The digital ammeter was set to measure current. Due to the small magnitude of the current involved, a check was done to verify if the resistance that gave off the 20-mA output from the electromagnetic flowmeter did give the 20-mA. It was observed that the resistance value set on the electromagnetic meter's control unit was less than the required value, and as a result, a current of 20.1 mA was found across the meter at maximum flow. This error was addressed by inputting the correct resistance on the electromagnetic flow meter.

Next, a check to verify if the electromagnetic flowmeter gave of 4 mA when there was zero flow through the meter and 20-mA at 5 L/s (maximum flow). The 20-mA output was verified by a function on the meter that allows the user to check the current at various simulated flow rates, as percentages, thus 100% would represent the maximum flow rate of 5 L/s. These checks meant that the flow meter was now correctly programmed, and its signal output was now correctly calibrated.

The programmed logger was then connected to the flow meter and at no flow, i.e. 0 L/s the logger displayed a negative flow rate. This informed that the current delivered to the logger from the flow meter was less than 4 mA. It was believed that this disparity was because of an increase in resistance along the point of connection to the logger. A continuity test on the logger-meter connection cable was done, using a digital ammeter and revealed that the cables were intact. It was believed that the error could be as a result of the cables being poorly connected to the electromagnetic meter, thus affecting the resistance and current recorded. The connections were thus checked and reconnected. The logger then displayed the expected flow

rate of 0 L/s. However, when the pump was switched on albeit with the valve was still shut, the logger displayed a flow rate of 0.03 L/s, this was believed to be because of a slight change in the current from the meter due to electrical interference. The interference was addressed by splitting the power points of the meter and variable speed drive and installing a noise filter. This reduced the interference to allow the 4-mA value to be recorded as 0.01 L/s. The logger was then programmed to measure every 0.01 L/s change in flow rate and to record the flow data every second.

4.1.2.1 Instrument Verification Results

A comparison of the flow rates on the electromagnetic flow meter and the logger display was made, and the results are shown in Table 4-1.

Table 4-1 - Displayed values from the electromagnetic flow meter and Sensus data logger

Electromagnetic Flow Meter (L/s)	Sensus Data Logger (L/s)
0.0000	0.01
0.1765	0.19
0.2920	0.31
0.3771	0.39
0.4969	0.51
0.9721	0.98
1.2771	1.28
1.8591	1.86
2.1250	2.13
2.2056	2.21
2.3124	2.31
2.4323	2.44

The data points obtained were plotted to establish the relationship between the electromagnetic flowmeter readings and the data logger. A regression analysis revealed an R^2 value of 1, which shows that there is a strong positive relationship between the observed and expected data. The gradient of 1.005 shown in Figure 4-1, also communicates that the logger and the displayed values are similar.

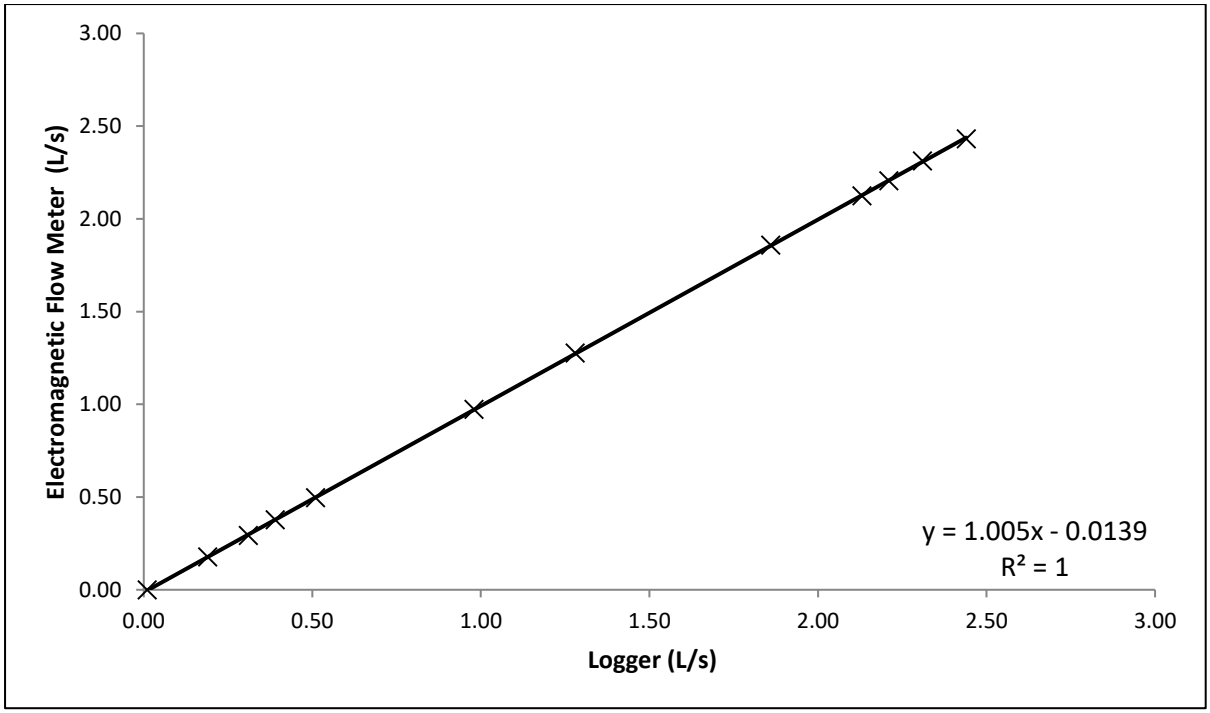

Figure 4-1 - Logger data verification

However, the sensitivity of the current output meant some minor discrepancies were to be expected and corrected for through the obtained equation. After verification, the logger could be used to collect data to a satisfactory level of confidence.

4.1.3 Calibrating the Pressure Transducer and Pressure Logger Programming

In this study, the PrimeLog+ water data logger was used for logging the pressure values obtained from the experiments. The logger was chosen as an alternative to the Sensus Pressure transducer, which was faulty and needing replacement.

The logger used, the PrimeLogger 2i can simultaneously record the flow and pressure in a system. Other functionalities such as depth and height logging are available. The logger has an accuracy of 0.1% on all logger functions. The PrimeLogger used in this study had an internal pressure transducer with a pressure rating of 20 bar. This transducer was calibrated at Signal Instrumentation, and the calibration certificate can be found in Appendix B. The logger was programmed via the Primeworks software. This was done by connecting the logger to the same computer used to programme the Sensus data logger via a USB connection. On the software, the user inputs the logger information such as the site name and site ID.

Additionally, the logger parameter to be used, in this instance pressure logging, is chosen. The logger interval was also set to record and store data every second. As the logger did not have an inbuilt display, a XAP display from the same manufacturer was used. This was connected

to the PrimeLogger via a USB data cable which allowed the interface between the two devices. The display unit also allows the data logger to be zeroed. The logger was reconnected to the computer, and the logged valued were downloaded to obtain the values after a test, as a Microsoft Excel file.

4.1.4 Test Procedure

To characterise leakage on the standardised setup, an 800 mm long uPVC pipe sample was connected to the setup and held in place by Viking Johnson couplings. An in-depth experimental description is found in chapter 3.2.1. A programmed pressure and flow logger were connected to their respective connection points, as shown in Figure 4-2.

Six uPVC pipe samples were used each with one leak, namely 6 mm and 12 mm round holes, 50 mm and 100 mm longitudinal cracks, and 50 mm and 100 mm circumferential cracks. The leaks were created by mechanically machining the pipes. Each sample pipe was individually tested. For each pipe sample, ten tests were done on the test rig that was used by Van Zyl and Malde (2017) which was slightly modified by adding an air valve and an extra inlet/outlet point.

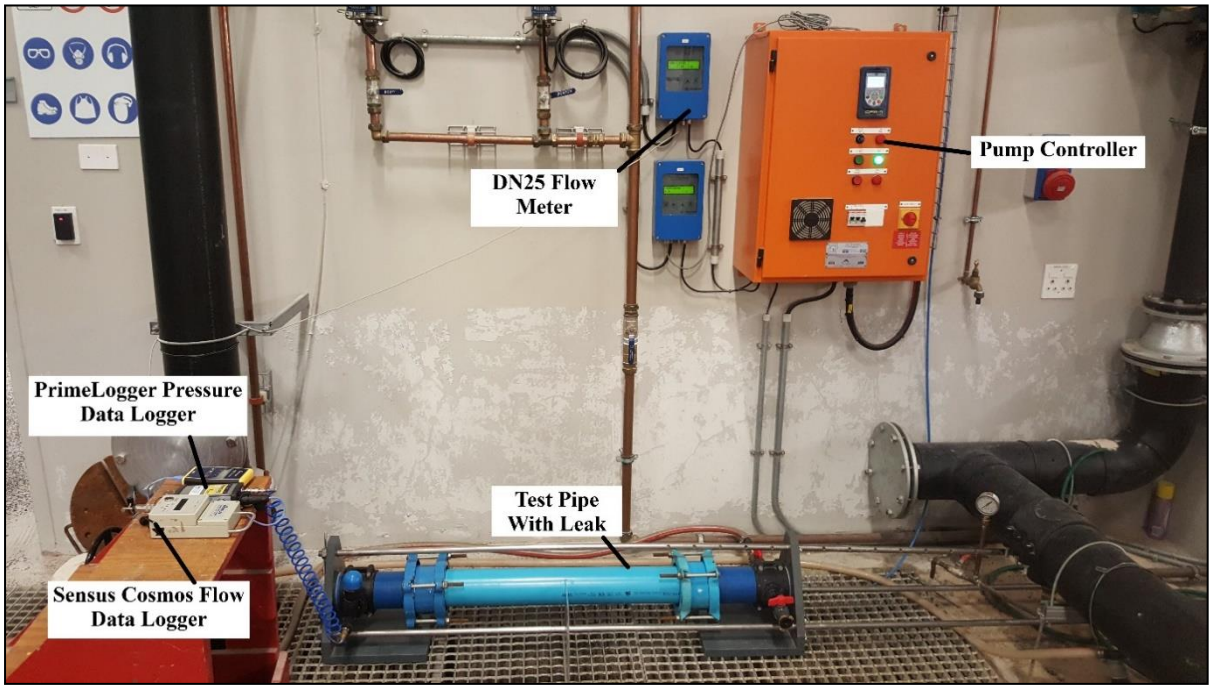

Figure 4-2 - Test setup with the data loggers connected

Water was pumped from the sump and conveyed via a pipe connected on the setup connection point via quick-release brass fittings and allowed to run and discharge into the atmosphere for 60 seconds. This was to ensure the pipe was full and that any trapped air escaped through the air valve and leak. For the test, the pressure was increased and then held constant in 60-second

steps. The different pressure steps were obtained by varying the pump speed on the pump controller. The pressure was incrementally increased in 5 steps from the lowest pump speed to the maximum speed, as shown in Figure 4-3.

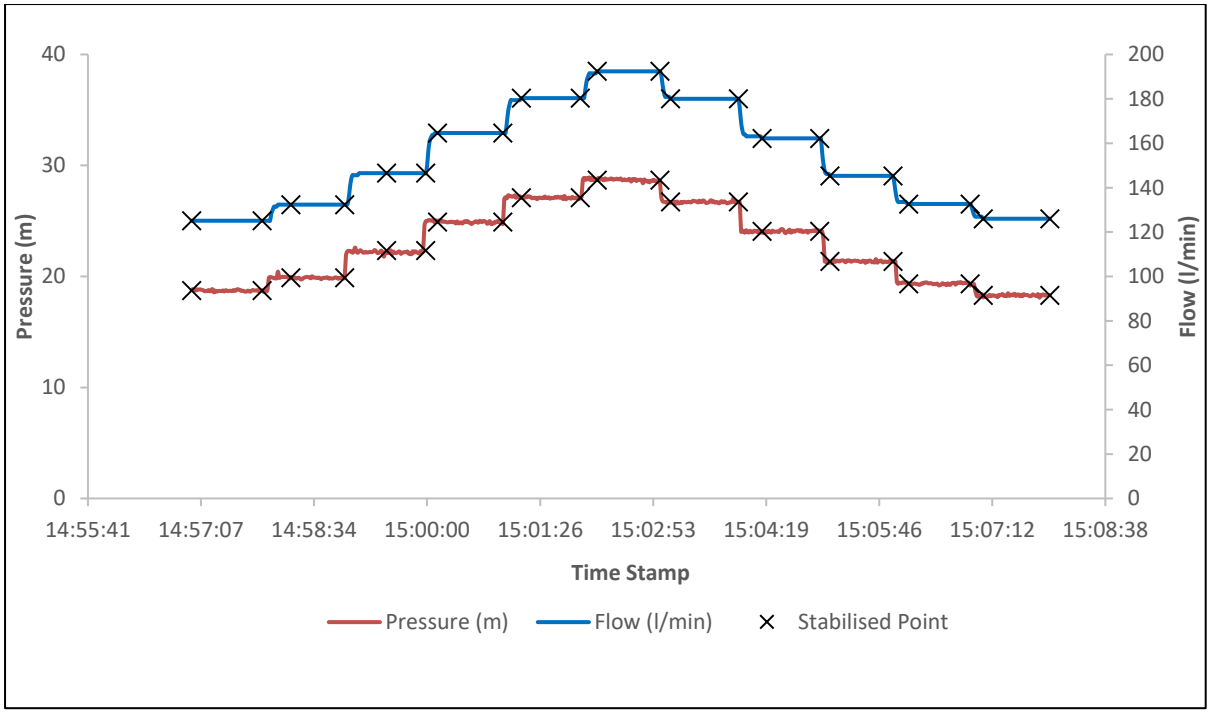

Figure 4-3 - Pressure and flow rate variations during a test

The pressure was then decreased in steps until the minimum pump speed was attained. Initially, the pressure alternation was conducted three times to obtain 31 data points for pressure, and the flow rate values as Van Zyl and Malde (2017) had similarly done.

A minimum of three pressure alternations was performed, each producing 31 data points per test. The subsequent tests were then done with one set of pressure alternation, and each test produced 11 data points. This was done after considering the volume of water used in 15 up and down steps and comparing with the volume of the PCAD tank which is only 200 L and would not be adequate to produce 31 data points. Furthermore, having a similar number of steps between the laboratory and PCAD experiments meant that the confidence intervals of the experimentations would have a similar width which allows for better comparison.

Caution was taken to ensure that there were no leaks through the Viking Johnson coupling and at the quick fit couple at connection point such that water only flowed through the leak opening. The leak was oriented in such a manner that the leak and the pressure transducer were at the same level to simplify calculations by eliminating the need to account for elevation differences in determining the actual pressure at the leak. Ten tests were conducted for each pipe sample

at random times of the day and over 1 to 3 days. The data points from all the tests per sample were then combined, and regression analysis performed to obtain the effective area and the effective head-area slope for the pipe sample.

A slight variation in the test procedure for the circumferential crack was found necessary. During the sample setup, it was observed that the magnitude of the torque used to tighten the bolts that kept the steel rods in a place affected the initial leak area. Large forces closed off the leak and resulted in a leak area that was smaller than the machined area. Loosening the bolts too much also resulted in longitudinal forces playing a significant role in the sample and the effective head area being positive at times.

Thus, a way was sought to standardise the torque required and to incorporate the variations into the results. One suggested method was to use a torque wrench that measured the torque applied, however, such a device could not be obtained and instead it was resorted to measuring the thread length after each bolt had been tightened using digital Vernier callipers as shown in Figure 4-4.

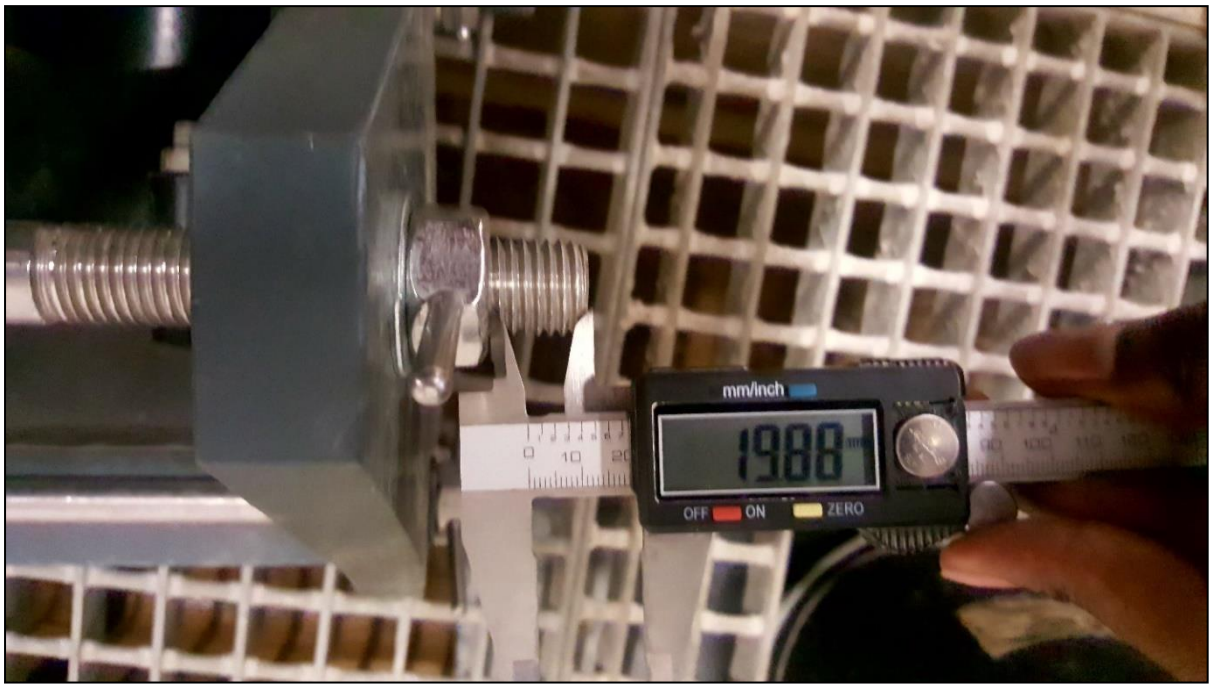

Figure 4-4 - Measuring the thread length during a sample setup for circumferential crack

After measuring the leak area, i.e. length and width after every 1 mm change in the thread length, an average thread length of 20 mm was found to be adequate to ensure the original orifice area did not change. This thread length was also believed to be adequate to ensure the longitudinal forces were accounted for by the steel rods. The flow and pressure through each orifice were recorded on the Prime logger and Sensus data loggers. The collected data was

retrieved via the logger software and analysed on Microsoft Excel to obtain leak characteristics such as the effective area-head slope, N1, coefficient of discharge and the effective area. Experimental data points were obtained by observing the stabilised points on each step and averaging the flow and pressure values between the identified ranges on Microsoft Excel.

Initially, data from each test was exported to an excel data sheet with linked equations, and the flow and pressure readings from the PrimeLog data logger were analysed. By rearranging the orifice equation, as shown in equation 20, the effective areas of the leaks were found.

$$C_d A = \frac{Q}{\sqrt{2gh}} \qquad (20)$$

Where $C_d A$ is the effective area, Q is the flow rate in m^3/s and h is pressure head in meters. The values of the $C_d A$ obtained were then plotted against their associated the pressure heads to produce a linear graph. The initial effective area and effective head area slopes are respectively, the intercept and the gradient of the graph. The leakage exponent, N1 was found by plotting the logarithmic values of the leak flow rate against the logarithmic values of their respective pressure heads. The slope of this graph then gives the N1 exponent.

The head-area slope was compared with values from the experiment by Van Zyl & Malde (2017) and predicted by Cassa & van Zyl (2013) and Nsanzubuhoro, Van Zyl and Zingoni, (2017) for the various leak types. Statistical inference theory was used to obtain the 95% single parameter confidence intervals for each of the parameters.

4.2 Results and Discussions

4.2.1 12 mm uPVC Round Hole

Ten tests were done on the 12 mm uPVC pipe section, and the following results were obtained. The pressure and flow were recorded, and the stabilised steps defined as periods were the pressure variation was less than 0.1 m were then used to analyse the data. Figure 4-5 shows a typical uPVC round hole pressure and flow relationship at each step.

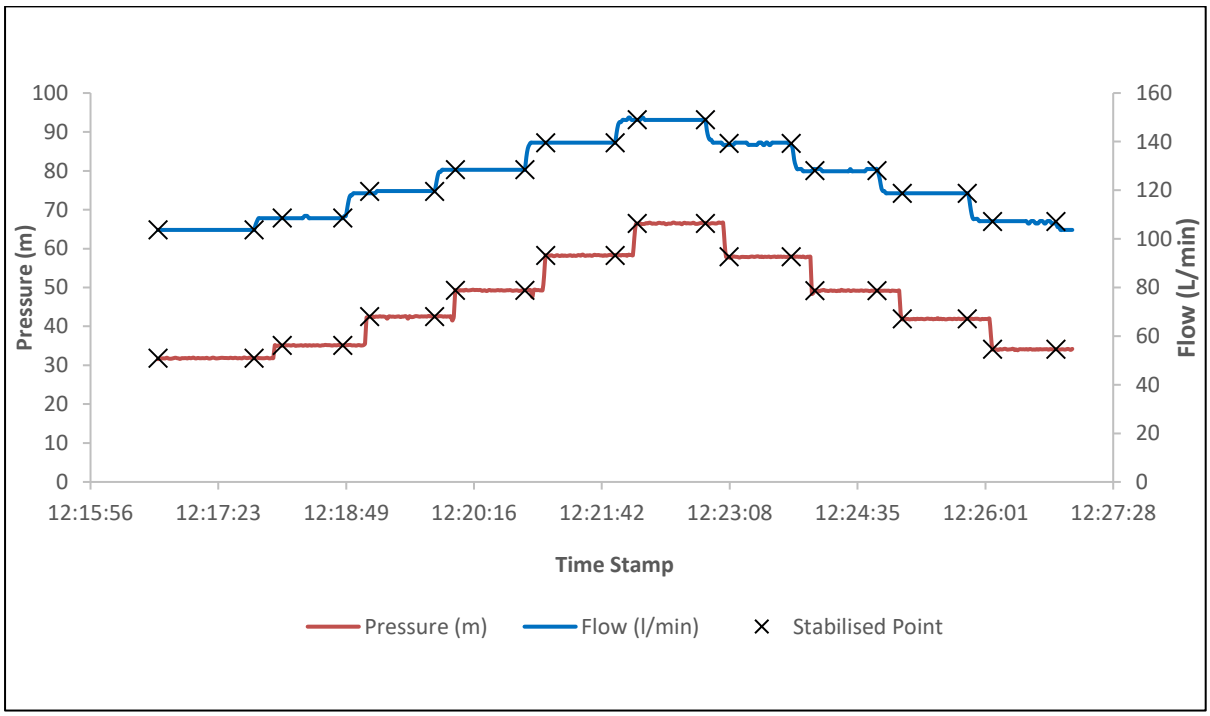

Figure 4-5 - Pressure head-flow rate relationship for a typical test

As explained in section 4.1.4. above, the pressure and flow rate values were analysed and manipulated to allow for the evaluation of the required leakage characteristics.

The data points from the ten tests were combined to enable better analysis, and Figure 4-6 shows the power relationship between the flow rate and the pressure head. The figure also shows the gives the N1 as the exponent of the power relationship.

The N1 value for the combined data points of pipe sample tests was found to be 0.496. The standard deviation on the N1 value across all tests conducted was 0.0027 and sample variance (variance of the N1 values of the ten conducted tests) of 7.32E-06 (0.002% of the N1 value). This showed little variance in the values found in the tests and represents excellent repeatability and reliability of the conducted tests for the N1 exponent.

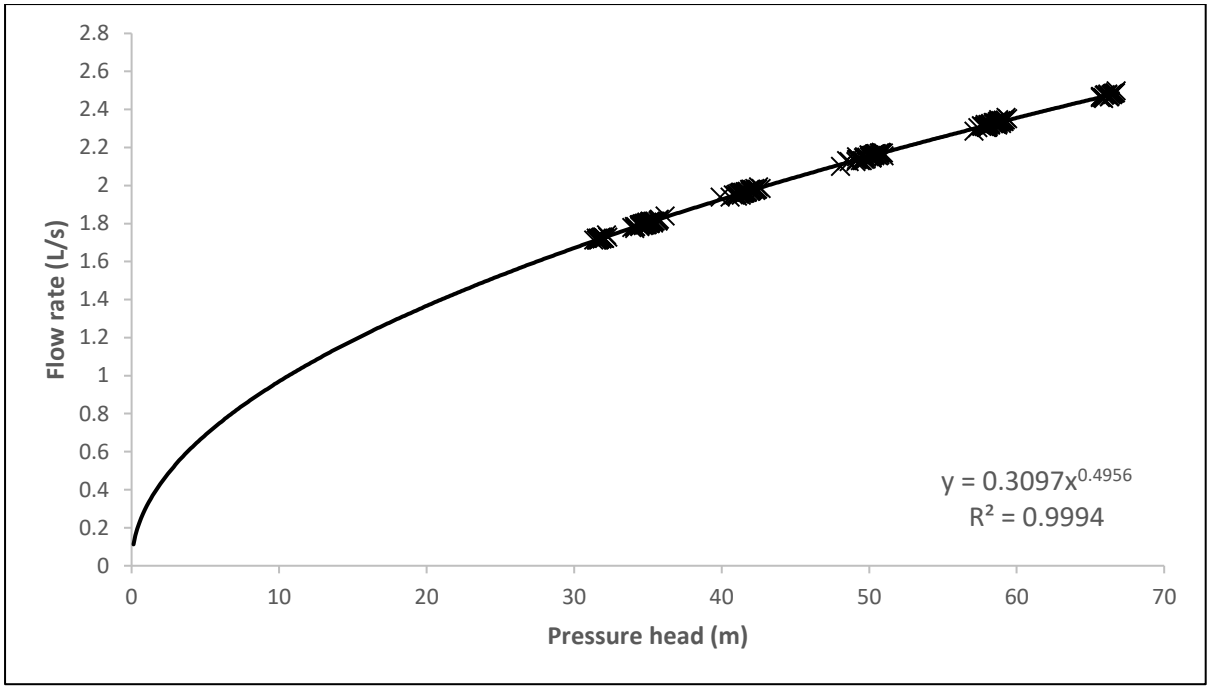

Figure 4-6 - Flowrate-pressure power relationship

From equation 20, the effective areas for the different flowrates and their respective pressure heads were found as explained in section 4.1.4. The effective areas for all data points across ten tests were then plotted against their associated pressure heads. Figure 4-7 graphically shows the relationship between the effective area and pressure head.

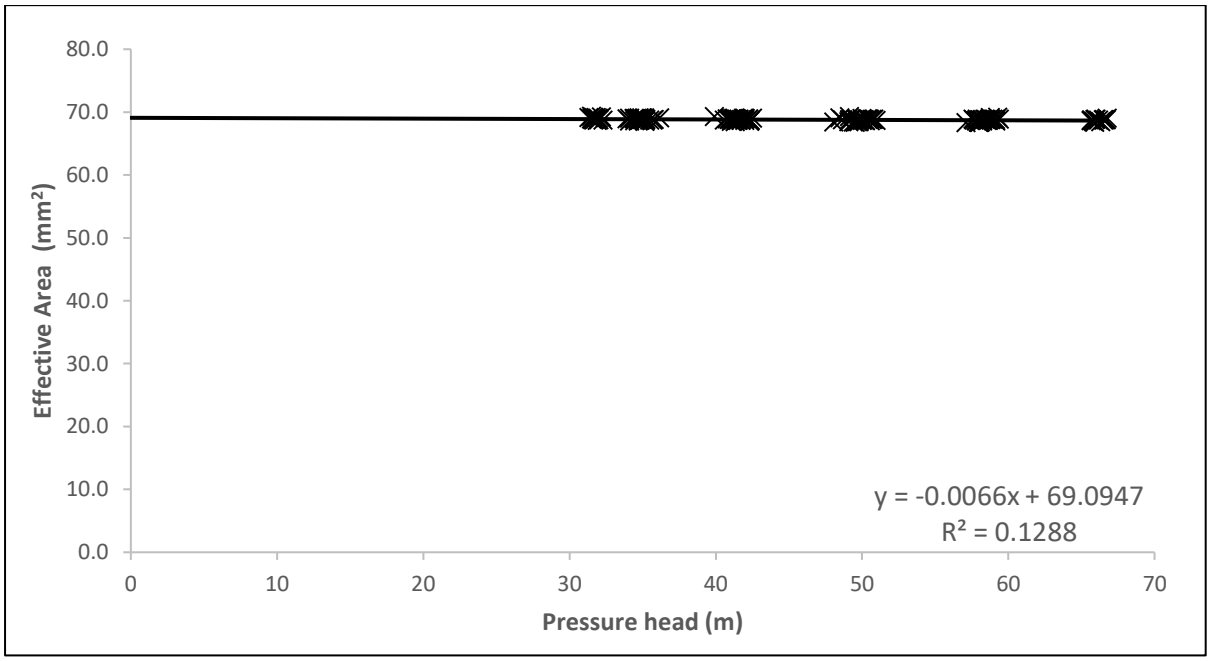

Figure 4-7 - Graph showing the effective head area slope of a 12 mm uPVC round hole

The effective area-head slope (C_dm/ m') was found to be negative with the slope value of the combined data points for the pipe sample being - 0.00661 mm^2/m meaning for every meter of

the pressure head, the orifice area reduced by 0.00661 mm^2. Van Zyl and Malde, (2017); Nsanzubuhoro et al., (2019), also found similar small negative effective area-head slopes for uPVC round holes in the pipe samples they tested using a similar laboratory setup. The single parameter confidence interval for the effective area-head slope is 0.00278 mm^2/m. The standard deviation of the effective area-head slope was found to be 0.0063 mm^2/m, while the sample variance which measures how far each test value is from the sample mean was found to be 4.01E-05 mm^2/m (0.61% of the mean). This shows little variance between test values and shows excellent repeatability in the test.

A test statistic to evaluate whether the slope of the line was zero was conducted. In this test, the null hypothesis, H_0, was taken to be that; the slope is equal to zero. The alternative hypothesis, H_1, was then that the slope is not equal to zero, with an alpha value of 0.05. The test revealed a t-statistic of 8.33 E-05 which is less than 0.05, and therefore the null hypothesis was rejected, and the slope was deemed to be statistically not equal to zero. However, as shown by the range of values of m' for various leak types by Van Zyl and Malde, (2017); Nsanzubuhoro et al., (2019), the slope obtained in this study is very small and can practically be deemed as zero.

The flow rate predictions of the FAVAD (modified orifice equation) and N1 equations were compared, as shown in the graph in Figure 4-8.

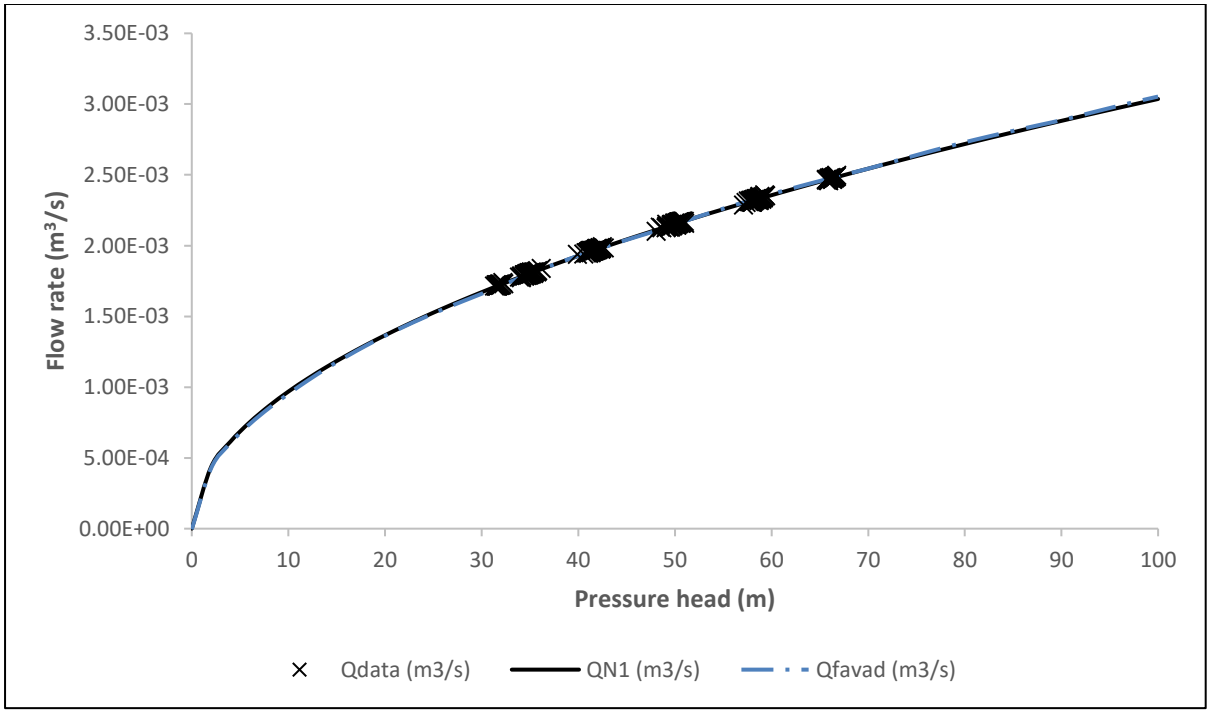

Figure 4-8 - Comparison of the FAVAD and N1 equation flow predictions and observed data

These predictions were made by evaluating the flowrates obtained from the two equations, equation 9 and equation 12, for the N1 and FAVAD, respectively. The flowrate and the associated pressure heads used to derive them were then plotted on a single graph. The data points of the combined tests were also plotted on that same graph to verify if these two models can predict the behaviour of the 12 mm round hole leak. Both models fit the data well, even outside the measured pressure range for the 12 mm uPVC round hole. The near-perfect alignment of the FAVAD and N1 models is to be expected as the N1 model will fit the FAVAD model for N1 values of 0.5. In this study, the N1 value was 0.496, which is very close to 0.5.

This phenomenon has also been explored by Van Zyl and Malde, (2017) who attributed the fit to very small head area slopes which can practically be considered as zero slopes and this enables pure orifice flow that is well described by both models.

The variation of the results for the ten tests was analysed, and Table 4-2 shows the summary of the parameters obtained in each of the ten tests conducted for this sample.

Table 4-2 - Summary of results for the ten 12 mm round hole tests

Experiment ID	A_0' (mm^2)	m' (mm/m)	C_d	N1	c
A	69.0	-0.0124	0.610	0.495	3.10E-04
B	69.3	-0.0141	0.613	0.494	3.12E-04
C	68.9	-0.0010	0.609	0.499	3.06E-04
D	68.8	-0.0003	0.608	0.500	3.05E-04
E	68.8	-0.0043	0.608	0.498	3.06E-04
F	68.8	-0.0002	0.608	0.500	3.05E-04
G	69.1	-0.0078	0.611	0.497	3.09E-04
H	69.3	-0.0152	0.613	0.494	3.13E-04
I	69.3	-0.0132	0.613	0.495	3.11E-04
J	69.1	-0.0191	0.611	0.492	3.13E-04

The ten test results were also analysed graphically and compared with Van Zyl and Malde, (2017) results. In this comparison, the combined dataset was also included to aid in the repeatability analysis of the ten individual tests. The leakage parameters are visually represented on the graphs below.

Figure 4-9 shows the comparison for combined data points from this study, the individual tests and the Van Zyl and Malde, (2017) study for the effective area parameter.

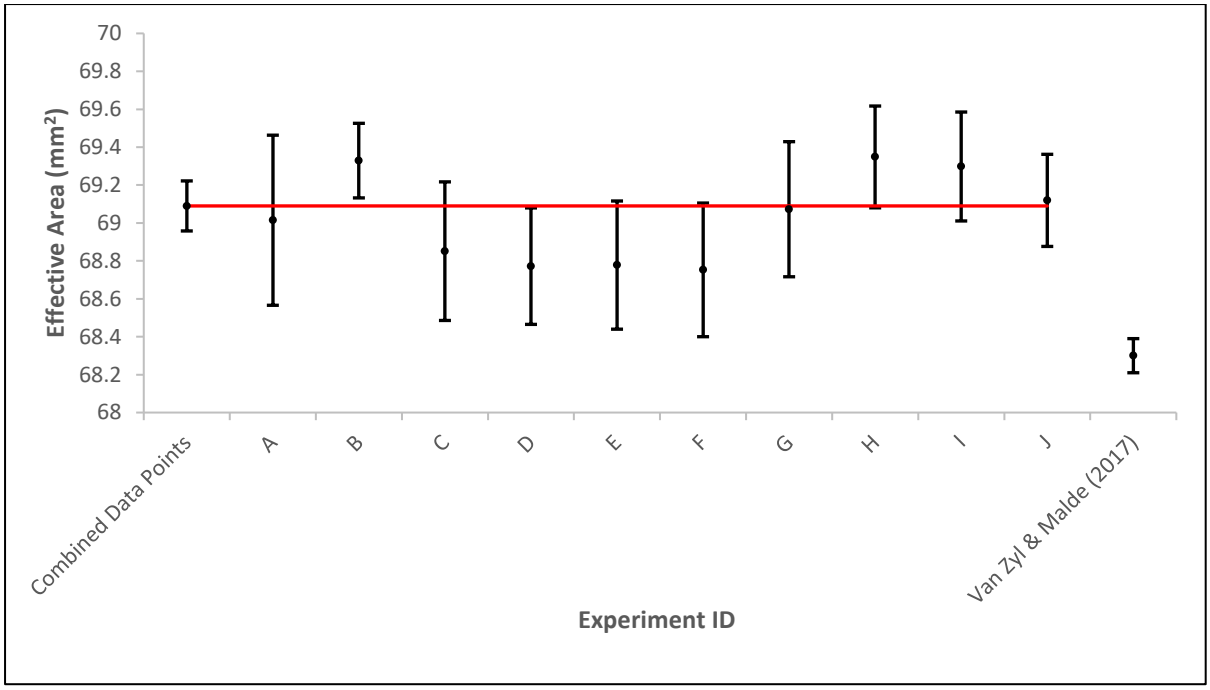

Figure 4-9 - Repeatability analysis of the effective area of the ten 12 mm round hole tests and comparison with Van Zyl & Malde (2017) results

Figure 4-10 displays the effective head-area slope comparison for combined data points from this study, the individual tests and the Van Zyl and Malde, (2017) study with their associated single parameter confidence intervals.

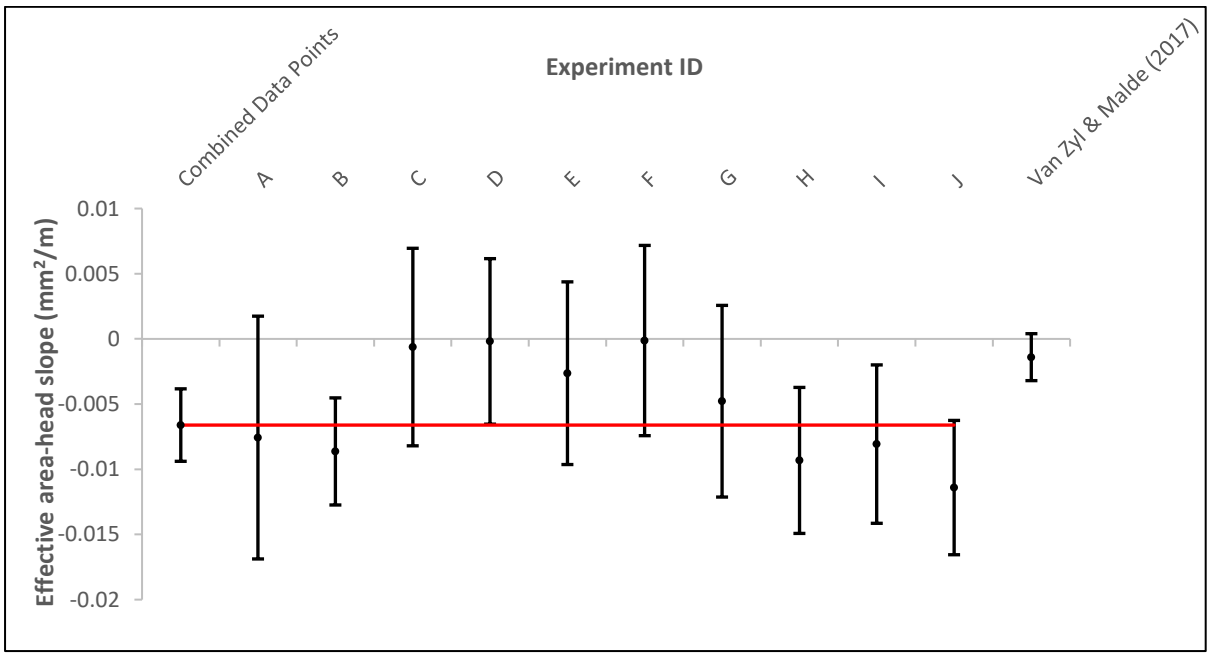

Figure 4-10 - Repeatability analysis of the effective area-head slope of the ten 12 mm round hole tests and comparison with Van Zyl & Malde (2017) results

From Figure 4-10 it can be seen that the individual effective area-head slopes values for the 12 mm round hole contain the combined m' value, however, when inspecting the effective areas shown in Figure 4-9. One test (test B) does not contain the combined effective area value.

Upon inspection, variation in the individual test results can be seen. This seems contrary to the variance found using statistical inference methods. However, the visually apparent variation of the results is attributed to the magnitude of the values in question; being is very small while the scale used to show the variation is large. Thus, while there appears to be significant variation in the results, this due to the magnitude of the test parameter being very small such that small deviations in the data collected have significant effects

An analysis of the parameters from the individual tests from this study and the Van Zyl and Malde (2017) study was conducted. It was observed that there was some overlap between the Van Zyl and Malde (2017) and the individual test parameters. This implies that some of the individual tests conducted produced statistically similar results to the Van Zyl and Malde (2017) study

An assessment of the single parameter confidence intervals revealed that when considering the combined datasets from this study, the intervals for the two datasets did not overlap. The lack of overlap was believed to be a result of Van Zyl and Malde (2017) only conducting one test for the 12 mm round hole leak, and consequentially the results lie outside the 95% interval of the combined data points of this study. However, the result from the Van Zyl and Malde (2017) study overlaps with 9 of the individual tests.

The equation used to derive the two-sided 95% confidence interval and found in most statistical textbooks is shown as equation 21:

$$\overline{X_n} \pm t_{\frac{\alpha}{2},n-1}\frac{\sigma}{\sqrt{n}} \qquad (21)$$

Where $\overline{X_n}$ is the mean of the parameter (A_0' or m') for n observations, $t_{\alpha/2}$, is the t-test parameter for a set alpha value, α (0.05 in this case for 95% level of confidence), n - 1 represents the degrees of freedom for the test statistic, σ is the standard deviation of the observations.

The Van Zyl and Malde (2017) study had a smaller confidence interval, although it had fewer data points. As the t-test parameters are the same for both studies, the difference is thus due to different standard deviations. It then means that the data points from that study had a smaller standard deviation compared to the standard deviation of the combined tests from this study.

On the other hand, the individual tests had fewer data points (10 per tests) than the Van Zyl and Malde (2017) study (31 data points), and as a result, their confidence intervals are wider than the latter's confidence interval. Finally, the combined parameters for this study had larger confidence intervals as shown in Table 4-3. As the dataset from this study had significantly more data points, this implies that a combination of data points results in a more significant standard deviation in the data, which is to be expected in an experimental setup.

Table 4-3 - Summary of results and comparison with Van Zyl & Malde (2017) study

	N1	**A_0' (mm^2)**	**95% SPCI for A_0' (mm^2)**	**m' (mm^2/m)**	**95% SPCI for m' (mm^2/m)**	**p for m' (%)**	**C_d**
Van Zyl & Malde (2017)	0.499	68.3	± 0.09	- 0.00141	± 0.00180	12.5	0.603
This Study	0.496	69.1	± 0.132	- 0.00661	± 0.00278	< 0.1	0.610

4.2.2 6 mm uPVC Round Hole

Ten tests were also conducted on the uPVC pipe section with a 6 mm round hole. The pressure and flow were recorded, and the stabilised steps were then used to analyse the data. Figure 4-11 shows a typical 6 mm uPVC round hole pressure and flow relationship at each step.

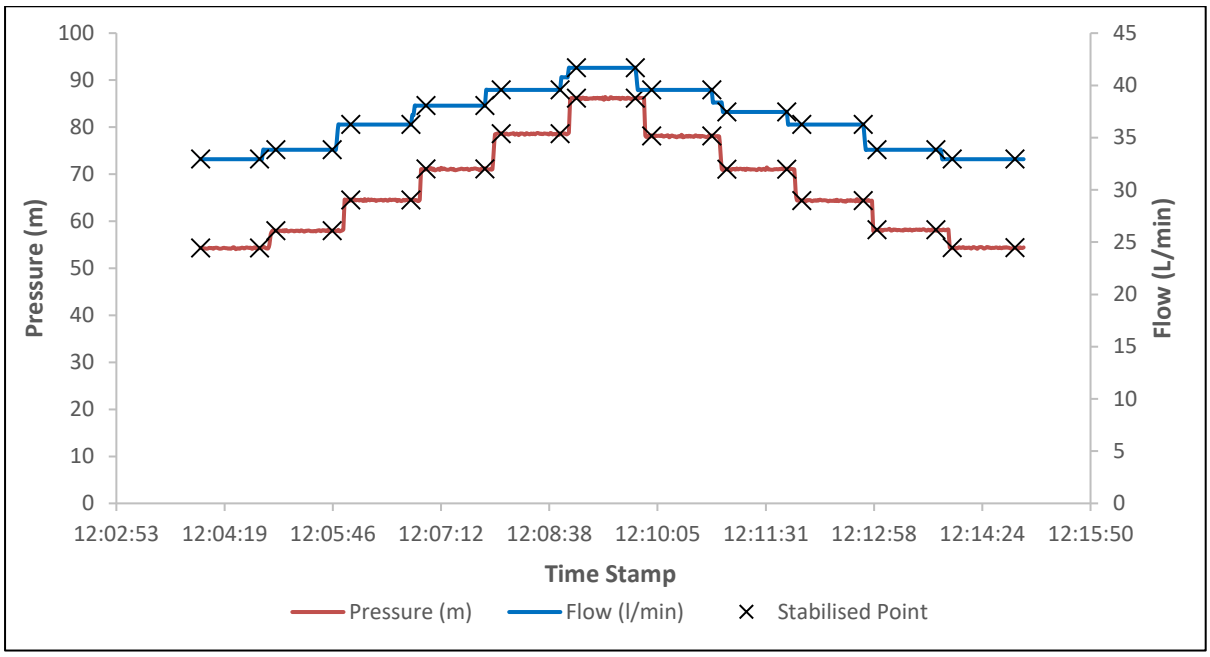

Figure 4-11 - Pressure head-flow rate relationship for a typical test

The pressure and flow rate values were analysed and manipulated to allow for the evaluation of the required leakage characteristics. The data points from the ten tests were combined, and Figure 4-12 shows the power relationship between the flow rate and the pressure head.

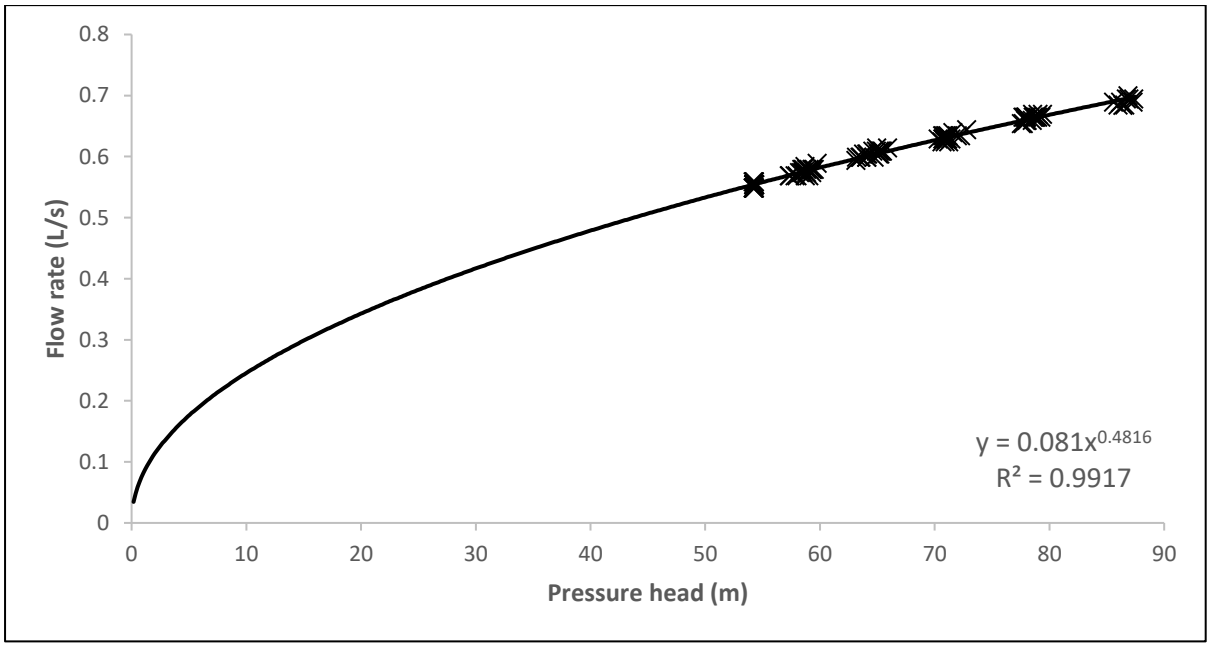

Figure 4-12 - Flowrate-pressure power relationship

The N1 is the exponent of the power relationship. The combined N1 value for the pipe sample was found to be 0.482. A standard deviation of 0.009 was found across all ten tests conducted.

The sample variance, which communicates the variance of the N1 values of the ten conducted tests, was found to be 9.23E-05. This shows that there is a 0.02% variation from the mean N1 value. This result showed little variance in the tests and represented excellent repeatability and reliability of the conducted tests for the N1 exponent.

The effective areas for the different flowrates and their respective pressure heads were found as explained in section 4.1.4. The effective areas for all data points across ten tests were then plotted against their associated pressure heads. Figure 4-13 graphically shows the relationship between the effective area and pressure head.

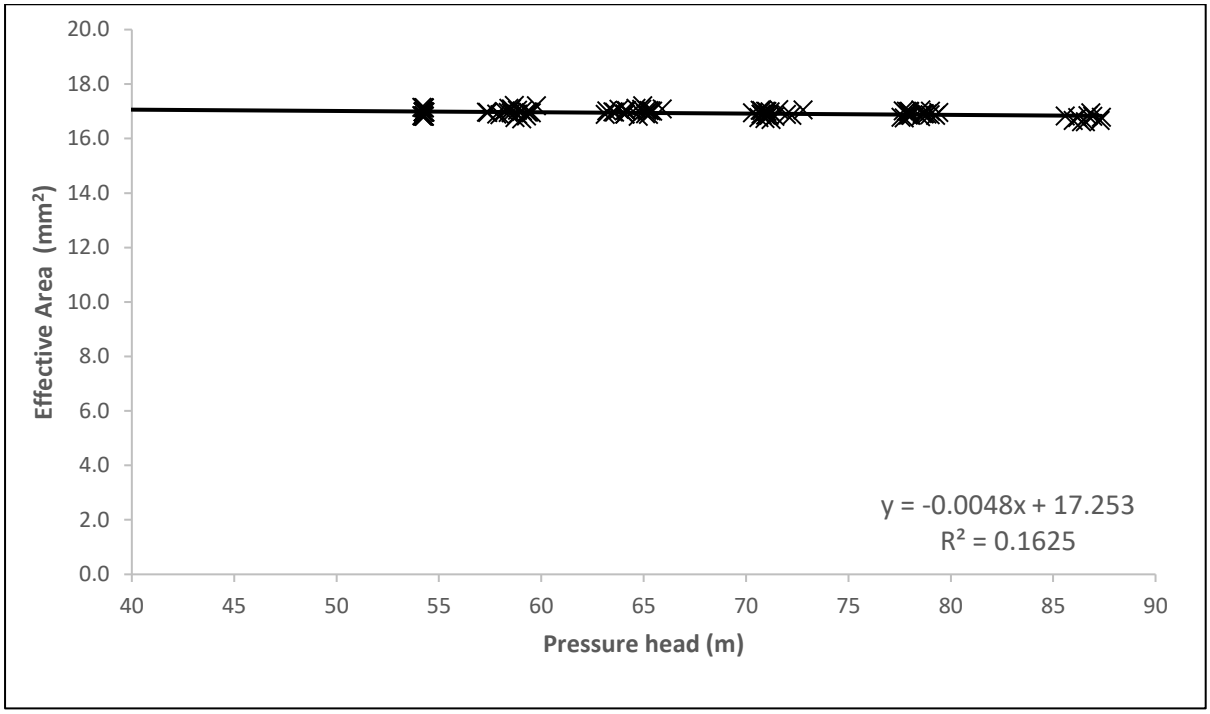

Figure 4-13 - Graph showing the effective head area slope of a 6 mm uPVC round hole

The effective area-head slope (C_dm) was found to be negative with the slope value for the pipe sample being - 0.0042 mm^2/m meaning for every meter of the pressure head the orifice area reduced by 0.0042 mm^2. The single parameter confidence interval for the effective area-head slope is 0.0021 mm^2/m. The standard deviation of the effective area-head slopes of the ten tests was found to be 0.0022 mm^2/m, while the sample variance which measures how far each test value is from the sample mean and other test results was found to be 4.89E-06 mm^2/m.

The flow rate predictions of the FAVAD and N1 equations were compared, as shown in Figure 4-14.

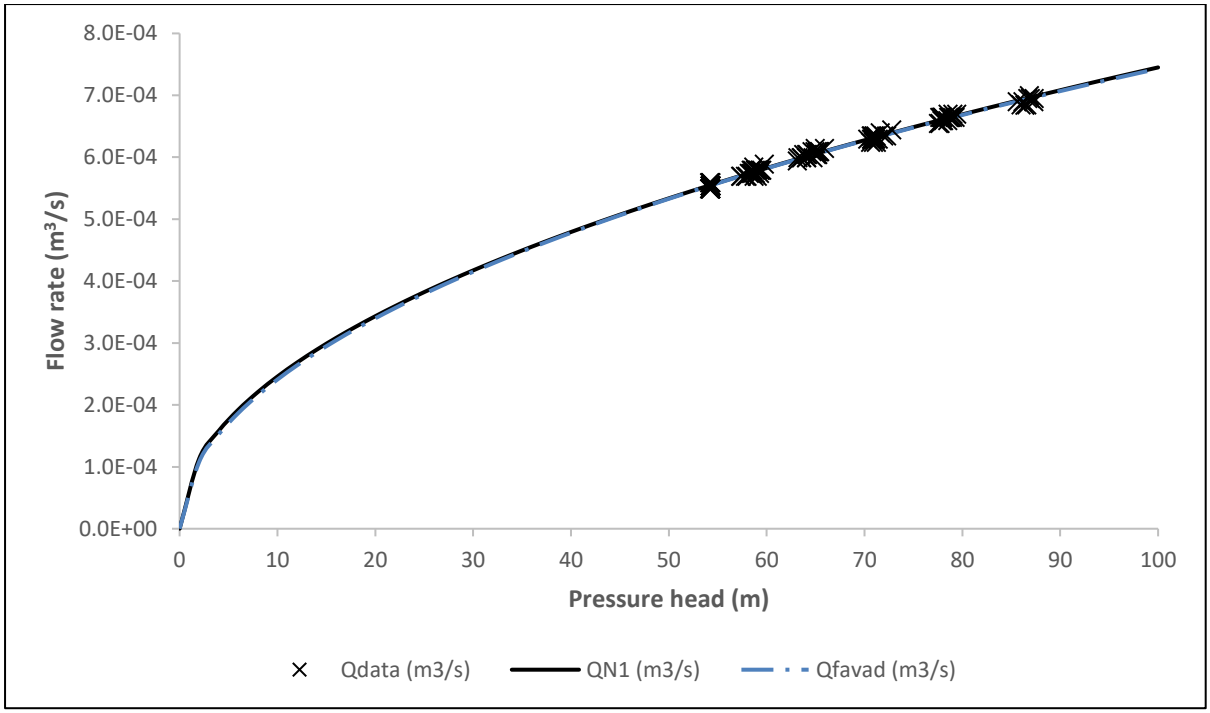

Figure 4-14 - Comparison of the FAVAD and N1 equation flow predictions and observed data

Both models fit the data well, even outside the measured pressure range for the 6 mm uPVC round hole. This is because the round hole appears to obey the orifice equation as the leak area does not significantly change with pressure and the leakage exponent, N1 is close to 0.5. Thus, the N1 equation fits/aligns with the modified orifice equation for this sample. Table 4-4 then shows a summary of the results for the data presented above.

Table 4-4 - Summary of results

	N1	**A_0' (mm^2)**	**95% SPCI for A_0' (mm^2)**	**m' (mm^2/m)**	**95% SPCI for m' (mm^2/m)**	**p for m' (%)**	**C_d**
This Study	0.482	17.25	± 0.143	- 0.0042	± 0.0021	< 0.05	0.61

The variation of the ten tests was analysed graphically and Figure 4-15 and Figure 4-16 show the graphs that describe the repeatability and reliability of the results conducted on a 6 mm uPVC round hole using the standardised method. Two parameters, the effective area-head slope and effective area, were used to establish the repeatability and reliability of the results across

the ten tests. These figures also visually depict the repeatability of the experiment. Figure 4-15 shows the repeatability of the effective head area slope parameter across the tests.

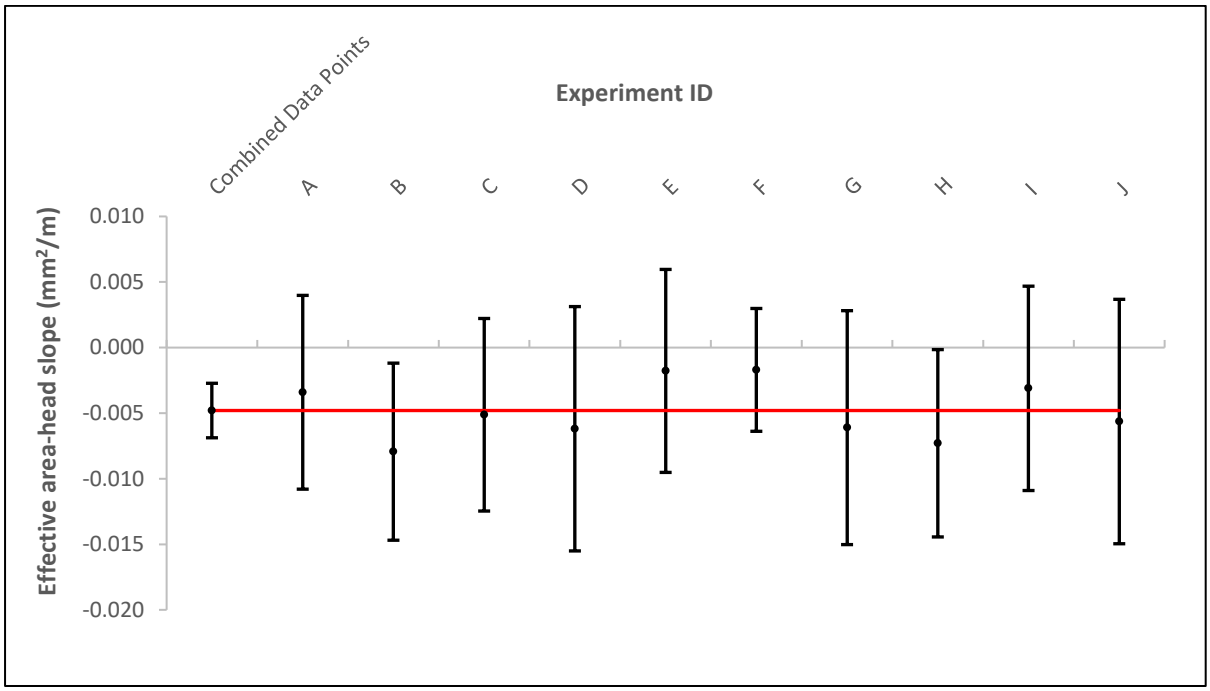

Figure 4-15 - Effective area -head comparison and repeatability analysis of the 6 mm round hole tests

As seen in Figure 4-15, the effective area-head area slopes obtained from the ten tests were all within the 95% confidence interval of the combined data value. A similar observation is made when analysing the effective areas of the ten tests, as shown in Figure 4-16.

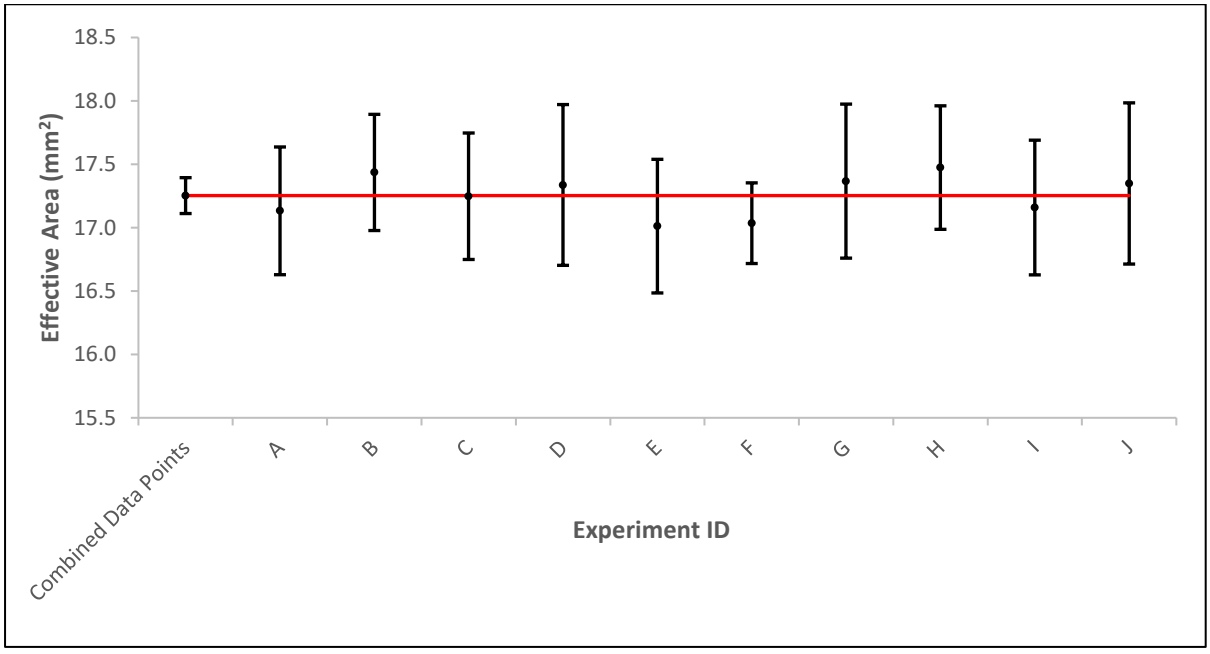

Figure 4-16 - Effective area comparison and repeatability analysis of the 6 mm round hole tests

The results of these tests reveal that, for this leak type, it is possible to obtain consistent values from the standardised method. The figure thus visually confirms the excellent repeatability of the experiment. Table 4-5 then shows a summary of the parameters obtained in each of the ten tests.

Table 4-5 - Summary of results for the ten 6 mm round hole tests

Experimental ID	A_0' (mm^2)	m' (mm/m)	C_d	N1	c
A	17.1	-0.00341	0.606	0.486	7.93E-05
B	17.4	-0.00794	0.617	0.468	8.56E-05
C	17.2	-0.00512	0.610	0.480	8.16E-05
D	17.3	-0.00619	0.613	0.476	8.29E-05
E	17.0	-0.00178	0.602	0.494	7.69E-05
F	17.0	-0.00170	0.602	0.494	7.70E-05
G	17.4	-0.00611	0.614	0.494	8.24E-05
H	17.5	-0.00730	0.618	0.471	8.50E-05
I	17.2	-0.00311	0.607	0.489	7.85E-05
J	17.3	-0.00564	0.614	0.480	8.18E-05

4.2.3 100 mm uPVC Longitudinal Crack

For the ten tests conducted on the 100 mm uPVC longitudinal crack, the results documented below were obtained. As with the 12 mm round hole, the typical pressure and flow rate relationship with time for the tests is shown in Figure 4-17.

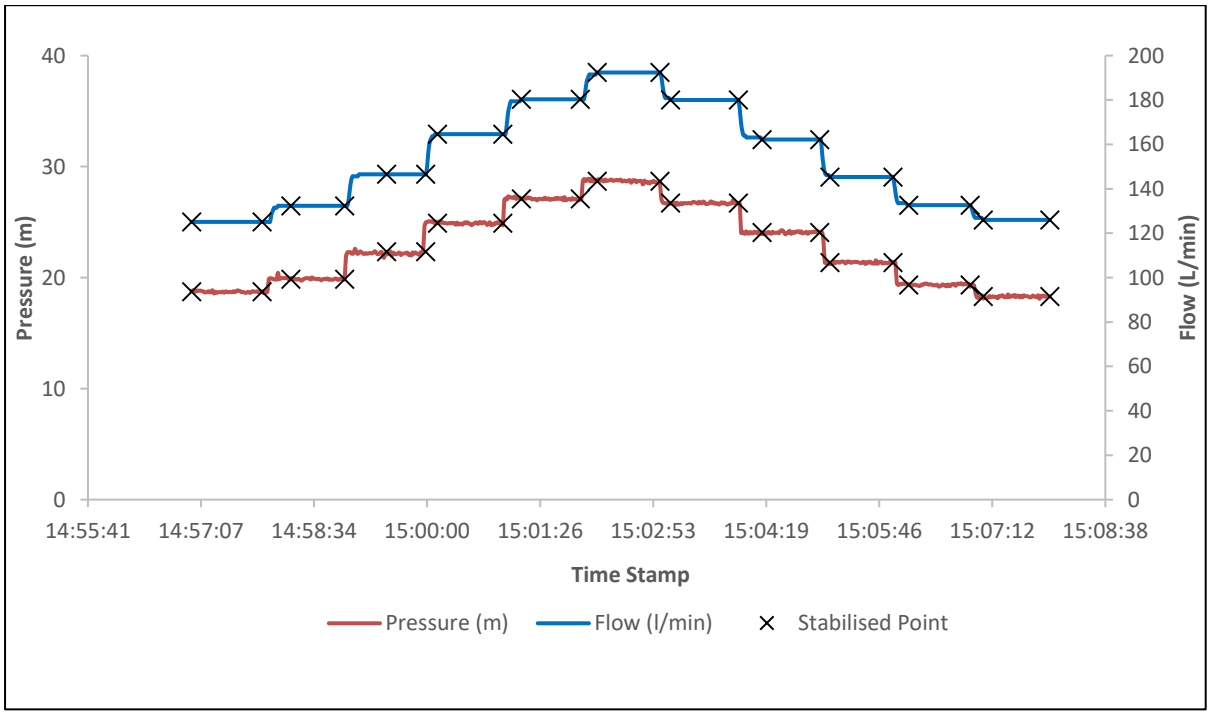

Figure 4-17 - Pressure head-flow rate relationship for a typical test

The stabilised points on each step were noted and used to analyse and derive the leakage characteristics of this leak opening. As explained in section 4.2.1 above, the pressure and flow rate values were analysed and manipulated to allow for the evaluation of the required leakage characteristics.

The data points from the ten tests were combined to enable better analysis, and Figure 4-18 shows the power relationship between the flow rate and the pressure head. The figure also shows the N1 as the exponent of the power relationship.

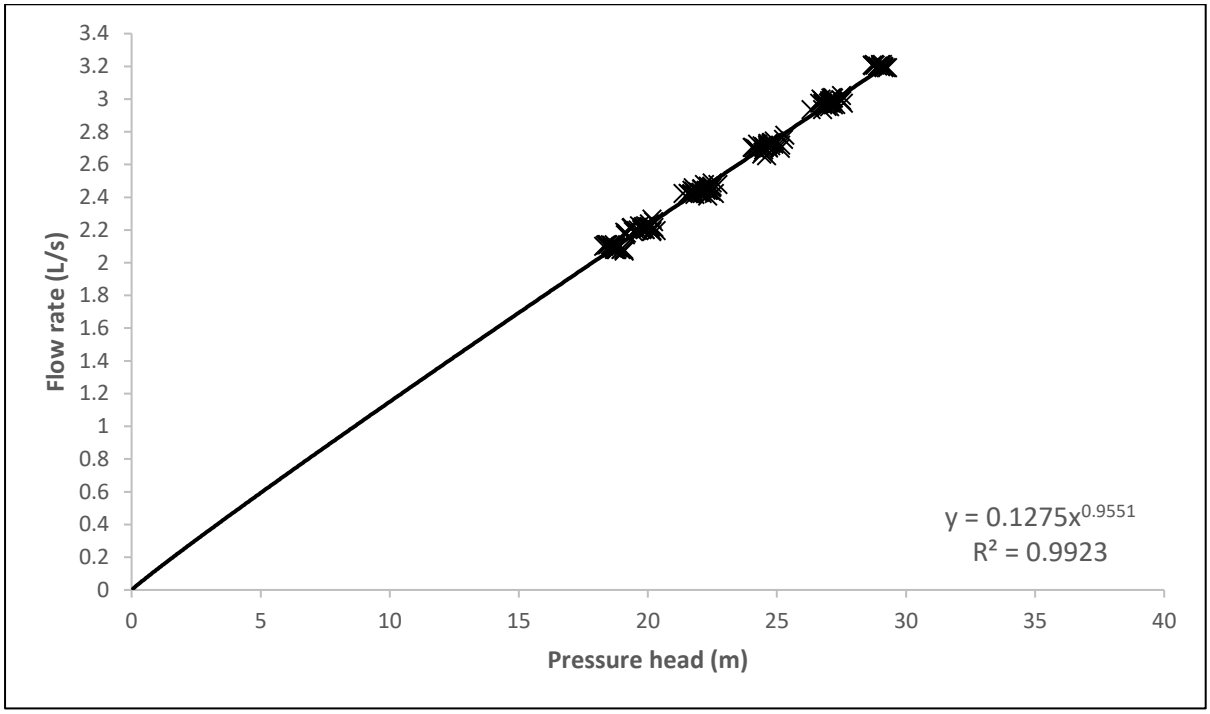

Figure 4-18 - Flowrate-pressure power relationship of a 100 mm longitudinal crack

From the analysis, the N1 value for the pipe sample was found to be 0.955 with a standard deviation of 0.00848 and sample variance (variance of the N1 values of the ten conducted tests) of 7.19E-05 (0.008% of the mean N1).

These results implied little variance in the tests and represented the repeatability and reliability of the ten conducted tests. It can be observed that due to the exponent being approximately equal to one, the graph obtained is almost linear.

From the data obtained through equation 20, a graph of the effective area against the pressure head was obtained and is shown in Figure 4-19 which graphically shows the relationship between the effective area and pressure head.

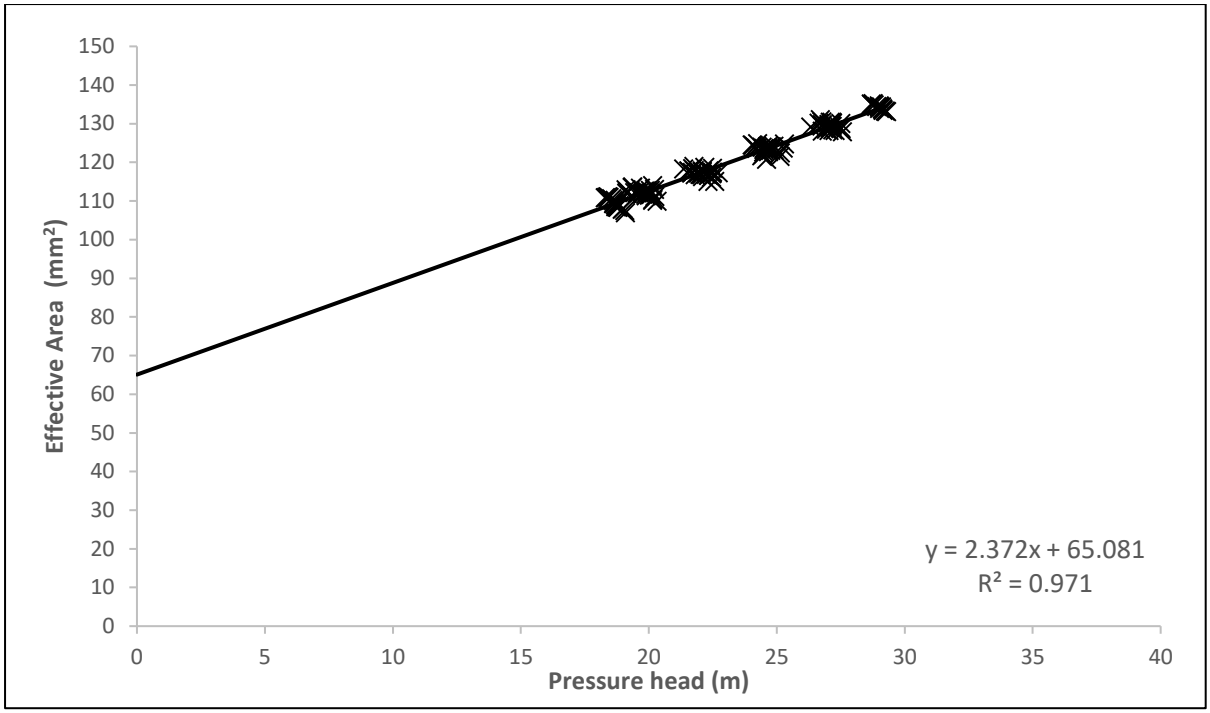

Figure 4-19 - Graph showing the effective head area slope of a 100 mm uPVC longitudinal crack

For this pipe sample, the effective area-head slope (Cdm) was positive with a positive slope value of 2.37 mm^2/m meaning for every meter of pressure head the leak area increased by 2.37 mm^2. This is a significant change in the area with respect to pressure and shows that leak areas on longitudinal cracks vary more in response to pressure variations. This means that the leakage flow rate of a longitudinal crack is more dependent on the pressure head of the fluid flowing through the leak. The single parameter confidence interval for the effective area-head slope (mm^2/m) is ± 0.066 mm^2/m.

The effective area-head slope was comparatively large, which is anticipated in a longitudinal crack Nsanzubuhoro et al., (under review),. The standard deviation of the effective area-head slopes was found to be 0.0439, while the sample variance of the effective area-head slopes from the ten tests, which measures how far each test value is from the sample mean was found to be 0.00193 (0.08% of the mean). These two statistical values report little variance between the ten test results and show excellent repeatability in the test. The ANOVA and regression analysis of the combined data points revealed a coefficient of determination, R^2, of 0.97.

The flow rate predictions from the FAVAD and N1 equations were compared, as shown in Figure 4-20. As above, the predictions were made by evaluating the flowrates obtained from the two equations, equation 9 and equation 12.

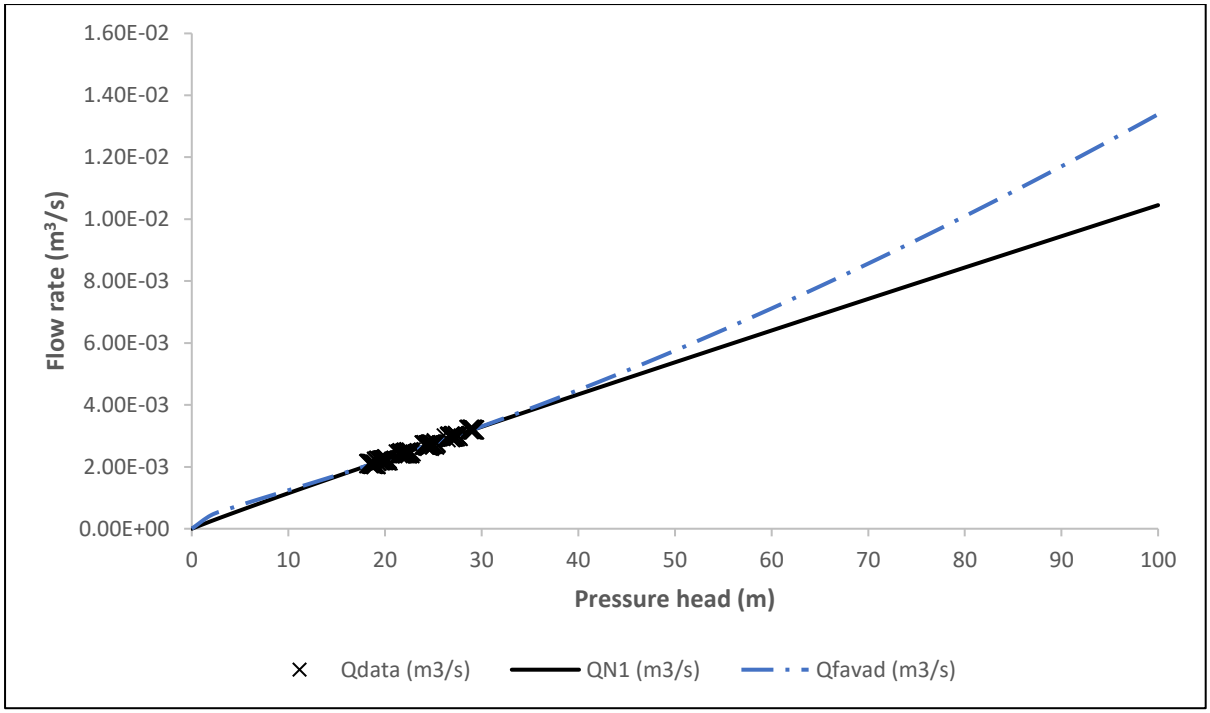

Figure 4-20 - Comparison of the FAVAD and N1 equation flow predictions and observed data

For the N1 and FAVAD respectively, and both models fit the data well within the measured pressure range for the 100 mm uPVC longitudinal crack. However, beyond the measured range, i.e. pressure values larger than the maximum obtained from the study, the two equations deviated.

Van Zyl and Malde, (2017) attributed the deviation to the N1 equation being an empirical equation that mostly depends on the data and consequently, the pressure range used. In contrast, the FAVAD equation is derived from the fluid mechanics and observed properties of the leak and is, therefore, more reliable. Therefore, the N1 equation can only be used to predict/model leakage within the range of pressure values wherein it was calibrated.

The nature of the leak and the pump used in this study did not allow for higher pressure values to be recorded, as such it could not be determined if the FAVAD equation would also match the experimental data.

The variation of the 10 test results was analysed, and Table 4-6 shows a summary of the parameters obtained in each of the ten tests conducted for this sample.

Table 4-6 - Summary of results for the ten 100 mm longitudinal crack tests

Experiment ID	A_0' (mm^2)	m' (mm/m)	C_d	N1	c
A	65.1	2.33	0.651	0.954	1.27E-04
B	66.1	2.34	0.661	0.950	1.30E-04
C	63.8	2.37	0.638	0.961	1.24E-04
D	62.2	2.45	0.622	0.976	1.18E-04
E	63.3	2.44	0.633	0.970	1.22E-04
F	65.4	2.38	0.654	0.952	1.29E-04
G	65.5	2.40	0.655	0.953	1.29E-04
H	64.3	2.43	0.622	0.961	1.26E-04
I	64.4	2.45	0.644	0.962	1.26E-04
J	65.5	2.41	0.655	0.954	1.29E-04

The ten test results were also analysed graphically and compared with Van Zyl and Malde, (2017) results. In this comparison, the combined dataset was also included to aid in the repeatability analysis of the ten individual tests. The leakage parameters are visually represented on the graphs below.

Figure 4-21 displays the effective head-area slope comparison for combined data points from this study, the individual tests and the Van Zyl and Malde, (2017) study with their associated single parameter confidence intervals.

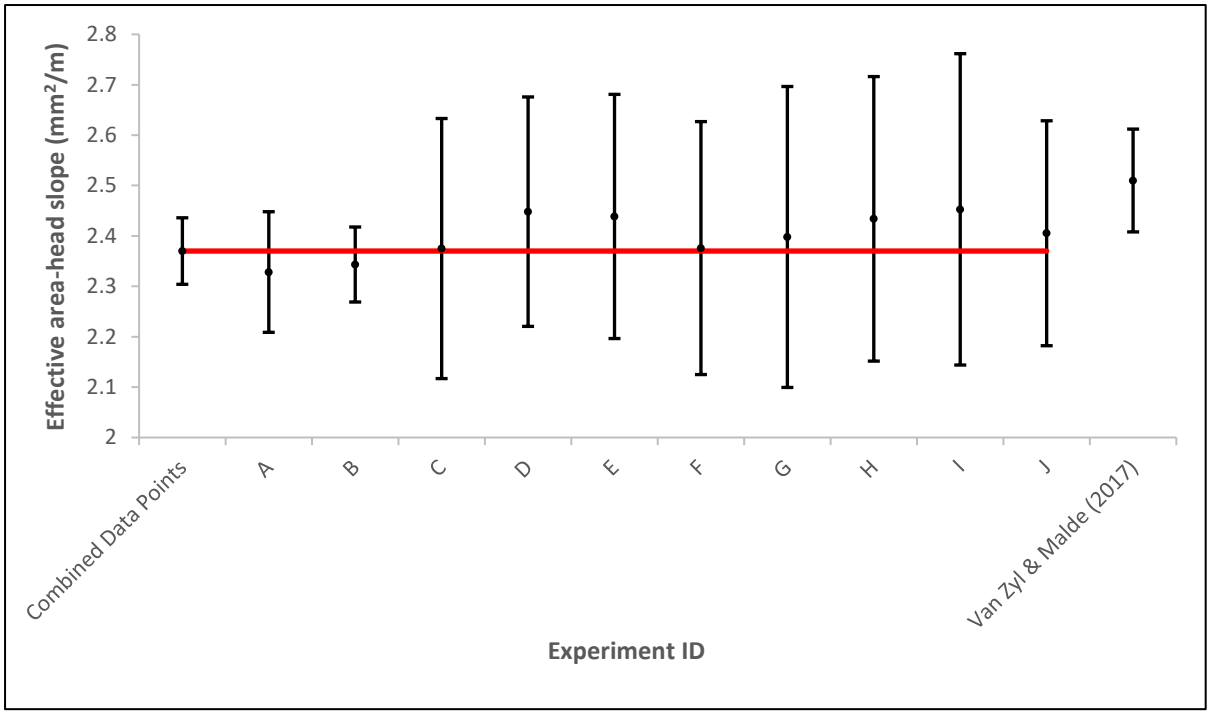

Figure 4-21 - Repeatability analysis of the effective area-head slope of the ten 100 mm longitudinal crack tests and comparison with Van Zyl & Malde (2017) results

Figure 4-22 shows the comparison for combined data points from this study, the individual tests and the Van Zyl and Malde, (2017) study for the effective area parameter.

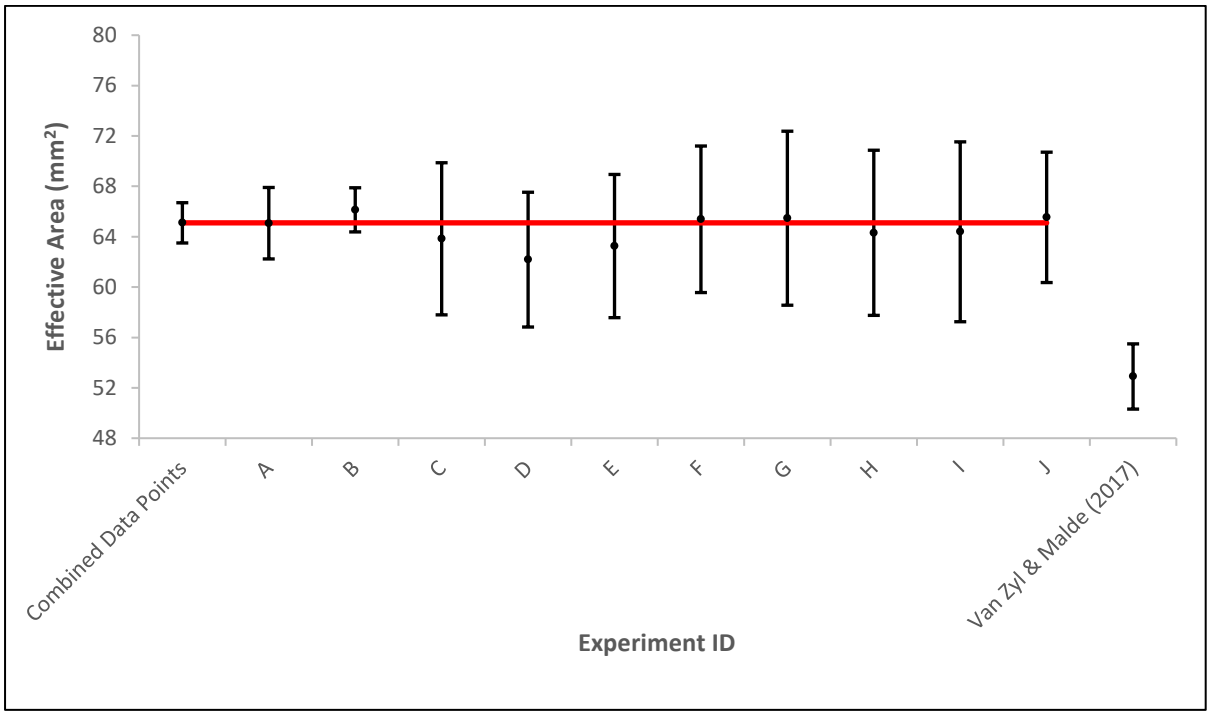

Figure 4-22 - Repeatability analysis of the effective area of the ten 100 mm longitudinal crack tests and comparison with Van Zyl & Malde (2017) results

As shown in Figure 4-21, all individual effective area-head slope values with their respective confidence intervals for the 100 mm longitudinal crack overlap with combined effective area-head slope value and all test results overlapped with each other. The difference in confidence interval width in test A and B is due to the two tests containing 31 data points each, while the rest have only 10 data points.

A similar analysis of the effective areas from the ten conducted tests was done, and the results are graphically shown in Figure 4-22. As with the effective area-head slope parameter shown above, the effective area of the ten tests all overlapped with the combined effective area. The figure thus visually confirms the excellent repeatability of the experiment.

Finally, comparisons between the observed results and Van Zyl and Malde, (2017) results were made. An assessment of the single parameter confidence intervals of the effective area-head slope revealed that the intervals for the two datasets, i.e., this study and Van Zyl and Malde (2017) had an overlap as shown in Figure 4-21. This means for the one test Van Zyl and Malde, (2017) conducted on a 100 mm uPVC longitudinal crack, and its confidence interval was large enough to accommodate the results from this study.

Furthermore, the Van Zyl and Malde, (2017) study overlapped with 9 of the individual tests conducted in this study even though their test had fewer data points.

Figure 4-22 reveals that no overlap exists between the two datasets for the effective area parameter. However, as the two studies had the same leak size, the discrepancy of the figures is believed to be a result of experimental variations. An analysis of the coefficients of discharge reveals that this study has a higher coefficient of discharge (0.643) meaning that the orifice jet for this study is closer to the actual leak area than the Van Zyl and Malde, (2017) study which has a smaller coefficient of discharge (0.529) as shown in Table 4-7.

Table 4-7 - Summary of results and comparison with Van Zyl & Malde (2017) study

	N1	**A_0' (mm^2)**	**95% SPCI for A_0' (mm^2)**	**m' (mm^2/m)**	**95% SPCI for m' (mm^2/m)**	**p for m' (%)**	**C_d**
Van Zyl & Malde (2017)	1.04	52.9	± 2.59	2.51	± 0.129	< 0.1	0.529
This Study	0.959	65.08	± 1.55	2.37	± 0.066	< 0.1	0.643

In their study which involved leakage characterisation using the same method, Nsanzubuhoro et al., (under review) alluded that there might be some consistent error from the Van Zyl and Malde, (2017) dataset or significant differences in pipe and leak properties.

4.2.4 50 mm uPVC Longitudinal Crack

Ten tests were done on the uPVC pipe section with a 50 mm longitudinal crack. The pressure and flow were recorded, and the stabilised steps used to analyse the data. Figure 4-23 shows the pressure and flow relationship at each step in a typical 50 mm longitudinal crack test.

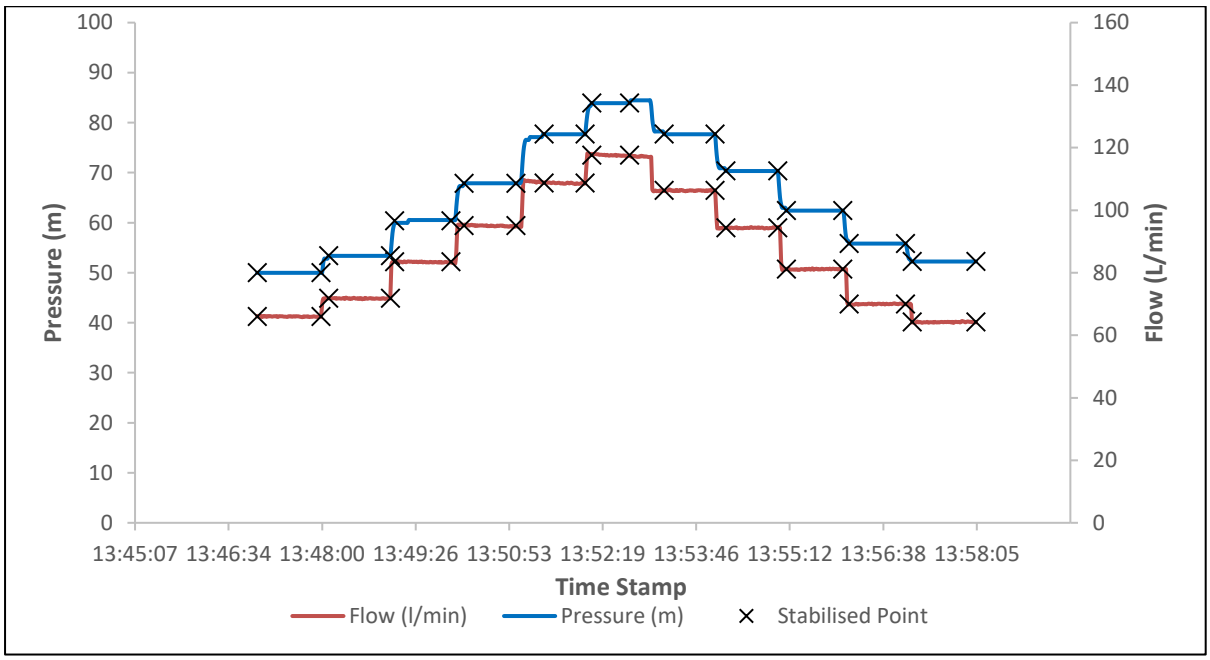

Figure 4-23 - Pressure head-flow rate relationship for a typical test

From the stabilised points, the pressure head and its respective flow rate were plotted, and Figure 4-24 shows the relationship between the two.

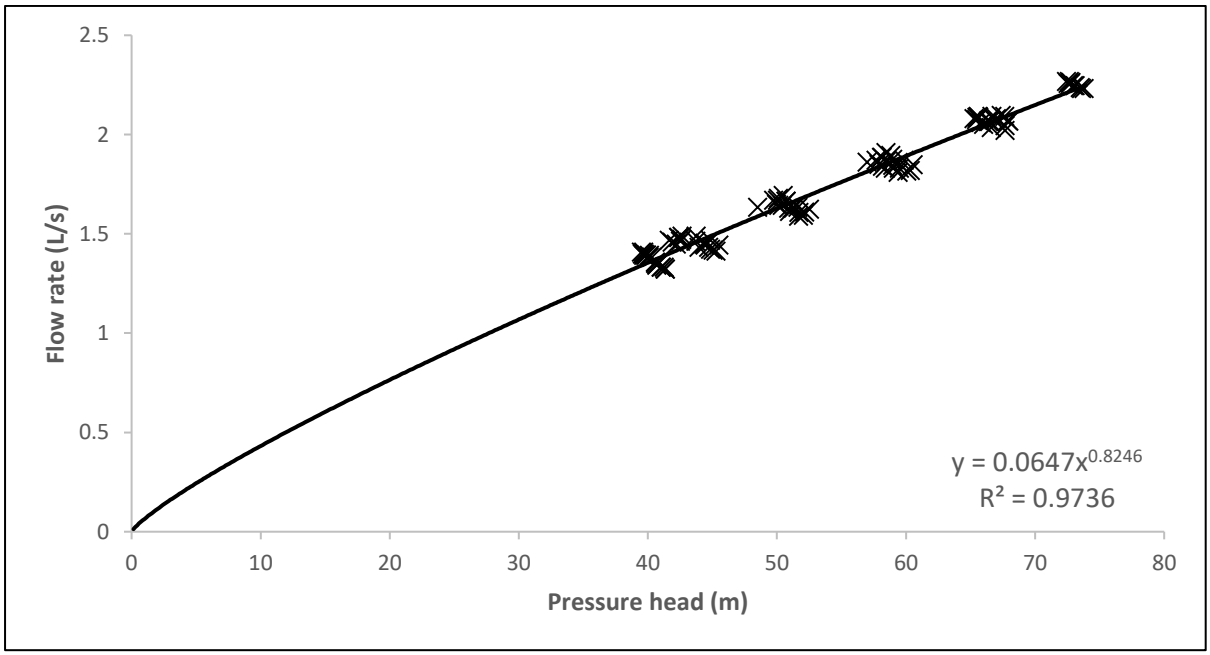

Figure 4-24 - Flowrate-pressure power relationship of a 50 mm longitudinal crack

This relationship between the flow rate and the pressure head is a power relationship and gives the N1 as the exponent of the power relationship. The N1 value for the pipe sample was found to be 0.82 with a standard deviation of 0.005 across all ten tests conducted. The sample variance the N1 values obtained from the ten tests conducted in the laboratory was 2.84E-05 (with is 0.003% of the mean). The small magnitude of the sample variance in relation to the N1 value showed little variance in the tests and represented excellent repeatability and reliability of the conducted tests for the N1 exponent.

The individual tests data points were combined. The effective areas for all combined data points across ten tests were then plotted against their associated pressure heads. Figure 4-25 graphically shows the relationship between the effective area and pressure head.

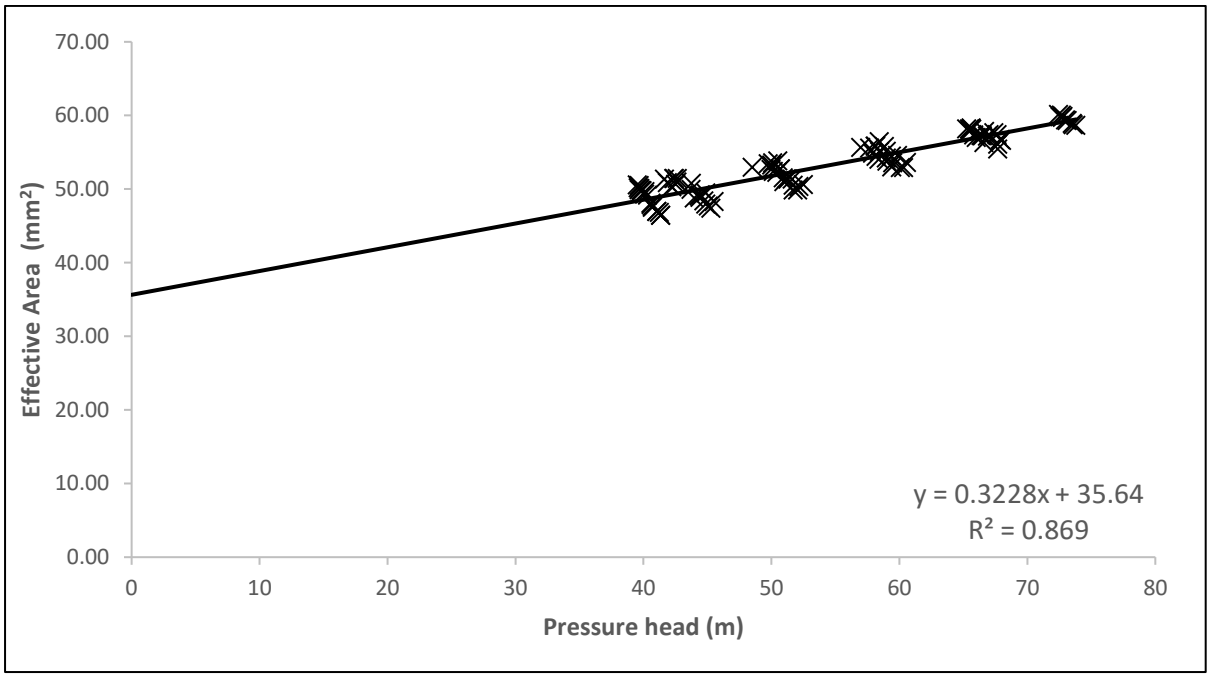

Figure 4-25 - Graph showing the effective area-head slope of a 100 mm uPVC longitudinal crack

For this sample, the effective area-head slope (m') was found to be 0.323 mm^2/m meaning for every meter increment of the pressure head; the orifice area increased by 0.323 mm^2. The simultaneous confidence interval for the effective area-head slope is 0.0239 mm^2/m. The standard deviation of the effective area-head slopes of the ten tests was found to be 0.00429 mm^2/m, while the sample variance which measures how far each test value is from the sample mean was found to be 1.84E-05 mm^2/m. This was a 1.33% deviation from the mean and reports little variance between test values and shows good repeatability in the test.

The flow rate predictions of the FAVAD and N1 equations were compared with the measured data, as shown in Figure 4-26.

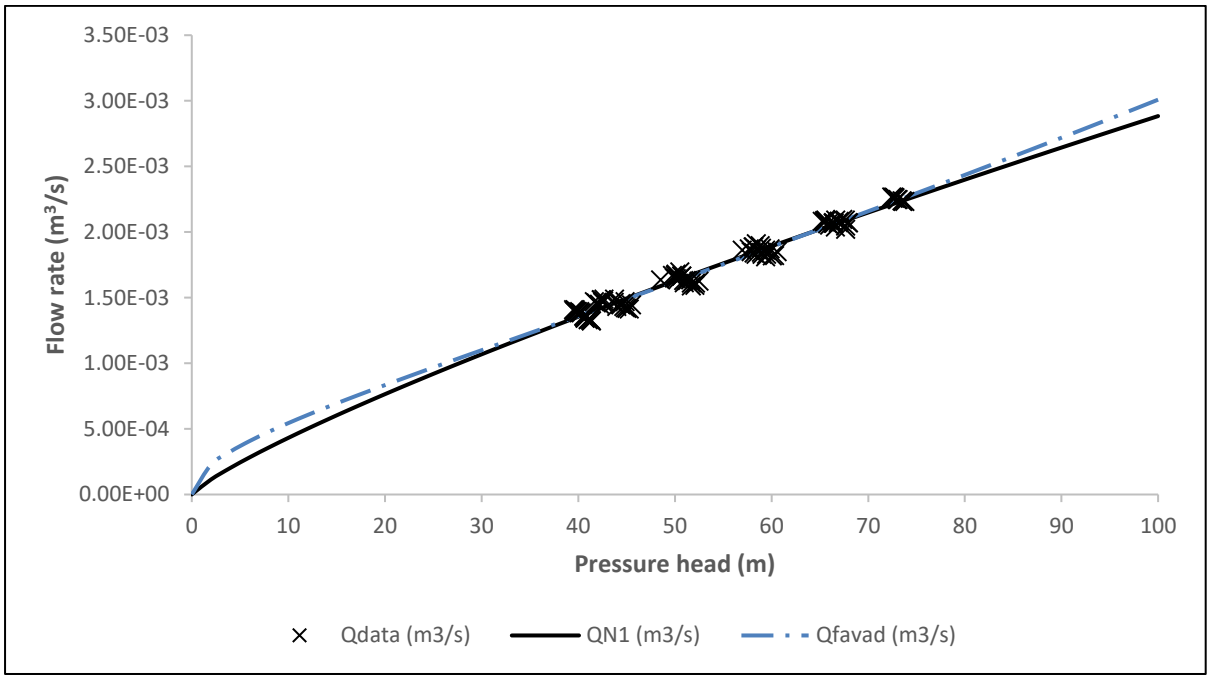

Figure 4-26 - Comparison of the FAVAD and N1 equation flow predictions and observed data

Both models can be seen to fit the data well within the measured pressure range for the 50 mm longitudinal crack. Beyond the measured data range, the two models differ. This difference is due to the N1 equation being an empirical equation that mostly depends on the data and consequently, the pressure range used.

The variation of the 10 test results was analysed, and Table 4-8 shows the summary of the parameters obtained in each of the ten tests conducted for this sample.

Table 4-8 - Summary of results for the ten 50 mm longitudinal crack tests

Experiment ID	A_0' (mm^2)	m' (mm/m)	Cd	N1	c
A	34.7	0.321	0.694	0.832	6.15E-05
B	34.8	0.322	0.697	0.830	6.23E-05
C	35.1	0.324	0.701	0.831	6.24E-05
D	35.5	0.320	0.709	0.824	6.45E-05
E	35.2	0.328	0.704	0.830	6.31E-05
F	35.7	0.328	0.714	0.827	6.44E-05
G	36.0	0.328	0.720	0.825	6.53E-05
H	35.6	0.333	0.712	0.831	6.36E-05
I	36.4	0.321	0.729	0.818	6.73E-05
J	36.3	0.323	0.727	0.818	6.73E-05

The ten test results were also analysed graphically and compared with Van Zyl and Malde, (2017) results. In this comparison, the combined dataset was also included to aid in the repeatability analysis of the ten individual tests. The leakage parameters are visually represented on the graphs below.

Figure 4-27 shows the comparison for combined data points from this study, the individual tests and the Van Zyl and Malde, (2017) study for the effective area parameter.

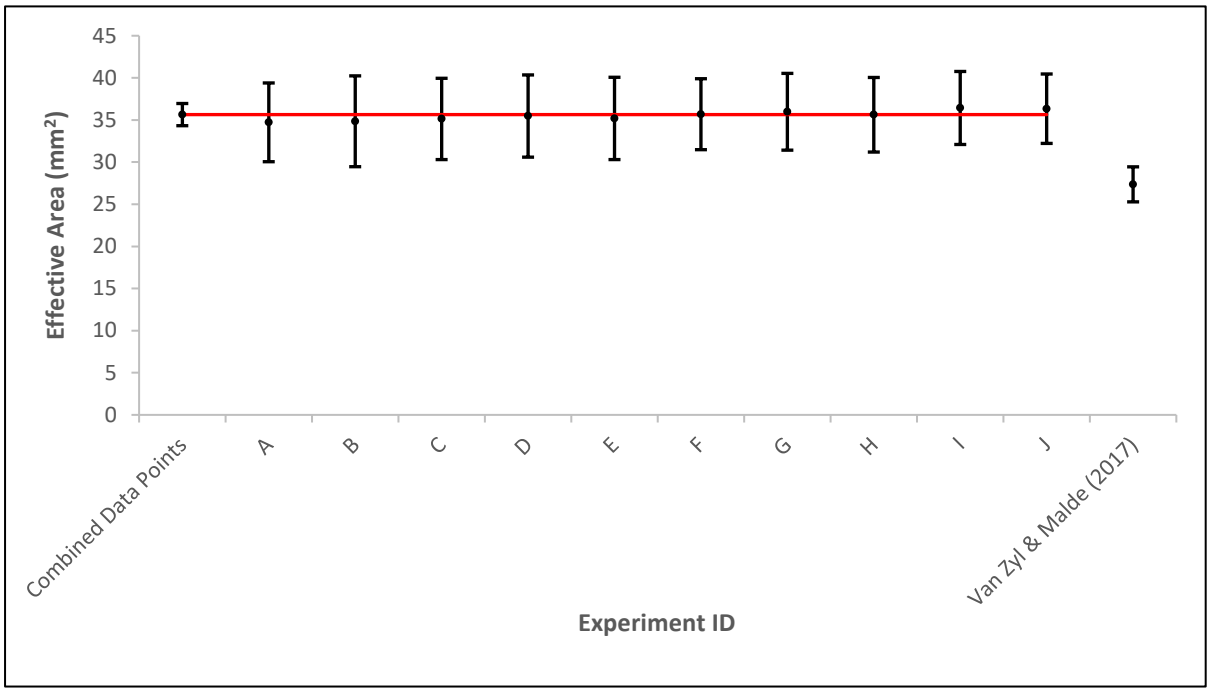

Figure 4-27 - Repeatability analysis of the effective area of the ten 50 mm longitudinal crack tests and comparison with Van Zyl & Malde (2017) results

The effective area values (both the individual and combined datasets) and the Van Zyl and Malde, (2017) study did not overlap. The previous explanation for this difference in the effective area parameter for the two studies in the 100 mm longitudinal crack still holds for the 50 mm longitudinal crack. The effective areas of the ten individual tests are consistent, and all fall within each other's single parameter's confidence intervals. This observation reports good repeatability of the results for this pipe sample.

A similar observation is made from analysing the values and confidence intervals of the effective area-head area slopes of the ten tests. This is shown in Figure 4-28 shows the comparison of the effective area-head slope results from this study for both the combined dataset and individual tests, and the Van Zyl and Malde, (2017) study.

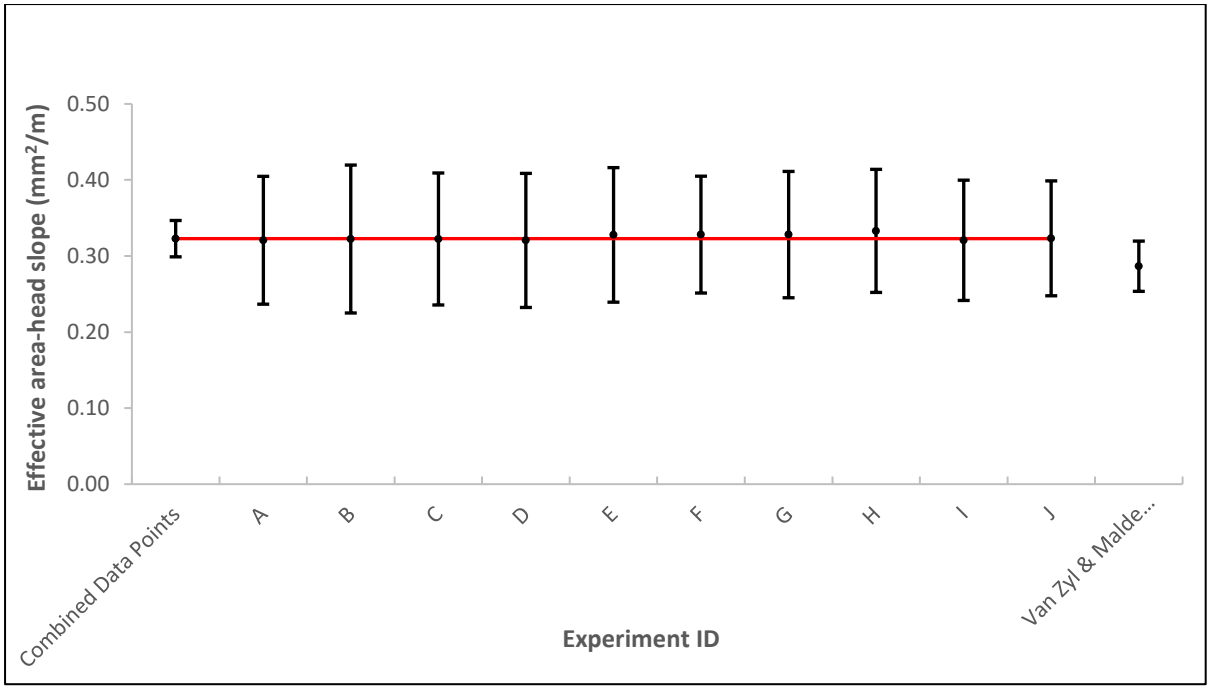

Figure 4-28 - Repeatability analysis of the effective area-head slope of the ten 50 mm longitudinal crack tests and comparison with Van Zyl & Malde (2017) results

Analysing the single parameter confidence intervals revealed that for the effective area-head slopes, the combined dataset value ± SPCI for this study overlapped with the Van Zyl and Malde, (2017) results. The Van Zyl and Malde, (2017) result also overlapped with all ten individual test results. This means the effective area-head slope for the single test Van Zyl and Malde, (2017) conducted on the 50 mm uPVC longitudinal crack exists in the single parameter confidence interval of this study. Table 4-9 shows a summary of the parameters analysed.

Table 4-9 - Summary of results and comparison with Van Zyl & Malde (2017) study

	N1	**A_0' (mm^2)**	**95% SPCI for A_0' (mm^2)**	**m' (mm^2/m)**	**95% SPCI for m' (mm^2/m)**	**p for m' (%)**	**C_d**
Van Zyl & Malde (2017)	0.904	27.37	± 2.08	0.287	± 0.0331	< 0.05	0.54
This Study	0.824	35.6	± 1.32	0.322	± 0.0239	< 0.05	0.71

4.2.5 100 mm uPVC Circumferential Crack

Ten tests were conducted on the uPVC sample with a 100 mm uPVC circumferential crack. The typical pressure and flow rate relationship with time for the tests are shown in Figure 4-29.

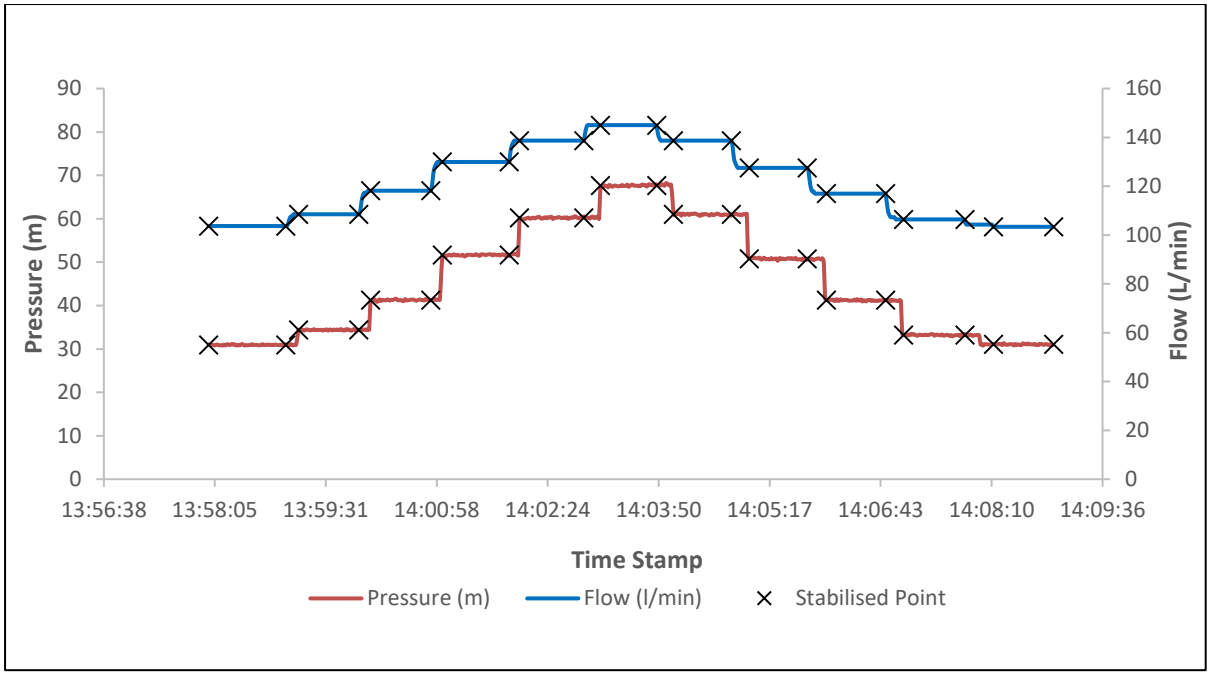

Figure 4-29 - Pressure head-flow rate relationship for a typical test

The stabilised points on each step were used to analyse and characterise the leakage characteristics of the leak opening. From the stabilised points, the pressure head and its respective flow rate were plotted, and Figure 4-30 shows that relationship.

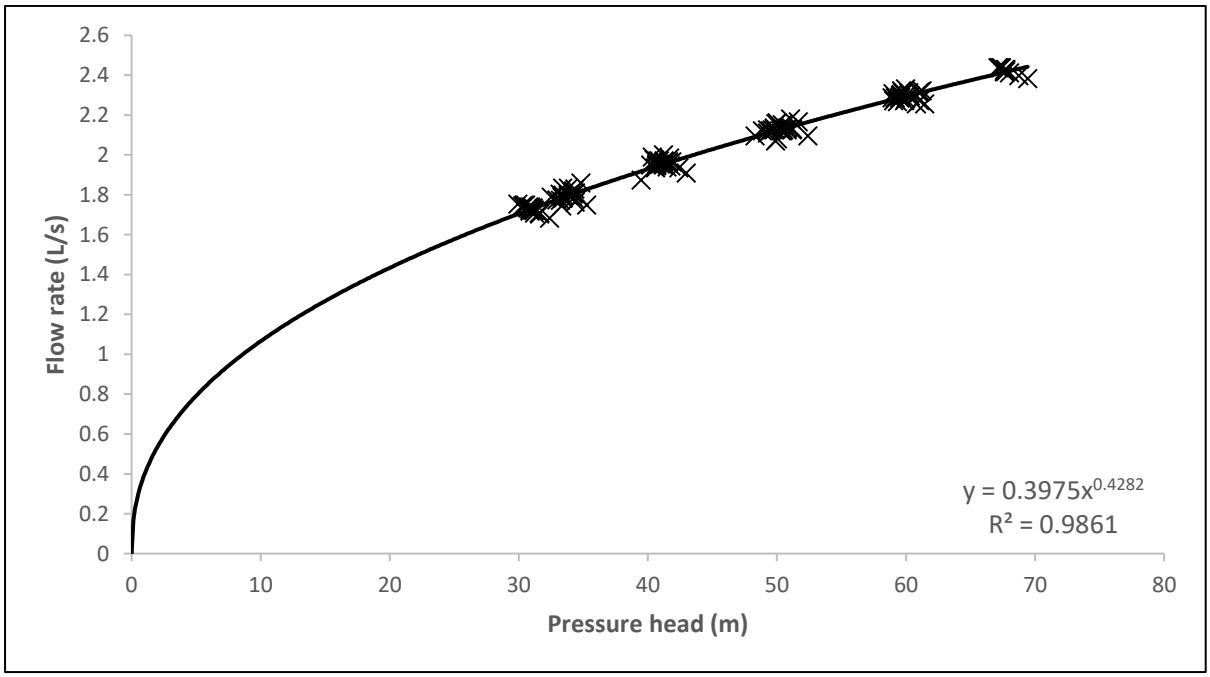

Figure 4-30 - Flowrate-pressure power relationship of a 100 mm circumferential crack

The relationship between the flow rate and the pressure head is a power relationship and gives the N1 as the exponent of the power relationship. The N1 value for the pipe sample was found to be 0.428, with a standard deviation of 0.0083. The sample variance of the N1 values of the ten conducted tests was found to be 6.97E-05 which represents 0.02% of the mean N1 value. This showed little variance in the tests and represented excellent repeatability and reliability of the conducted tests for the N1 analysis.

The effective areas for all data points across ten tests were then plotted against their associated pressure heads. Figure 4-31 graphically shows the relationship between the effective area and pressure head.

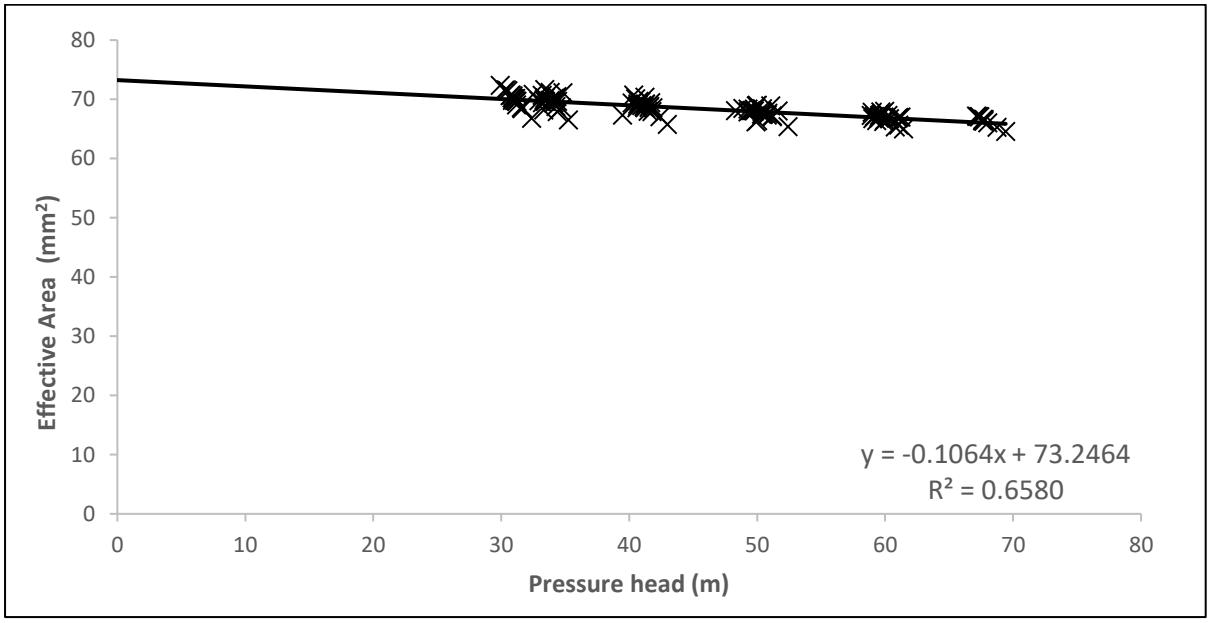

Figure 4-31 - Graph showing the effective head area slope of a 100 mm uPVC circumferential crack

The graph gave negative effective area-head slope (C_dm) of - 0.106 mm^2/m for the pipe sample. Denotating that, for every meter of pressure head the leak area reduced by 0.106 mm^2. Thus, for a circumferential crack, the leak area closes due to the expansion of the pressurised pipe. The standard deviation, across the ten tests, of the effective area-head slope, was found to be 0.0147 mm^2/m. The sample variance of the same parameter, which measures how far each test value's m' is from the sample mean was found to be 0.000216 mm^2/m which is 0.2% of the mean. The 95% simultaneous confidence interval for the effective area-head slope is 0.0134 mm^2/m.

The value of the effective area-head slope reveals that for a 100 mm circumferential crack, there is a negative and significant change in the area with respect to pressure. It further shows

that leak areas for circumferential cracks are more responsive to pressure variations than round holes but less responsive as compared to longitudinal cracks. Nsanzubuhoro et al., (under review) also obtained similar findings. The standard deviation of the initial effective area was found to be 1.58 mm^2/m. The sample variance of the initial effective area, which measures how far each test value is from the sample mean was found to be 2.497 mm^2/m which is 3.4% of the mean effective area. These two statistical values report a considerable variation in the effective initial areas of the tests conducted.

An explanation for this variation was found through the observation of how the initial leak is dependent on the tension in the steel rods in place during the setup for the test which was controlled by how tight the bolts at one end of the rods were bolted on. The nature of the test procedure for the circumferential leak, as explained in section 4.1.4 meant that variation in the results was to be expected. The magnitude of the variation in this case, however, points to the considerable effect the longitudinal stresses have on the circumferential crack leak area. Cassa and Van Zyl, (2013) made a similar observation although from data obtained through finite element modelling. Flow rate predictions of the FAVAD and N1 equations were compared, as shown in Figure 4-32.

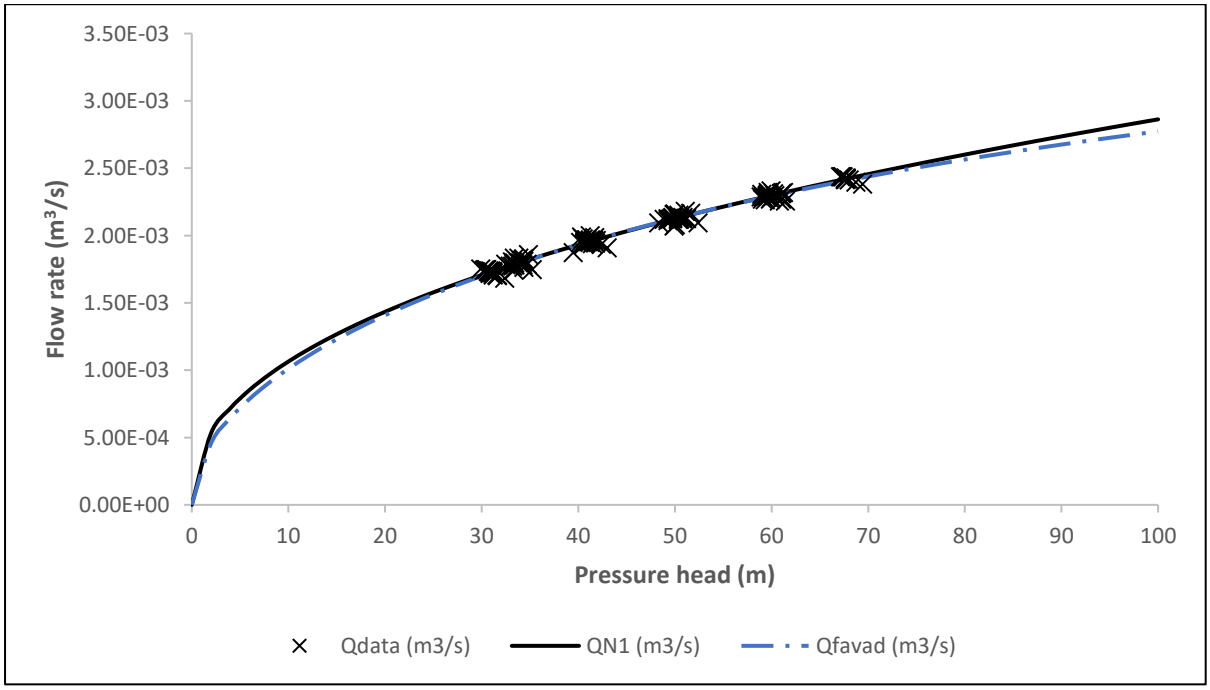

Figure 4-32 - Comparison of the FAVAD and N1 equation flow predictions and observed data

Both models fit the data well within the measured pressure range for the 100 mm uPVC circumferential crack.

The variation of the 10 test results was analysed, and Table 4-10 shows the summary of the parameters obtained in each of the ten tests conducted for this sample.

Table 4-10 - Summary of results for the ten 100 mm circumferential crack tests

Experiment ID	A_0' (mm^2)	m' (mm/m)	C_d	N1	c
A	73.0	-0.101	0.730	0.431	3.93E-04
B	74.0	-0.107	0.740	0.430	3.99E-04
C	70.1	-0.080	0.701	0.443	3.65E-04
D	71.6	-0.096	0.716	0.434	3.83E-04
E	72.5	-0.097	0.725	0.434	3.87E-04
F	75.7	-0.136	0.757	0.411	4.30E-04
G	74.5	-0.117	0.745	0.422	4.11E-04
H	74.1	-0.111	0.741	0.427	4.03E-04
I	72.9	-0.098	0.729	0.434	3.89E-04
J	73.2	-0.103	0.732	0.431	3.94E-04

The ten test results were also analysed graphically and compared with Van Zyl and Malde, (2017) results. In this comparison, the combined dataset was also included to aid in the repeatability analysis of the ten individual tests. The leakage parameters are visually represented on the graphs below. Figure 4-33 shows the comparison for combined data points from this study, the individual tests and the Van Zyl and Malde, (2017) study for the effective area parameter.

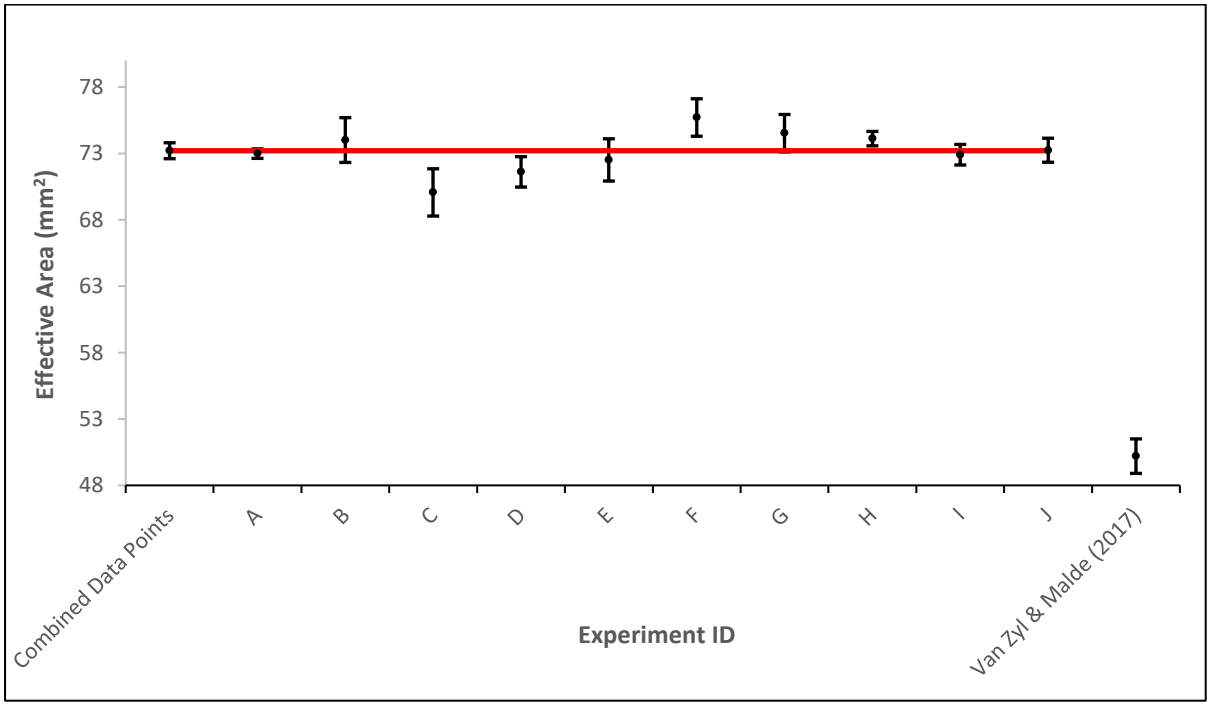

Figure 4-33 - Repeatability analysis of the effective area of the ten 100 mm circumferential crack tests and comparison with Van Zyl & Malde (2017) results

The effective area values from the two studies considering both the combined dataset and ten individual tests did not overlap. This variability was explained earlier on in this section. All individual effective area-head slope values for the circumferential crack were found to contain the combined effective area-head value and overlapped with one another, thus showing good repeatability. It was also observed that there was more variance in the effective area parameter, as suggested by the earlier reported statistical analysis. This is an effect of the inconsistent tightening of the steel rods after each test such that some leak areas were initially smaller than the original machined leak area. Interestingly, this variation is not observed in the effective area-head slope values. This can be seen in Figure 4-34 which shows the comparison for combined data points from this study, the ten individual tests and the Van Zyl and Malde, (2017) study for the effective area-head slope parameter. This informs that, for this sample, the effective area-head slope might not be greatly dependent on the initial leak size.

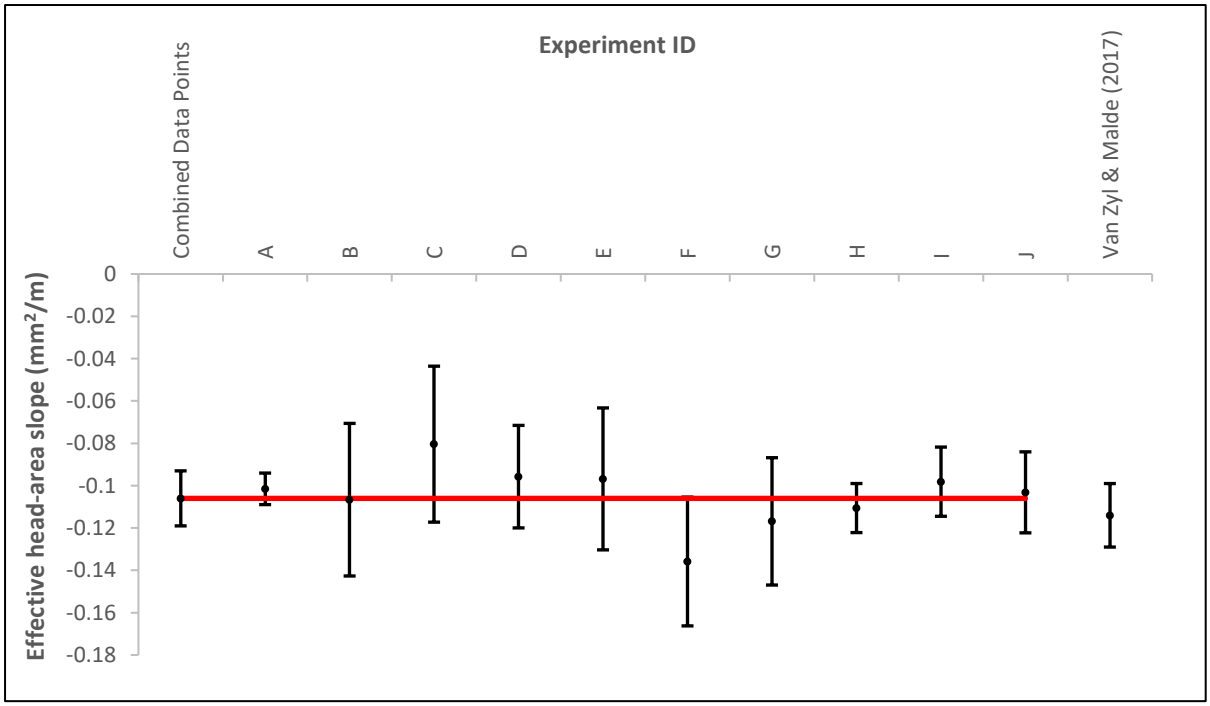

Figure 4-34 - Repeatability analysis of the effective area-head slopes of the ten 100 mm circumferential crack tests and comparison with Van Zyl & Malde (2017) results

Unlike the effective area-head slope, the effective area parameter was found to be different, as shown in Figure 4-34. Three of the effective area values with their 95% confidence intervals were found to be inconsistent with the combined effective area as there was no overlap of the single parameter confidence intervals.

Analysing the single parameter confidence intervals revealed that for the effective area-head slope, the results ± SPCI for this study overlapped with the Van Zyl and Malde, (2017) results.

Correspondingly, the Van Zyl and Malde, (2017) SPCI also overlap with this study's results. Additionally, the Van Zyl and Malde, (2017) result overlapped with all ten of the individual tests conducted in this study.

This means the effective area-head slope for the single test Van Zyl and Malde, (2017) conducted on the 100 mm uPVC circumferential crack exists in the single parameter confidence interval of this study. Table 4-11 then shows a summary of the parameters analysed.

Table 4-11 - Summary of results and comparison with Van Zyl & Malde (2017) study

	N1	**A_0' (mm^2)**	**95% SPCI for A_0' (mm^2)**	**m' (mm^2/m)**	**95% SPCI for m' (mm^2/m)**	**p for m' (%)**	**C_d**
Van Zyl & Malde (2017)	0.327	50.2	± 1.28	- 0.114	± 0.0189	< 0.05	0.502
This Study	0.429	73.2	± 0.63	- 0.106	± 0.013	< 0.05	0.732

4.2.6 50 mm uPVC Circumferential Crack

Ten tests were done on the uPVC pipe section with a 50 mm circumferential crack. Figure 4-35 shows the pressure and flow relationship at each step in a typical test. These were recorded, and the stabilised steps were then used to analyse the determine the leak characteristics.

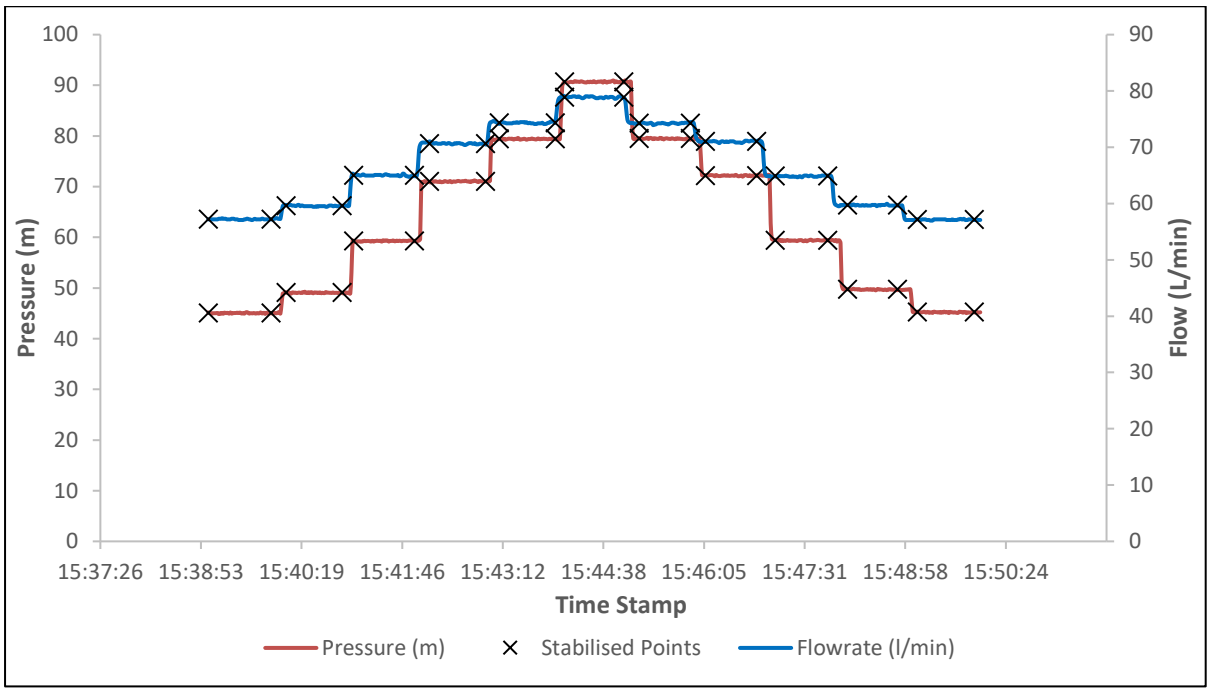

Figure 4-35 - Pressure head-flow rate relationship for a typical test

From the stabilised points, the pressure head and its respective flow rate were plotted, and Figure 4-36 shows the relationship between the two.

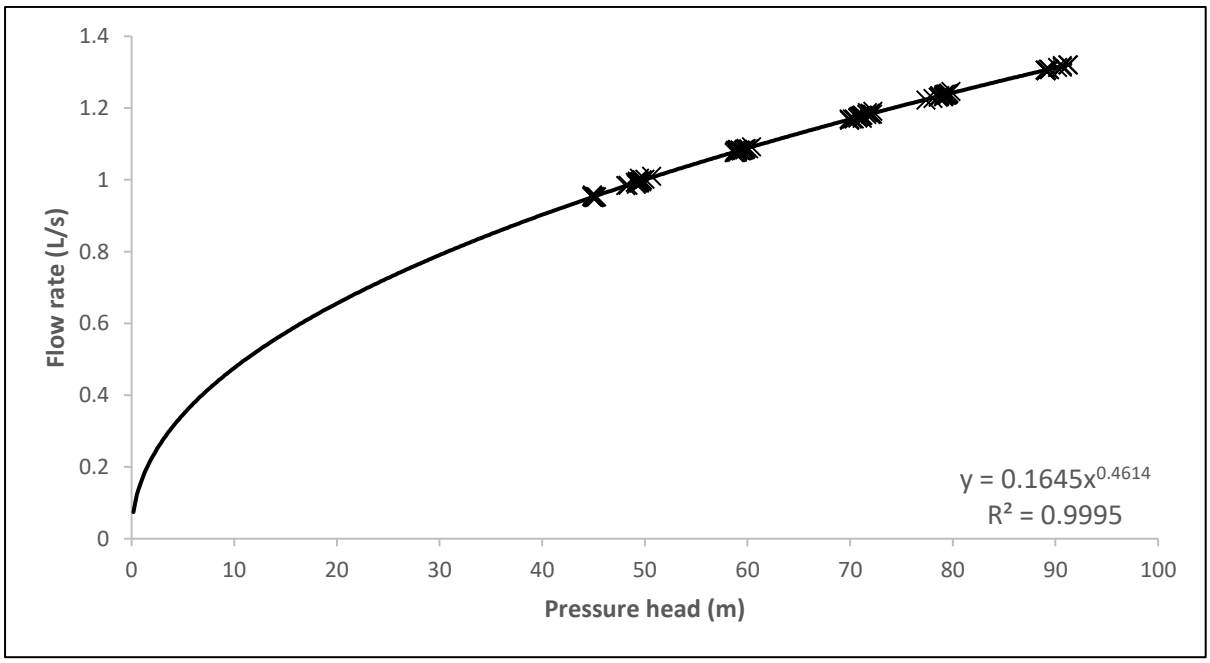

Figure 4-36 - Flowrate-pressure power relationship of a 50 mm circumferential crack

This relationship between the flow rate and the pressure head is a power relationship and gives the N1 as the exponent of the power relationship. The N1 value for the pipe sample was found to be 0.461, with a standard deviation of 0.0019 across all ten tests conducted. The sample variance the N1 values obtained from the ten tests conducted in the laboratory was 3.60 E-06 (with is 0.78E-03% of the mean). The small magnitude of the sample variance in relation to the N1 value showed little variance in the tests and represented excellent repeatability and reliability of the conducted tests for the N1 exponent.

The individual tests data points were then combined, and the effective areas for all combined data points across ten tests were plotted against their associated pressure heads. Figure 4-37 graphically shows the relationship between the effective area and pressure head.

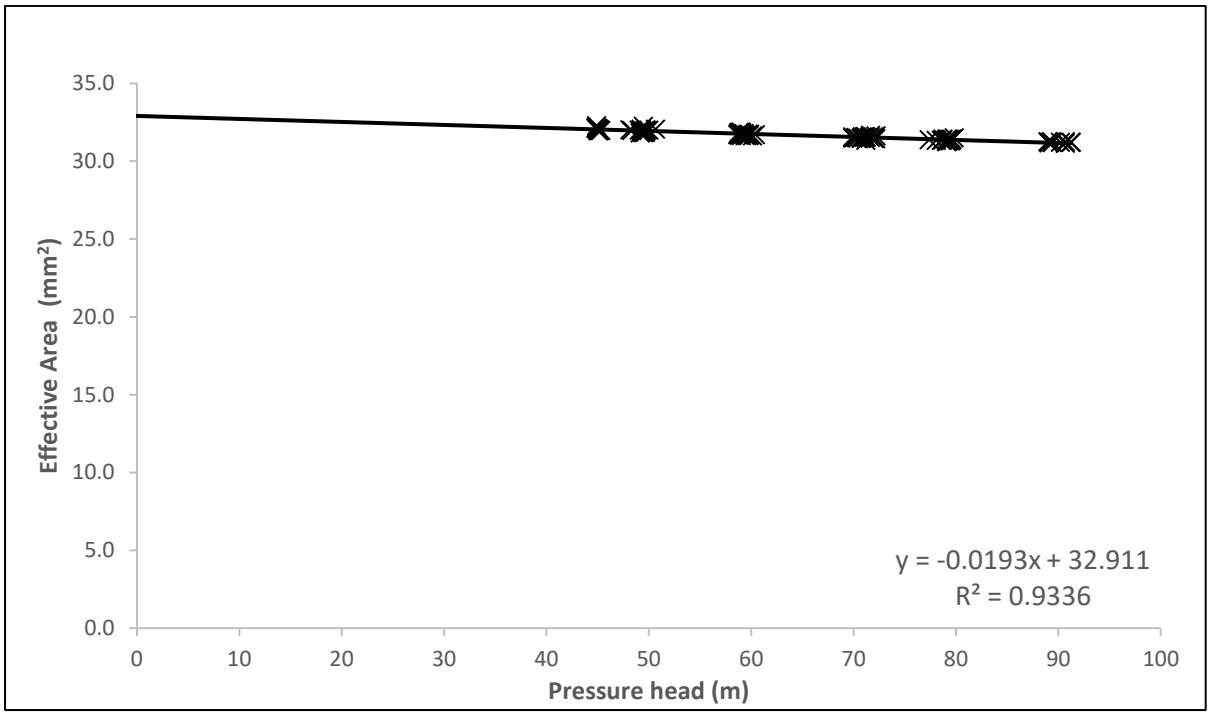

Figure 4-37 - Graph showing the effective head area slope of a 50 mm uPVC circumferential crack

For this sample, the effective area-head slope was found to be - 0.0193 mm^2/m meaning for every meter increment of the pressure head; the orifice area decreased by 0.0193 mm^2. The single parameter confidence interval for the effective area-head slope is 0.0304 mm^2/m. The standard deviation of the effective area-head slopes of the ten tests was found to be 0.00149 mm^2/m, while the sample variance which measures how far each test value is from the sample mean was found to be 2.24E-06 mm^2/m. This was a 0.01% deviation from the mean m' and reports little variance between test values and shows excellent repeatability in the test.

The flow rate predictions of the FAVAD and N1 equations were then compared with the measured data, as shown in Figure 4-38.

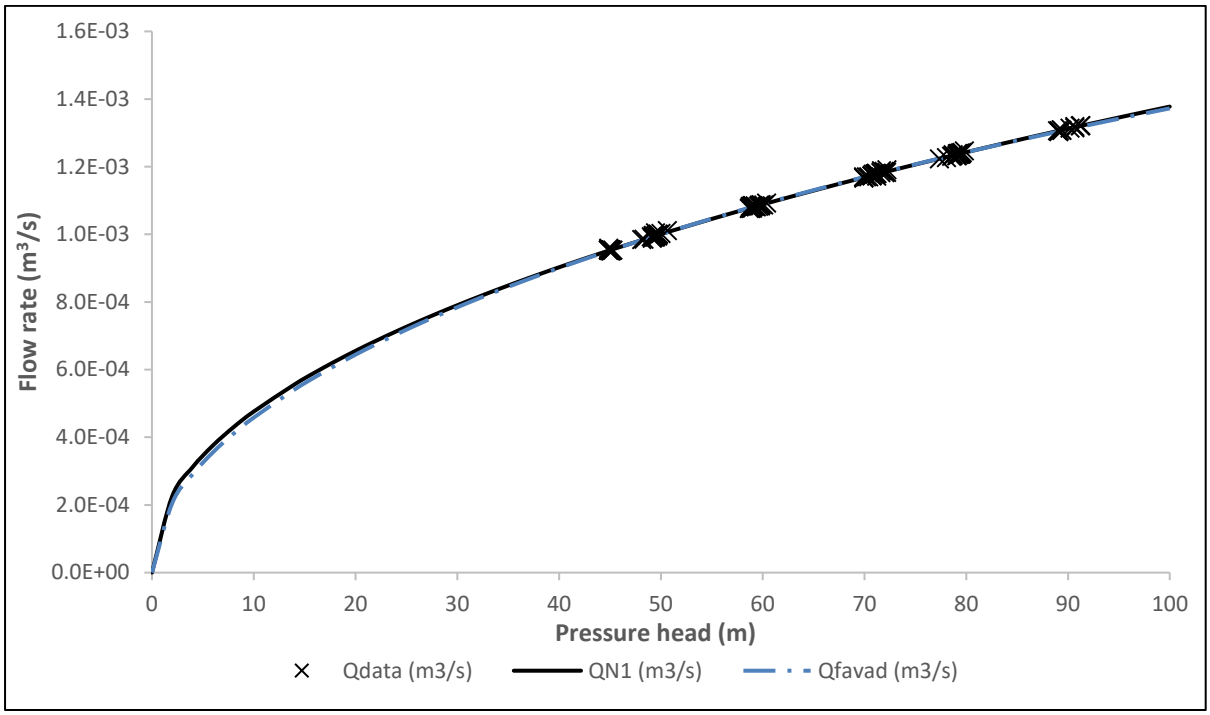

Figure 4-38 - Comparison of the FAVAD and N1 equation flow predictions and observed data

Both models can be seen to fit the data well within the measured pressure range. The relationship cannot be established beyond the measured data range, as it exceeds the maximum pressure rating of the pipe.

The variation of the 10 test results was analysed, and Table 4-12 then shows the summary of the parameters obtained in each of the ten tests conducted for this sample.

Table 4-12 - Summary of results for the ten 50 mm circumferential crack tests

Experiment ID	A_0' (mm^2)	m' (mm/m)	N1	C_d	c
A	33.0	-0.0208	0.459	0.66	0.00017
B	32.8	-0.0169	0.467	0.66	0.00016
C	33.1	-0.0223	0.456	0.66	0.00017
D	32.9	-0.0185	0.463	0.66	0.00016
E	33.0	-0.0204	0.459	0.66	0.00017
F	32.9	-0.0187	0.463	0.66	0.00016
G	32.9	-0.0187	0.463	0.66	0.00016
H	32.9	-0.0186	0.463	0.66	0.00016
I	32.9	-0.0195	0.461	0.66	0.00016
J	32.9	-0.0190	0.462	0.66	0.00016

The ten test results were also analysed graphically and compared with Van Zyl and Malde, (2017) results. In this comparison, the combined dataset was also included to aid in the repeatability analysis of the ten individual tests. Figure 4-39 shows the comparison for combined data points from this study, the individual tests and the Van Zyl and Malde, (2017) study for the effective area parameter.

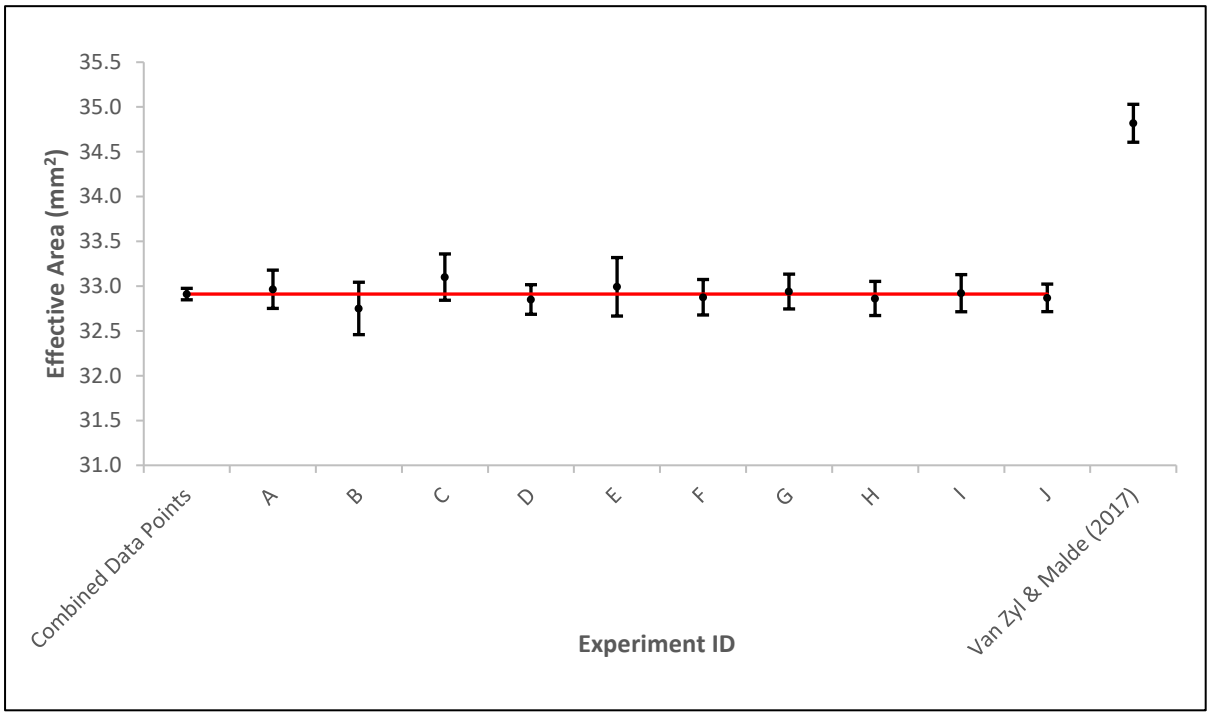

Figure 4-39 - Repeatability analysis of the effective area of the ten 50 mm circumferential crack tests and comparison with Van Zyl & Malde (2017) results

The effective area values from the two studies considering both the combined dataset and ten individual tests did not overlap. This variability could be due to different material and leak properties from the two studies. Additionally, the difference could be due to different forces values used on the longitudinal steel rods, which were identified as having a significant effect on the leakage parameters. All individual effective area-head slope values for the circumferential crack were found to contain the combined effective area-head value and overlapped with one another. The figure thus visually confirms the good repeatability of the experiment.

As with the 100 mm circumferential crack, this variation is not observed in the effective area-head slope values. This can be seen in Figure 4-40 which shows the comparison for combined data points from this study, the ten individual tests and the Van Zyl and Malde, (2017) study for the effective area-head slope parameter.

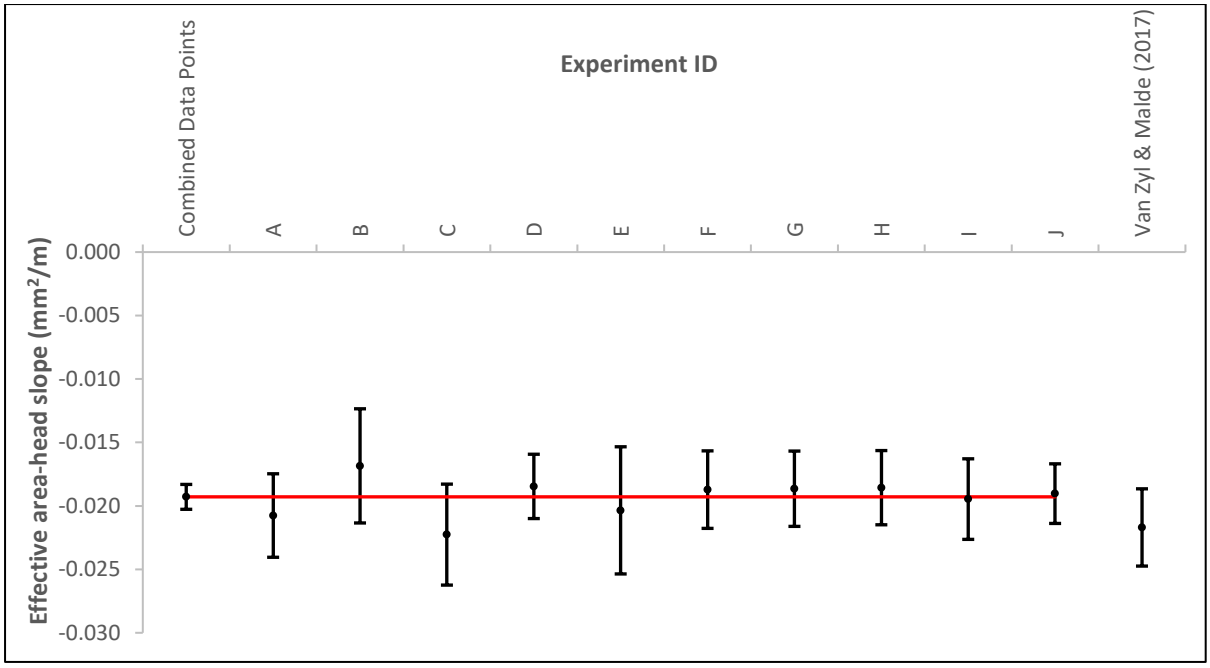

Figure 4-40 - Repeatability analysis of the effective area-head slope of the ten 50 mm circumferential crack tests and comparison with Van Zyl & Malde (2017) results

As with the effective area parameter, the effective area-head slope of the ten tests all overlapped with the combined effective area this is visually represented in the previous graph. Further analysis of the single parameter confidence intervals revealed that for the effective area-head slope, the results ± SPCI for this study overlapped with the Van Zyl and Malde, (2017) results. Correspondingly, the Van Zyl and Malde, (2017) SPCI also overlap with this study's results. This means the effective area-head slope for the single test Van Zyl and Malde, (2017) conducted on the 50 mm uPVC circumferential crack exists in the single parameter confidence interval of this study. Table 4-13 then shows a summary of the parameters analysed

Table 4-13 - Summary of results and comparison with Van Zyl & Malde (2017) study

	N1	**A_0' (mm^2)**	**95% SPCI for A_0' (mm^2)**	**m' (mm^2/m)**	**95% SPCI for m' (mm^2/m)**	**p for m' (%)**	**C_d**
Van Zyl & Malde (2017)	0.455	34.8	± 0.212	- 0.0217	± 0.00304	< 0.05	0.696
This Study	0.461	32.9	± 0.064	- 0.0193	± 0.0304	< 0.05	0.658

4.3 Chapter Summary

To fulfil the first objective of this study which was to calibrate the Pipe Condition Assessment Device (PCAD), six uPVC pipes with individual leaks of varied sizes and types, were tested using an experimental but standardised method. The leakage parameters and characteristics thereof were analysed and compared to expected results.

The aim was to ascertain if it would be possible to replicate the results obtained in an earlier study by Van Zyl and Malde, (2017) within an acceptable statistical confidence region. In the initial study by Van Zyl and Malde, (2017) one test was done per sample where a test consisted of increasing the pressure in 5 pressure steps (increments) and decreasing the pressure by the same magnitude with five decrements. This was done thrice, in succession. For this study, ten tests were done per pipe sample. This was done to establish the repeatability of the tests, with ten tests rather than one. Furthermore, the setup used was modified for ease of use.

The results displayed above revealed that for all six samples, the tests had excellent repeatability, which was inferred from the minimal deviations and sample variance, with the notable exception of the circumferential crack. This exception was explained as being due to the sensitivity of the circumferential leak to longitudinal stresses. It is recommended that for a more standardised method of assessing leakage parameters of circumferential cracks and possibly other leak types there is need to account and record the torque used to fasten the bolts that keep the steel rods in place such that a uniform set of results are obtained and can be replicated.

The effective area-head slope (m’), which was deemed to be the parameter of importance as it helps identify was the type of leak is on a pipe, was analysed for all six samples. Of importance in the analyses was whether the 95% single parameter confidence regions obtained in this study overlapped with the range obtained by Van Zyl and Malde, (2017).

For the 12 mm round hole, it was found that the 95% SPCI did not overlap. However, the values of the effective area head slope were small and close to zero, which was expected and revealed that the tests were able to characterise the leakage parameter effectively for the leak type. The lack of overlap was explained by that the study conducted by Van Zyl and Malde, (2017) only had one test and as such the repeatability of the study was not established; thus, the values could have been outside the range even at a 95% confidence interval as more observations tend to reduce the width of the confidence region. It is therefore believed that the values from this

study that were obtained from more data points, with more tests, and a higher coefficient of discharge is more accurate and show good repeatability.

As above, an analysis of the 6 mm uPVC round hole was conducted and these tests revealed that there was low variance in the results for the m', A_0' and N1 parameters. The obtained m' was also found to be a small negative value that can practically be referred to as a zero-grade line. However, a t-test to check if the line was statistically zero revealed that within a 95% level of confidence, the line is statistically not zero. This test revealed that the experiment is repeatable with all the ten tests overlapping for all the m' and A_0' parameters.

In like manner, the results for the 100 mm uPVC longitudinal crack were analysed with importance being laid on the m' parameter. The m' values obtained were as expected with a larger change in area due to pressure, the same inference had been made in the study by Van Zyl and Malde, (2017) and Nsanzubuhoro et al., (under review),. As with the 12 mm round hole, the 95% single parameter confidence intervals were compared, and the results showed that the SPCI in the Van Zyl and Malde, (2017), the study contained the values for m' but the SCI from this study did not contain the m' range obtained by Van Zyl and Malde, (2017). However, an overlap of the confidence intervals exists. This overlap is due to the large SCPI on the Van Zyl and Malde, (2017). This value of the confidence interval informed that the Van Zyl and Malde, (2017) experiment had more variance in results as compared to this study, which, and had fewer data points.

The 50 mm longitudinal crack tests also showed good repeatability with all the 95% confidence intervals if the tests conducted overlapping. The rate of leak expansion was also appreciably significant as expected for a longitudinal crack

An analysis of the results obtained in the tests for the 100 mm uPVC circumferential crack revealed that the effective area-head slope for one test Van Zyl and Malde, (2017) conducted exists in the simultaneous confidence interval of this study and that the 95% SPCI for both studies overlap.

In all the samples tested in this study, the sample variance of the effective area-head slope was small for the (less than 0.001 mm^2/m). Statistical inference theories state that; the higher the variance, the more heterogeneous a parameter is, and the smaller the variance, the more homogeneous is it. When the variance is zero, it implies that all the values are equal. Thus, for this study, the sample variances revealed that the data (which is the obtained effective area-head slopes) were homogenous and therefore, the tests had good repeatability.

However, as stated above, when the sample variance of the effective area of the circumferential crack was analysed, it was found that the sample variance was large and therefore, more heterogeneous.

There also was a discrepancy in the number of collated data points for the six tests which stem from the various observations made with each test. These observations included the effect the magnitude of the torque used to tighten the bolts that kept the steel rods in place, on the circumferential crack parameters. These observations warranted more data points to be collected under different conditions for the same sample to get a better average of the leakage parameters.

In all the sample tests, it was noted that there was a significant difference in the coefficient of discharges, and this can be explained by several factors. Firstly, the orifices for the two studies were manufactured differently, with this study employing drilling with a steel drill bit and the Van Zyl and Malde, (2017) study employing water jets. The different procedures could produce variations at the edges of the leak opening, which alter the coefficient of discharge. Additionally, the variations can also be attributed to the leak areas not being precisely the dimensions specified because of the limitations of the drilling equipment used and human error. Likewise, it is possible that the thickness of the pipe materials used in the two studies was significantly different, and this could also explain the differences in the coefficient of discharges obtained.

To summarise this discussion, the results from this study show excellent repeatability of the parameters obtained using the standardised method developed by Van Zyl and Malde, (2017). The results also show that the standardised method can be replicated to obtain leakage parameters and that the results obtained are repeatable. While there are some notable variations in some of the leakage parameters obtained in the two studies, they have been explained in this discussion as far as possible.

The next chapter will now discuss the results of the additional tests that were required to establish a baseline for evaluating the PCAD's efficacy and reliability.

5 LEAKAGE CHARACTERISATION WITH THE STANDARDISED METHOD AT LOWER PRESSURES

After the tests on the six samples had been conducted, a trial test on the 12 mm round hole sample was conducted with the PCAD. This was to evaluate whether the results from the samples tested using the standardised method were comparable with the PCAD derived leak characteristics. It was found that the PCAD pump was unable to deliver pressure values like the ones used in characterising the leaks in Chapter 4. Therefore, tests on three samples at pressure ranges compatible with the PCAD capabilities were conducted. The exercise undertaken to establish this finding is described below.

5.1 Trial Test on 12 mm uPVC round hole with PCAD

Results from the PCAD trial tests conducted on the 12 mm round hole were found to be inconsistent with the expected results. It was initially was suspected that the instrumentation could be the source of the discrepancies. As a result, external instrumentation (the same setup that was used to calibrate the device flow meter and pressure sensor) was used to record the data while a leak test was conducted via the PCAD.

The test produced only five stabilised points due to the high flow rate and long stabilisation times. Figure 5-1 shows the flow and pressure data for one of the tests.

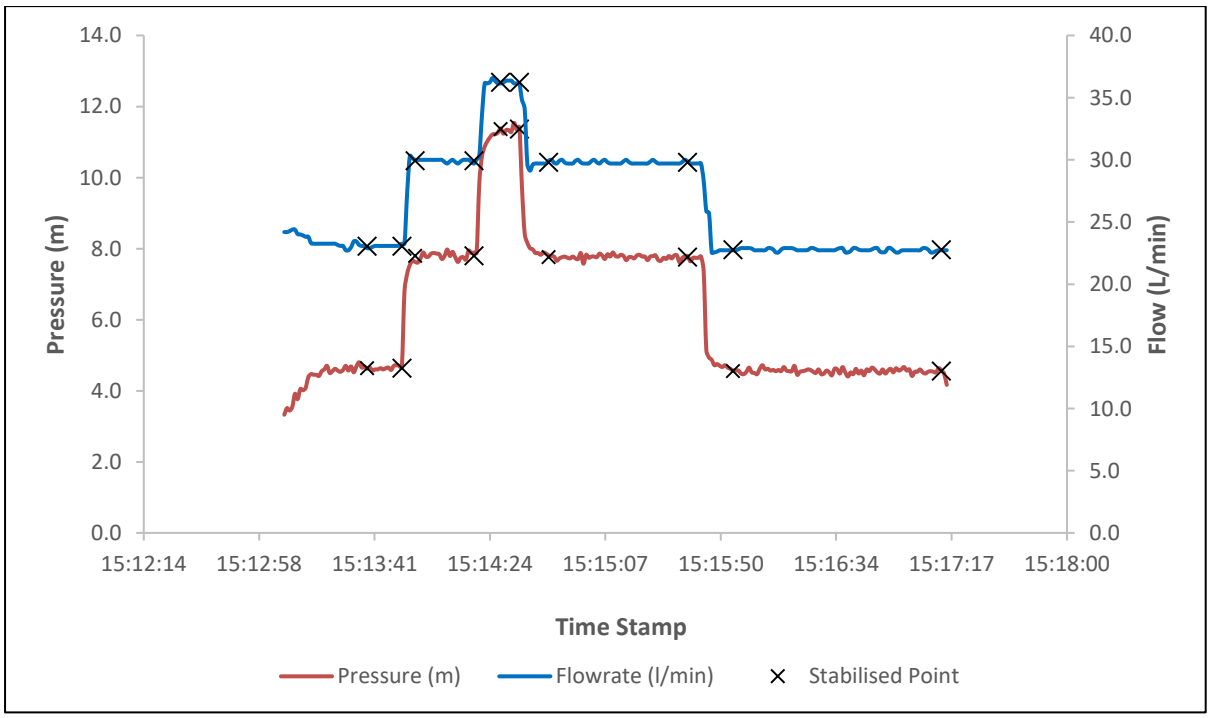

Figure 5-1 - Pressure head-flow rate relationship for a test on a 12 mm round hole using the PCAD

The data from the test conducted using the PCAD show that the pressure was low, compared to the pressure values obtained using the laboratory equipment.

The effective area-head slope for the test was found to be 0.0341 mm^2/m, which is a positive value that is 5.4 times the value obtained using laboratory equipment and out of the range of values expected. In addition, the effective area, shown in Figure 5-2, was found to be 40.04 mm^2, with a coefficient of discharge of 0.36, which communicated that there were significant variations in the orifice opening.

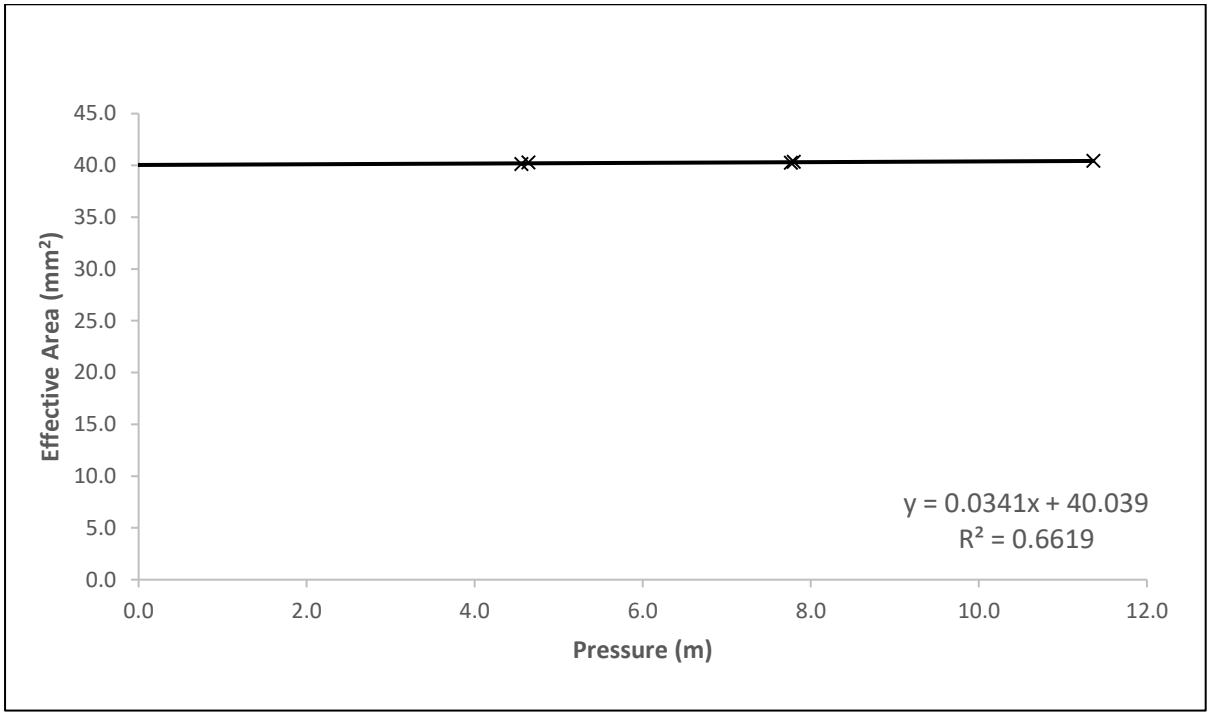

Figure 5-2 - Graph showing the effective area-head slope of a 12mm uPVC round hole with PCAD

The source of these variations was investigated, and since the pipe sample was exactly the sample used in the previous tests, the dimensions were not expected to be the source of the error. Nonetheless, the orifice opening was measured again, and the opening checked to investigate if the integrity of the orifice had been compromised.

Next, the code of the device was checked and debugged, and no error was found. The final check was then the device instrumentation. The flow meter and pressure sensor were tested to inspect if they still functioned as expected. The leak test was also conducted with external instruments to compare with the device instrumentation.

Finally, the pump in the PCAD was investigated. The first check was to verify if the pump was operating at 100% power output. This was done by opening the side panel on the PCAD and

viewing the pump controller, and the pump found to be the operating as expected. Next, the pump curve of the pump accounting for the losses in the system was considered, and it was found that the maximum pressure the pump can deliver at 100% power was 39.2 m.

The system curve, which was the orifice equation for the 12 mm round hole, was also drawn on the same curve. For the 12 mm round hole and larger orifice areas, the pump was found to be working off its curve, which explained the comparatively low pressures observed during the trial tests. The parameters used to obtain the head losses, and system curves are found in Table 5-1. The orifice equation was used to model the system characteristics. A coefficient of discharge of 0.61 was used as it was the value obtained in the laboratory tests.

Table 5-1 - Parameters used to determine system and pump curves

Parameter	**Value**
C_d	0.61
Orifice diameter (m)	0.012
Orifice area (m^2)	0.000113097
k_L (tee threaded)	0.9
K_L (elbow threaded 90)	1.5
ν (m^2/s)	1.14E-06
ε (mm)	0.000075

Water was pumped from the PCAD tank at different pressure heads and flow rates using the device pump, and those values were recorded. The Reynolds number and subsequent head losses were calculated and shown in Table 5-2 with the friction factor, f, being found through the application of the Haaland equation found in most hydraulics textbooks such as Chadwick, Morfett and Borthwick, (2013).

Table 5-2 - PCAD pump characteristics

Q (m^3/h)	**H (m)**	**Re**	**f**	**H_f (m)**	**H_L (m)**	**Total loss (m)**	**True H (m)**
0	39.2	0.000	0.000	0.000	0.000	0.000	39.2
0.22	37.9	3350.6	0.043	0.004	0.007	0.011	38.0
0.54	35.7	8376.6	0.033	0.019	0.045	0.064	35.8
1.33	27.6	20662.2	0.026	0.092	0.276	0.368	27.9
1.98	17.5	30714.1	0.023	0.185	0.609	0.794	18.3
2.38	10.5	36856.9	0.022	0.256	0.877	1.133	11.6
2.45	9.86	37973.8	0.022	0.269	0.931	1.201	11.1

As the pressure logger was located after the pump and there were bends and friction losses in the pipes connecting the two, the head loss was added on the obtained pressure from the logger to obtain the real head from the pump.

Figure 5-3 then shows the pump curves obtained from the manufacturer and the laboratory exercise described above.

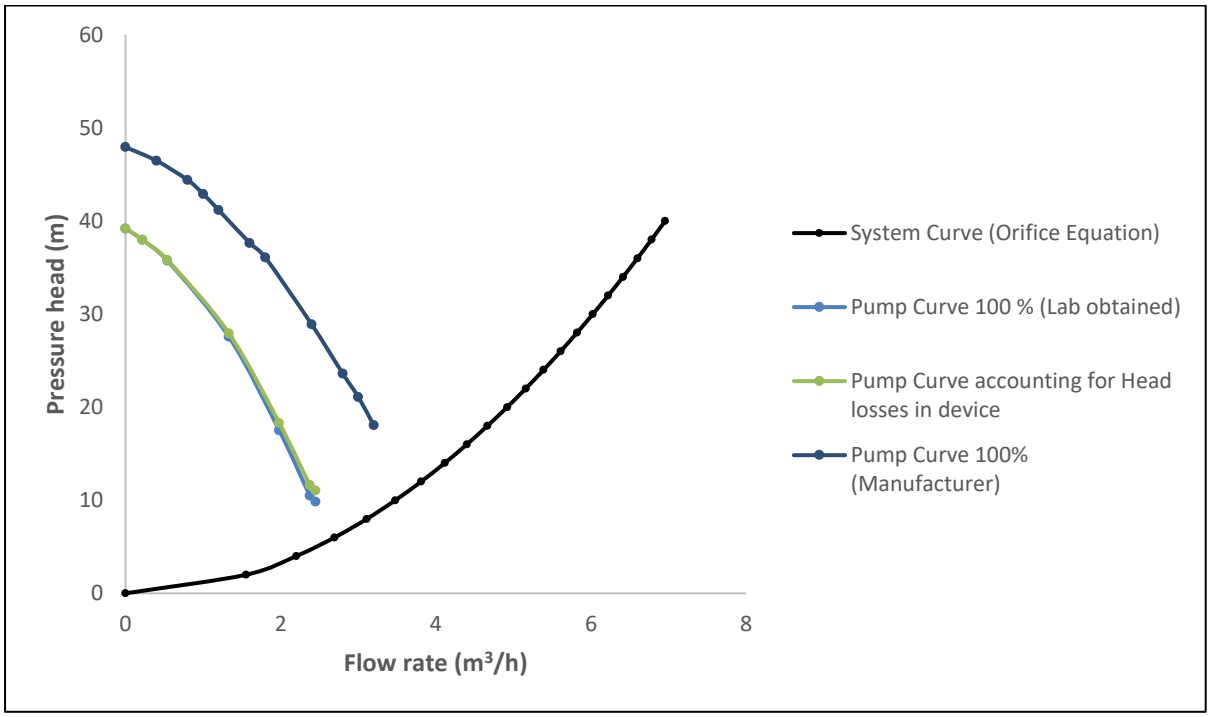

Figure 5-3 - Pump curves for PCAD and the 12 mm round hole characteristic curve

The laboratory-derived curve has a lower maximum achievable pressure value as compared to the manufacturer, and this is believed to be due to the pump speed being controlled by the microprocessor which could be deliberately supplying less power to the pump, to prevent it from burning out. From the curves, it was determined that the 12 mm round hole was too large for the device pump to characterise.

This finding revealed one limitation of the device. The curves were then used to determine the size of the leaks to be used to establish the repeatability and reliability of the PCAD results. From the derived pump curves, a 6 mm round hole, 50 mm longitudinal crack, and 50 mm circumferential cracks were chosen as their system curves intersected with the pump curve.

Figure 5-4 shows how the 6mm round hole system curve intersects with the pump curve.

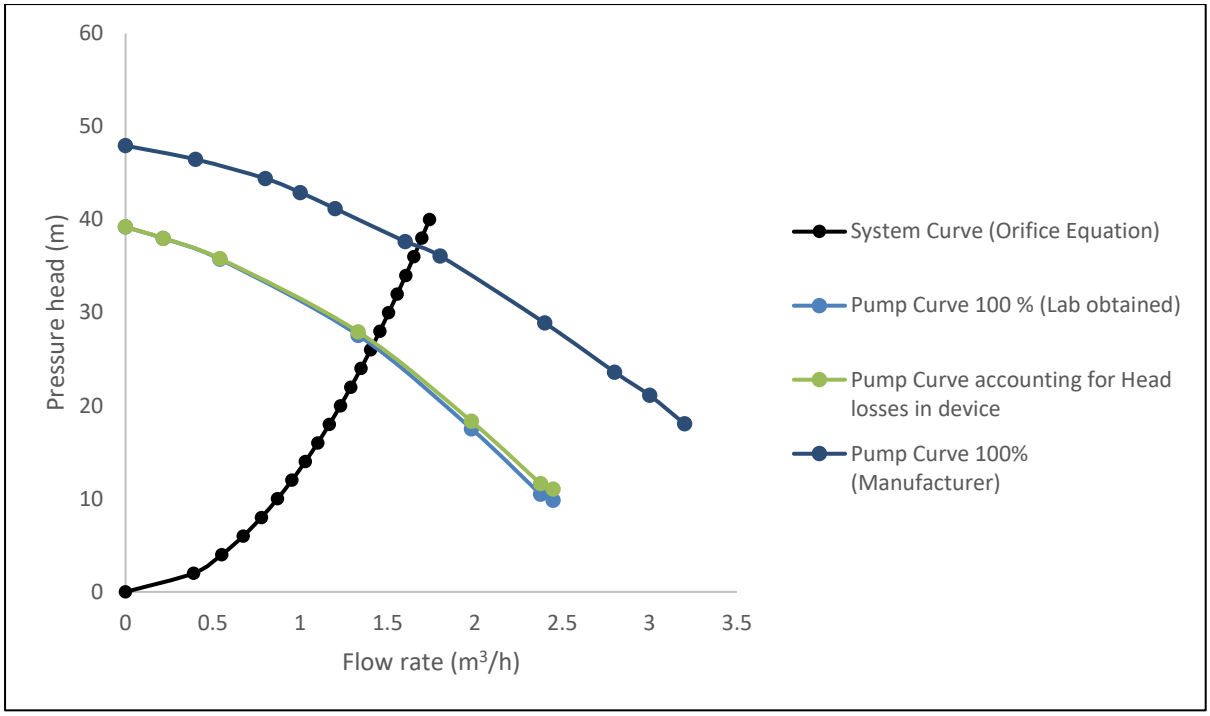

Figure 5-4 - Pump curves for PCAD and the 6mm round hole characteristic curve

The next section describes the results obtained from the three pipe samples using the same methodology and equipment, as described in section 4.1.

5.2 Low-Pressure Test Results and Discussions

In this section, lower pressures (6.5 m – 39 m) were used as this was the range of pressures at which the device can operate and intersect with all the leak types system curves.

5.2.1 6 mm Round Hole (Low Pressure)

Ten tests were done on the uPVC pipe section with a 6 mm round hole at a pressure range of 9.8 meters to 25.7 meters head. This pressure range was comparable with what the device could deliver for this leak type.

The following results were obtained from the tests. The pressure and flow were recorded on the data loggers, and the stabilised steps then used to analyse the data. Figure 5-5 shows the pressure and flow relationship at each step in a typical 6 mm round hole leakage characterisation test.

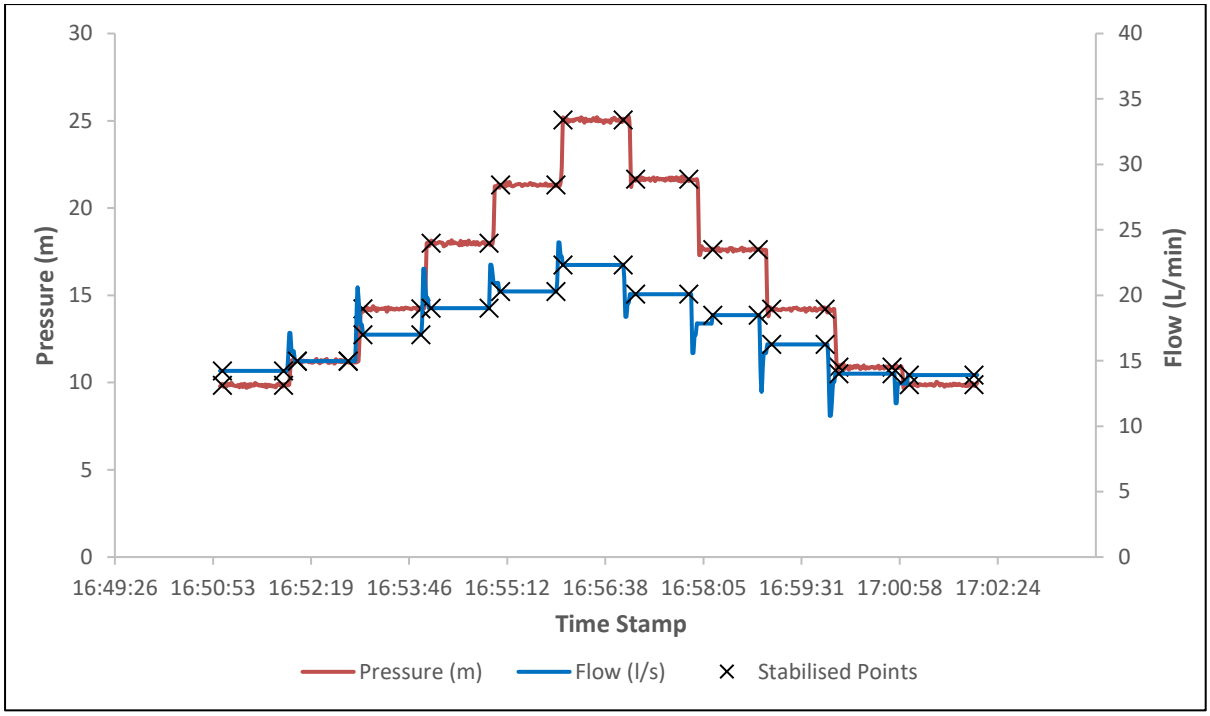

Figure 5-5 - Pressure head-flow rate relationship for a typical test

From the stabilised points, the pressure head and its respective flow rate were plotted, and Figure 5-6 shows the relationship between the two. This relationship between the flow rate and the pressure head is a power relationship and gives the N1 as the exponent of the power relationship. The N1 value for the pipe sample was found to be 0.501 with a standard deviation of 0.0069 across all ten tests conducted. The sample variance the N1 values obtained from the ten tests conducted in the laboratory was 4.76E-05 (0.0095% of the mean).

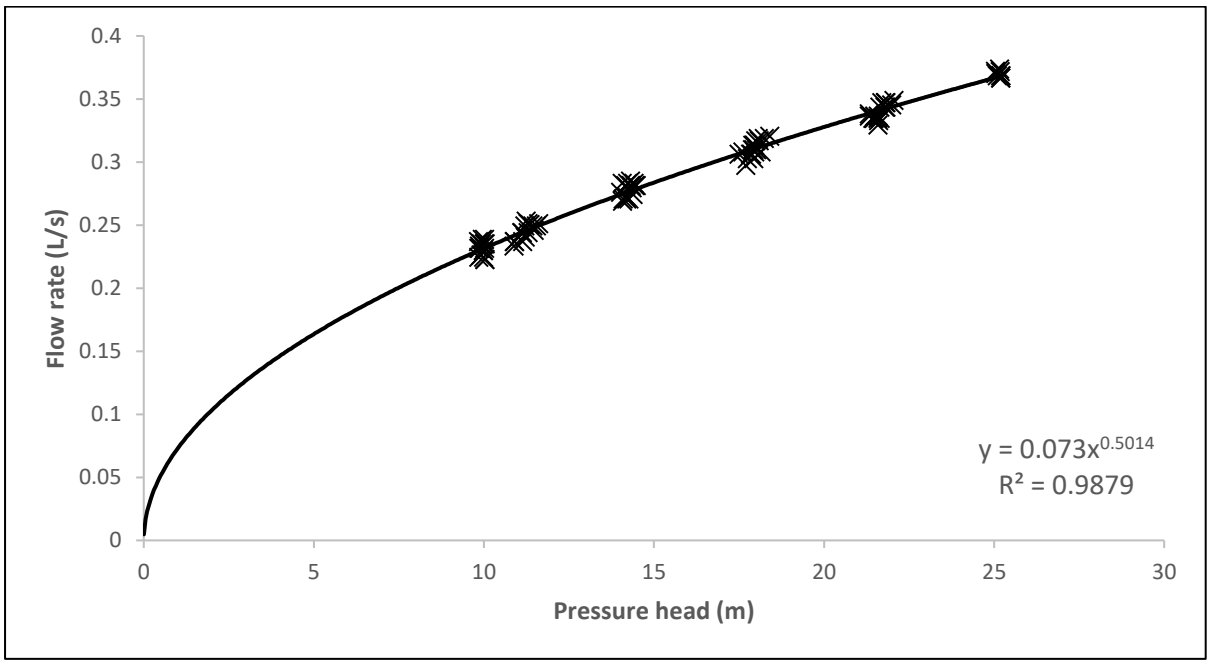

Figure 5-6 - Flowrate-pressure power relationship of a 6 mm round hole

The small magnitude of the sample variance in relation to the N1 value showed little variance in the tests and represented excellent repeatability and reliability of the conducted tests for the N1 exponent.

The individual tests data points were combined, and a regression analysis was done using the combined data. The effective areas for all combined data points across ten tests were then plotted against their associated pressure heads. Figure 5-7 graphically shows the relationship between the effective area and pressure head.

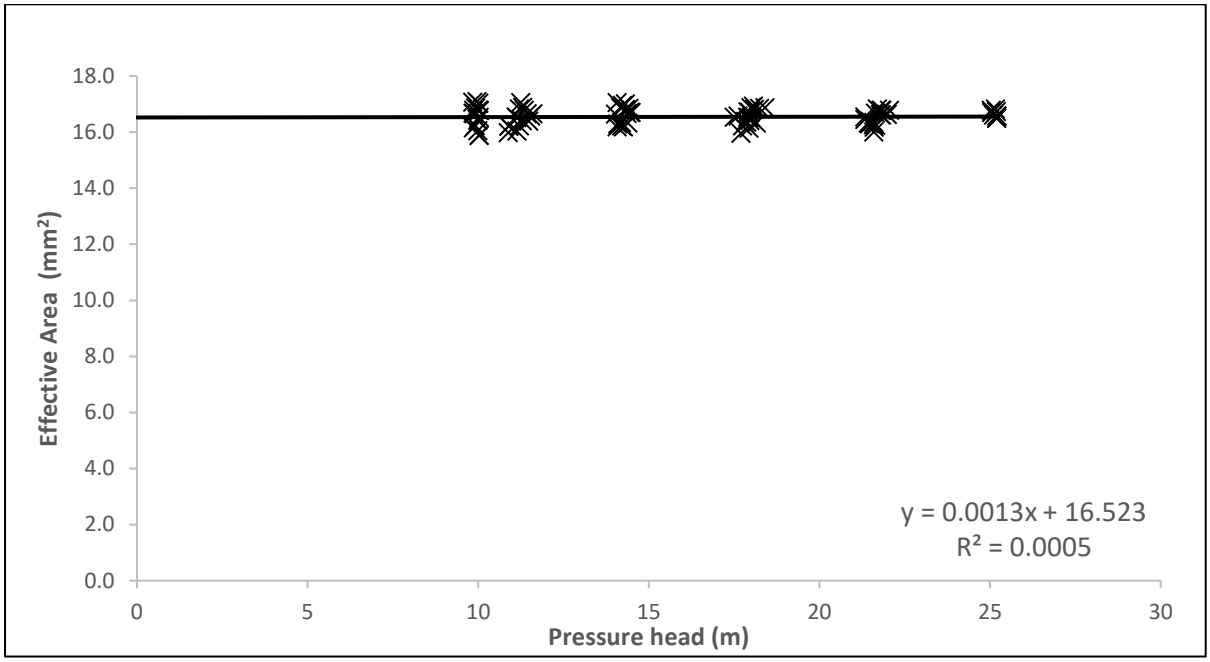

Figure 5-7 -Graph showing the effective area-head slope of a 6 mm uPVC round hole

From the linear regression analysis, the effective area-head slope (C_dm) was found to be 0.00129 mm^2/m meaning for every meter of the pressure head the orifice area increased by 0.00129 mm^2 (0.00456% of the original area). The simultaneous confidence interval for the effective area-head slope is 0.0117 mm^2/m. The effective area-head slope derived is very small and near-zero, as suggested by Nsanzubuhoro et al., (under review).

The standard deviation of the effective area-head slopes of the ten tests was found to be 0.00672 mm^2/m, while the sample variance which measures how far each test value is from the sample mean was found to be 4.52E-05 mm^2/m. This was a 3.5% deviation from the mean and reports little variance between test values and shows acceptable repeatability in the test.

The flow rate predictions of the FAVAD and N1 equations were compared with the measured data as shown in Figure 5-8, and both models fit the data well within the measured pressure range for the 6 mm round hole.

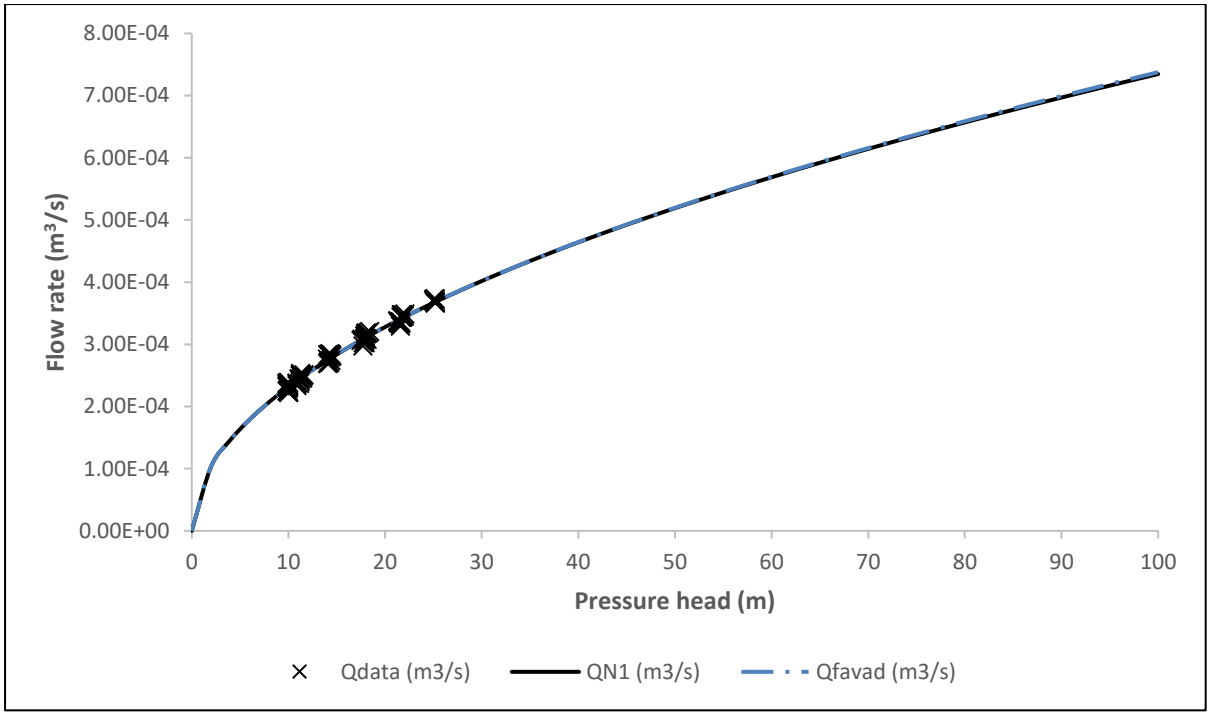

Figure 5-8 - Comparison of the FAVAD and N1 equation flow predictions and observed data

Beyond the measured data range, the two modes are found to align still. This is as a result of N1 value being 0.501, which then allows the equation to predict perfect orifice flow while the FAVAD equation parameters also model a perfect orifice flow regime.

Table 5-3 then shows a summary of the results for the data presented above.

Table 5-3 - Summary of results

	N1	**A_0' (mm^2)**	**95% SPCI for A_0' (mm^2)**	**m' (mm^2/m)**	**95% SPCI for m' (mm^2/m)**	**p for m' (%)**	**C_d**
This Study	0.501	16.5	± 0.198	0.00129	± 0.0117	<0.05	0.58

The variation of the ten tests was analysed graphically, and Figure 5-15 and Figure 5-16 show the graphs that describe the repeatability and reliability of the results conducted on a 6 mm round hole using the standardised method at lower pressures. Two parameters, the effective area-head slope and effective area, were used to establish the repeatability and reliability of the results across the ten tests. These figures also visually depict the repeatability of the experiment. Figure 5-9 shows the repeatability of the effective area-head slope parameter across the tests.

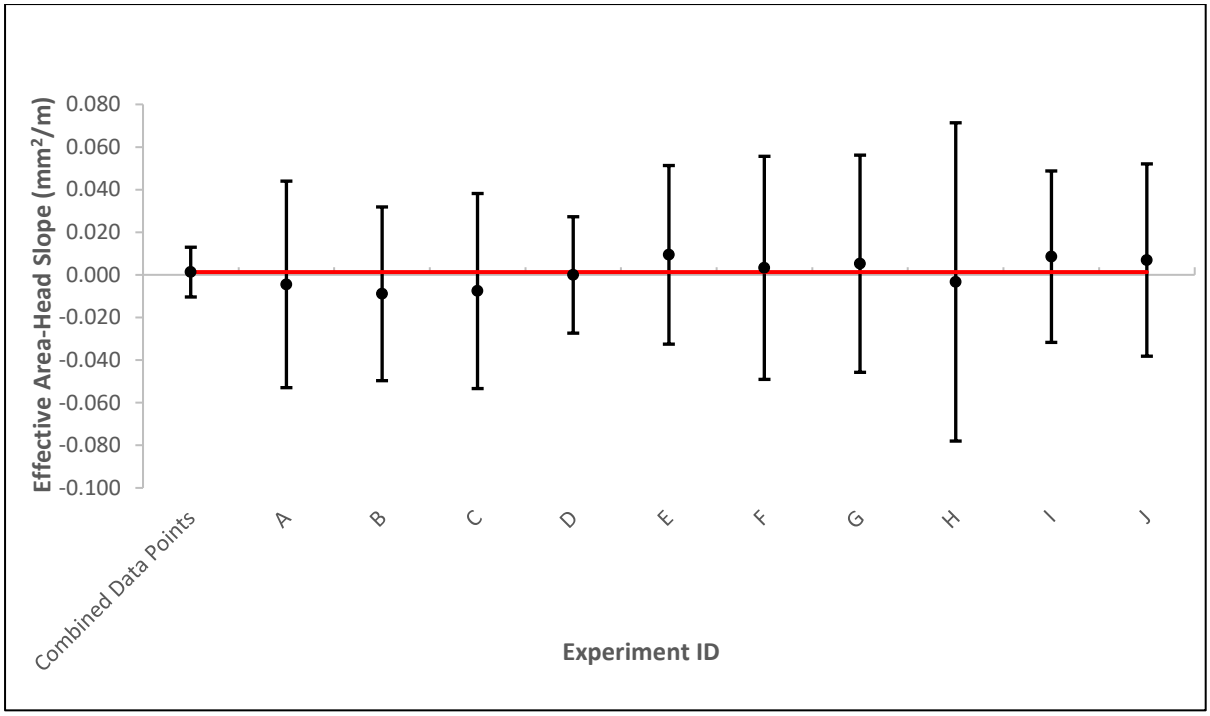

Figure 5-9 - Effective area-head slope repeatability analysis of the 6 mm round hole

The effective area-head area slopes of the ten tests are consistent and all fall within each other's single parameter's confidence intervals. A similar observation is made from analysing the values and confidence intervals of the effective area of the ten tests, as shown in Figure 5-10

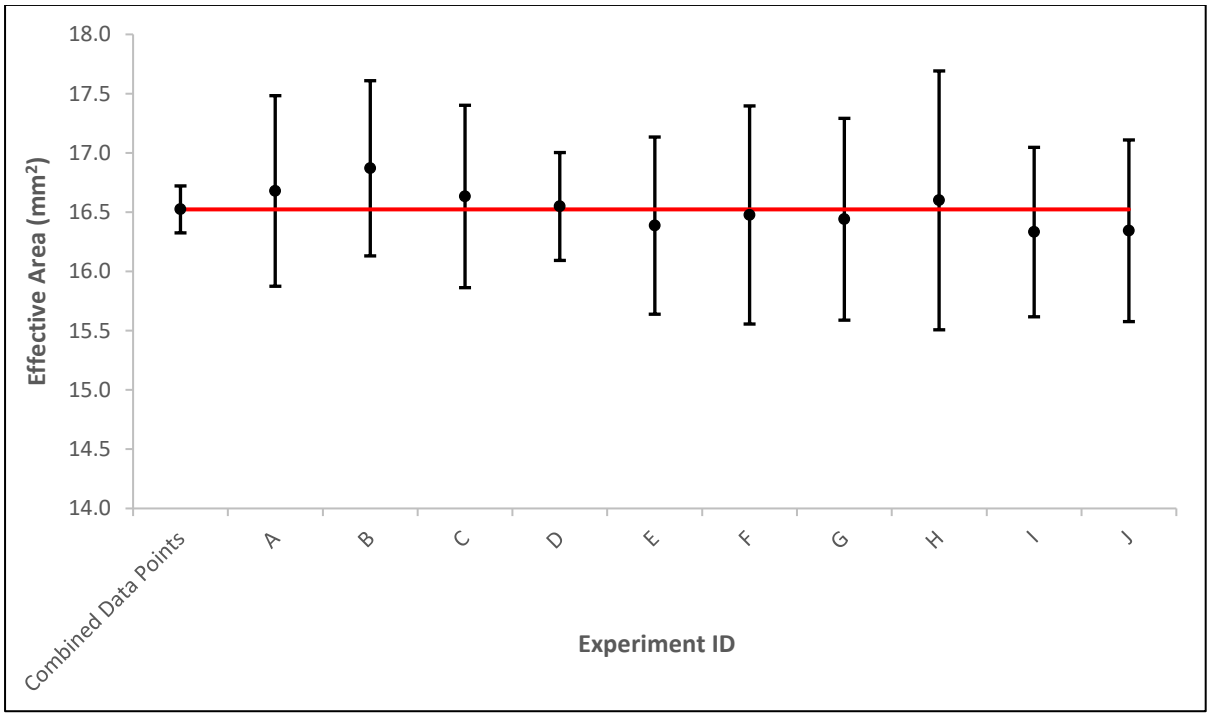

Figure 5-10 - Effective area repeatability analysis of the 6 mm round hole

Table 5-4 then shows the summary of the parameters obtained in each of the ten tests conducted.

Table 5-4 - Summary of results for the ten 6 mm round hole

Experiment ID	A_0' (mm^2)	m' (mm/m)	N1	C_d	c
A	16.7	-0.004	0.495	0.590	7.45E-05
B	16.9	-0.009	0.492	0.597	7.58E-05
C	16.6	-0.008	0.491	0.588	7.49E-05
D	16.5	0.000	0.500	0.585	7.33E-05
E	16.4	0.009	0.509	0.580	7.15E-05
F	16.5	0.003	0.506	0.583	7.20E-05
G	16.4	0.005	0.503	0.581	7.26E-05
H	16.6	-0.003	0.501	0.587	7.32E-05
I	16.3	0.009	0.509	0.578	7.12E-05
J	16.3	0.007	0.509	0.578	7.12E-05

5.2.2 50 mm uPVC Longitudinal Crack (Low Pressure)

Ten tests were done on the uPVC pipe section with a 50 mm longitudinal crack at a pressure range of 6.8 meters to 13.2 meters head. This pressure range was comparable with what the device could deliver for this leak type. The following results were obtained from the tests.

Figure 5-11 shows the pressure and flow relationship at each step in a typical 50 mm longitudinal crack leakage characterisation test.

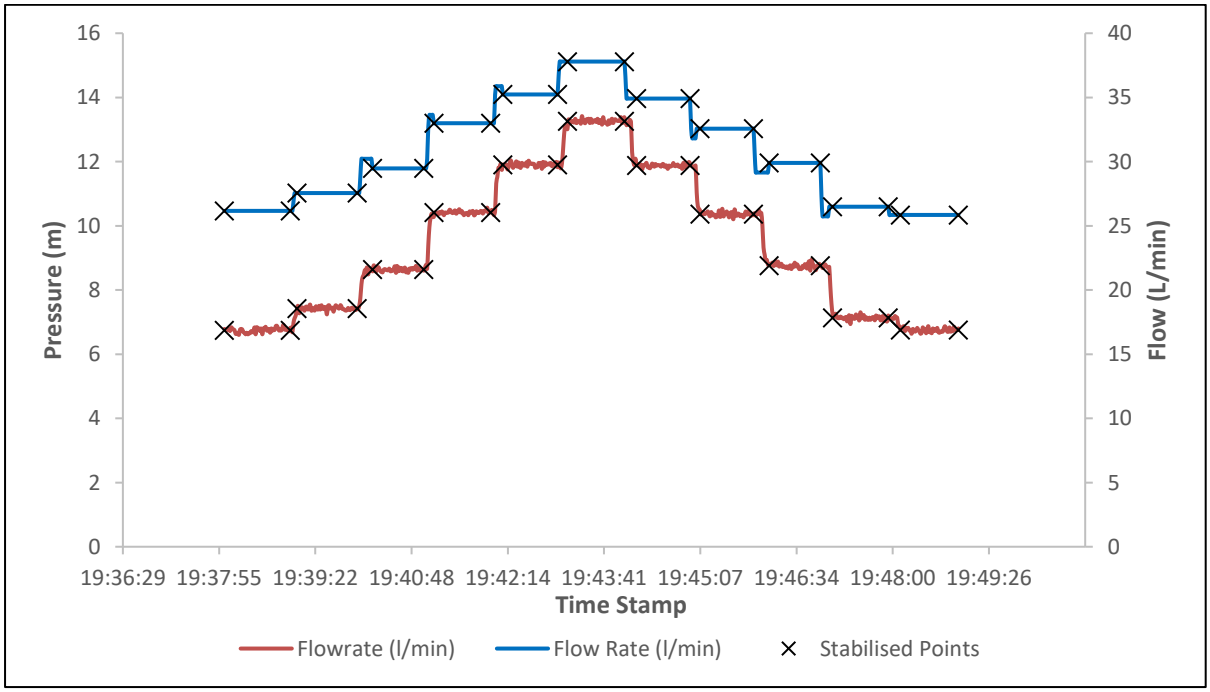

Figure 5-11 - Pressure head-flow rate relationship for a typical test

From the stabilised points, the pressure head and its respective flow rate were plotted, and Figure 5-12 shows the relationship between the two. This relationship between the flow rate

and the pressure head is a power relationship and gives the N1 as the exponent of the power relationship.

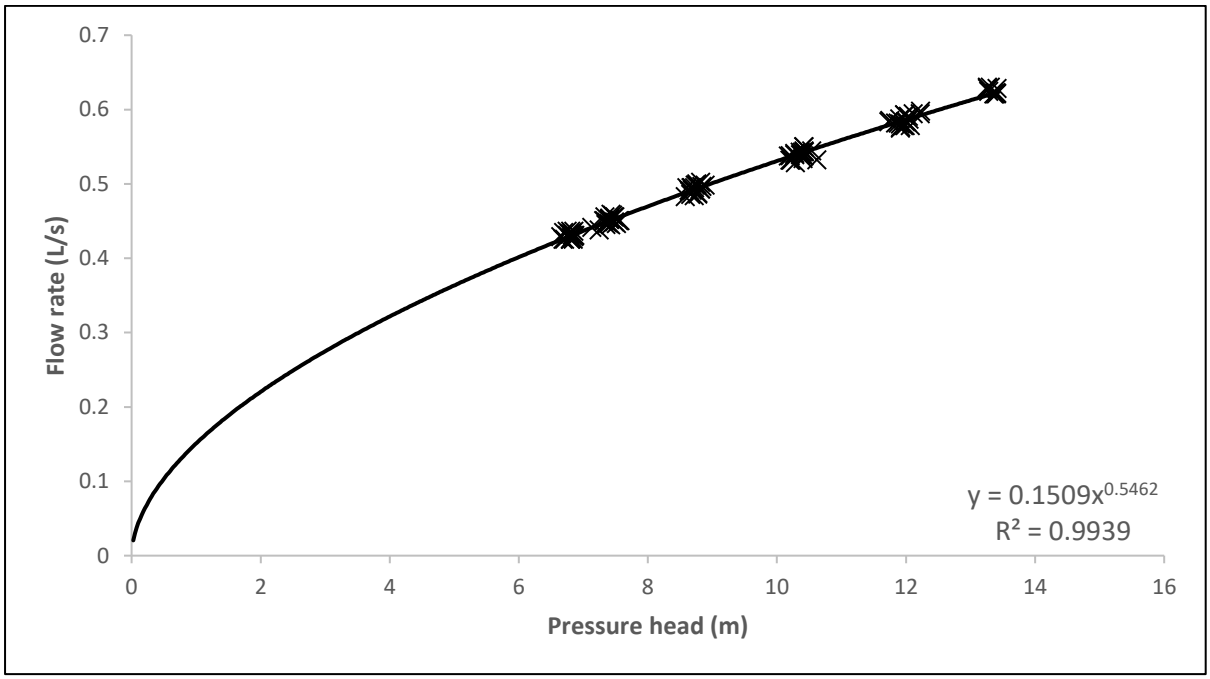

Figure 5-12 - Flowrate-pressure power relationship of a 50 mm longitudinal crack

The N1 value for the pipe sample was found to be 0.55 with a standard deviation of 0.009 across all ten tests conducted. The sample variance the N1 values obtained from the ten tests conducted in the laboratory was 7.99E-05 (0.015% of the mean N1 value). The small magnitude of the sample variance concerning the N1 value showed little variance in the tests and represented good repeatability and reliability of the conducted tests for the N1 exponent.

The individual tests data points were combined, and a regression analysis was done using the combined data. The effective areas for all combined data points across ten tests were then plotted against their associated pressure heads. Figure 5-13 graphically shows the relationship between the effective area and pressure head. The effective area-head slope was found to be 0.186 mm^2/m meaning for every meter of the pressure head the orifice area increased by 0.186 mm^2. The simultaneous confidence interval for the effective area-head slope is 0.0320 mm^2/m. The derived effective area-head slope was within the typical pressure range for longitudinal cracks suggested by Nsanzubuhoro et al., (under review). The standard deviation of the effective area-head slopes of the ten tests was found to be 0.0327 mm^2/m, while the sample variance which measures how far each test value is from the sample mean was found to be 0.00107 mm^2/m. This was a 0.58% deviation from the mean and reports little variance between test values and shows good repeatability in the test.

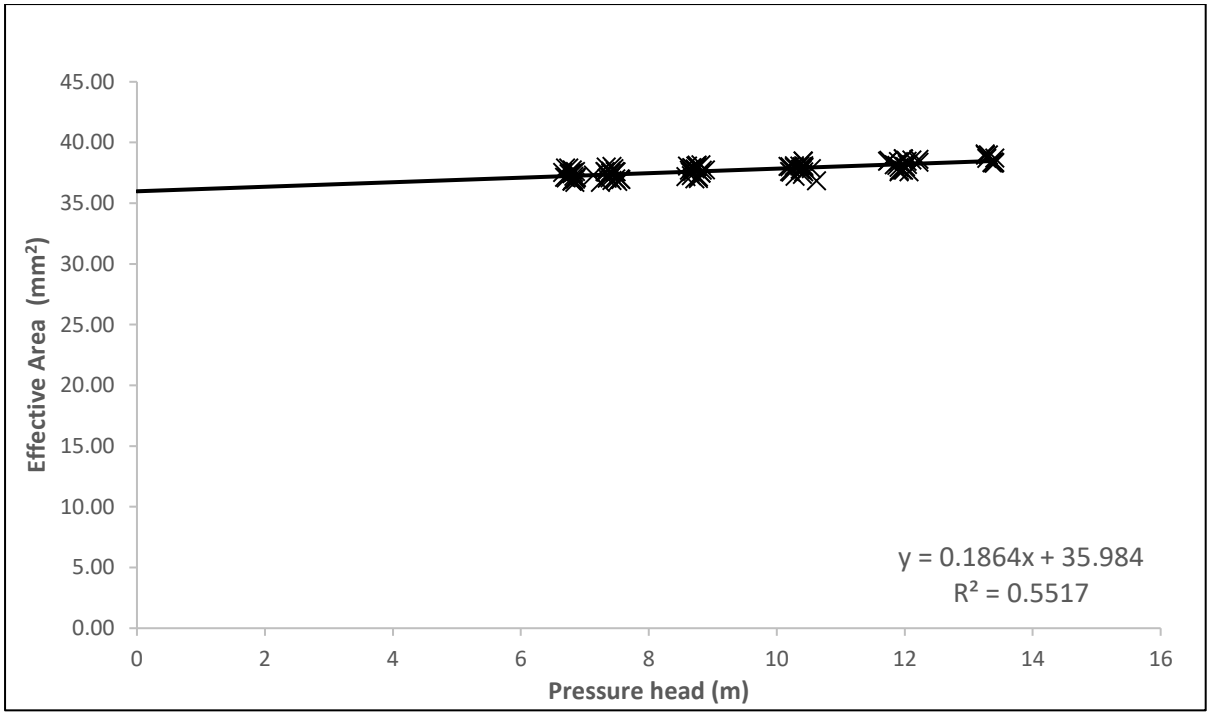

Figure 5-13 - Graph showing the effective area-head slope of a 50 mm uPVC longitudinal crack

The flow rate predictions of the FAVAD and N1 equations were compared with the measured data, as shown in Figure 5-14.

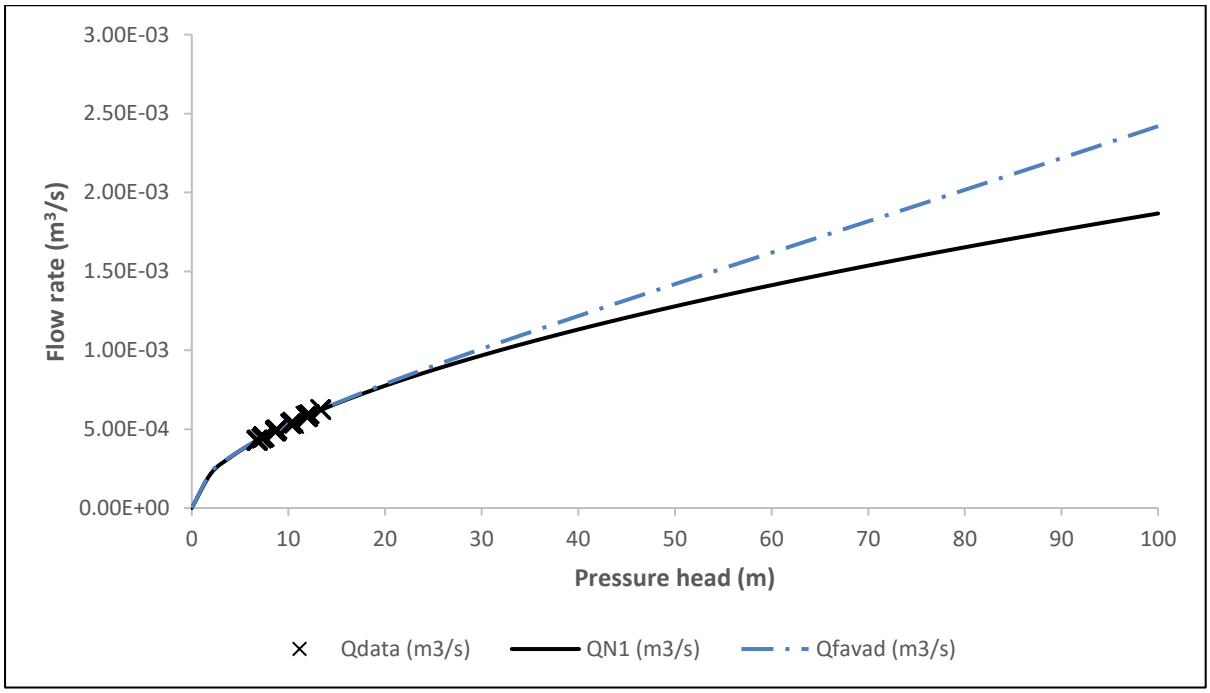

Figure 5-14 - Comparison of the FAVAD and N1 equation flow predictions and observed data

Both models fit the data well within the measured pressure range for the 50 mm longitudinal crack. Beyond the measured data range, the two models differ. The deviation of the N1 equation

from the FAVAD equation is more pronounced for this sample due to the lower range of pressures obtained for this sample. This deviation is due to the N1 equation being an empirical equation that is dependent on the data and consequently, the pressure range used. Table 5-5 then shows a summary of the results for the data presented above.

Table 5-5 - Summary of results

	N1	A_0' (mm^2)	95% SPCI for A_0' (mm^2)	m' (mm^2/m)	95% SPCI for m' (mm^2/m)	p for m' (%)	C_d
This Study	0.546	35.9	± 0.31	0.186	± 0.0320	<0.05	0.72

The variation of the ten tests was analysed graphically, and Figure 5-15 and Figure 5-16 show the graphs that describe the repeatability and reliability of the results conducted on a 50 mm longitudinal crack using the standardised method at lower pressures. Two parameters, the effective area-head slope and effective area, were used to establish the repeatability and reliability of the results across the ten tests. Figure 5-15 shows the repeatability of the effective area-head slope parameter across the tests.

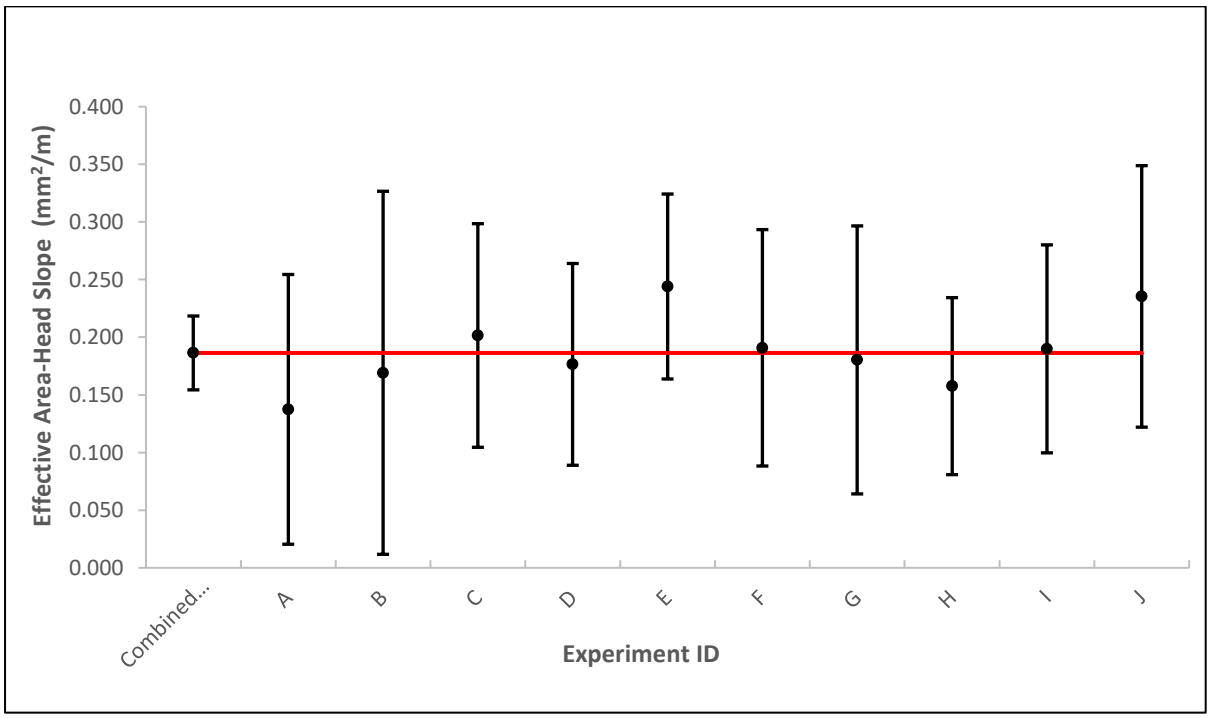

Figure 5-15 - Effective area-head slope repeatability analysis of the 50 mm longitudinal crack tests

The effective area-head area slopes of the ten tests are consistent and all fall within each other's single parameter's confidence intervals. A similar observation is made from analysing the values and confidence intervals of the effective area of the ten tests, as shown in Figure 5-16.

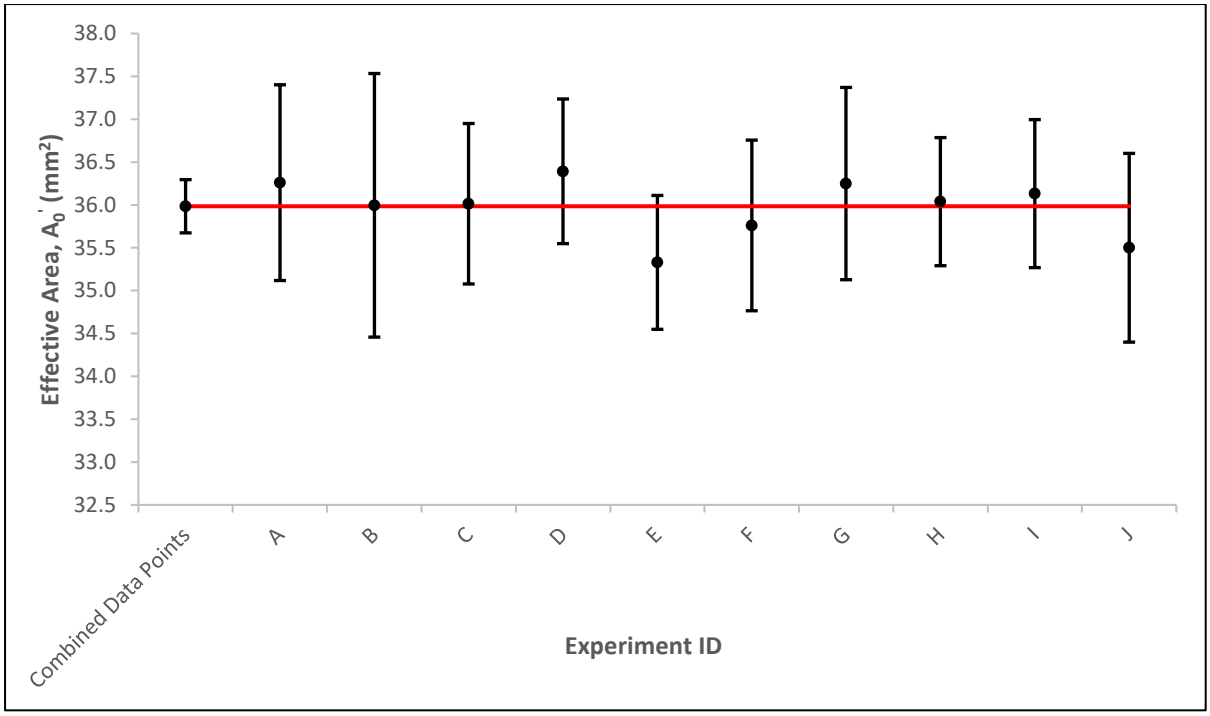

Figure 5-16 - Effective area repeatability analysis of the 50 mm longitudinal crack

Table 5-6 then shows the summary of the parameters obtained in each of the ten tests conducted for this sample.

Table 5-6 - Summary of results for the ten 50 mm longitudinal crack tests

Experiment ID	A_0' (mm^2)	m' (mm/m)	N1	C_d	c
A	36.3	0.137	0.533	0.73	1.55E-04
B	36.0	0.169	0.542	0.72	1.52E-04
C	36.0	0.202	0.549	0.72	1.51E-04
D	36.4	0.176	0.543	0.73	1.53E-04
E	35.3	0.244	0.563	0.71	1.45E-04
F	35.8	0.191	0.549	0.72	1.49E-04
G	36.2	0.180	0.543	0.72	1.53E-04
H	36.0	0.158	0.540	0.72	1.52E-04
I	36.1	0.190	0.546	0.72	1.52E-04
J	35.5	0.235	0.559	0.71	1.46E-04

5.2.3 50 mm uPVC Circumferential Crack (Low Pressure)

Ten tests were done on the uPVC pipe section with a 50 mm circumferential crack at a pressure range of 6.2 meters to 15.3 meters head. This pressure range was comparable with what the device could deliver for this leak type. The following results were obtained from the tests. The pressure and flow were recorded, and the stabilised steps then used to analyse the data. Figure 5-17 shows the pressure and flow relationship at each step in a typical 50 mm circumferential crack leakage characterisation test.

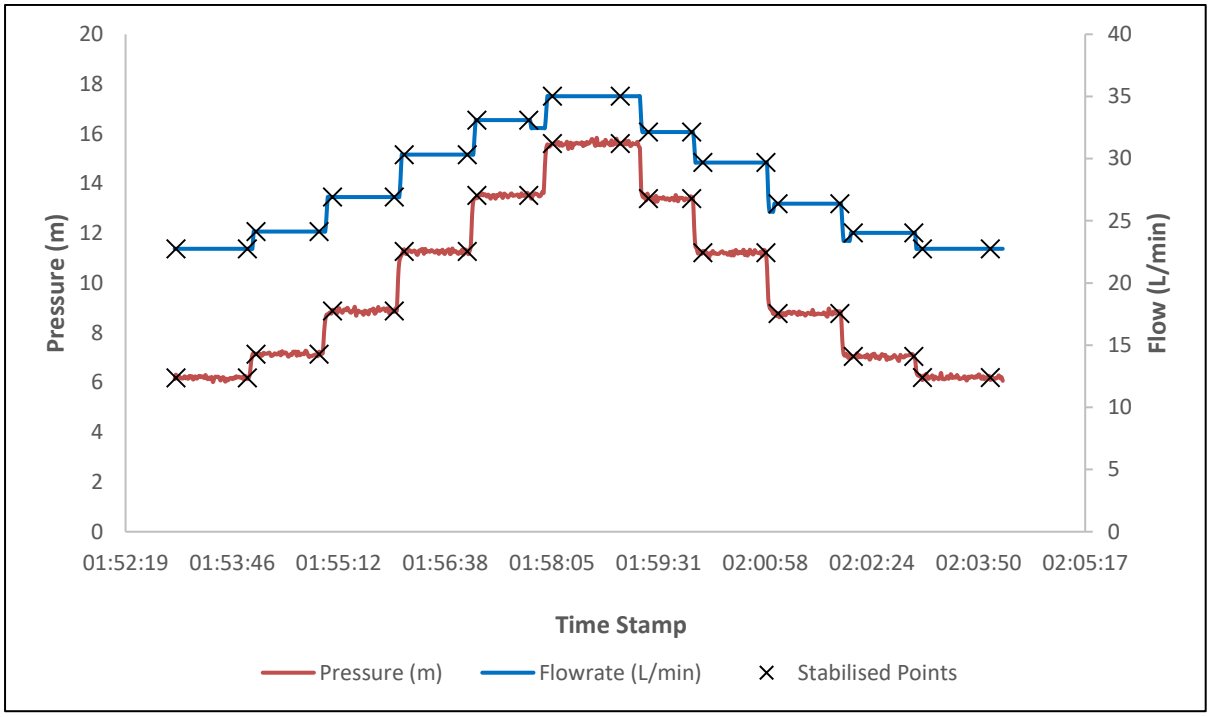

Figure 5-17- Pressure head-flow rate relationship for a typical test

From the stabilised points, the pressure head and its respective flow rate were plotted, and Figure 5-18 shows the relationship between the two parameters. This relationship between the flow rate and the pressure head is a power relationship and gives the N1 as the exponent of the power relationship.

The N1 value for the pipe sample was found to be 0.47 with a standard deviation of 0.0.00265 across all ten tests conducted. The sample variance the N1 values obtained from the ten tests conducted in the laboratory was 7.07E-05 (0.02% of the mean N1).

The small magnitude of the sample variance in relation to the N1 value showed little variance in the tests and represented good repeatability and reliability of the conducted tests for the N1 exponent.

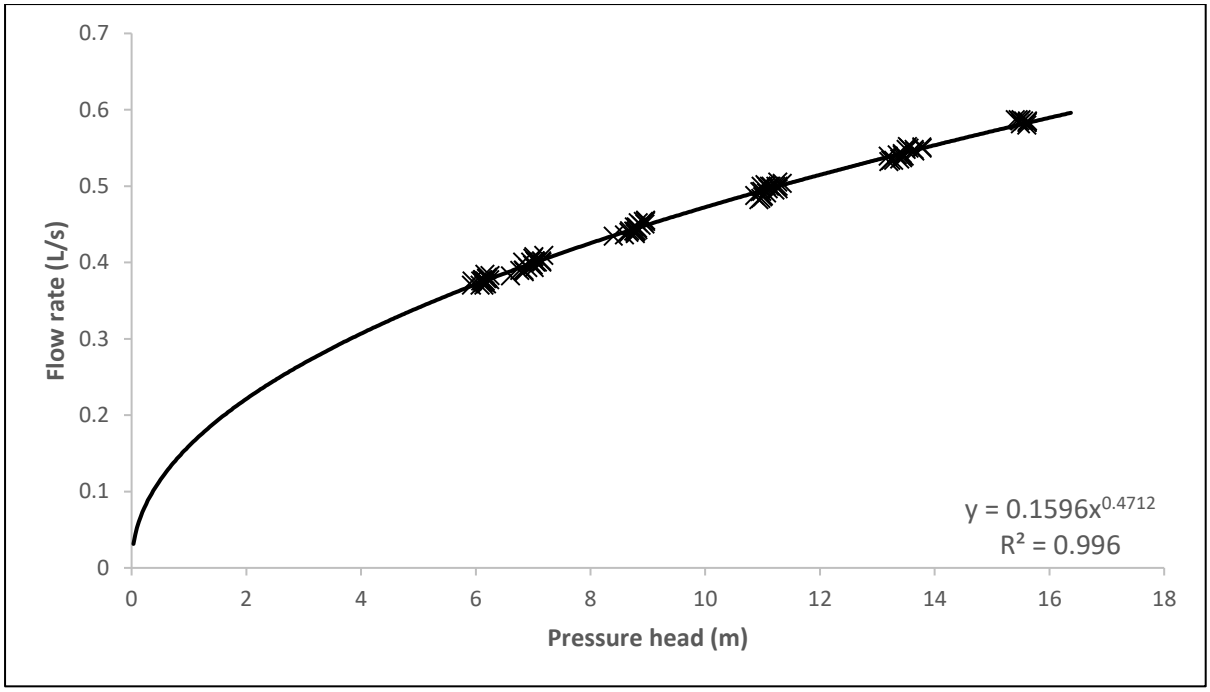

Figure 5-18 - Flowrate-pressure power relationship of a 50 mm circumferential crack

The individual tests data points were combined. The effective areas for all combined data points across ten tests were then plotted against their associated pressure heads. Figure 5-19 graphically shows the relationship between the effective area and pressure head.

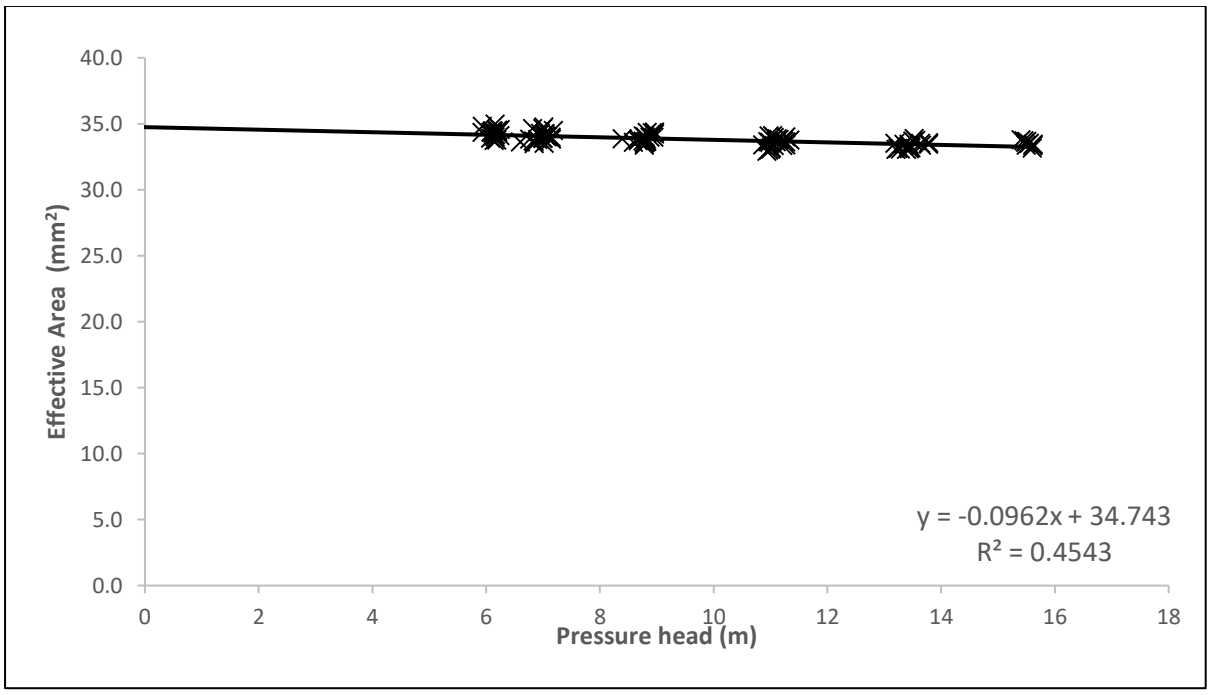

Figure 5-19 - Graph showing the effective area-head slope of a 50 mm uPVC circumferential crack

The effective area-head slope (Cdm) was found to be - 0.096 mm^2/m meaning for every meter of the pressure head the orifice area increased by 0.096 mm^2. The simultaneous confidence

interval for the effective area-head slope is 0.0204 mm^2/m. The derived effective area-head slope was outside the typical pressure range for longitudinal cracks suggested by Nsanzubuhoro et al., (under review).

The standard deviation of the effective area-head slopes of the ten tests was found to be 0.00792 mm^2/m, while the sample variance which measures how far each test value is from the sample mean was found to be 6.26E-05 mm^2/m. This was a 0.07% deviation from the mean and reports little variance between test values and shows good repeatability in the test.

The flow rate predictions of the FAVAD and N1 equations were compared with the measured data, as shown in Figure 5-20.

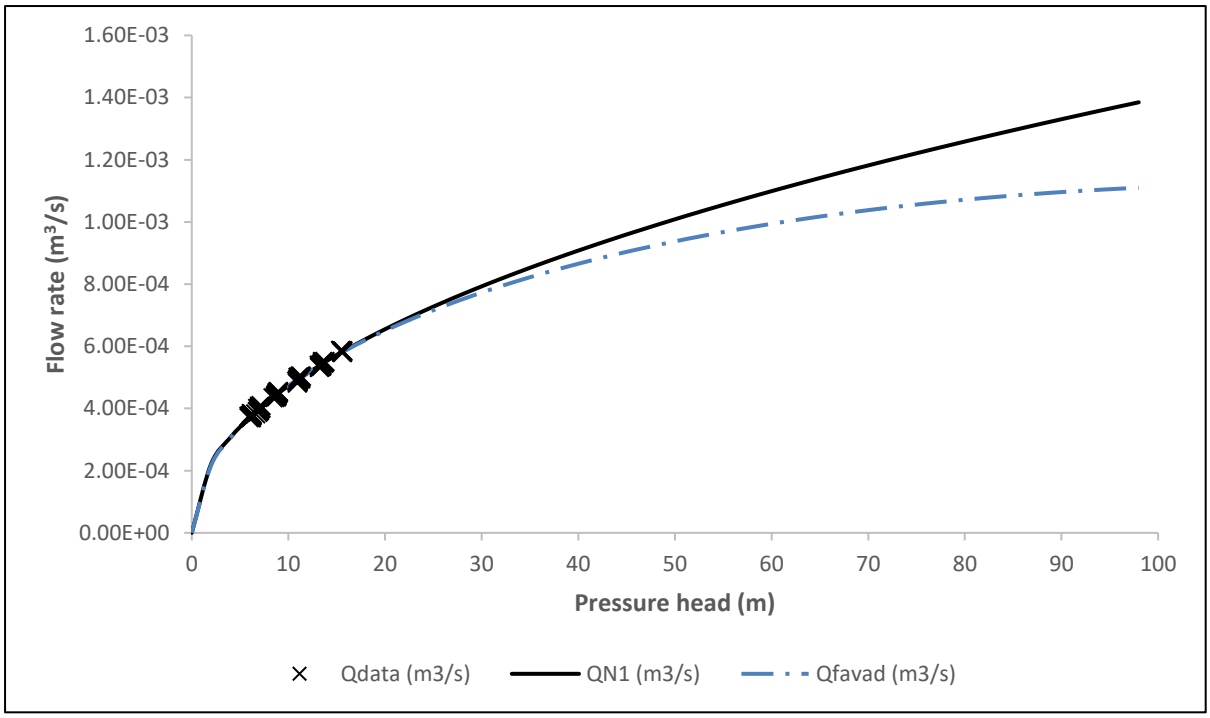

Figure 5-20 - Comparison of the FAVAD and N1 equation flow predictions and observed data

Both models fit the data well within the measured pressure range for the 50 mm longitudinal crack, but beyond the measured data range, the two models differ. The deviation of the N1 equation from the FAVAD equation is more pronounced due to the lower range of pressures obtained for this sample. This deviation is due to the N1 equation being an empirical equation that is dependent on the data and consequently, the pressure range used.

Table 5-7 then shows a summary of the results for the data presented above.

Table 5-7 - Summary of results

	N1	A_0' (mm^2)	95% SPCI for A_0' (mm^2)	m' (mm^2/m)	95% SPCI for m' (mm^2/m)	p for m' (%)	C_d
This Study	0.471	34.7	± 0.21	- 0.0962	± 0.004	<0.05	0.69

The variation of the ten tests was analysed graphically, and Figure 5-21 and Figure 5-22 show the graphs that describe the repeatability and reliability of the results conducted on a 50 mm circumferential crack using the standardised method with lower pressure ranges. Two parameters, the effective area-head slope and effective area, were used to establish the repeatability and reliability of the results across the ten tests. These figures also visually depict the repeatability of the experiment. Figure 5-21 shows the repeatability of the effective area-head slope parameter across the tests.

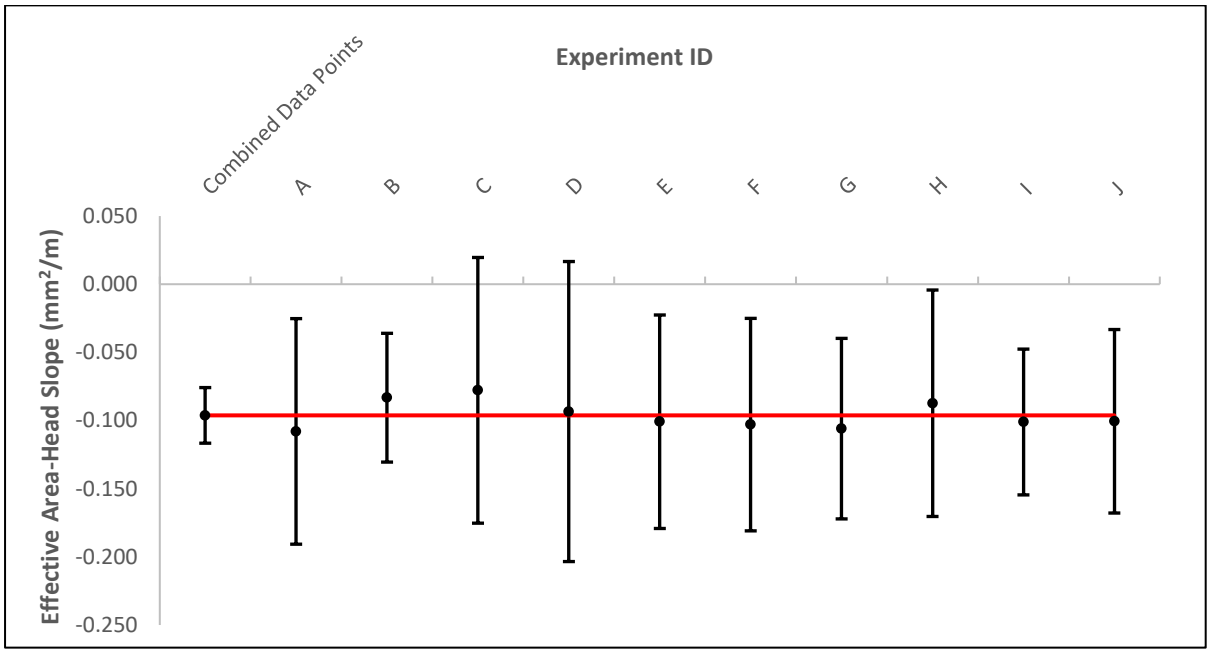

Figure 5-21 - Effective area-head slope repeatability analysis of the 50 mm circumferential crack tests

The effective area-head area slopes of the 10 tests are consistent and all fall within each other's single parameter's confidence intervals. A similar observation is made from analysing the values and confidence intervals of the effective area of the ten tests, as shown in Figure 5-22.

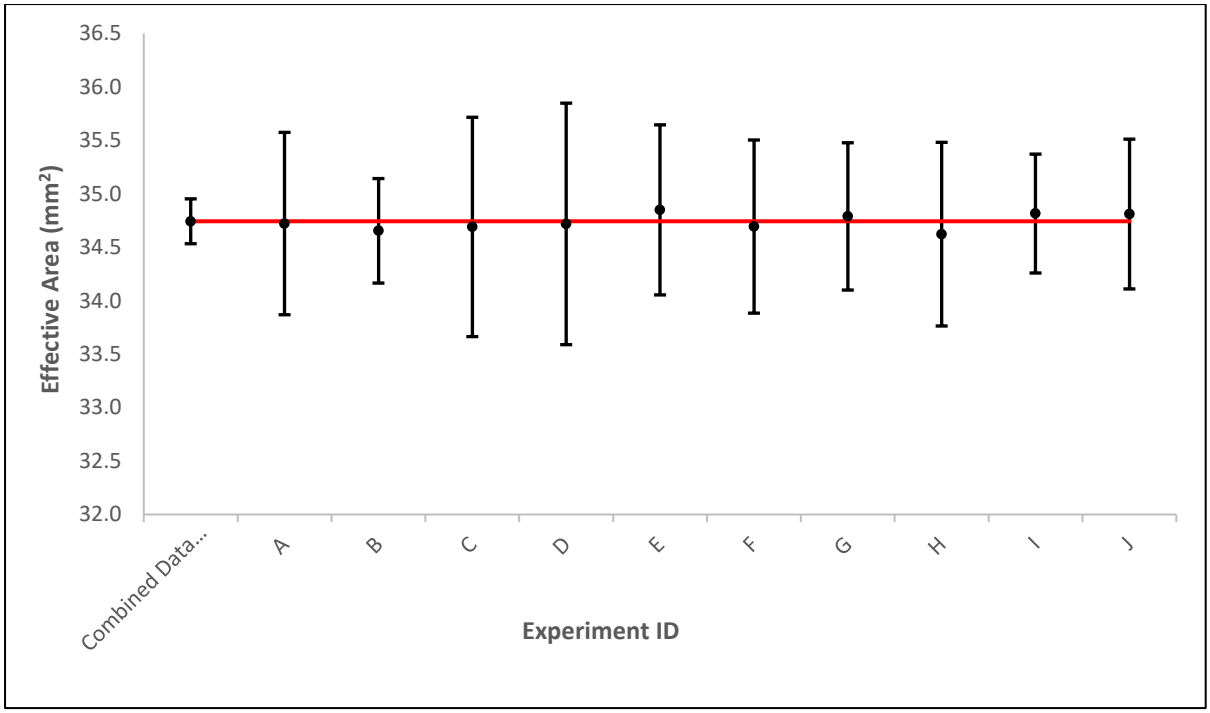

Figure 5-22 - Effective area repeatability analysis of the 50 mm circumferential crack

Table 5-8 then shows the summary of the parameters obtained in each of the ten tests conducted for this sample.

Table 5-8 - Summary of results for the ten 50 mm circumferential crack tests

Experiment ID	A_0' (mm^2)	m' (mm/m)	N1	C_d	c
A	34.7	-0.108	0.468	0.694	1.60E-04
B	34.7	-0.083	0.475	0.693	1.58E-04
C	34.9	-0.097	0.471	0.699	1.60E-04
D	34.7	-0.093	0.472	0.694	1.59E-04
E	34.8	-0.101	0.470	0.697	1.60E-04
F	34.7	-0.103	0.469	0.694	1.60E-04
G	34.8	-0.106	0.467	0.696	1.61E-04
H	34.6	-0.087	0.474	0.692	1.59E-04
I	34.8	-0.101	0.471	0.696	1.60E-04
J	34.8	-0.101	0.470	0.696	1.60E-04

5.3 Comparing Low-Pressure Method Derived Parameters with Standard Pressure Derived Parameters

From the results obtained in Chapter 4 and the previous section, it was noted how the parameters for the same leak types varied when the pressure range used in the characterisation tests was changed. Table 5-9 below shows a summary of these observed changes for the three pipe samples. The two different pressure ranges are denoted by the abbreviation's HP and LP, where HP represents the high/standard pressure, based on previous studies whose values match the ones used in the study. LP denotes low pressure ranges used to ascertain the leak characteristics which were in range with what the PCAD pump could deliver.

Table 5-9 - Comparison of leakage characteristics at different pressure ranges

Experiment	A_0' (mm^2)	95% SPCI for A_0' (mm^2)	m' (mm^2/m)	95% SPCI for m' (mm^2/m)	C_d
6mm Round Hole (HP)	17.25	0.1415	- 0.0048	0.0021	0.61
6mm Round Hole (LP)	16.52	0.1980	0.0013	0.0117	0.58
50mm Longitudinal Crack (HP)	35.64	1.3168	0.3228	0.0239	0.71
50mm Longitudinal Crack (LP)	35.98	0.3107	0.1864	0.0320	0.72
50mm Circumferential Crack (HP)	32.91	0.0639	- 0.0193	0.0010	0.66
50mm Circumferential Crack (LP)	34.74	0.2099	- 0.0962	0.0204	0.69

5.3.1 Effective Area Comparison

For the round hole and circumferential crack, the effective areas were different and did not overlap, as shown in Figure 5-23. Discharge coefficients, shown in Table 5-9, are also different for the two leak types which can be explained by the different flow regimes that occur due to the different pressure values. As the circumferential crack closes less at lower pressures, this means the flow regime will form a Vena contracta that is closer in size to the original area than at standard pressures. Furthermore, these differences in effective areas can also be because of the effective area is dependent on the distribution of the effective areas derived at every pressure step. Thus, a slight variation in the effective area can create residuals which affect the value of the effective area.

For the longitudinal cracks effective area parameters, an overlap was observed for the two pressure ranges also shown Figure 5-23.

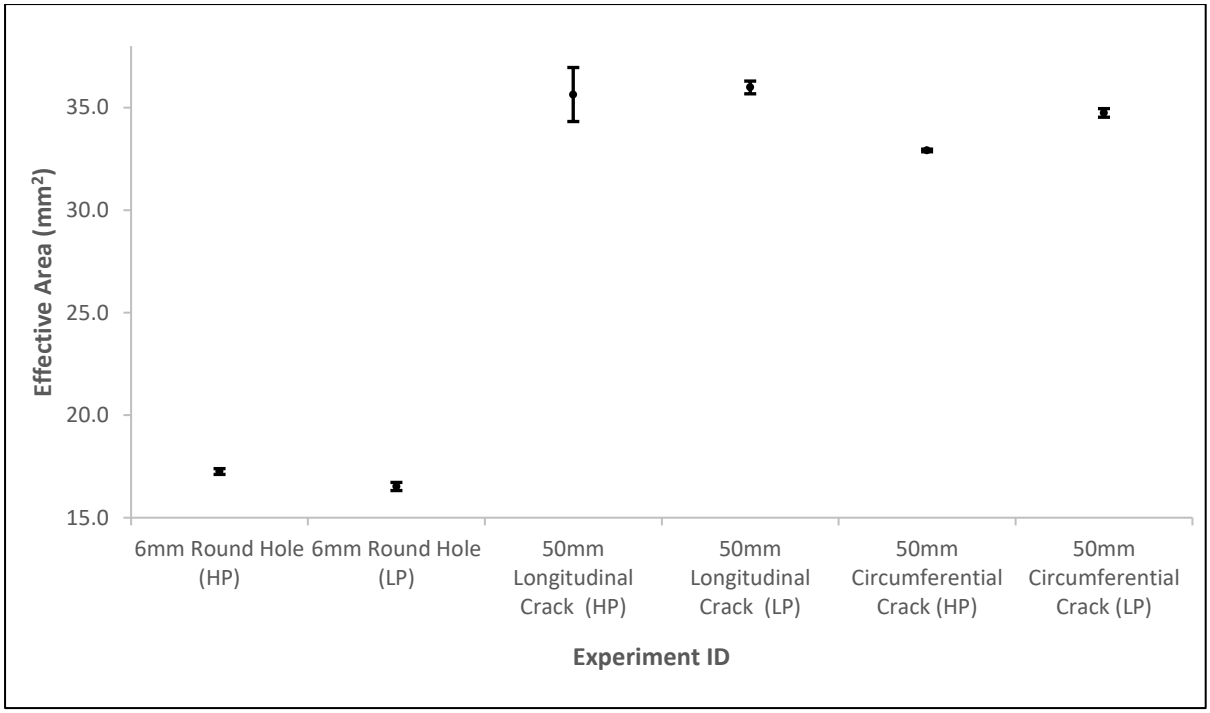

Figure 5-23 - Effective area comparison at different pressure ranges

5.3.2 Effective Area - Head Comparison

The effective area – head slope parameter for all three leak types was different at the two different pressure ranges with no overlap, as seen in Figure 5-24.

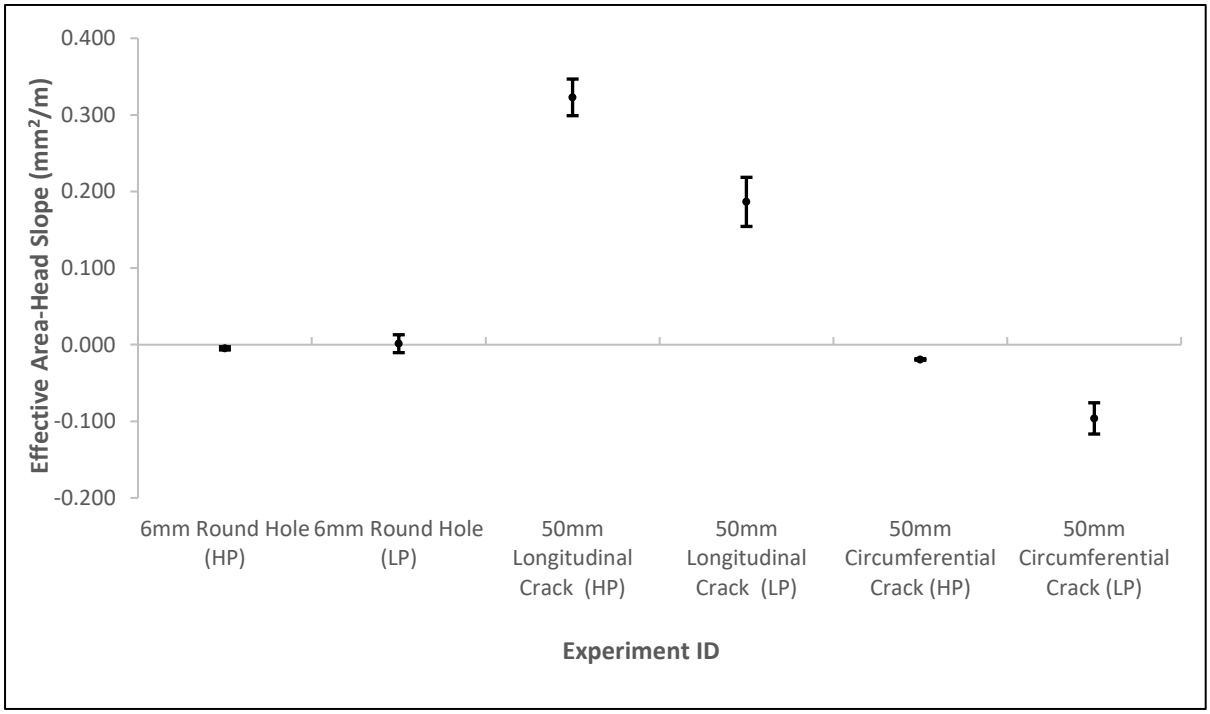

Figure 5-24 - Effective area-head comparison at different pressure ranges

The lack of overlap suggests that the effective area-head slope might be pressure dependent. That is to say, the value of m' for a sample is only valid within its measured pressure range,

much like the N1 parameters. The implied pressure dependence contradicts previously stated claims such as the one made by Kabaasha, (2017) who claimed that the benefits of the modified orifice equation is that it is independent of the system pressure. This study, using 3 different leak types, tested 30 times, suggests that these two parameters might be pressure dependent.

Possible reasons for this may be found by considering the basic mechanics of materials. A circumferential crack of length L, on a pipe sample shall be considered for ease of demonstration an o aid in explaining this phenomenon. In the analysis of leakage parameters, the pipe material is assumed to deform elastically and obey Hooke's law.

Hooke's law from the mechanics of materials theory states that the stress in a material is directly proportional to the strain induced on the material (Hibbeler, 2016). The constant of proportionality is called the modulus of elasticity or Young's modulus. This law can thus be represented as an expression of the form:

$$E = \frac{\sigma}{\epsilon}$$

Where E is Young's modulus, σ is the stress and ϵ is the nominal strain. Substitution and simplification give an expression that explains the change in length of a sample in relation to the pressure and Young's modulus as:

$$\delta = P\frac{L_0}{E}$$

Where δ is the change in the length of the material, P is the pressure and L_0, is the original material length.

Now, considering a small, thin strip of material just adjacent to a circumferential crack of length L_0, it can then be seen that by applying a circumferential force (as is the case during a leak characterisation test), there will be a resultant change in length δ. On the leak area, this change in length translates to a change in the area. Within the elastic limit, E is considered constant, and thus with an increase in pressure, there will be an increase in the extension of the strip length. The area of the leak will also change such that the rate of increase of the area becomes pressure-dependent with units (mm^2/m), which is the area-head slope. In a perfectly elastic material, this rate should be constant. However, as Hibbeler, (2016) points out, materials are not perfectly elastic.

It is then believed that there is a force value that needs to be met before near-perfect elastic behaviour is observed. Before this point, the internal materials stress is large enough to offer resistance and thus the rate of elongation (and m') is lower at lower forces and by extension, lower pressures.

5.4 Comparing Experimental Results with FEM Predicted Head Area Slopes

In section 2.2.5.2, a discussion was held wherein it was noted that a few studies had been conducted with the explicit aim of using a finite element method to model leakage behaviour in water pipes.

For these models, a regression analysis was conducted which helped to reduce the various factors that influence the behaviour of leakage to basic equations that could predict the head-area slopes of various leak types and sizes given the geometric properties of the leak and the pipe type.

Of note, are the three equations derived by Cassa and Van Zyl, (2014) to predict the behaviour of longitudinal, circumferential and spiral cracks, these are found as equation 13, equation 14 and equation 15, respectively, on this document. An additional equation referenced as equation 17 was developed by Nsanzubuhoro et al., (2017) this equation is used to predict the behaviour of round holes.

In this study, the three prediction equations were used to obtain the predicted head area slopes. Some of the parameters, such as pipe length and thickness, were obtained from measuring the pipe samples.

The parameters for the elastic modulus used were obtained from a PVC manual by Richardson, (2006) and compared with an experimental investigation conducted by Kowalska et al., (2014). Other required parameters, such as pipe thickness and orifice dimensions were measured in the laboratory Other parameters inherent to the sample such as the modulus of elasticity, E, were obtained from manufacturers data sheets and literature.

The predicted results obtained from finite element modelling were then compared to the experimental tests; these are shown and discussed below.

5.4.1 Round Hole Prediction

Nsanzubuhoro et al., (2017) derived equation was used in this study to predict the head-area slope of the 12 mm and 6 mm uPVC round holes.

Table 5-10 shows a summary of the parameters used to derive the predicted head area slopes.

Table 5-10 - Parameters used to predict the head area slope using equation 17 by Nsanzubuhoro, Van Zyl and Zingoni, (2017)

Data		
	12 mm Round Hole	**6 mm Round Hole**
Leak Diameter (m)	0.012	0.012/0.006
E (Pascals)	2.80E+09	2.80E+09
Poisson's Ratio, v	0.4	0.4
Internal Pipe Radius, r (m)	0.0535	0.0535
Pipe Thickness, t (m)	0.0452	0.0452

From equation 17, Nsanzubuhoro et al., (2017) predict an area-head slope, and it was found that for the 0.0127 mm^2/m for 12 mm and 0.0032 mm^2/m for the 6 mm uPVC round hole. The values obtained were then compared with the experimentally obtained values, as shown in Table 5-11.

For both orifice sizes, the head area slopes are small and represent a slight change in the area with respect to pressure and are near zero. However, the equation does not predict the negative area-head slope found in uPVC round holes.

Table 5-11 - Head-area slope values from this study and equation 18

Experiment	**m' (mm^2/m)**	**95% SPCI for m' (mm^2/m)**
Predicted (12mm)	0.0127	-
Experimental (12mm)	- 0.0103	0.004
Predicted (6mm)	0.0032	-
Experimental (6mm)	- 0.0079	0.0034

An effort was then made to determine if the predicted head-area slope values were within the 95% confidence region of this study's results. It was found that the predicted effective head-area slope did not lie within that confidence region, as shown in Figure 5-25.

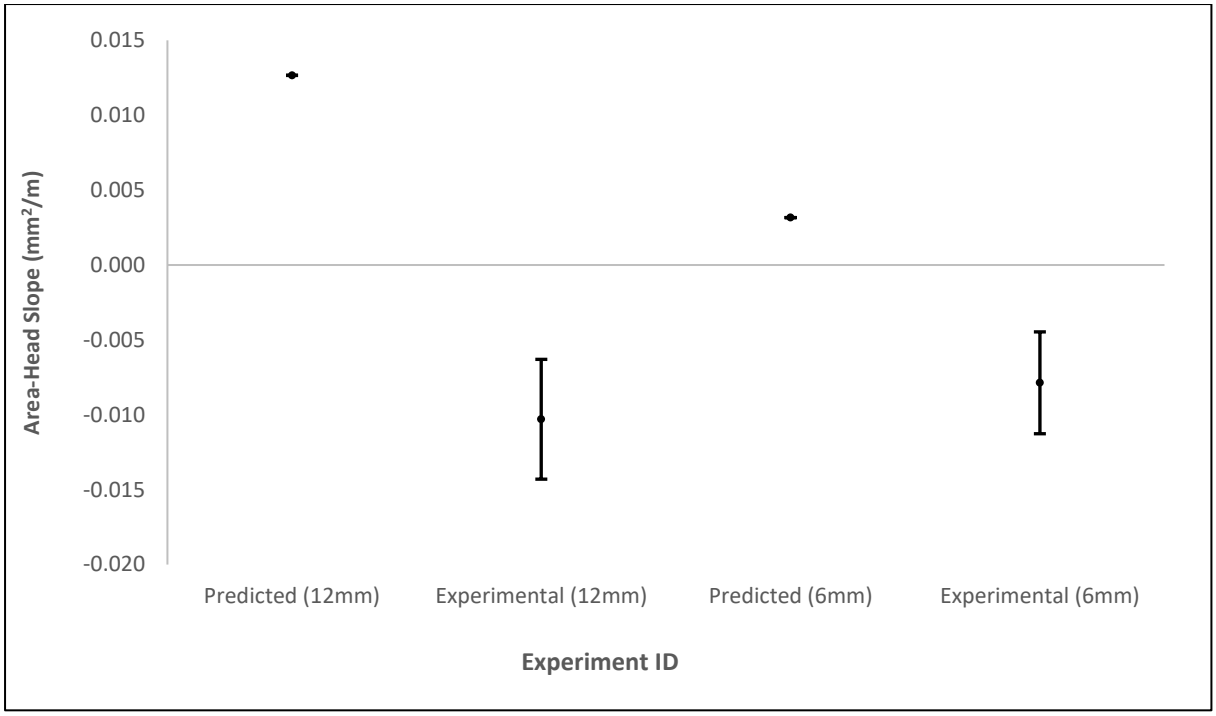

Figure 5-25 - Comparing the predicted head-area slopes of the round holes with the experimentally determined values

However, to one significant figure, the slope predicted by Nsanzubuhoro, Van Zyl and Zingoni, (2017) becomes additive inverse head-area slope of the slope found in this study with a value of 0.01 mm^2/m.

The same analysis was conducted for the 6 mm round hole, and it was found that the predicted head area slope did not lie within the 95% confidence interval of the experimentally determined values. This overlap was still not found even the inverse additive value of the predicted head area was compared with the experimental value of the head area slope.

The lack of negatives from the predicted values stems from generic PVC parameters, which have a generally positive head area slopes for round holes (Van Zyl and Malde, 2017), being used to derive an empirical equation meant to predict the head area slopes of round holes for all types of materials. Nsanzubuhoro et al., (2017) accounted for this discrepancy by analysing results from previous experimental results and modifying equation 17 to the form shown as equation 18. However, as this equation was found using a rather small dataset, it was not used to compare predicted values and the experimental values obtained from this study. In addition,

the negative head-area slope for a non-metal round hole appears to be a phenomenon inherent to uPVC pipes, and this is confirmed by analysing data from Van Zyl and Malde, (2017) who also found a negative slope for uPVC round holes.

5.4.2 Longitudinal Crack Prediction

An equation developed by Cassa and Van Zyl, (2014), was used to obtain the predicted values for the 50 mm and 100 mm longitudinal crack orifices. Table 5-12 contains a summary of the parameters used to predict the head area slope of a longitudinal crack using the equation

Table 5-12 - Parameters used to predict the head area slope using equation 13 by Cassa and Van Zyl, (2014)

Data		
	100 mm Longitudinal Crack	50 mm Longitudinal Crack
Length of Crack (m)	0.1	0.05
E (Pascals)	2.80E+09	2.80E+09
Internal Diameter, d (m)	0.0535	0.0535
Pipe Thickness, t (m)	0.00452	0.0452

Cassa and Van Zyl, (2014) predict an area-head slope of 3.706 mm^2/m for a 100 mm long by 1 mm wide and 0.346 mm^2/m for the 50 mm long by 1 mm wide uPVC longitudinal crack. This represents a significant positive change in the area with respect to pressure (3.07% and 0.692% of the original area for every meter of pressure head for the 100 mm and 50 mm crack respectively). Thus, equation 13, regardless of its limitations and within the bounds of the regression used to derive it (Cassa and Van Zyl, 2013), manages to reasonably predict the behaviour of longitudinal cracks. However, as seen in Table 5-13, the 50 mm crack prediction did not fall within the 95% SPCI of the experimentally obtained results.

Table 5-13 - Head-area slope values from this study and Cassa and Van Zyl, (2014)

Experiment	**m' (mm^2/m)**	**95% SPCI for m(mm^2/m)**
Predicted (100 mm)	3.706	-
Experimental (100 mm)	3.640	0.102
Predicted (50 mm)	0.346	-
Experimental (50 mm)	0.454	0.034
Experimental (50 mm) Low Pressure	0.259	0.045

Moreover, the head-area slope of the 50 mm longitudinal crack derived from the low-pressure tests was lower than the normal pressure range's head area slope. The predicted head-area slope values for the 100 mm crack were within the 95% confidence region of this study's results, as shown in Figure 5-26. This meant that the results obtained from this study contained the predicted value within the 95% confidence region. Thus, the equation performs well considering it is derived from empirical data and is valid within a particular pressure range.

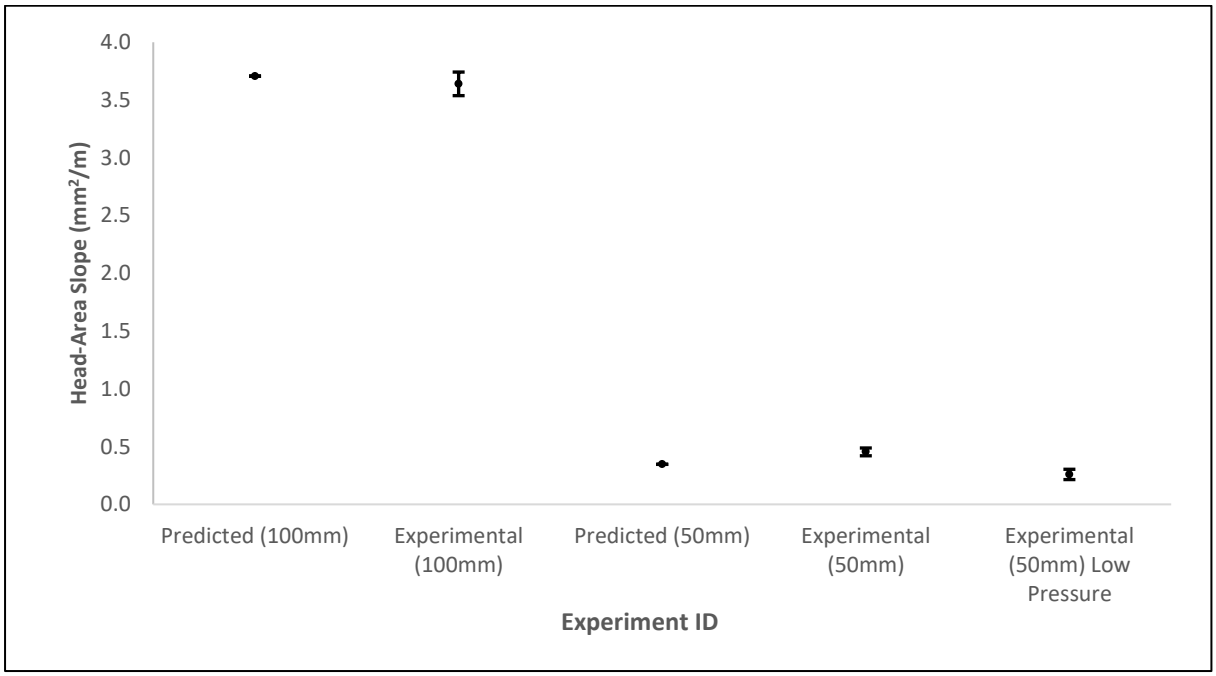

Figure 5-26 - Comparing the predicted head-area slope of a 100 mm longitudinal crack with the experimentally determined value

5.4.3 Circumferential Crack Prediction

The equation developed by Cassa and Van Zyl, (2013) for the circumferential crack has a component of longitudinal stresses acting on the pipe. This meant that the predictions conducted by utilising this equation could not be reasonably compared to the experimentally derived parameters. This was because the experimental setup was designed in such a way that eliminates longitudinal stresses in the test pipe, as explained in section.

In this study, there appeared to be some influence of longitudinal stresses due to the varying tension in the steel rods that were meant to eliminate the stresses. However, the overall values of effective area-head obtained were all negative which reflects that the longitudinal stresses were at most, minimum. This inference is reinforced by the observation made by Cassa and Van Zyl, (2013) who disclosed that negative head slopes were obtained in the biaxial loading state only for circumferential crack.

5.5 Chapter Summary

The aim of this chapter was to conduct tests using pressure ranges comparable with what the PCAD's pump can deliver to obtain a baseline for comparing PCAD derived leakage parameters. Leakage characterisation of the three pipe samples was conducted. The chosen leak sizes had system curves that were all within the pump's pressure curve.

It was observed that the parameters obtained from these tests were significantly different from the parameters obtained using standard pressures ranges. The effective area variance was explained as being due to the flow regimes being different, thus changing the coefficient of discharge and by extension, the effective area.

It was also perceived that the effective area-head slope might be pressure dependent. To explain this finding, it was suggested that there is a force value that needs to be met before near-perfect elastic behaviour is observed. Before this point, the internal materials stress is large enough to offer resistance and thus the rate of elongation (and m') is lower at lower forces and by extension, lower pressures. However, the effective are-head slope remains essential as it still provides results that are physically meaningful in leakage modelling and analysis.

A comparison of the experimental results obtained from this study with equations derived to predict the area-head slope was also made. For the equation used to predict the area-head slope of round holes, it was found that while the equation was able to reasonably predict the area-head slope. It was, however, unable to predict the area-head slopes of uPVC. This is due to the material properties of the uPVC pipe, which result in negative area-head slopes for round holes. While the equation had been updated to account for this finding, it was believed that the dataset used to derive the updated equation was too small to be used with confidence. It is thus recommended that that more tests on round holes with different materials and leak sizes be conducted and a better-calibrated equation be developed to predict the leak area-head slope better.

A similar comparison on the longitudinal crack predictions revealed mixed results. Firstly, for both the 50 mm and 100 mm cracks, the FEM equation was able to reasonably estimate the area-head slopes within the range suggested by (Nsanzubuhoro et al., 2019). The 100 mm laboratory obtained longitudinal crack area-head slope was found to contain the FEM predicted value within its 95% confidence interval. No overlap of the predicted area-head slope was observed for the 50 mm longitudinal crack. No comparison was made with the circumferential

crack results as the prediction equation has a component for longitudinal stresses, and the standardised method is designed to eliminate longitudinal stresses via the steel rods.

In conclusion, the work done on this chapter produced results that can could then be used for comparison with PCAD results to ascertain its efficacy and reliability.

6 LEAKAGE CHARACTERISATION WITH PCAD

This chapter contains a description of how the PCAD was used to conduct the leakage characterisation tests on the same pipe samples using the same setup as in section 4.11. The PCAD was used to pressurise the pipes and to record the flow rate and pressure values. The first step in conducting this test was to verify the accuracy of the instrumentation on the device and then calibrate the device. The procedure employed to conduct the verification and calibration is described below.

6.1 PCAD Instrumentation Calibration and Checks

For the device calibration and check, the pressure and flow rate instrumentation were checked to verify if the values they record are accurate. The device was then calibrated.

6.1.1 Pressure Instrumentation

For the calibration of the device transducer, an external sensor was connected on the same line and elevation as the device transducer. The connection made is shown in Figure 6-1. The calibration exercise was used to calibrate the reading from the device's sensor, which was inside the device to obtain the reading to be expected just outside the device, accounting for head losses.

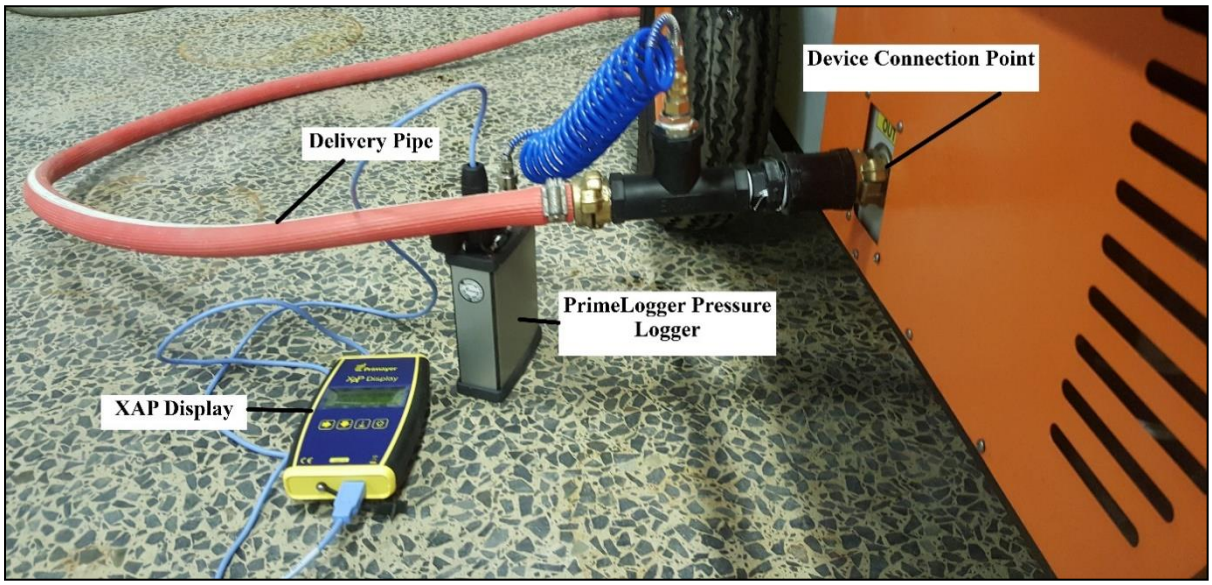

Figure 6-1 - Calibrating the PCAD's pressure transducer

The PCAD has one pressure sensor that records the pressure. The external sensor, which was connected in line with the PCAD's pressure transducer was the pre-calibrated Primayer Data Logger. Two operations were then done to simultaneously record the pressure on both devices, namely, filling up the tank and carrying out the pressure step test.

In the filling up procedure, water was pumped from the wall unit into the device via the inlet connection. On the inlet, there existed an external transducer that recorded the pressure from the pump, which would be recorded as the system pressure by the PCAD. The time at which this procedure was done was recorded. After the tank was full and the inlet valve into the tank had closed the stable pressure from the external water source was noted down and recorded on both devices, i.e. the pressure logger and PCAD.

The second procedure was to conduct a leak test. The PCAD's pump was used to pump water from the tank and discharged via the delivery pipe with no pipe connected. A pressure step test was used, where the pressure head was increased after the pressure had stabilised. Both the PCAD and data logger were again used to record the data. The data obtained from the two devices was recorded, and the pressure values at the same time (up to 1-second accuracy) was compared. A comparison of the datasets from the device and logger in relation to time is shown in Figure 6-2.

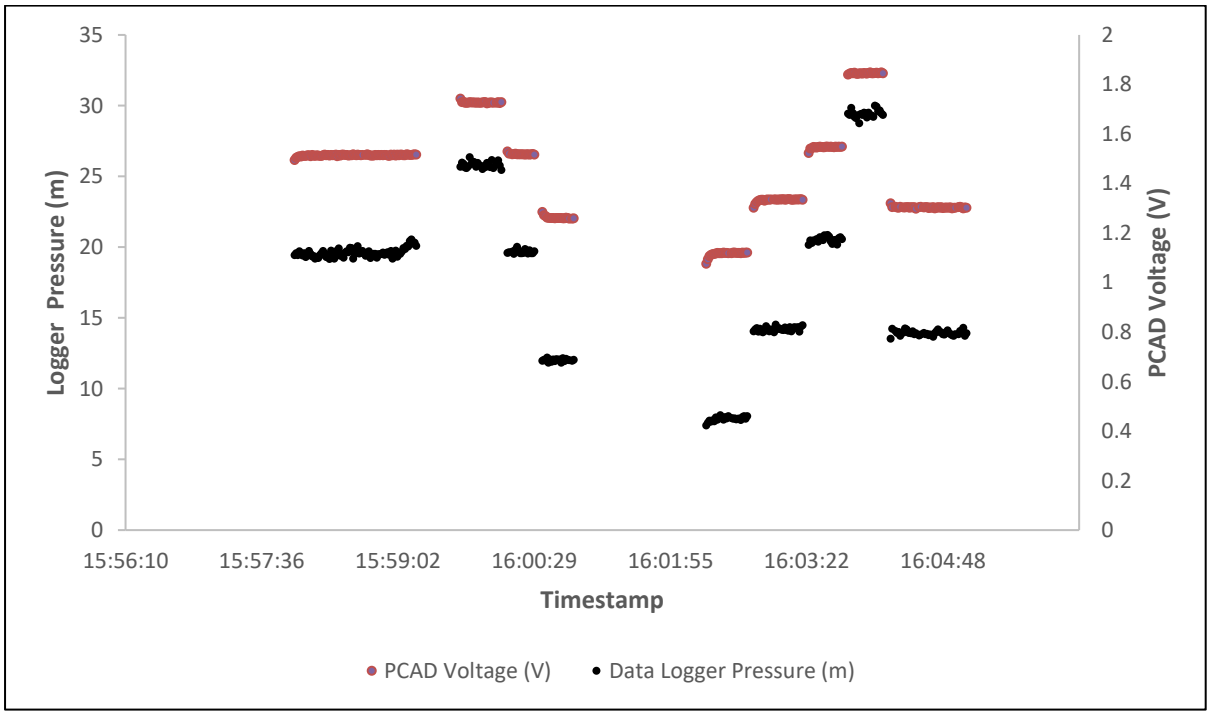

Figure 6-2 - Comparing the PCAD's voltage and the logger pressure

The data collected from the test was analysed to obtain the linear regression equation shown in Figure 6-3 that explains the relationship between the two datasets. From this relationship, a regression analysis output sheet was obtained through MS Excel's Regression Analysis data pack and was used to calibrate the PCAD's pressure sensors. This equation was then programmed onto the PCAD's system to adjust the voltages and convert them to calibrated pressure readings.

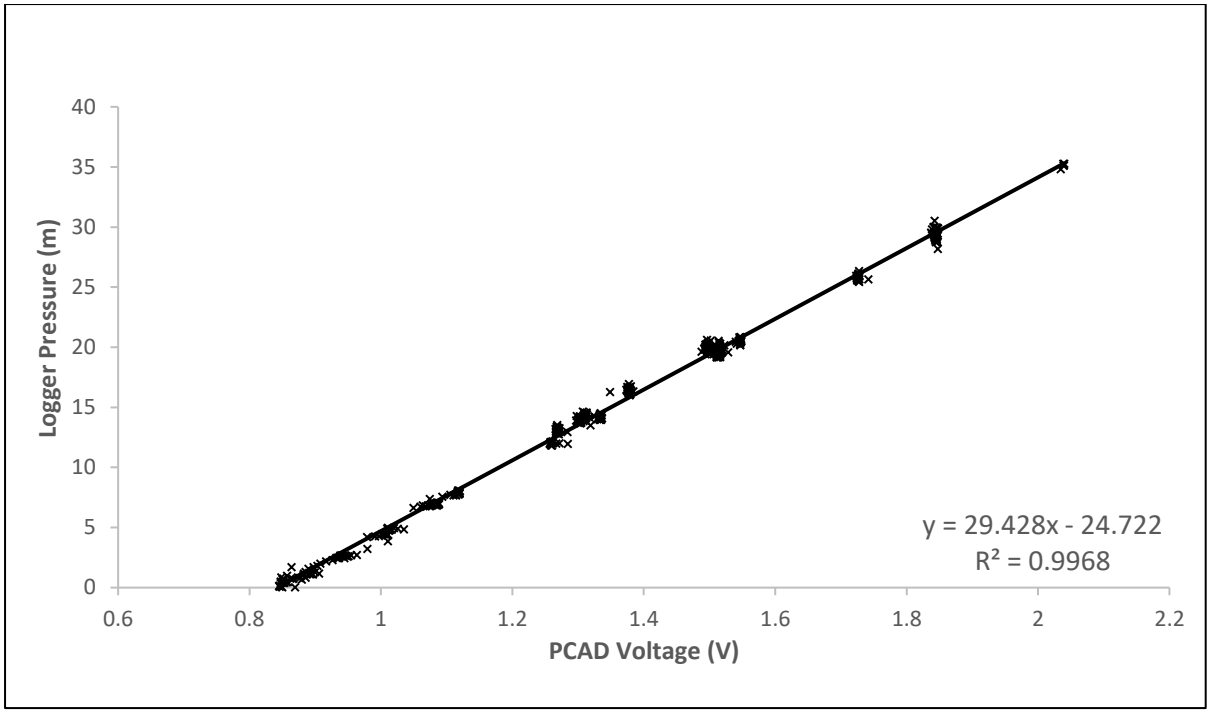

Figure 6-3 - Linear regression equation for the PCAD pressure calibration

However, the equation obtained via the regression analysis did not give a 100% match due to the variability of the data. This meant there would be an error in the devices' flow measurements. The error in the data obtained via the PCADs' pressure sensors was established by initially finding the error in the values obtained from the PCAD's calibrated flowrate measurements. This is described by equation 22:

$$\boldsymbol{PCAD\ Error = Logger\ Pressure - PCAD\ Calibrated\ Pressure} \quad \boldsymbol{(22)}$$

A statistical analysis of the error terms was then conducted using a statistical analysis pack on Microsoft Excel, and from this, the mean of the error terms at a 95% level of the confidence interval was obtained.

The PCAD pressure measurements were found to have a mean error of 0.006 m which deviated by 0.04 m. This is a comparatively small error when compared to the error from the logger's pressure transducer.

6.1.2 Flow Instrumentation

The PCAD has two Itron Aquadis+ volumetric cold-water flowmeters with a nominal flow rate of 1.5 m^3/h, a maximum flow rate of 3.5 m^3/h and a minimum flow rate of 7.5 l/h. The flowmeters are connected to the device's microcontroller, which records the readings the meters pick up. To ensure the accuracy and reliability of measurements obtained from the

device via these meters required that the meters be checked against an established accurate meter.

The ideal meter would have been the electromagnetic flowmeter in the lab. However, this could only be used to record flow in the ‘in” direction of the device and can thus only check one meter. To check both meters required a meter that would allow bidirectional flow or be easily changed to align with the flow direction.

To that end, another Itron Aquadis meter was used in a setup shown in Figure 6-4. The meter was equipped with quick-release fittings for an easy and fast connection. Volumetric water pulses from the meter were recorded with a Sensus logger on the pulse function. This meter was then checked against the electromagnetic flowmeter, and a relationship was found. The Itron Aquadis meter was then connected at the PCAD inlet and was used to check the PCAD flowmeters.

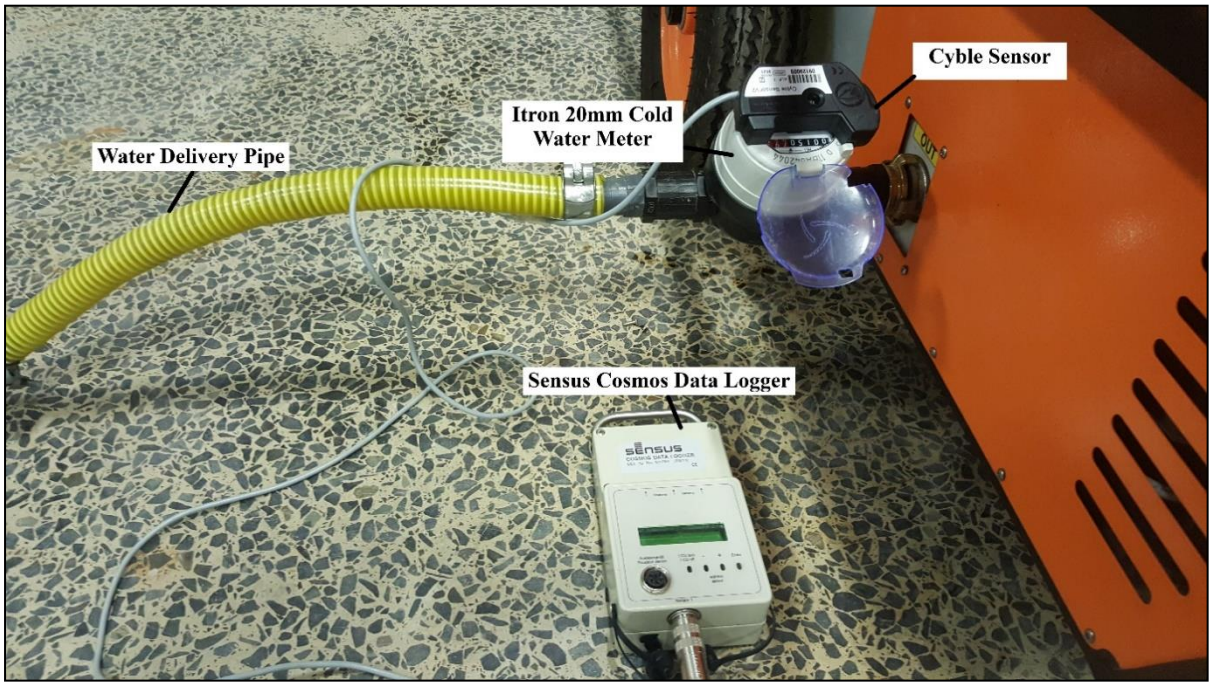

Figure 6-4 - Checking the PCAD's flow sensors

The inlet meter’s accuracy was checked by allowing water to flow through the outside meter and the PCAD inlet meter during the filling up, as described in chapter 3.3.3. The PCAD outlet meter’s accuracy was checked by pumping out the water in the tank and increasing the pumping speed to obtain different flow rates.

The flow readings which the two devices (PCAD meters and calibrated meter) picked up were recorded, downloaded and compared. The data from the flow meter and the PCAD was

downloaded and analysed on a Microsoft Excel spreadsheet. The aim was to match the flow rates from the logger with the device's flowrate using the timestamps found on every reading.

After a match had been established the two datasets could then be analysed, and a regression analysis was done to determine the equation that relates the device flowrate to the actual flow rate as measured by the external meter.

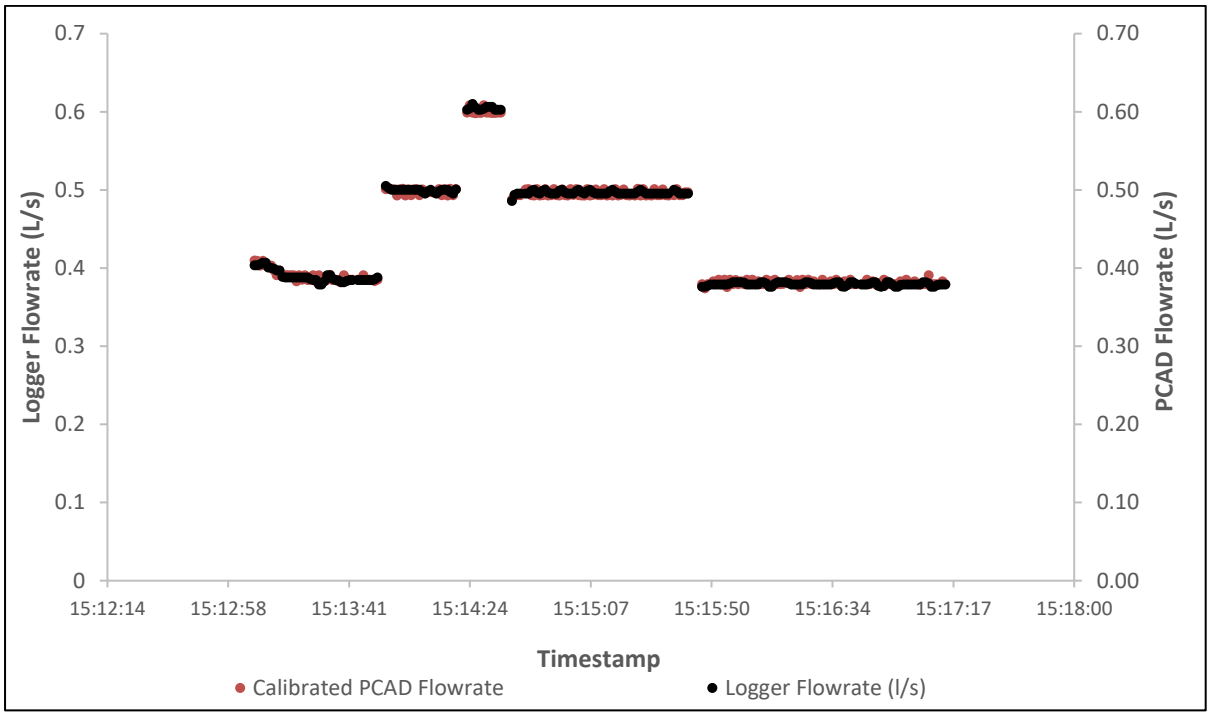

Figure 6-5 - Comparing the PCAD's flow rate and the logger flow rate

The relationship between the flow rate through the external meter and the pipe condition assessment devices' flow sensor was statistically compared and a relationship established.

Using the same error analysis as described above, the PCAD was found to have an error of - 0.00016 L/s, which deviated by ± 0.00051 L/s. This is a moderately small error which is comparable to the error from the electromagnetic flowmeter given in Chapter 4. This was expected as the external and device flow meters are from the same manufacturer, and both were fairly new.

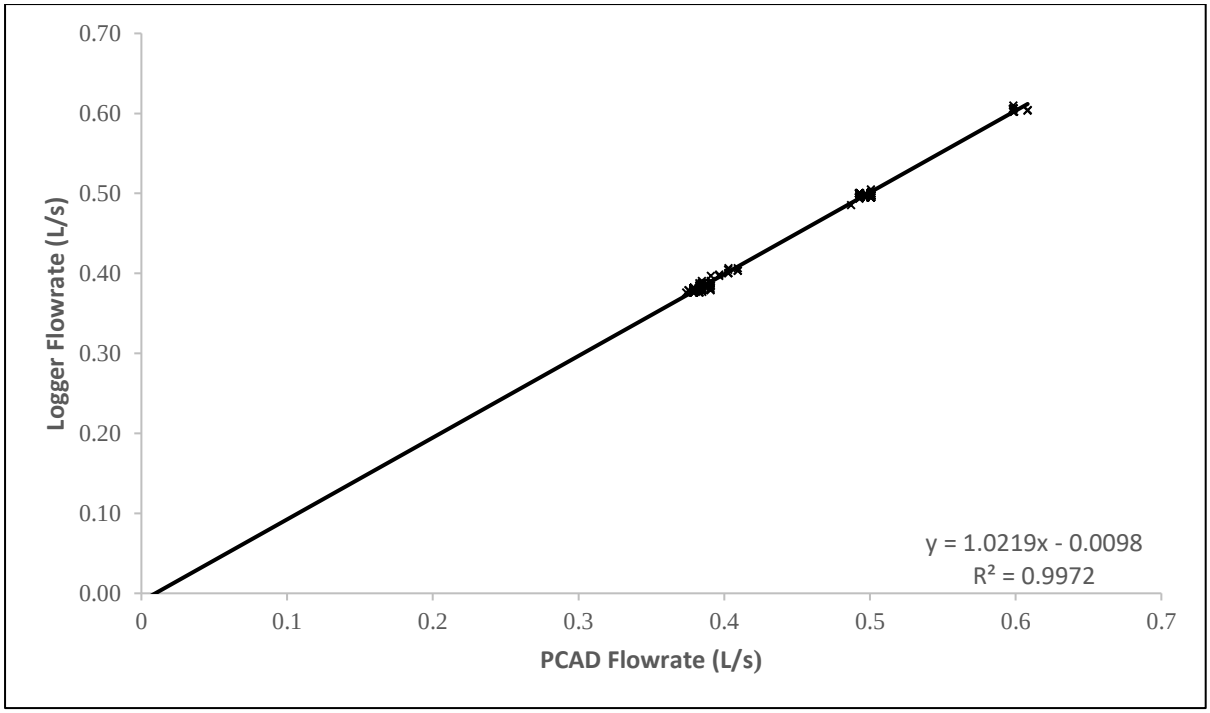

Figure 6-6 - Linear regression equation for the PCAD pressure calibration

The statistic of concern, however, was the range in the error terms which was found to be 0.023 L/s. This range in the errors could have a noticeable effect when characterising leakage with small flow rates

6.2 Calibrating Head Losses in the System

As with any pipe system conveying a fluid, it was realised that there would be losses in the system, from the PCAD pressure sensor to the actual leak. Initially, these losses were accounted for by using basic hydraulic equations for pipe flow losses, found in most hydraulic textbooks such as Chadwick et al., (2013). A pressure transducer and a data logger were connected to the pipe tests setup, downstream of the leak to calibrate the equation through obtaining the actual loss coefficients.

The logger was programmed on the same computer that had access to the PCAD's code, and a check was made to ensure that the timestamps of the logger and the PCAD matched. A leak test was then performed with the PCAD with the pressure values at the device outlet being recorded by the device sensor.

The pressure values obtained from the leak test via the external transducer and PCAD sensor were collected and compared on a graph. The flow rate of the fluid was also recorded on the PCAD, and that data was downloaded and saved. The pressure values obtained from this exercise were then copied onto an analysis sheet that had the loss equation derived from

hydraulic principles. The expected pressure was subsequently copied and pasted on the same table that had the logger and the raw PCAD pressure values. A graph with a visualisation of the pressure values is shown in Figure 6-7. An analysis of the error values, i.e. the difference in the predicted equation and actual logger pressure was done, and points with an error of more than 10% were noted. These were all identified as high error points and were also plotted on the same graph.

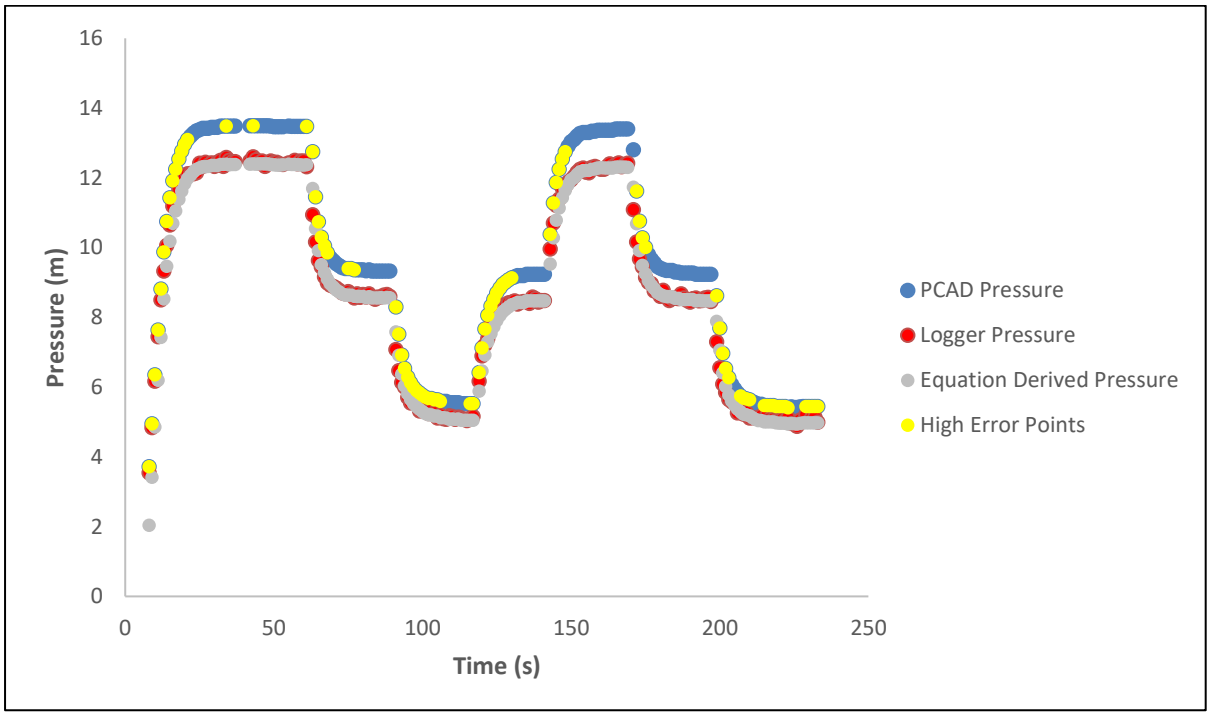

Figure 6-7 - Comparing the pressure values

An analysis of the data revealed that there were more errors during the step-change periods and on low-pressure steps. The step-change periods are not used in the leak tests and thus could be omitted. Thus, these error points were omitted from further analysis of the loss coefficients. From the figure, the stabilised pressure points were identified, and the flow rate and pressure data pertaining to those areas were extracted. This resulted in 5 pressure steps being obtained, each with their respective flow rate values.

From the data collected, it was found that the coefficients used to determine the PCAD pressure using the hydraulics derived equation were incorrect for this system. This could because the coefficients found in standard texts are derived from industry conditions using specific materials. It was therefore required to find the actual loss coefficients for this system which is shown in Figure 6-8. This would aid in calibrating the PCAD and enable it to give more accurate values.

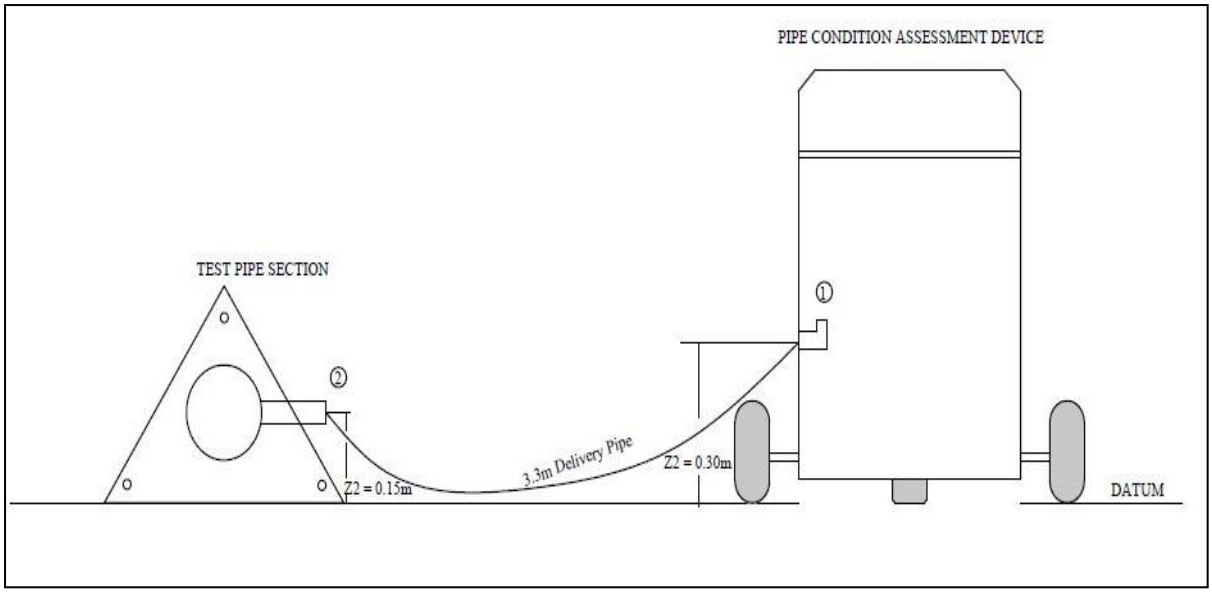

Figure 6-8 - Schematic of the system

The system-specific loss coefficients were found through initially analysing the system as two points 1 and 2, with different pressure components, as shown in Figure 6-8 where point 1 is the pressure transducer downstream of the leak and point 2 is the PCAD pressure sensor. An analysis of the pressure heads between the two points was done using the energy equation, as shown in equation 23. The equation consists of the static pressure head, the elevation head, the velocity head, minor losses including (entry losses) and friction loss in the pipe.

$$H_1 + \frac{{V_1}^2}{2g} + Z_1 = H_2 + \frac{{V_2}^2}{2g} + Z_2 + \frac{K_L {V_1}^2}{2g} + \frac{fL{V_1}^2}{2gD} \qquad (23)$$

Where H_1 and H_2 are the pressure head values recorded by the PCAD pressure sensor and the logger, respectively. V is the velocity and Z is the elevation from the datum, which is the ground level. K_L and f are the minor loss coefficient and friction factors, respectively. Through manipulating the flow rate-velocity relationship and identifying that V_2 is zero, the equation was simplified to, and the following expression was derived:

$$(H_1 - H_2) = \frac{8K_L Q^2}{\pi^2 g D^4} + \frac{8fLQ^2}{\pi^2 g D^5} - \frac{8Q^2}{\pi^2 g D^4} + (Z_2 - Z_1) \qquad (24)$$

The values of the pressure head from the logger and PCAD were used to obtain the LHS of the equation for every step. These values were recorded on a table in the Microsoft Excel package. The RHS of the expression was evaluated by first deriving the Reynolds number at every step. Haaland's approximation to the Colebrook-White equation for obtaining the friction factor of fluid under turbulent flow was applied. This equation is as equation 25:

$$\frac{1}{\sqrt{f}} = -1.8\, log\left[\left(\frac{e}{3.7D}\right)^{1.11} + \frac{6.9}{Re}\right] \qquad (25)$$

Where D is the diameter of the pipe; Re is the Reynolds number and *e* is the absolute roughness of the pipe. A randomised value of *e* was then used to obtain the friction factors. The RHS of the equation was then solved by using the friction factor, f generated from the Haaland equation and a randomised value of K_L initially set as 0.5. An evaluation of the difference between the LHS and RHS of equation 25 was then done. The sum of the differences was subsequently found. A solver on the Microsoft Excel software was then used to minimise these values by optimising the values of K_L and *e*.

The values obtained from the solver then gave the actual pipe absolute roughness and loss coefficients for the system. For this system, the K_L was found to be 0.593 and *e* was found to be 1.31E-04. Table 6-1 shows the results from this optimisation and reveals that the obtained values minimise the error to 9.47E-07 m or 0.000945 mm.

Table 6-1 - Values used to evaluate the loss coefficients

H_1 (m)	H_2 (m)	Q^2 (10^{-5})	H_1-H_2	LHS	Re (10^4)	f	RHS	L -R	% Error
13.4	12.24	5.84	1.16	1.52	3.43	0.035	1.46	0.06	0.53
9.21	8.547	4.79	0.669	0.96	2.81	0.035	0.99	-0.02	-0.33
13.29	12.21	5.82	1.08	1.45	3.42	0.035	1.45	-0.002	-0.02
13.35	12.28	5.83	1.06	1.43	3.43	0.035	1.46	-0.02	-0.20
13.26	12.18	5.81	1.07	1.44	3.42	0.036	1.45	-0.008	-0.06
								Σ=9.47E-07	Σ = -0.02

The values obtained using the hydraulic derived equation and the optimised $K_L$and *e* were then found to have an error of 0.02% which means the PCAD could now evaluate the pressure values at the leak to a 0.02% accuracy of the logger values.

6.3 Leakage Characterisation Tests

6.3.1 Test Procedure

To characterise leakage on the uPVC sections using the PCAD, the following procedure was used:

1. The user-programmed the device via the device control panel, accessed via a webpage as described by Lopez and Zyl, (2019). On the webpage, the user-specified the number of pressure steps for the test mode. The available choices were; to either have the steps controlled by the device identifying stabilised points and varying the pressure or to have the steps controlled by a set duration, for instance, thirty (30) seconds. The user also entered the test pipe parameters such as the length of the pipe and the pipe type.
2. Next, the device was connected to the test setup, as shown in Figure 6-9. The connection to the 20 mm fire hose has quick release fittings on both ends.

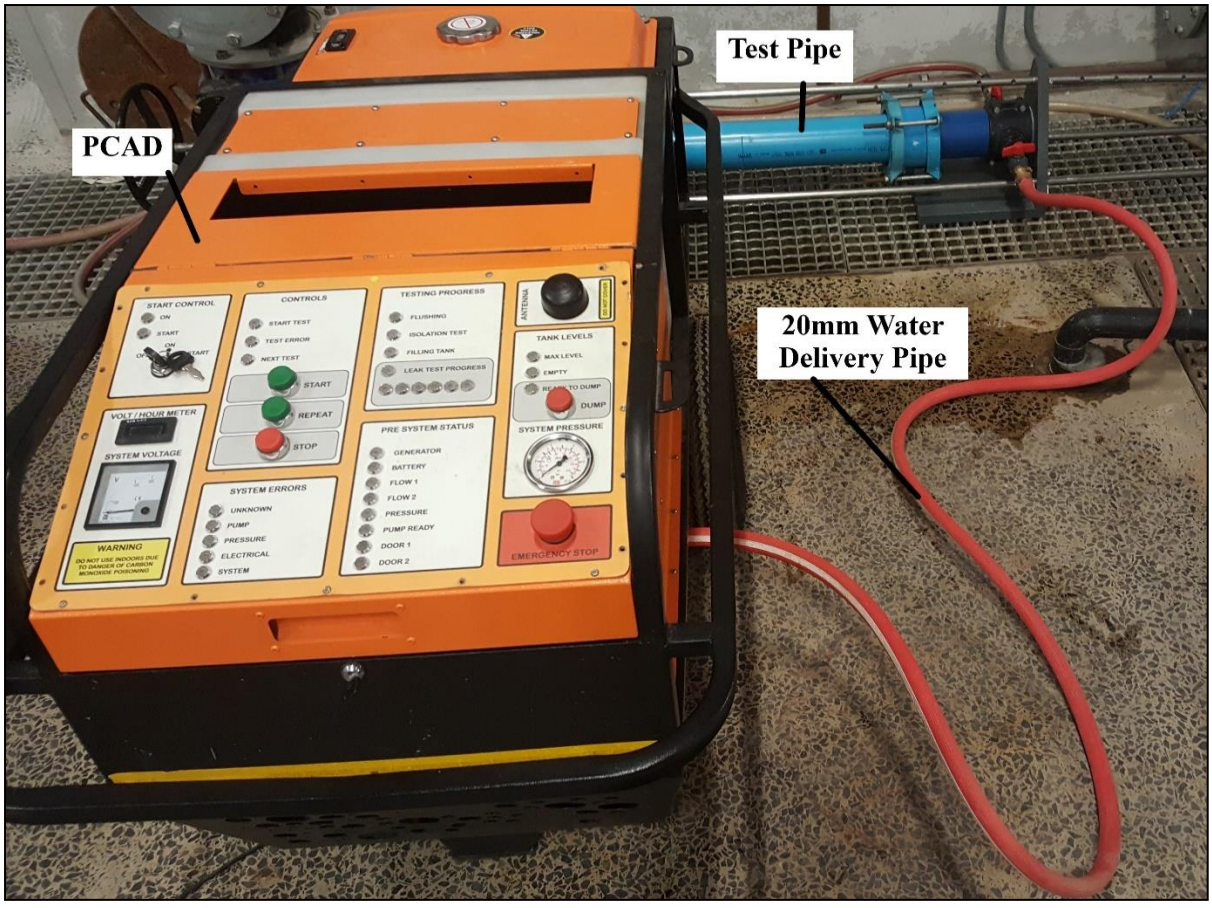

Figure 6-9 - PCAD connection to standardised setup

3. The wall unit was switched on to allow water to be pumped through the pipe and into the device's onboard tank, with the device on the "Tank Fill" operation. When the tank was full, the device automatically shut the valve into the tank, and the wall unit was switched off.
4. The "Leak Test" function on the PCAD was then selected, and this initiated the leak test. In the leak test function, the device pumped water into the test pipe. As the only opening available on the setup was the machined crack, the water flowed through it, and a flow and pressure measurement was recorded on the device. The pressure during the test was varied as programmed on step 1, by changing the device's pump speed.
5. The test data was then downloaded from the device webpage and analysed on the Microsoft Excel program.
6. The test was repeated ten (10) times for each pipe sample.

The results of the tests and calibration operations are discussed in the next section

6.3.2 6 mm uPVC Round Hole

After the instrumentation had been calibrated, ten tests were done on the uPVC pipe section with a 6 mm round hole. As with previous experiments, the pressure and flow were recorded, and the stabilised steps were then used to analyse the data. Figure 6-10 shows a typical 6mm uPVC round hole pressure and flow relationship at each step.

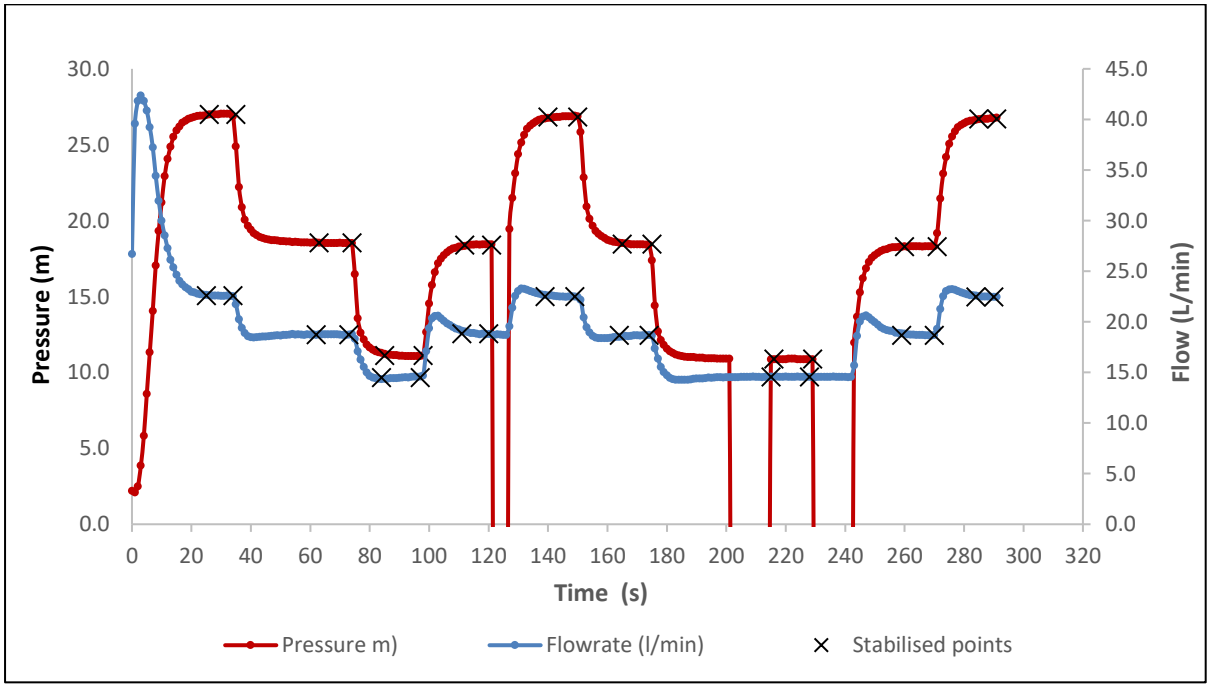

Figure 6-10 – Typical pressure head-flow rate relationship for a test with the PCAD

The drops in the pressure readings were due to one of the components in the PCAD malfunctioning due to electric current leakage during a test, which resulted in the device detecting negative pressures. The flow rate and pressure head at each step were recorded then plotted on a graph. Figure 6-11 this relationship between the flow rate and the pressure head. The N1 is found as the exponent of the relationship, which is a power relationship.

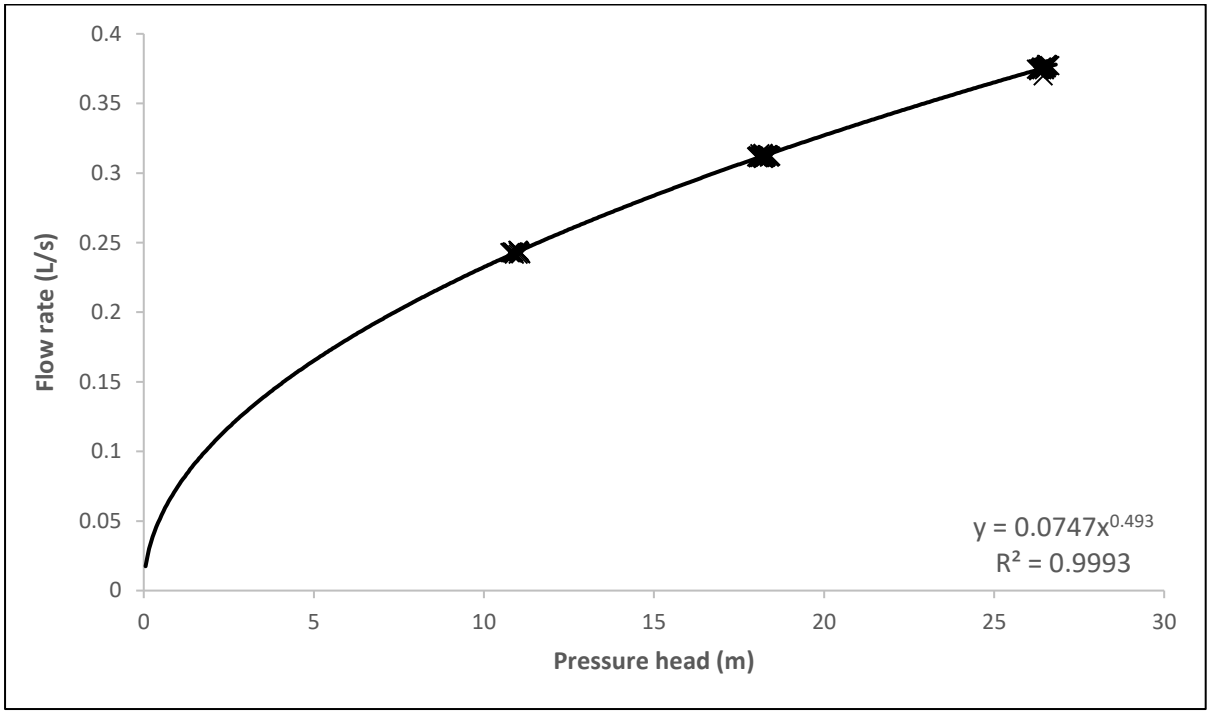

Figure 6-11 - Flowrate-pressure power relationship of a 6mm uPVC round hole

The N1 value for the pipe sample was found to be 0.493 with a standard deviation of 0.0022 and sample variance (variance of the N1 values of the ten conducted tests) of 5.26E-06. These results communicated that there was little variance in the tests and represent excellent repeatability and reliability of the conducted tests for the N1 parameter.

Through manipulating the orifice equation, the effective area for every pressure and flow step was found. The effective area was then plotted against the pressure head. The data were also analysed using the regression package on Microsoft Excel, and the effective area-head slope for the pipe sample was found to be - 0.00615 mm^2/m meaning for every meter of pressure head the orifice area decreased by 0.00615 mm^2 (a 0.02% reduction in leak area). This is a minimal change in the area with respect to pressure and reinstates the observation that round-shaped leak areas are not very responsive to pressure changes. This effective area-head slope was comparatively small, and near-zero as suggested by Nsanzubuhoro et al., (under review).

The effective area-head slope (C_dm) is shown in Figure 6-12. The standard deviation of the effective area-head slope was found to be 0.00206 mm^2/m, while the sample variance effective area-head slope, which measures how far each test value is from the sample mean was found to be 4.25E-06 mm^2/m (0.07% of the mean C_dm). These statistical values report little variance between test values and show excellent repeatability in the test. The single parameter confidence interval for the effective area-head slope (mm^2/m) is ± 0.0053 mm^2/m.

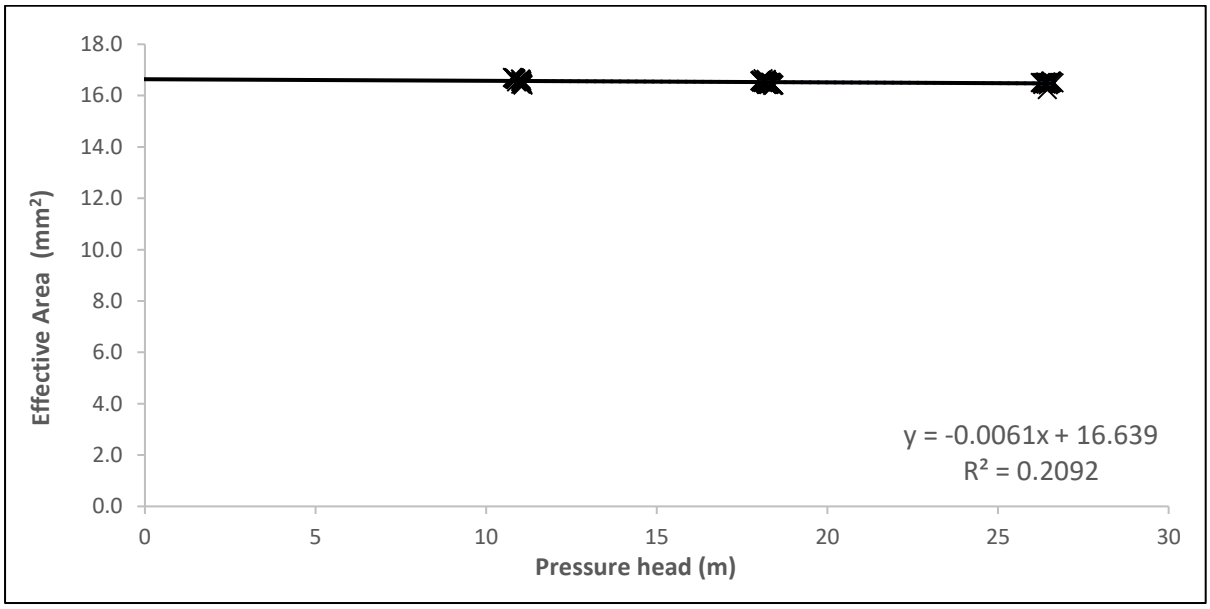

Figure 6-12 - Graph showing the effective head area slope of a 6mm uPVC round hole

The flow rate predictions derived from the FAVAD and N1 equations using the parameters found in this study were compared, as shown in Figure 6-13.

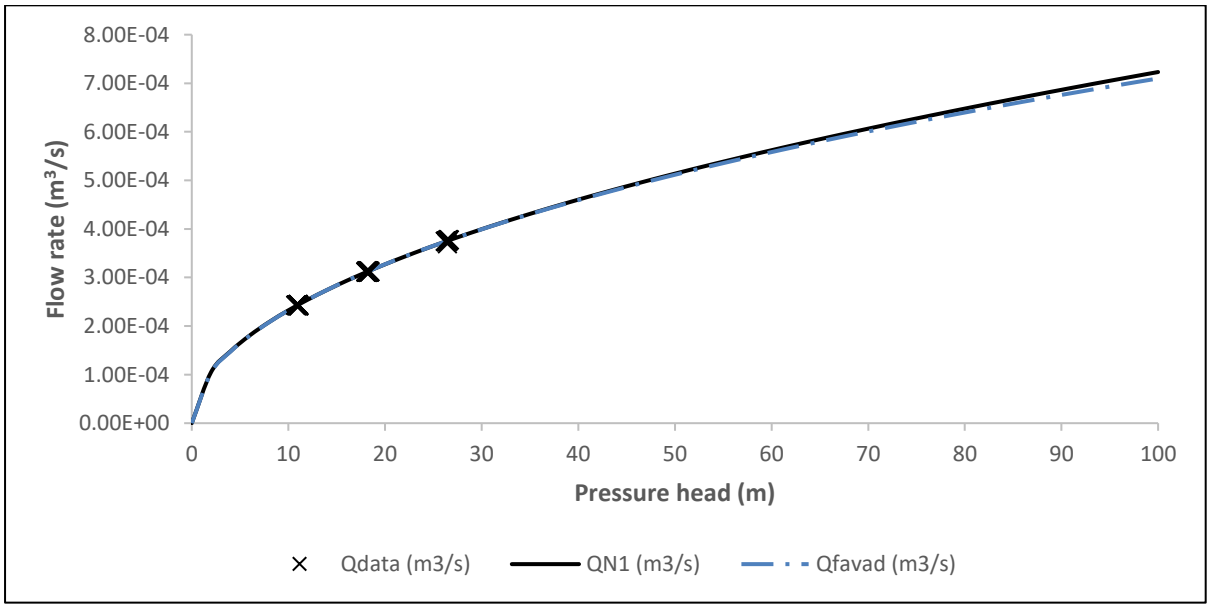

Figure 6-13 - Comparison of the FAVAD and N1 equation flow predictions and observed data

Within the measured pressure range for the 6 mm uPVC round hole, both models fit the data well. This is because the round hole appears to obey the orifice equation as the leak area does not substantially change with pressure, and as a result, the N1 equation aligns with the modified orifice equation. Table 6-2 then shows a summary of the results for the data presented above.

Table 6-2 - Summary of Results

	N1	**A_0' (mm^2)**	**95% SPCI for A_0' (mm^2)**	**m' (mm^2/m)**	**95% SPCI for m' (mm^2/m)**	**p for m' (%)**	**C_d**
This Study	0.493	16.63	± 0.0511	- 0.00615	± 0.0053	<0.05	0.59

Further analysis of the parameters obtained from the ten (10) individual tests conducted using the PCAD revealed that it has excellent repeatability. The parameters analysed were the effective area and effective area-head being the parameters of importance as they are the main parameters used in the characterisation of leaks. This is because these parameters are essential in modelling and managing leakage. Figure 6-14 and Figure 6-15 show the graphs that describe the repeatability and reliability of the results conducted on a 6 mm uPVC round hole using the PCAD.

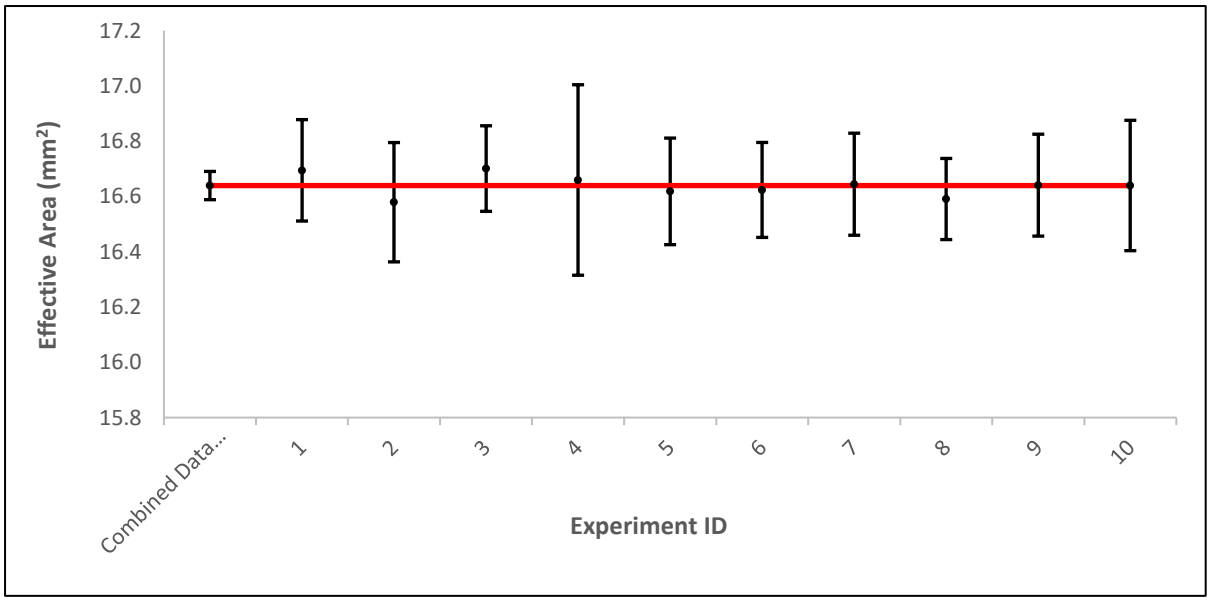

Figure 6-14 - Effective area comparison and repeatability analysis of the 6mm round hole tests with the PCAD

In Figure 6-14, the effective areas obtained from the 10 tests all fall within the 95% confidence interval of the average value of the tests and within each of the ten tests conducted. A similar observation is made from analysing the values and confidence intervals of the effective area-head area slopes of the ten tests, as shown in Figure 6-15.

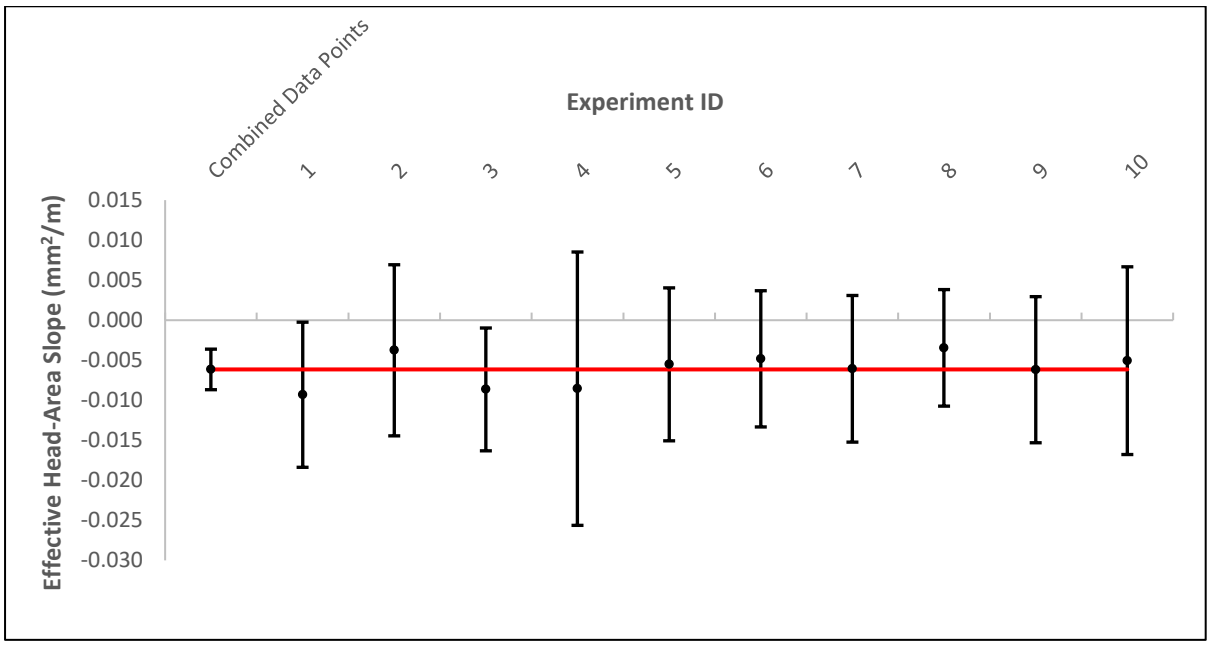

Figure 6-15 - Effective area – head slope comparison and repeatability analysis of the 6mm round hole tests with the PCAD

The figures thus visually confirm the good repeatability of the experimental results using the PCAD. Table 6-3 then shows a summary of the parameters obtained in each of the ten tests.

Table 6-3 - Summary of results for the ten 6 mm Round Hole tests with the PCAD

Experiment ID	A_0' (mm^2)	m' (mm/m)	N1	C_d	c
1	16.7	-0.00931	0.489	0.590	0.00008
2	16.6	-0.00376	0.496	0.587	0.00007
3	16.7	-0.00864	0.490	0.591	0.00008
4	16.7	-0.00855	0.491	0.589	0.00007
5	16.6	-0.00551	0.494	0.588	0.00007
6	16.6	-0.00483	0.494	0.588	0.00007
7	16.6	-0.00607	0.493	0.589	0.00007
8	16.6	-0.00345	0.496	0.587	0.00007
9	16.6	-0.00618	0.493	0.589	0.00007
10	16.6	-0.00505	0.495	0.589	0.00007

Figure 6-16 shows the comparison of the m' of the tests conducted with standard laboratory equipment and the PCAD. It also shows overlaps of the 95% single parameter confidence

interval of the m' values. A two-sample t-test with variance assumed as unknown was conducted using the data analysis tool pack on Microsoft excel. The hypotheses for the test were:

H_0: $m'_{\mathbf{pcad}} = m'_{\mathbf{lab}}$

H_1: $m'_{\mathbf{pcad}} \neq m'_{\mathbf{lab}}$

An alpha level of 0.05 was chosen**.** The decision criteria were to reject H_0 if p-stat (two tail) is less than 0.05. For the test and the following results were obtained:

	m' (mm/m) (PCAD)	***m' (mm/m) (LAB)***
Mean	-0.00614	0.000902
Variance	4.26E-06	4.52E-05
Observations	10	10
Hypothesized Mean Difference	0	
Degrees of freedom	11	
t Statistic	-3.16	
P(T<=t) one-tail	0.00451	
t Critical one-tail	1.796	
P(T<=t) two-tail	0.00902	
t Critical two-tail	2.20	

A p-value of 0.00902 which is less than the set alpha value of 0.05, was found. Therefore, the null hypothesis that the effective area-head slopes from the two sets of experiments are the same was rejected.

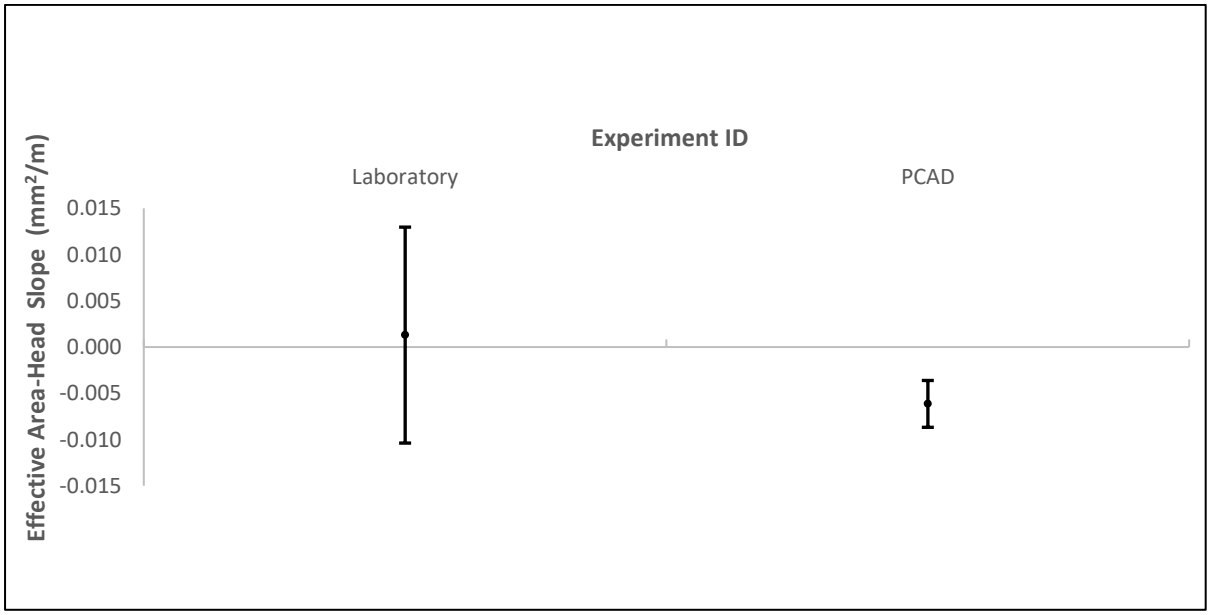

Figure 6-16 - Comparing the effective area-head slopes

Although the t-test revealed that the effective area-head slopes of the tests were statistically different, the confidence intervals of the set of experiments, however, overlapped. This finding communicated that within a 95% level of confidence, that is to say, 95 times out of a 100, the results from the laboratory tests will be obtained by the PCAD. The PCAD's single parameter confidence interval (SPCI) is smaller than the SPCI from the laboratory values. This is because the PCAD has less variance in how the pressure values for each step are determined as these are done via the code. In the laboratory experiments, the pressure values for each step are set by the user varying the pump's VSD manually, and thus it is hard to replicate the same pressure values during a test and across 10 tests. This variance is transferred to the effective area-head slopes per step, and this results in a large confidence interval.

Figure 6-17 then shows the comparison of the A_0' of the tests conducted with standard laboratory equipment and the PCAD. The 95% SPCI of the effective area also overlapped.

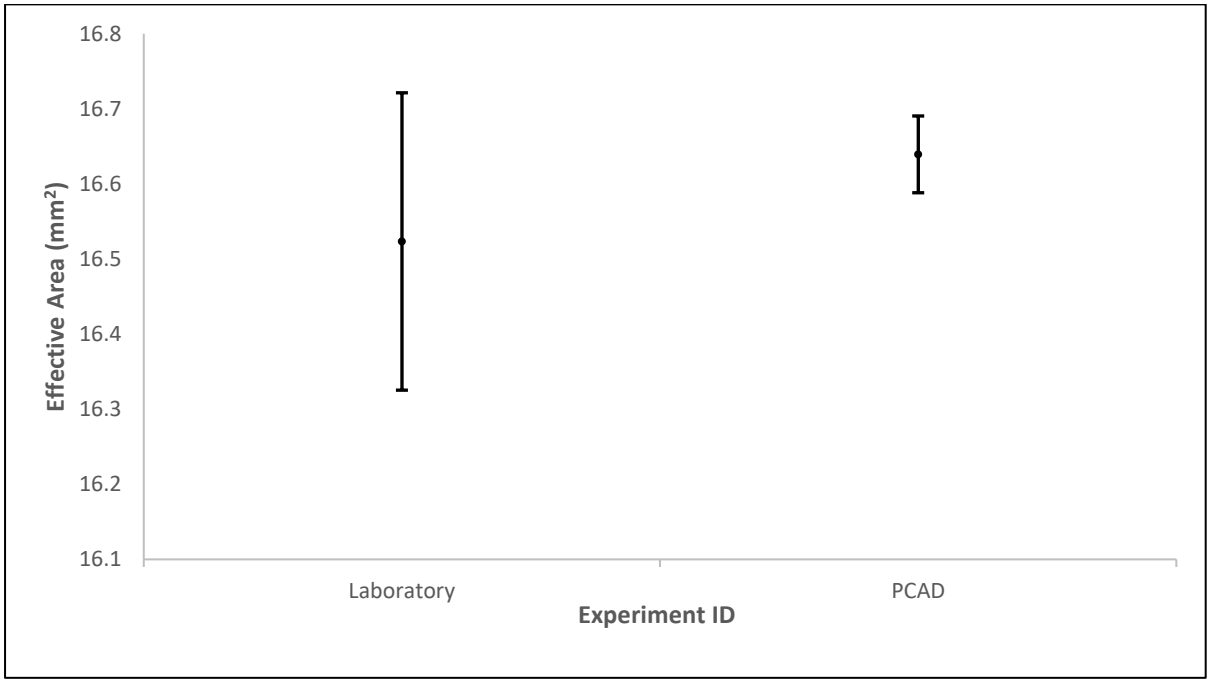

Figure 6-17 - Comparing the effective area values

As above, the SPCI of the PCAD is smaller than the laboratory experiments SPCI, and the above-mentioned reasons still apply for this parameter.

6.3.3 50 mm uPVC Longitudinal Crack

The pipe sample from the previous section was replaced with a uPVC pipe section with a 50 mm longitudinal crack, and ten tests were done using the PCAD. The pressure and flow were recorded on the device, and the stabilised steps used to analyse the data. Figure 6-18 shows a typical 50 mm longitudinal crack pressure and flow relationship at each step.

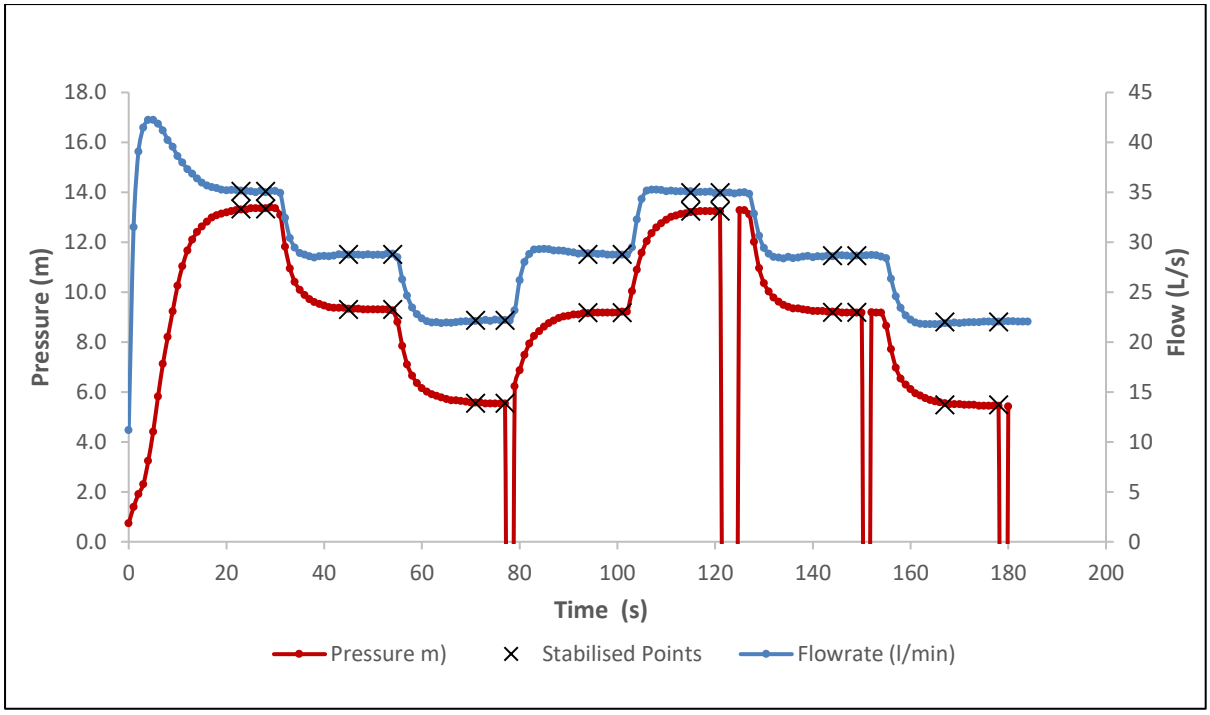

Figure 6-18 - Typical pressure head-flow rate relationship for a test with the PCAD

The flow rate and pressure head at each step were recorded then plotted on a graph. Figure 6-19 this relationship between the flow rate and the pressure head.

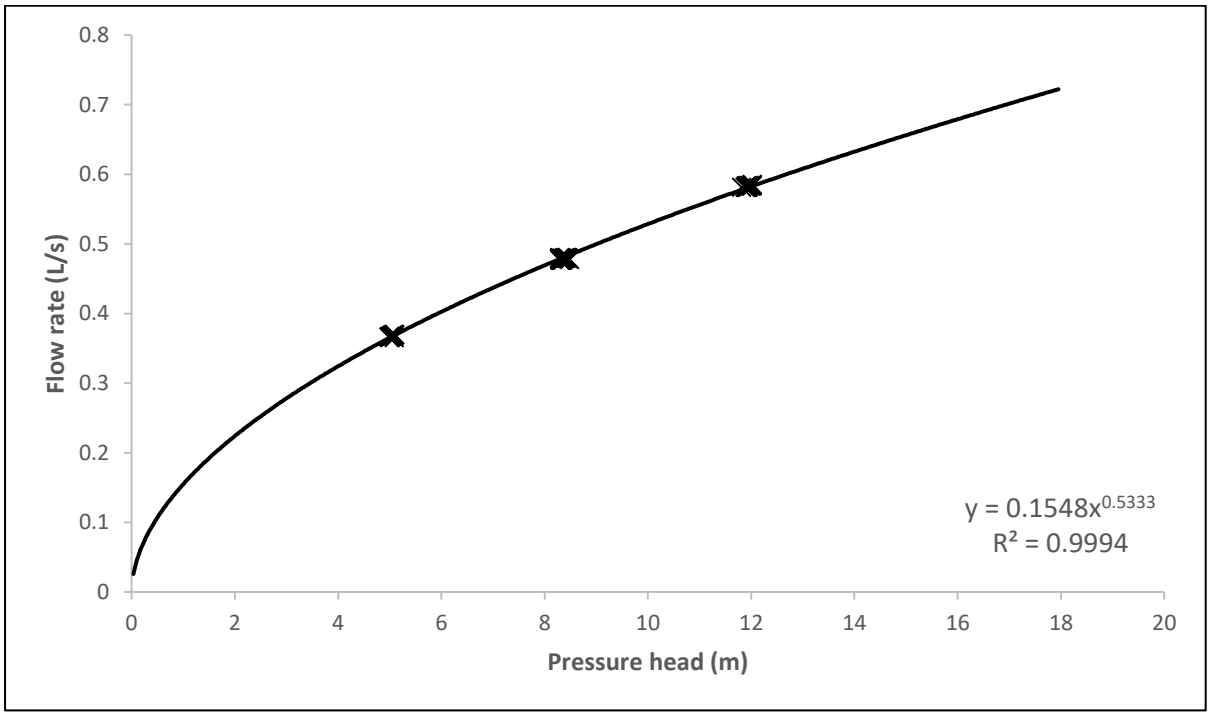

Figure 6-19 - Flowrate-pressure power relationship of a 50 mm uPVC longitudinal crack

The N1 is found as the exponent of the relationship, which is a power relationship. The N1 value for the pipe sample was found to be 0.533 with a standard deviation of 0.00197 and sample variance (variance of the N1 values of the ten conducted tests) of 3.91E-05 (0.007%

variance from the mean N1). These results communicated that there was little variance in the tests and represent good repeatability and reliability of the conducted tests for the N1 parameter.

Through manipulating the orifice equation, the effective area for every pressure and flow step was found. The effective area was then plotted against the pressure head. The effective area-head slope (C_dm) shown in Figure 6-20.

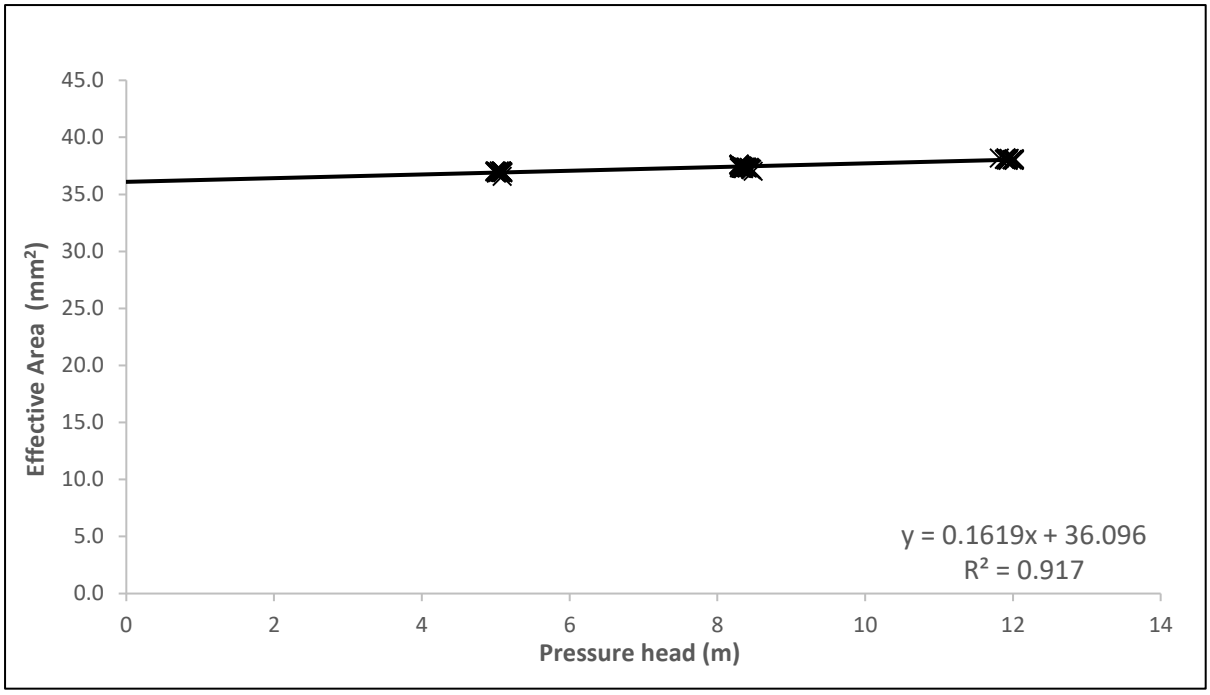

Figure 6-20 - Graph showing the effective area-head slope of a 50 mm uPVC longitudinal crack

The data was also analysed using the regression package on Microsoft Excel and the effective area- head slope for the pipe sample was found to be 0.161 mm^2/m meaning for every meter of pressure head the orifice area increased by 0.161 mm^2. This is a 0.32% increase in leak area for every meter of pressure head.

This is a significant change in the area with respect to pressure, although it is smaller than the typical longitudinal crack slope suggested by Nsanzubuhoro et al., (under review). This difference was explained earlier on in Chapter 5 as being due to the low-pressure ranges used to obtain the effective area-head slopes.

The standard deviation of the effective area-head slope was found to be 0.0103 mm^2/m, while the sample variance of the effective area-head slope, which measures how far each test value is from the sample mean was found to be 1.07E-04 mm^2/m. This is a 0.103% deviation from

the mean across the ten tests. These two statistical values report little variance between test values and show good repeatability in the test. The simultaneous confidence interval for the effective area-head slope (mm^2/m) is ± 0.0120 mm^2/m.

The regression analysis revealed a coefficient of determination, R^2 of 0.917 of the effective area – head relationship. this communicated that 91.7% of the variability of the effective area is accounted for by the variation in pressure head. The rest (9.3%) is a result of residual error.

The flow rate predictions derived from the FAVAD and N1 equations using the parameters found in this study were compared as shown in Figure 6-21, and both models can be seen to fit the data well within the measured pressure range for the 50 mm longitudinal crack.

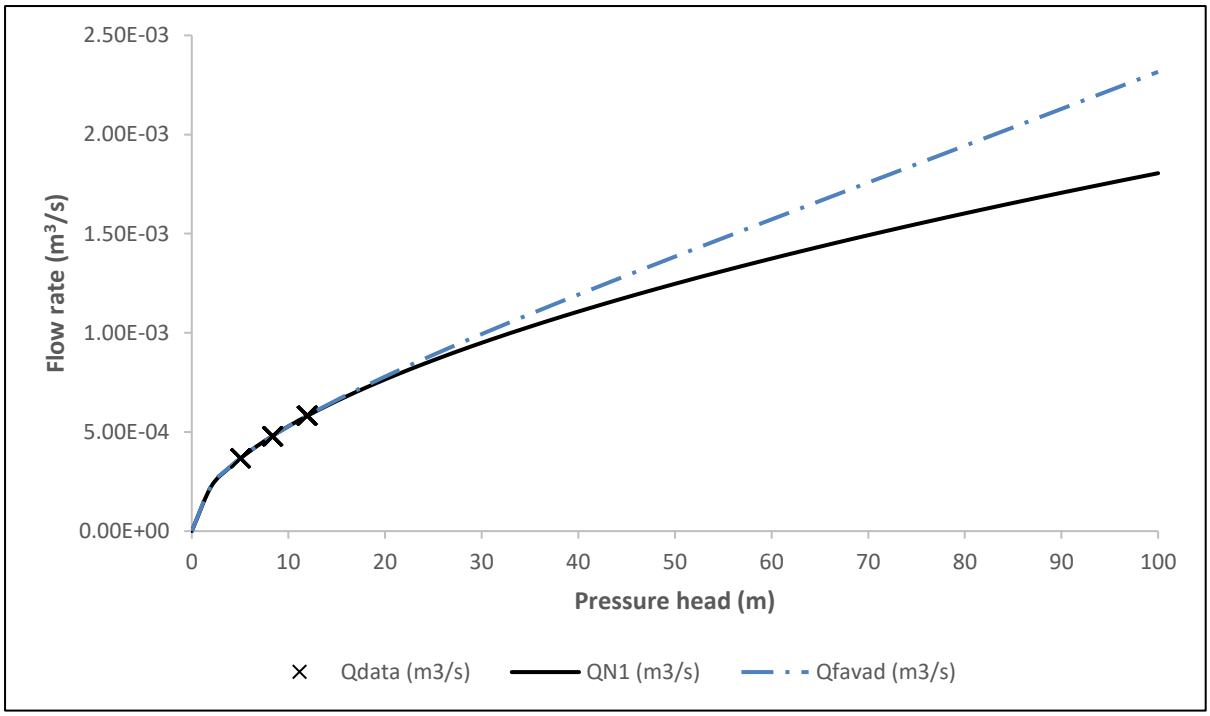

Figure 6-21 - Comparison of the FAVAD and N1 equation flow predictions and observed data

Beyond the measured data range, the two models differ. This difference is due to the N1 equation being an empirical equation that mostly depends on the data and consequently, the pressure range used.

Table 6-4 then shows a summary of the results for the data presented above.

Table 6-4 - Summary of results

	N1	A_0' (mm^2)	95% SPCI for A_0' (mm^2)	m' (mm^2/m)	95% SPCI for m' (mm^2/m)	p for m' (%)	C_d
This Study	0.533	36.10	±0.106	0.162	±0.012	<0.05	0.72

Further analysis of the parameters obtained from the ten (10) individual tests conducted using the PCAD revealed that it has excellent repeatability. The parameters analysed with the A_0' and m' being the parameters of importance as they are the main parameters used in the leakage modelling.

Figure 6-22 and Figure 6-23 show the graphs that describe the repeatability and reliability of the results conducted on a 50 mm longitudinal crack using the PCAD.

In Figure 6-22, the effective areas obtained from the 10 tests all fall within the 95% confidence interval of the average value of the tests and within each of the ten tests conducted.

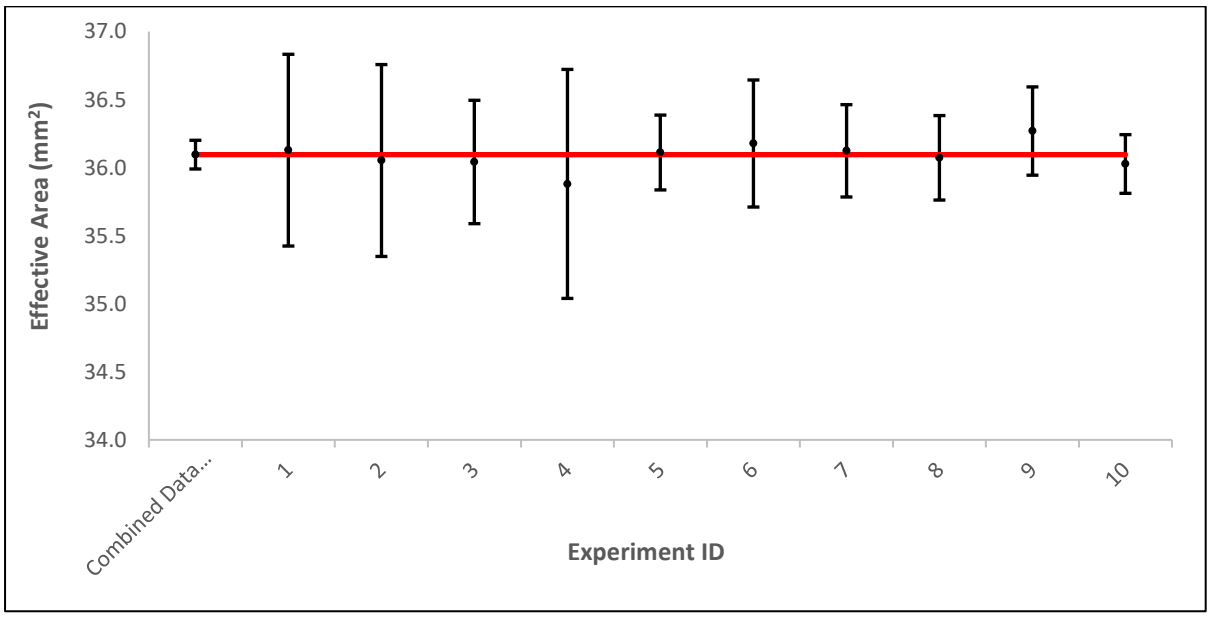

Figure 6-22 - Effective area comparison and repeatability analysis of the 50 mm longitudinal crack tests with the PCAD

A similar observation is made from analysing the values and confidence intervals of the effective area-head area slopes of the ten tests as shown in Figure 6-23

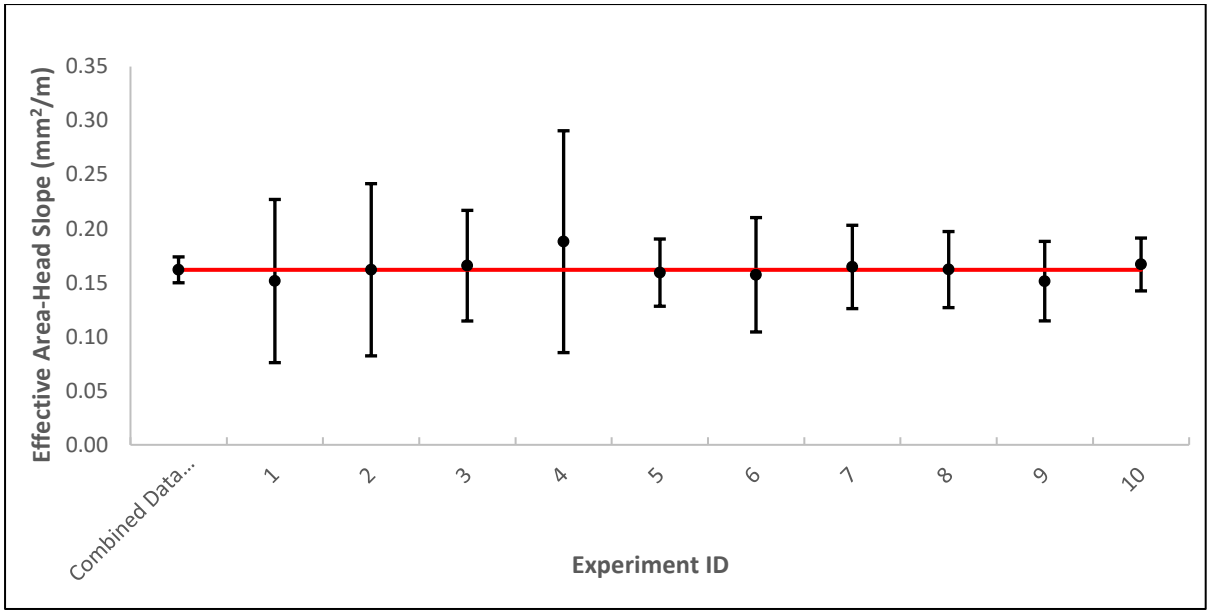

Figure 6-23 - Effective area-head slope comparison and repeatability analysis of the 50 mm longitudinal crack tests with the PCAD

The figure thus visually confirms the good repeatability of the experimental results using the PCAD.

Table 6-5 then shows a summary of the parameters obtained in each of the ten tests.

Table 6-5 - Summary of results for the ten 50 mm longitudinal crack tests with the PCAD

Experiment ID	A_0' (mm^2)	m' (mm^2/m)	N1	C_d	c
1	36.1	0.152	0.532	0.723	0.00016
2	36.1	0.162	0.532	0.721	0.00015
3	36.0	0.166	0.534	0.721	0.00015
4	35.9	0.188	0.538	0.718	0.00015
5	36.1	0.159	0.533	0.722	0.00015
6	36.2	0.157	0.532	0.724	0.00016
7	36.1	0.165	0.534	0.722	0.00015
8	36.1	0.162	0.533	0.721	0.00015
9	36.3	0.151	0.531	0.725	0.00016
10	36.0	0.167	0.535	0.721	0.00015

Figure 6-24 shows the comparison of the effective area head slopes of the tests conducted with standard laboratory equipment and the PCAD. The figure also shows overlaps of the 95% single parameter confidence interval of the effective area head slope values.

Figure 6-24 - Comparing the effective area-head slopes

A two-sample t-test with variance assumed as unknown was conducted using the data analysis tool pack on Microsoft excel. The hypotheses for the test were:

H_0: $m'_{pcad} = m'_{lab}$

H_1: $m'_{pcad} \neq m'_{lab}$

An alpha level of 0.05 was chosen**.** The decision criteria were to reject H_0 if p-stat (two tail) is less than 0.05. For the test and the following results were obtained:

	m' (mm/m) (PCAD)	***m' (mm/m) (LAB)***
Mean	0.163	0.188
Variance	0.000107	0.00107
Observations	10	10
Hypothesized Mean Difference	0	
Degrees of freedom	11	
t Statistic	-2.34	
P(T<=t) one-tail	0.01956	
t Critical one-tail	1.796	
P(T<=t) two-tail	0.0391	
t Critical two-tail	2.20	

A p-value of 0.0391, which is less than the set alpha value of 0.05, was found. Therefore, the null hypothesis that the effective area-head slopes from the two sets of experiments are the same was rejected. Although the t-test revealed that the effective area-head slopes of the tests

were statistically different, the confidence intervals of the set of experiments, however, overlapped. This finding communicated that within a 95% level of confidence, that is to say, 95 times out of a 100, the results from the laboratory tests will be obtained by the PCAD.

The region of overlap is acceptable but could be aided by the more significant deviation in the laboratory-derived results. This finding also communicated that there is less variation in the parameters obtained by the PCAD as compared to the standardised method using standard equipment. This is due to the PCAD's ability to provide similar pressure values at every step using pre-set constant voltage value. In contrast, for the lab experiment, the different pressure steps are obtained by manually varying the pump speed drive. This manual change of pressure heads results in more varied parameters as shown by the larger confidence intervals even when both methods have the same number of data points.

Figure 6-25 then shows the comparison of the effective areas of the tests conducted with standard laboratory equipment and the PCAD.

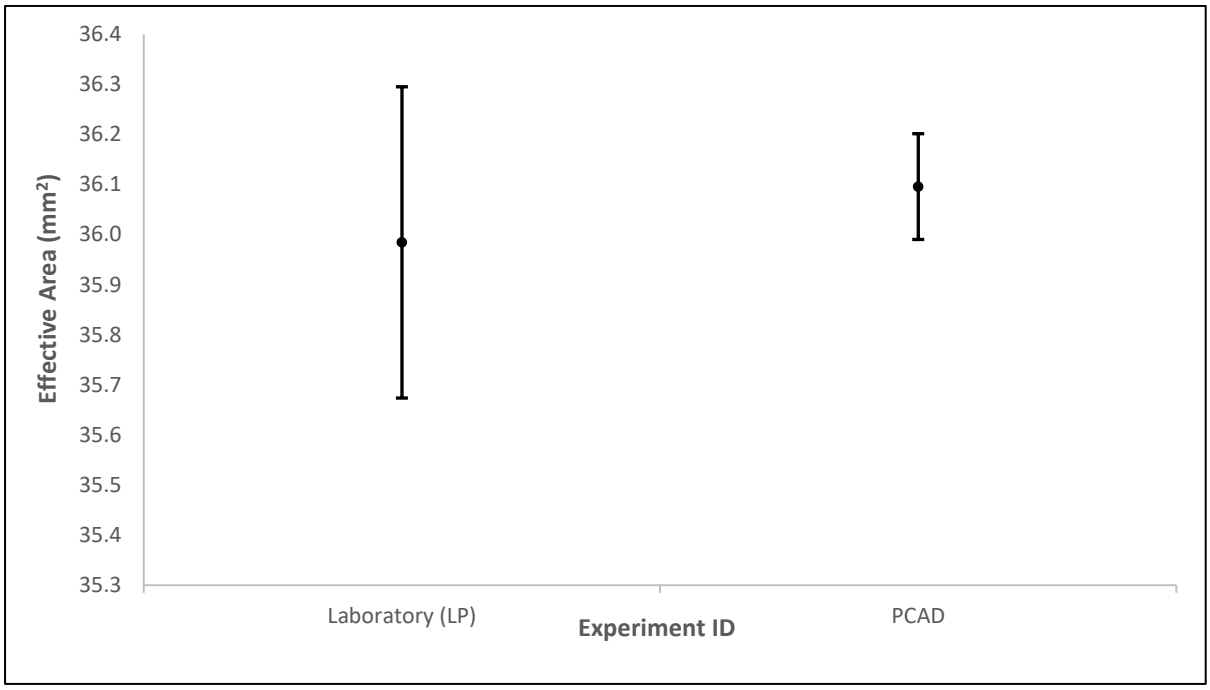

Figure 6-25 - Comparing the effective area values

The 95% single parameter confidence intervals of the effective areas overlap well. As above, the confidence interval of the laboratory experiments is larger than that of the PCAD, and the reason for this is the same as above.

6.3.4 50 mm uPVC Circumferential Crack

The pipe sample from the previous section was replaced with a uPVC pipe section with a 50 mm circumferential crack, and ten tests were done using the PCAD. The pressure and flow were recorded, and the stabilised steps used to characterise the leak. Figure 6-26 shows the typical pressure and flow relationship at each step.

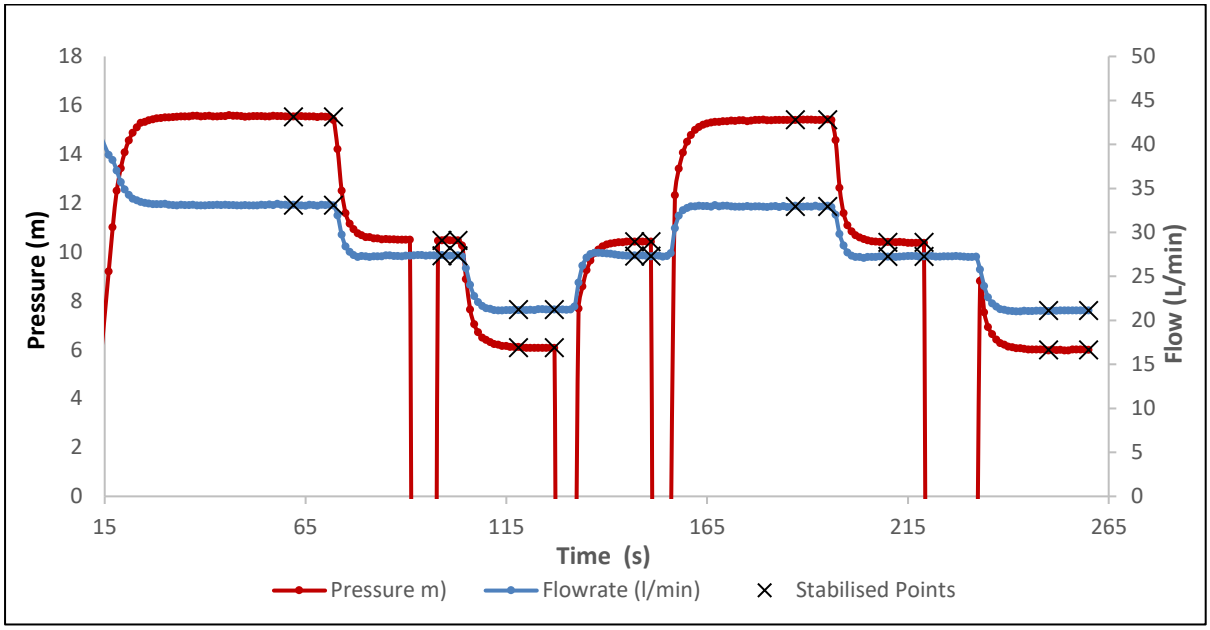

Figure 6-26 - Typical pressure head-flow rate relationship for a test with the PCAD

The flow rate and pressure head at each step were recorded then plotted on a graph. Figure 6-27 this relationship between the flow rate and the pressure head.

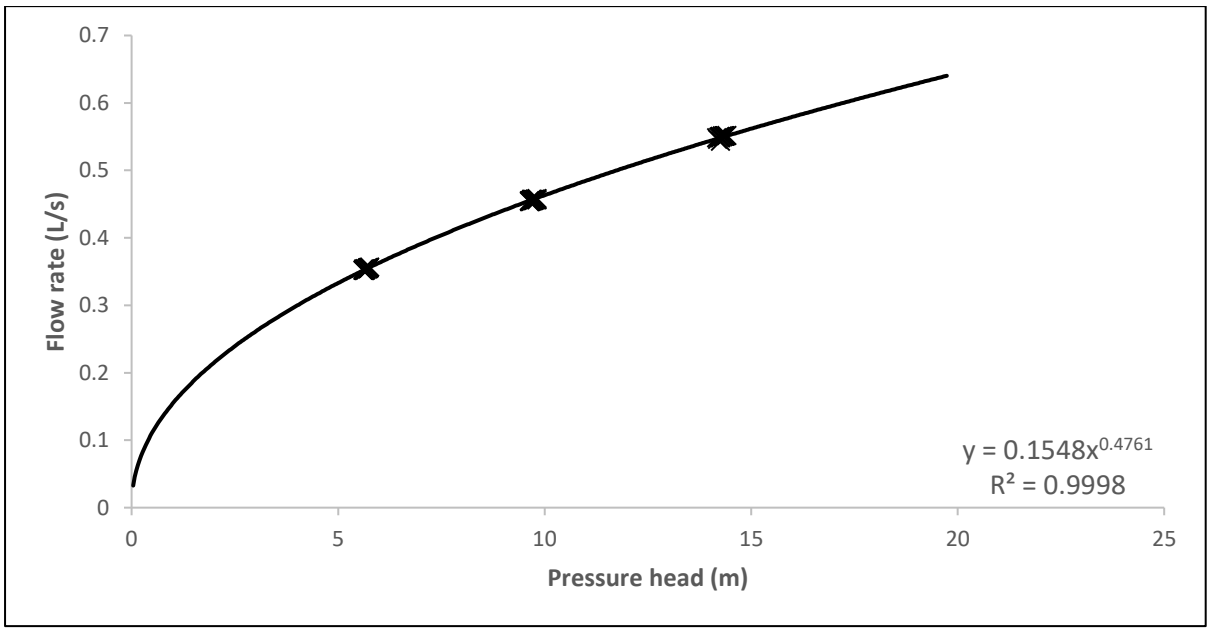

Figure 6-27 - Flowrate-pressure power relationship of a 50 mm uPVC circumferential crack

The N1 is found as the exponent of the relationship, which is a power relationship. The N1 value for the pipe sample was found to be 0.476 with a standard deviation of 0.0017 and sample variance (variance of the N1 values of the 10 conducted tests) of 2.76E-06. These results communicated that there was little variance in the tests and represent good repeatability of the conducted tests for the N1 parameter.

Through manipulating the orifice equation, the effective area for every pressure and flow step was found. The effective area was then plotted against the pressure head. The data was also analysed using the regression package on Microsoft Excel, and the effective area-head slope for the pipe sample was found to be - 0.0827 mm^2/m meaning for every meter of pressure head the orifice area decreased by 0.0827 mm^2. This is a minor change in the area with respect to pressure (0.17% of the original area). The effective area-head slope shown in Figure 6-28.

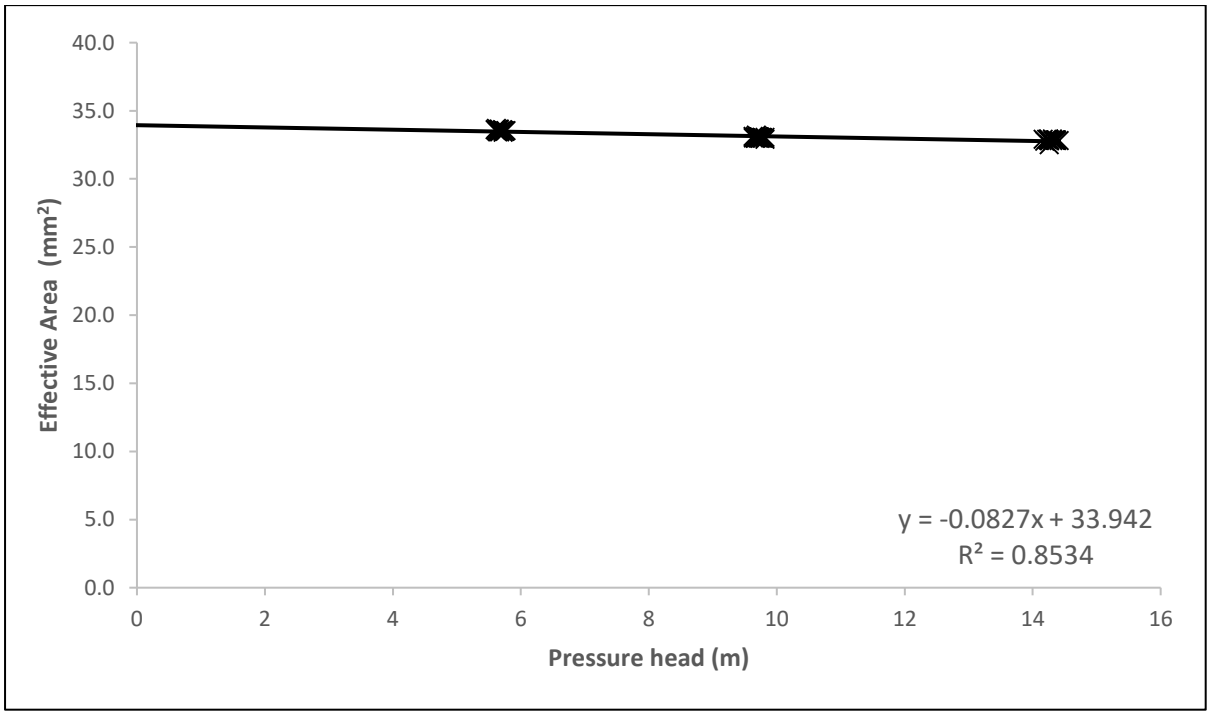

Figure 6-28 - Graph showing the effective area-head slope of a 50 mm uPVC circumferential crack

The standard deviation of the effective area-head slope was found to be 0.00694 mm^2/m, while the sample variance effective area-head slope, which measures how far each test value is from the sample mean was found to be 4.82E-06 mm^2/m. This value is a 0.006% deviation from the mean effective area head slope. These two statistical values report little variance between test values and show good repeatability in the test. The simultaneous confidence interval for the effective area-head slope (mm^2/m) is ± 0.0085 mm^2/m.

The regression analysis revealed a coefficient of determination, R^2 of 0.835 of the effective area – head relationship. This value communicated that, for the 50 mm circumferential crack, 83.5% of the variability of the effective area is accounted for by the variation in pressure head.

The leak was expected to have negative effective area-head slope as suggested to be the case for circumferential cracks by Nsanzubuhoro et al., (under review) although their range also includes the interval for round holes. For this leak and at the pressures used, it would be difficult to distinguish this leak from a round hole as both the effective area-slope and N1 values are similar to typical round hole values. However, the magnitude of the effective area-head slope was minimal and comparable to a round hole. This finding is believed to be due to the low pressures used in the characterisation tests. While it is generally accepted that uPVC material deforms elastically, the assumption that the material behaves like a perfectly elastic material does not hold as evidenced by the results from this study. It is thus reinstated that, at lower pressure, and by extension smaller forces, the deformation of the material is small as the material properties are strong enough to resist deformation. As the effective area-head slopes describe the rate of the leak/material's deformation, it then follows that this rate will be lower when the forces available to cause said deformation is smaller, in a non-idealised material.

The flow rate predictions derived from the FAVAD and N1 equations using the parameters found in this study were compared, as shown in Figure 6-29.

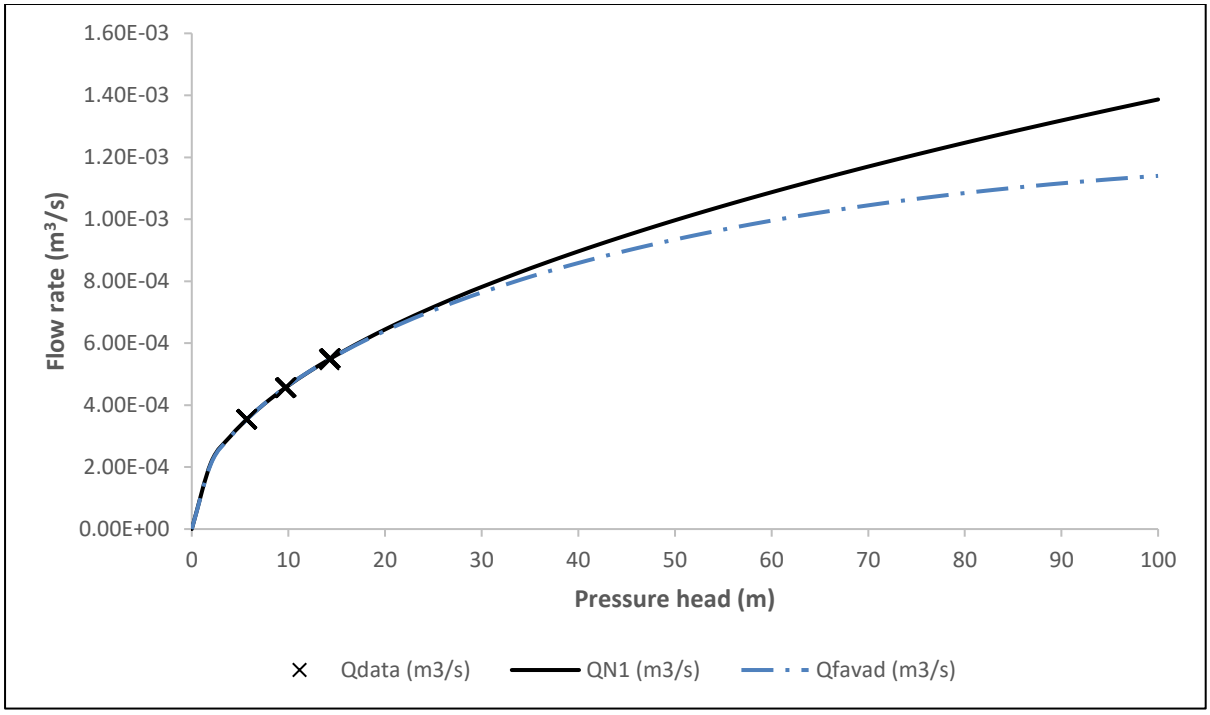

Figure 6-29 - Comparison of the FAVAD and N1 equation flow predictions and observed data

Both models fit the data well within the measured pressure range for the 50 mm circumferential crack. Beyond the measured pressure ranges the N1 model largely deviates from the FAVAD model as the N1 is only valid within its measure pressure range. Table 6-6 then shows a summary of the results for the data presented above.

Table 6-6 - Summary of results

	N1	**A_0' (mm^2)**	**95% SPCI for A_0' (mm^2)**	**m' (mm^2/m)**	**95% SPCI for m' (mm^2/m)**	**p for m'**	**C_d**
This Study	0.476	33.94	±0.0878	-0.0827	±0.00849	<0.05	0.68

Further analysis of the parameters obtained from the ten (10) individual tests conducted using the PCAD revealed that it has good repeatability. The parameters analysed with the effective are-head slope and the effective area being the parameters of importance as they are the main parameters used in the characterisation of leaks as they inform the leak size and rate of the increase thereof which aid in leakage modelling.

Figure 6-30 and Figure 6-31 show the graphs that describe the repeatability and reliability of the results conducted on a 50 mm circumferential crack using the PCAD.

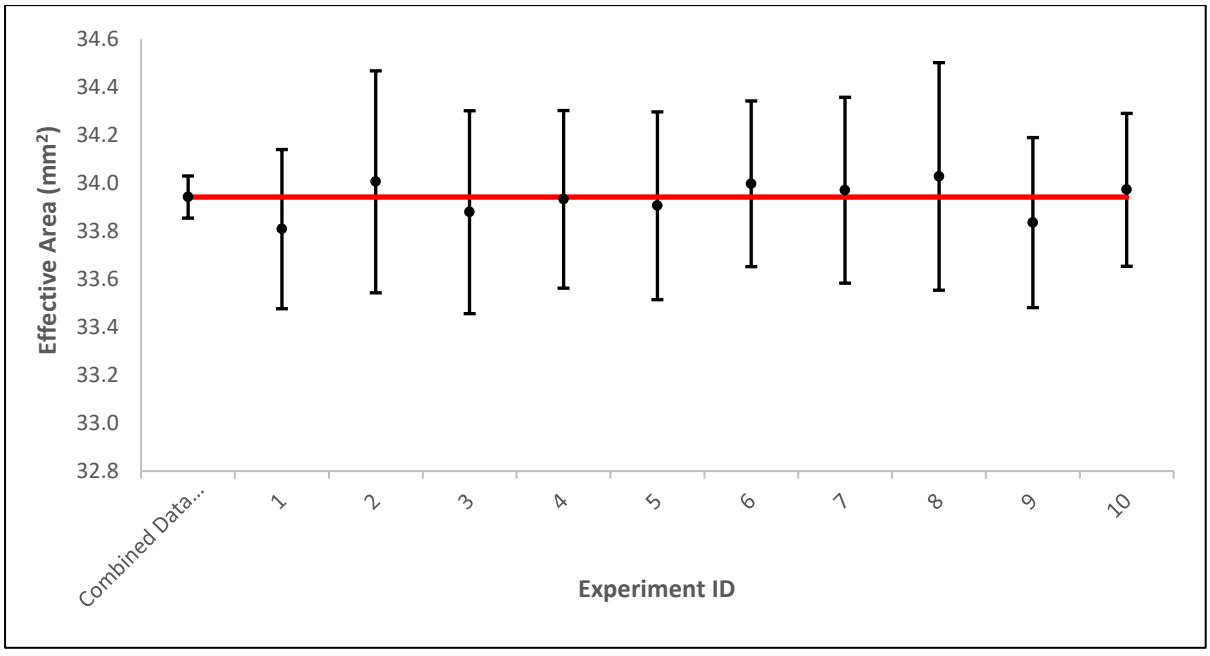

Figure 6-30- Effective area comparison and repeatability analysis of the 50 mm circumferential crack tests with the PCAD

In Figure 6-30, the effective areas obtained from the ten tests all fall within the 95% confidence interval of the average value of the tests and within each of the ten tests conducted. The comparable confidence interval widths also communicate that the variability of the data within the ten tests is also similar. A similar observation is made from analysing the values and confidence intervals of the effective area-head area slopes of the ten tests, as shown in Figure 6-31. As with the effective areas, the effective are-head slopes of the ten tests also all overlap and show that the PCAD produces repeatable results to a 95% level of confidence.

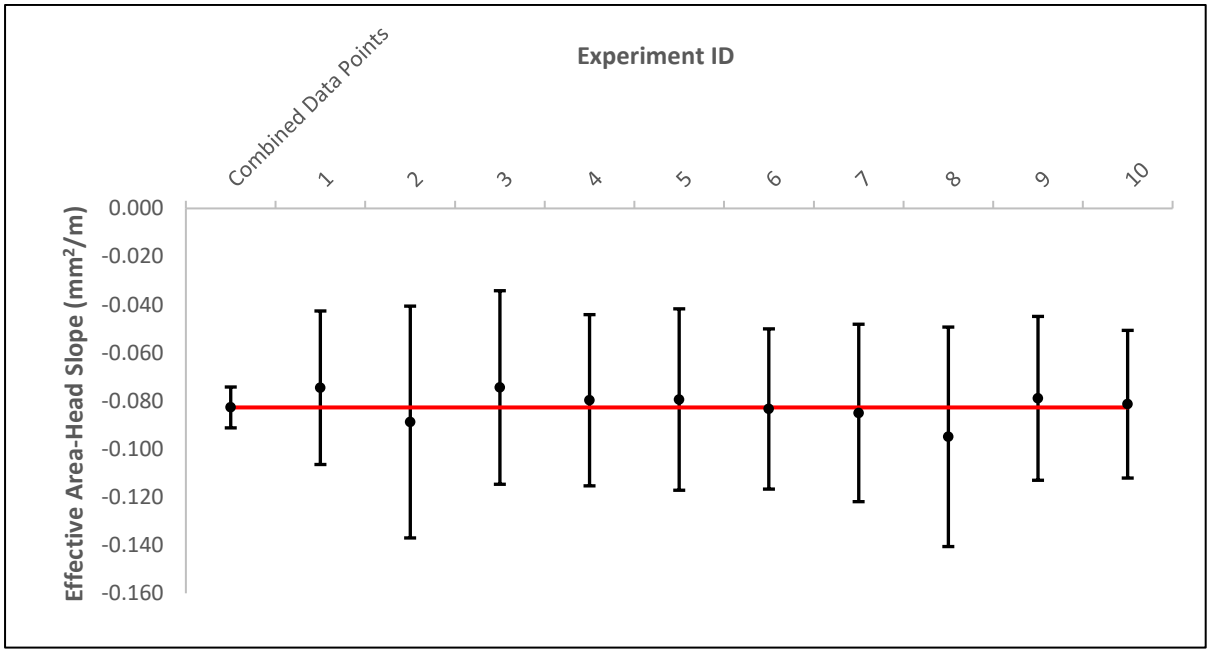

Figure 6-31 - Effective area-head comparison and repeatability analysis of the 50 mm circumferential crack tests with the PCAD

The figure thus visually confirms the good repeatability of the experimental results using the PCAD. Table 6-7 then shows a summary of the parameters obtained in each of the ten tests.

Table 6-7 - Summary of results for the ten 50 mm circumferential crack tests

Experiment ID	A_0' (mm^2)	m' (mm/m)	C_d	N1	c
1	33.8	-0.0746	0.676	0.478	0.00015
2	34.0	-0.0889	0.680	0.475	0.00016
3	33.9	-0.0744	0.678	0.478	0.00015
4	33.9	-0.0797	0.679	0.477	0.00015
5	33.9	-0.0795	0.678	0.477	0.00015
6	34.0	-0.0834	0.680	0.476	0.00016
7	34.0	-0.0850	0.680	0.475	0.00015
8	34.0	-0.0950	0.681	0.473	0.00016
9	33.8	-0.0790	0.677	0.477	0.00015
10	33.9	-0.0730	0.677	0.478	0.00015

Figure 6-32 shows the comparison of the effective area head slopes of the tests conducted with standard laboratory equipment and the PCAD.

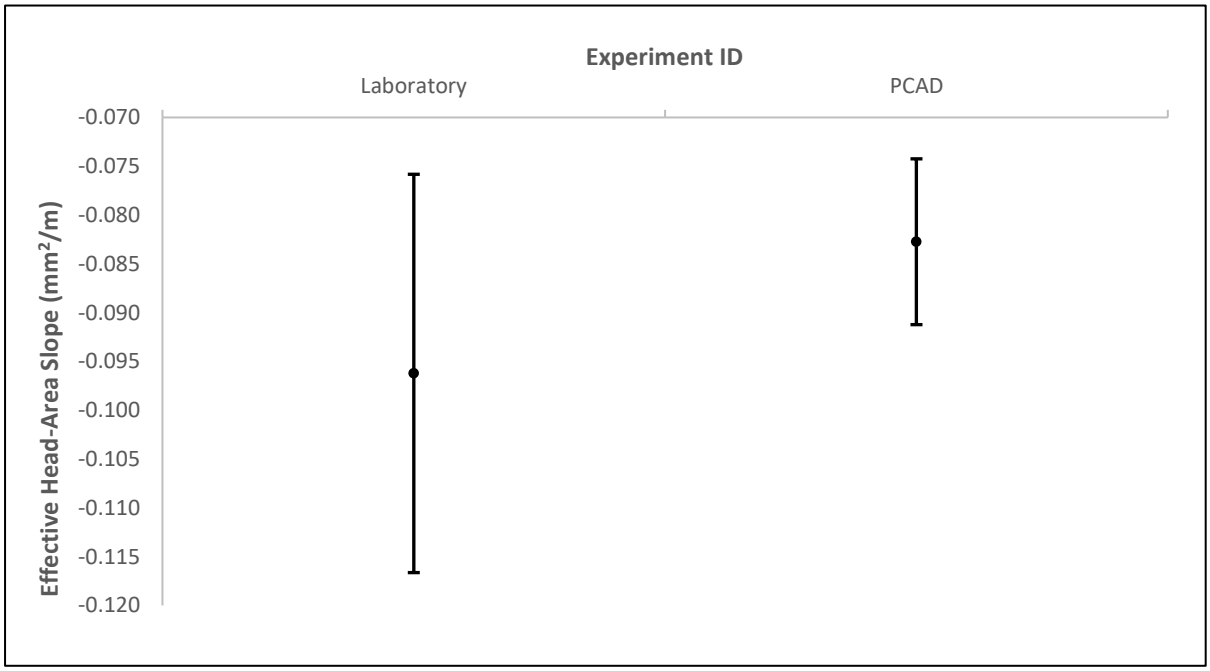

Figure 6-32 - Comparing the effective area-head slopes

It also shows overlaps of the 95% single parameter confidence interval of the effective area head slope values. A two-sample t-test with variance assumed as unknown was conducted using the data analysis tool pack on Microsoft excel. The hypotheses for the test were:

H_0: $m'_{\mathbf{pcad}} = m'_{\mathbf{lab}}$

H_1: $m'_{\mathbf{pcad}} \neq m'_{\mathbf{lab}}$

An alpha level of 0.05 was chosen**.** The decision criteria were to reject H_0 if p-stat (two tail) is less than 0.05. For the test and the following results were obtained:

	m' (mm/m) (PCAD)	***m' (mm/m) (LAB)***
Mean	-0.0812	-0.0954
Variance	4.82E-05	0.000141
Observations	10	10
Hypothesized Mean Difference	0	
Degrees of freedom	15	
t Statistic	3.25	
P(T<=t) one-tail	0.00268	
t Critical one-tail	1.75	
P(T<=t) two-tail	0.00536	
t Critical two-tail	2.13	

A p-value of 0.00536 which is less than the set alpha value of 0.05, was found. Therefore, the null hypothesis that the effective area-head slopes from the two sets of experiments are the same was rejected. Although the t-test revealed that the effective area-head slopes of the tests were statistically different, the confidence intervals of the set of experiments, however, overlapped. This finding communicated that within a 95% level of confidence, that is to say, 95 times out of a 100, the results from the laboratory tests will be obtained by the PCAD.

Figure 6-33 then shows the comparison of the effective areas of the tests conducted with standard laboratory equipment and the PCAD.

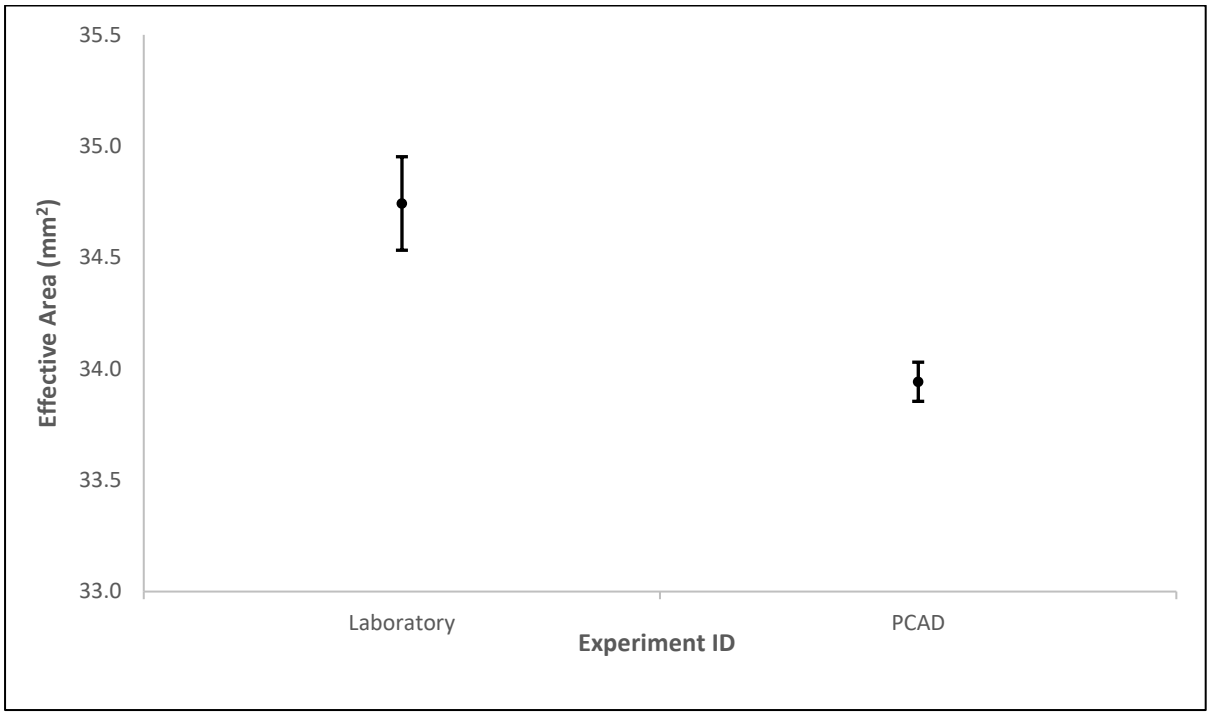

Figure 6-33 - Comparing the effective areas

The 95% single parameter confidence intervals of the effective areas do no overlap, and this may be a result of the variance in the effective areas that results in the intercept of the effective area-head graphs, being significantly different. As above, the confidence interval of the laboratory experiments is larger than that of the PCAD, and the reason for this is the same as above.

6.4 Chapter Summary

This section of the study sought to establish the efficacy of the PCAD in characterising leakage in pep system. This was done through conducting tests on pipe samples which had been previously tested using the standardised method. However, before the tests could be conducted, the PCAD instrumentation had to be calibrated and checked against pre-calibrated instrumentations whose accuracy had been verified. The calibration exercise enabled the accuracy of the PCAD to be established and informed that the instruments could be used with confidence. Additionally, the actual system characteristics of the experimental setup were assessed and verified to ensure that the calculations to determine the leakage characteristics using the PCAD were as accurate as possible.

Leakage characterisation tests on three leak types, namely, the 6 mm round hole and 50 mm longitudinal and circumferential cracks, were then conducted. It was anticipated that the device would not give the exact results as the laboratory equipment due to the different precision and accuracy levels of the instrumentation used. This assertion was verified by the abovementioned paired sample T-test results. The results from the study did, however, demonstrate that the device instrumentation could be relied on to verified levels of precision. The repeated ten leak characterisation tests demonstrated that the device had good repeatability as all the obtained values for the three leak types overlapped within their 95% confidence intervals. Furthermore, the PCAD was able to consistently produce leakage characterisation results that are similar to laboratory-derived results.

7 FIELD TESTS

7.1 Introduction

This section of the study documents the field tests conducted with the pipe condition assessment device. The tests were carried out in conjunction with the City of Cape Town and conducted on 5 residential pipe sections in the Kensington district metered area (DMA). Kensington is in the northern suburbs of Cape Town, South Africa and is a medium density area. The distribution of pipe types in the system is 38.2% Fibre Cement/Asbestos Cement, 16.6% cement-lined, 11.1% uPVC, 2.6% steel and 31.4% of the pipes are of unknown pipe type. The pipes in the DMA have diameters ranging from 100 mm to 225 mm.

Due to the ongoing drought in the region (at the time this section was authored); the input pressure had been dropped to an average of 30 metres to aid in water demand management and leakage control. It was thus required that the tests conducted on the pipes not exceed this average pressure to avoid creating new leaks in the system.

During the tests, the following aspects were considered:

- The ability of the device to detect leaks and assess the condition of the pipe in the field
- The ability of the device to successfully complete the test procedures
- The ease of operation and manoeuvrability of the device
- Modifications required (software and hardware)
- Data analysis and calculations
- Results and interpretations of results
- Assessment of the condition of the pipes tested.

The subsequent section will give an overview of these tests.

7.2 Assessments

In this exercise, initial preliminarily laboratory tests were conducted, and it was established that the device was functional in controlled laboratory conditions. Field tests were then conducted. These tests were conducted earlier on before the device had been fully calibrated. These tests were expected to illustrate how the device operates and functions in real water systems. It was also hoped to establish how an operator would cope while using the machine and establishing its ease of use.

The test procedure for the field tests is described in section 3.3.3 of this document. A total of 5 assessments in the Kensington DMA were conducted; however, due to various reasons discussed in sections below, only two pipes were analysed entirely.

7.2.1 Test 1 - 16th Street between 5th Ave & 6th Ave

The first test pipe tested was a 100 mm diameter, asbestos cement (AC) of 256-metre length which had 19 household connections. The tests pipe had isolation valves on both ends and one fire hydrant, as shown in Figure 7-1, which was used as the device connection point. The City of Cape Town water infrastructure maintenance section assisted in carrying out the isolation procedure and were able to isolate all the residential connections on this pipe section.

Figure 7-1 - Test 1 pipe located between 6th avenue/5th avenue & 16th street, Kensington.

7.2.1.1 Test Results

The flow and pressure parameters were obtained from the 6-step test. The presence of a flow rate indicated there was a leak in the pipe. The flow rate and pressure head values were plotted against time, as shown in Figure 7-2. From the data obtained from the test; an analysis to determine the stabilised points during the pressure steps was conducted. The average pressure head and flowrate values at each step were obtained from this analysis.

In this test, the flow rate at one-second intervals varied significantly, albeit within a fixed range during the tests. This was believed to be due to some electrical induced signal interference on the flow meter/sensor. It was thus possible to average the variations to obtain a mean flow rate.

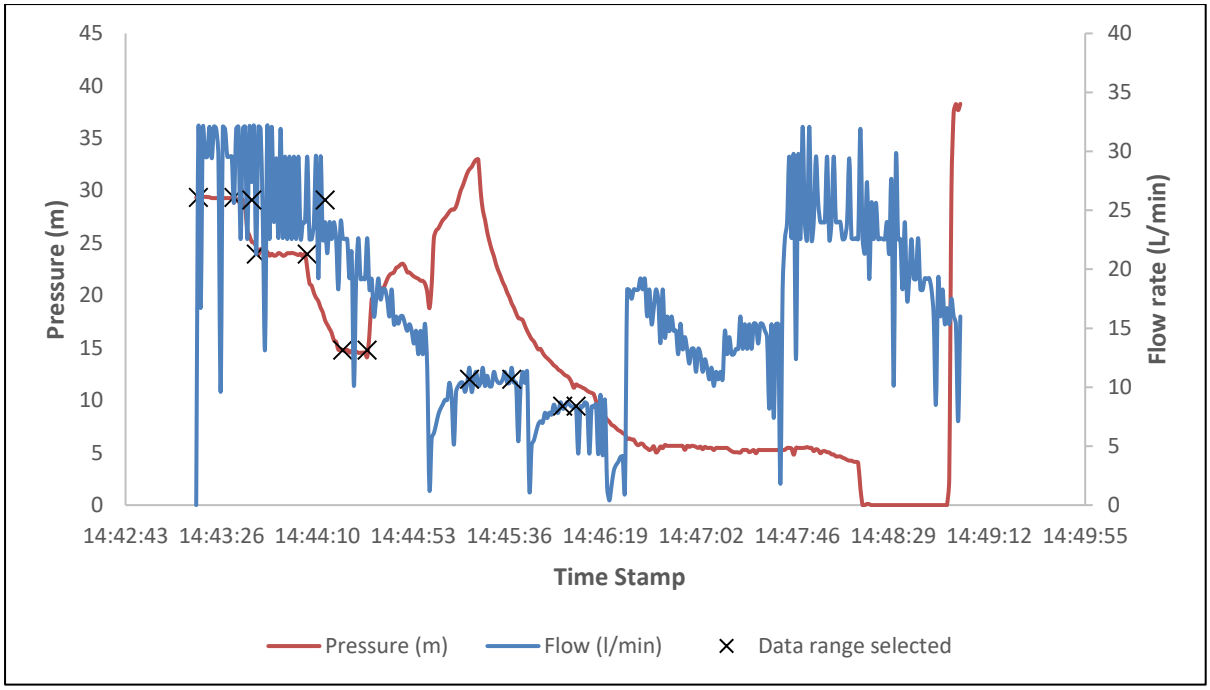

Figure 7-2 - Raw data showing pressure and flow rate variation for test 1

Figure 7-3 shows the graph of flow rate plotted against the pressure head for the Kensington test 1 pipe. A power function was fitted to the data, and from it, the leakage exponent of the leak was found.

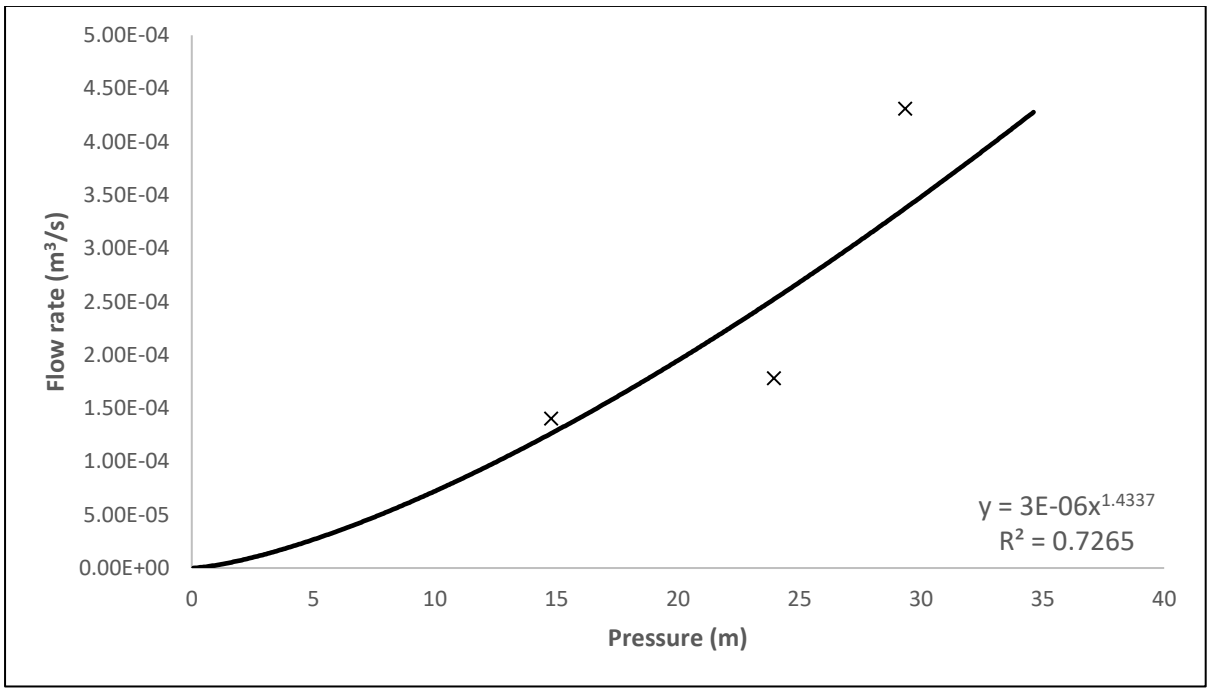

Figure 7-3 - Flow rate against pressure for test 1

From the power equation, the obtained leakage exponent, N1, was 1.43, and the obtained leakage coefficient (C) was 2.65×10^{-6}, for this test.

The effective leak area with respect to flow and pressure was found through manipulating the orifice equation. The effective leak areas per step were then plotted against their associated pressure head for every step, as shown in Figure 7-4.

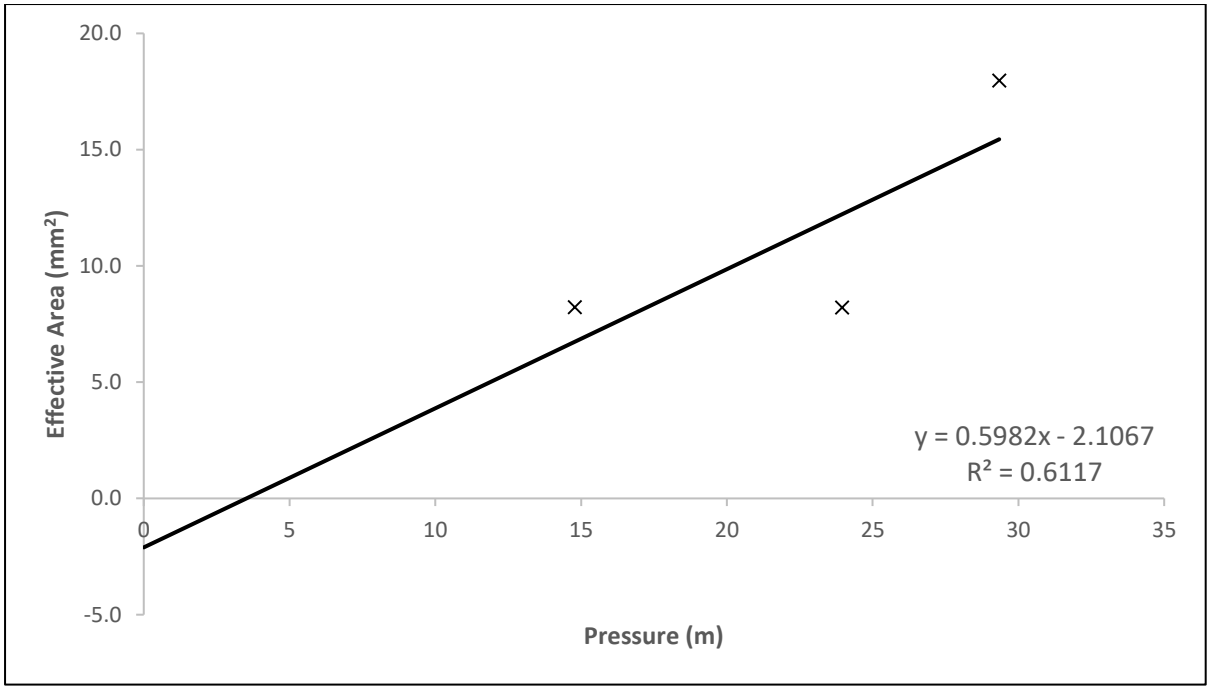

Figure 7-4 - Graph showing the effective head area slope for test 1

An initial effective leak area, A_0' of -2.11 mm^2 and effective area-head slope, *m'*, of 0.598 mm^2/m were obtained. The effective slope obtained is characteristic of a longitudinal crack (Nsanzubuhoro et al., under review).

The N1 value was found to be within the limits of 0.5 (for leak areas that are not responsive to pressure), to 1.5 (for leaks that are very responsive to pressure variations). Furthermore, the leak in this pipe was found to have a negative leak opening, which is not physically possible/realistic. This could point to some error in the data or imply that the leak is initially closed and opens when the pressure head exceeds 3.52 m.

Table 7-1 summarises the leakage parameters mentioned above.

Table 7-1 - Summary of results for Test 1

m' (mm^2/m)	**A_0' (mm^2)**	**N1**	**c**
0.598	-2.11	1.433729	2.65E-06

Other observations:

- It was observed that the device required at least three people to load and offload from the car.
- Isolating the valves was a bit difficult as the valves had not been maintained for a while. Thus, more work was required to seal the isolation valves. This exercise took at least 30 minutes.
- The Kensington residents were very understanding and willing to have their water supply cut off for the short duration of the test. They were also keen to learn more about the device and how it will assist in water conservation efforts in the city.

7.2.2 Test 2 – 5th Ave & 16th Street

The pipe section used in this test was 100 mm diameter, asbestos cement (AC) with a length of 100-metre which had ten household connections, one isolation valve and hydrant as shown in Figure 7-5.

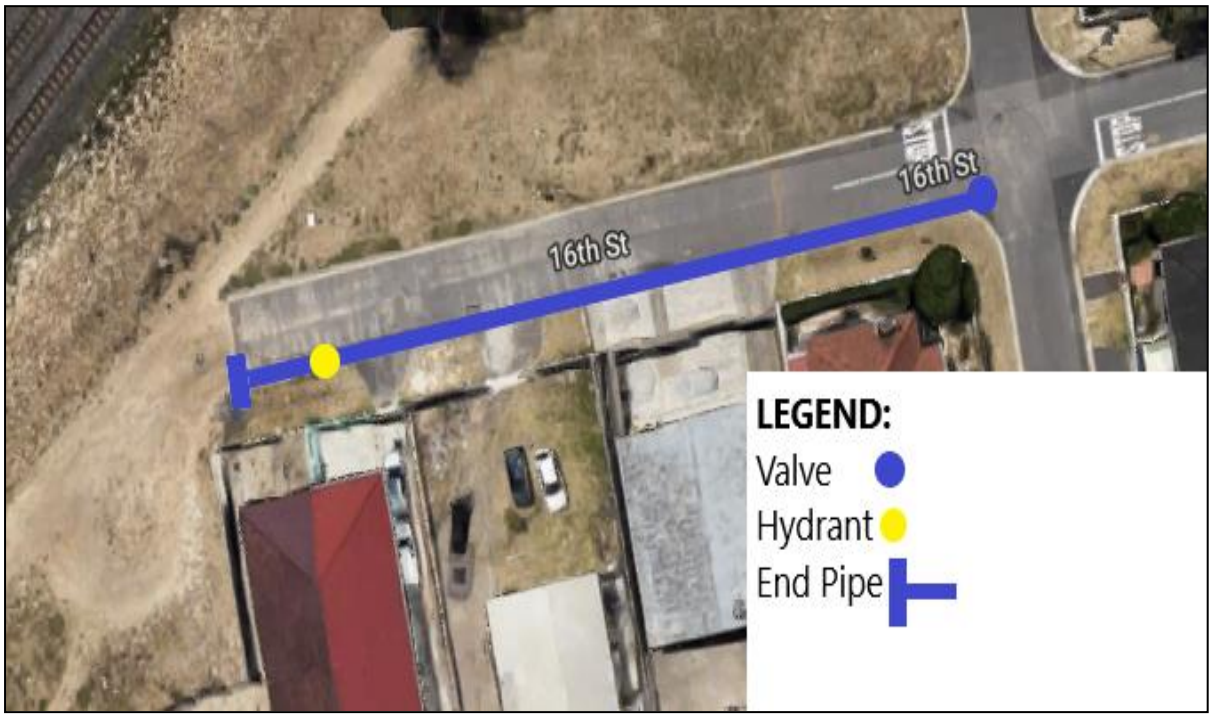

Figure 7-5 - Test 2 pipe located on 6th avenue and 16th street, Kensington.

7.2.2.1 Results

Using the same procedure as described in section 7.2.1, the results were analysed, and the following graphs and tables were obtained. Figure 7-6 shows the pressure and flow relationship at each step during the 6-step test. The stabilised points are also shown in the figure. For this

test, the flow rate and pressure measurements were found to be more stable with little electrical interference, as shown in the figure.

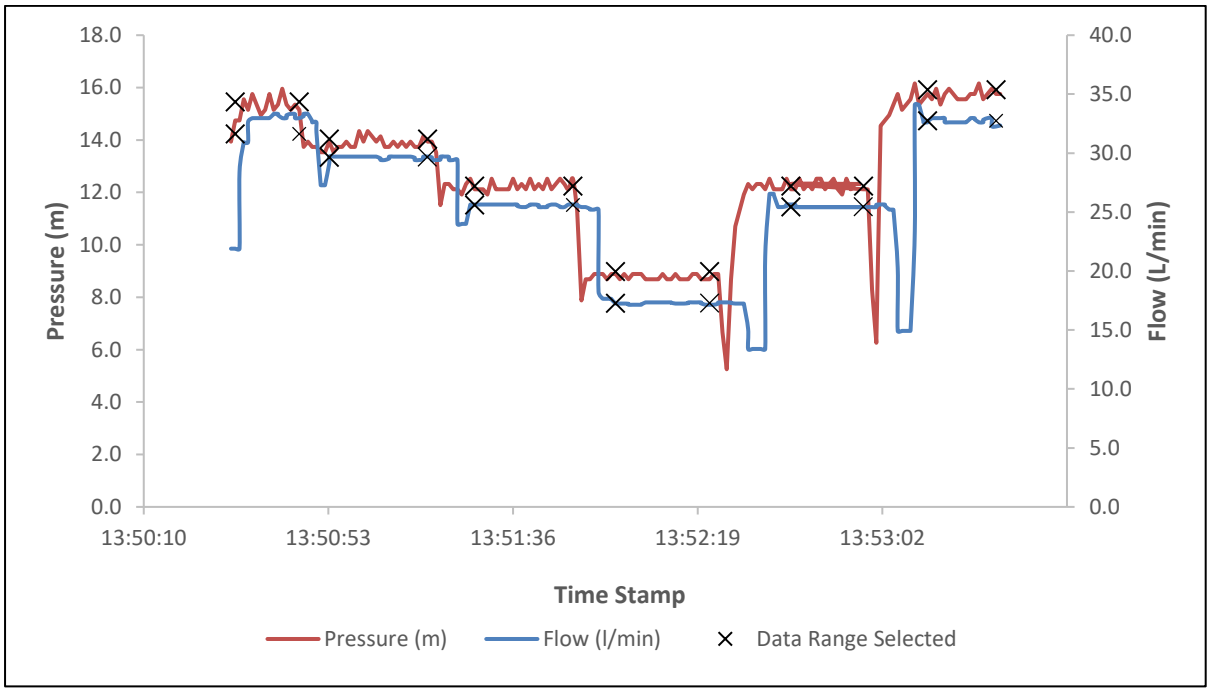

Figure 7-6 – Raw data showing the variation of Pressure and Flow for test 2

Figure 7-7 shows the relationship between flow rate plotted against the pressure head for the Kensington test 1 pipe. A power equation was fitted to the data points. From the power equation, the leakage exponent, N1, was 1.11, and the leakage coefficient (C) was 2.57×10^{-6}.

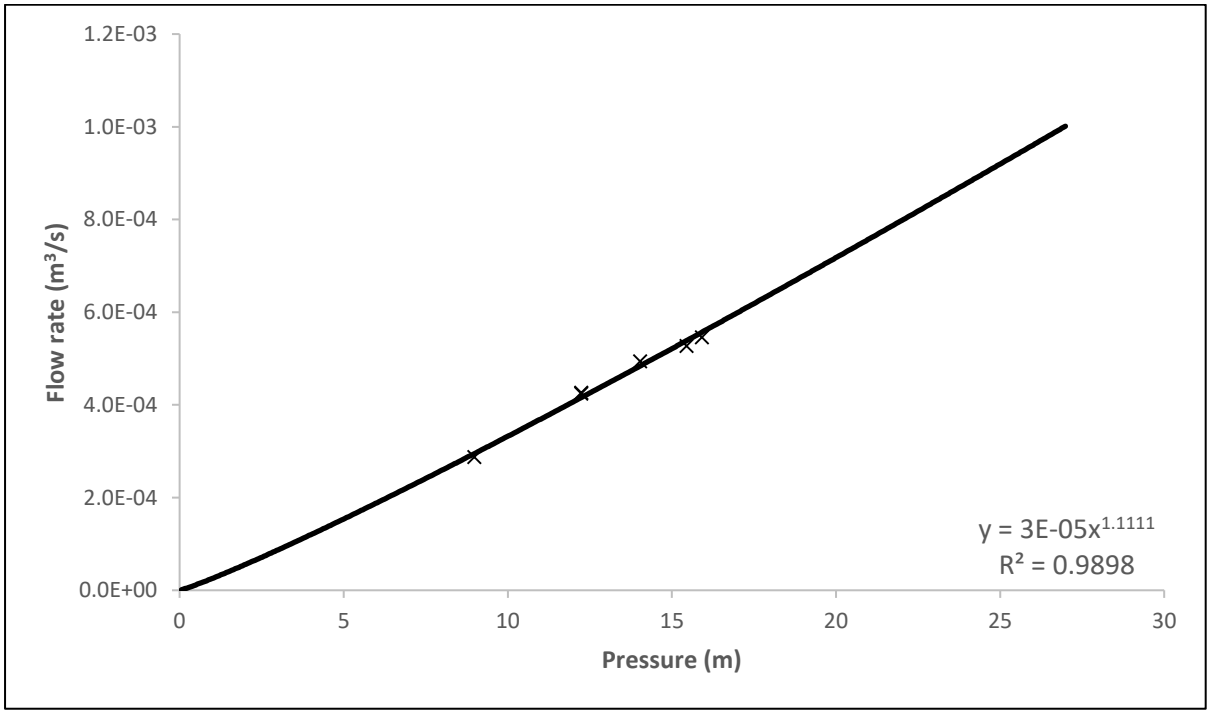

Figure 7-7 - Flow rate against pressure for test 2

The effective leak area with respect to flow rate and the pressure was found through manipulating the orifice equation. The effective leak area was then plotted against pressure, as shown in Figure 7-8. An effective area- the head slope of 1.29 mm^2/m with an effective area of 10.99 mm^2 was found for this test.

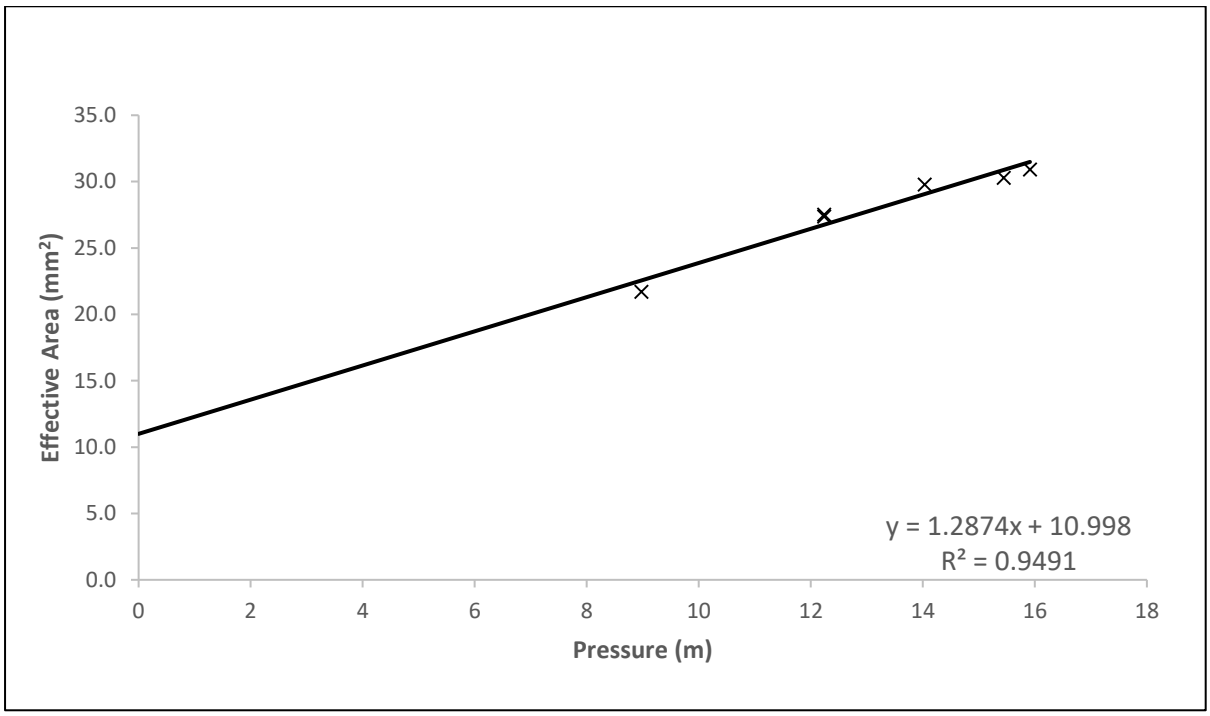

Figure 7-8 - Graph showing the effective head area slope for test 2

The effective area, in unison with an N1 value of 1.11, suggests that the leak or combination of leaks in the pipe section is a longitudinal crack whose area initial leak area of 10.99 mm^2 varies significantly with an increase in pressure head.

Table 7-2 summarises the leakage parameters mentioned above.

Table 7-2 - Summary of results for Test 2

m'(mm^2/m)	**A_0' (mm^2)**	**N1**	**C**
1.29	10.99	1.11	2.57E-05

7.2.3 Other Tests

7.2.3.1 5th Ave between 15th/16th Street

A leakage characterisation test on the pipe section shown in Figure 7-9 was attempted on the pipe section, but it was found that the valves could not be completely closed and as such the pipe could not be isolated Multiple attempts to close the valves were made including "exercising" the valves. This process involved the cyclic opening and closing of the valves to

remove any grit that could have caused the valves to no seal shut completely. The presence of leaking valves was confirmed by conducting an isolation test using the PCAD.

Figure 7-9 - Test pipe located on 5th Avenue between 15th and 16th Street, Kensington.

The isolation procedure only lasted thirty seconds due to how the PCAD had been programmed. This duration, however, was found to be insufficient to verify if the pipe has been isolated as some faulty valves may have very low flow rates such that the pipe may not have completely emptied in 30 seconds.

7.2.3.2 6th Avenue and 17th Street

To minimize instances where the tests could not be conducted due to faulty valves, it was decided to focus the tests on dead-end pipes which would only have one valve. The City of Cape Town's maintenance crew was able to assist in the isolation the pipe section shown in Figure 7-10, and a leak characterisation test was conducted.

However, the results from the test were odd in that the flow rate never stabilised during a test even after it had been established that the pipe is isolated. This meant that the device could not move on to the next step. As a result, the data from the test could not be analysed or used in this section. Nevertheless, the occurrence of a flow rate indicated the presence of a leak in the pipe section. This test informed that the device might need an option to trigger steps manually.

Figure 7-10 - Test pipe located on 6th Avenue and 17th Street, Kensington.

7.2.3.3 3rd Avenue and 12th Street

This was a dead-end pipe section with one valve and hydrant, respectively, as shown in Figure 7-11.

Figure 7-11 - Test pipe located on 3rd Avenue & 12th Street, Kensington.

The valve on this pipe section was successfully closed, and the device verified that the pipe had been successfully isolated. Still, the test could not be completed as the hydrant were the device was connected was found to be leaking. As a result, a test could not be conducted as

water leaked out from the hydrant. The positive in this test was that it was established that a hydrant was leaking and faulty and could be reported for repairs.

7.3 Chapter Summary

The objective of this section was to evaluate the efficacy of the PCAD in conducting condition assessments and evaluating the ease of use and limitations of its use in real water systems. This information is essential if the device is to be used to help address the vast quantities of water losses in our water networks. The findings described above, although limited, show that the device can detect leakage, characterise leakage, identify faulty valves and hydrants.

The objectives of this section were fulfilled by conducting five pipe condition assessment in Kensington as a pilot study for the PCAD. Concerning the use of the device, the device was found to be bulky and requires at least three people to offload it from a truck. Fortunately, it is easily manoeuvrable by one operator even over considerable distances. The leak test itself took a short period, usually less than 5 minutes. However, the pipe isolation exercise took more protracted periods, up to 30 minutes per pipe with a workforce of three city technicians.

One of the results from this study also revealed that the device is not able to successfully to characterise small leaks with its current procedure. They also communicated that the flow meter needed further calibration and work to filter out the electric noise/interference it picked up during the tests. The PCAD was also found to be unable to conduct leakage characterisation in pipe sections that could not be isolated. As a result, leakage characterisation was only done for two pipe sections. Consequently, the author suggests that a method be developed to characterise leakage in a pipe section that has faulty valves.

The results initially obtained did not account for all the losses in the pipe section that was tested, and future tests need to consider these losses as they could be considerable. Additionally, the isolation tests communicated that a modification to the code was required as the isolation test should not be determined by the duration of the test but by the absence of a flow rate to signify pipe isolation.

Finally, the tests revealed that the DMA might have significant challenges with regards to its operation and maintenance. This was shown by the number of valves and hydrants that were found to be faulty. However, the sample size of the pipes tested from which that assertion is made was admittedly small and may not be statistically significant. Thus, more tests need to be conducted in the DMA to assess the condition of the network entirely.

In conclusion, from the field test results, it is evident that the device can conduct pipe condition assessments in real water systems. While the tests were not perfect, they provided data on how the device use and data analysis can be improved. It is this data that informed the modifications in the experimental procedure, and data analysis explained in chapters 5, 6 and 7. The modification further reinforced the belief that the PACD can be used to characterise leakage in real water distribution networks.

8 DISCUSSION

At the beginning of this study, it was pointed out that a pipe condition assessment device had been developed at the University of Cape Town to assist in water conservation measures. It was also highlighted that this efficacy and reliability of the device had not yet been established. This then formed the core aim of this study.

The efficacy and reliability of this device were established by conducting thirty tests on different uPVC pipe samples using a standardised laboratory-based setup developed by Malde, (2015) and slightly modified for this study. The tests were done to establish the leakage characteristics of the leaks on the pipe samples. These leakage characteristics included the effective area, the effective area-head slope, the N1 and the discharge coefficient. The experiments of the pipe samples were repeated ten times to ascertain the repeatability and reliability of the standardised method. After the leakage characteristics had been found, the same pipes were then tested using the PCAD also, to obtain the leakage characteristics of the very same pipes tested using the PCAD. The tests were also ten times per sample. The variance and deviation of the results from these ten tests then informed the repeatability of the test results obtained by the PCAD to an acceptable level of confidence. After the reliability of the device in conducting leak assessments in a controlled laboratory environment had been established, the efficacy of the device was further investigated. This investigation was done by conducting tests in a real water network in Cape Town. From these tests, the reliability of the device and its ability to detect leakage and perform pipe condition assessments was evaluated and established.

The leakage characterisation tests conducted on the standardised setup revealed that to 95% level of confidence, the results of the test were repeatable. This communicated that the standardised method was a valid method for characterising leakage. These results from this study were then compared with previous results on similar pipe samples conducted by Van Zyl and Malde, (2017). For all six pipe samples, the results of the tests showed excellent repeatability with minimal standard deviations and low variance of less than 0.001 mm^2/m for the effective area-head parameter for all samples. Statistical inference theories state that; the higher the variance, the more heterogeneous a parameter is, and the smaller the variance, the more homogeneous is it. When the variance is zero, it implies that all the values are equal. Thus, for this study, the sample variances revealed that the data (which is the obtained effective area-head slopes) were homogenous and therefore the tests had excellent repeatability

The notable exception was the 100 mm circumferential crack whose variance was comparably significant as the pipe was disconnected and reattached after every test. The reason for this was that the circumferential crack is sensitive to longitudinal stresses. The magnitude longitudinal stresses were affected by the magnitude of the torque used to tighten the steel rods. It is thus recommended that a standardised method for securing the steel rods be developed and a set value be determined to ensure uniformity.

A comparison of the leakage parameters with their 95% single parameter confidence intervals revealed that the results of this study, from the standardised method, were significantly different from the Van Zyl and Malde, (2017) values. This finding was true for both the effective area-head slope and effective area. For the latter, the difference was believed to be a result of the parameter being reliant of the line of best fit of the effective areas and pressure heads. These parameters are established by the user by inspecting of the data to identify stable pressure and flow steps. This results in the variance of the values of the effective area and pressure head, which in turn affects the line of best fit and consequently, the effective area of the sample. That considered, the results from this study are more reliable as the analysis of the test results was done using more data points and repeated ten times with good consistency. Furthermore, a study conducted by Nsanzubuhoro et al., (under review) on the same modified standardised setup found statistically similar results with a 95% level of confidence as the ones found in this study.

Preliminary tests on a 12 mm round hole using the PCAD revealed that the PCAD was unable to adequately characterise leakage for large cracks due to the pump operation off its pump curve for these leak sizes. Further investigation and analysis of the device's pump curves informed that new leak areas would need to be tested using pressures comparable with the range of pressures the PCAD can deliver. As with the previous results, the outcome of the leak characterisation tests of these three samples at lower pressures revealed that the method produces results with low variances and small standard derivations. However, the test results found at the new pressure ranges were all found to be statistically different from the parameters obtained at standard, higher pressures. Of interest was the finding that the effective area-head slope might be pressure-dependent much like the N1 parameter which is contrary to existing opinions held by authors such as Kabaasha, (2019) and Lopez and van Zyl, (2019). The 95% confidence of the m' from the different pressure ranges for all three samples did not overlap. It was thus, believed that there is a force/pressure value that needs to be met before near-perfect elastic behaviour is observed. Before the point at which perfect plastic elastic behaviour is

observed, the material's internal stress is large enough to offer resistance and thus the rate of elongation (and m') is lower at lower forces and by extension, lower pressures. This belief is admittedly based on limited findings from this study. Therefore, more tests conducted on pipe samples at different pressure ranges to ascertain this claim. Nevertheless, the effective area-head slope remains an important leakage parameter as it still provides physically meaningful results for leakage modelling and analysis.

A comparison of the laboratory-derived area-head slope with finite element modelling derived equations developed by Cassa and Van Zyl, (2013) and Nsanzubuhoro et al., (2017) for longitudinal and round cracks respectively were conducted. While it was found that the FEM equations managed to reasonably predict the area head slopes of round holes and longitudinal cracks, these parameters were statistically different from the laboratory-derived parameters. There is then a need for additional work to calibrate both equations by comparing the predicted values with laboratory values and establishing the relationship that exists, if any exists, to aid in the prediction of the area-head slope.

After the baseline results had been established on the three pipe samples at pressure ranges comparable with the PCAD pressure, the device's instrumentation was calibrated. This calibration exercise allowed the accuracy of or the pressure and flow rate sensors on the device to be evaluated. The pressure sensor was found to have an error an average error of 0.006 m which varied by 0.04 m. The flow rate was found to have an error of 0.00016 L/s, which deviated by ± 0.00051 L/s. This was an acceptable error value when compared to the average pressure and flow rates the device would have to deliver.

The three pipe samples were then tested using the device. While paired sample t-tests informed that the leakage parameters were different, the 95% confidence intervals of all three samples were found to overlap with the results obtained with the standardised method. Furthermore, the PCAD was able to consistently produce leakage characterisation results that are similar to laboratory-derived results shown by the results from the ten tests performed for each sample having low variance and deviation from the mean. This finding confirmed the device's ability to characterise leakage reliably to acceptable statistical confidence.

One drawback was that the device's pump is smaller than the laboratory's pump and could not accurately characterise leakage for pipes with large leaks sizes. This apparent drawback would nevertheless, not be an issue in the field as leaks of such dimensions and flow rates are expected to be visible and therefore easily repaired.

Finally, the PCAD was then used to characterise leakage in a DMA in Cape Town, South Africa. The Kensington DMA, chosen for this exercise, has a flat terrain flat and was relatively safe. In this section of the study, the efficacy of the device in conducting leakage in real water distribution systems was assessed. It was observed that the device was unable to characterise leakage in pipe sections that could not be isolated. However, that finding also informed that PCAD was able to aid in identifying valves that did not shut and leaking hydrants. The device was found to be easily manoeuvrable by one operator but was however found to be heavy to load and offload the vehicle. While the field tests themselves were not perfect, they provided data on how the device use and data analysis can be improved. It is recommended that a method be developed that would enable pipe section with faulty valves to be characterised.

From the laboratory and field test results, it is evident that the device can conduct pipe condition assessments in real water systems to an acceptable level of confidence.

9 CONCLUSION AND RECOMMENDATIONS

9.1 Conclusion

In response to the increase in water scarcity which is exacerbated by water wastages due to loss events such as leaks, a pipe condition assessment device (PCAD) was developed at the University of Cape Town. However, the efficacy and reliability of the PCAD in detecting and characterising leakage while conducting pipe condition assessments had not yet been established. This then, is what this study sought to achieve.

In this study, the setup and standard method used to conduct leakage characterisation were found to be reliable as the test conducted using the setup all showed excellent repeatability. A few modifications to the experiments were however found necessary. The repeatability of the leakage characterisation using the standardised method was displayed by low variance across sixty tests conducted on six different pipe samples. The only exception was the 100 mm circumferential crack which had a comparatively high variance. This section of the study contributed to the existing literature by providing a statistical method and evidence that to 95% level of confidence, the standardised method developed by Van Zyl and Malde, (2017) is reliable and repeatable. The standardised method can thus be used to conduct laboratory-based leakage characterisation tests.

By comparing the leak characterisation results conducted using the PCAD and the standard laboratory equipment, the reliability of the PCAD was established. The reliability and repeatability of the PCAD were demonstrated by the overlap of the 95% single parameter confidence intervals of the two main parameters analysed, namely the effective area-head slope and effective area intervals, in the ten tests conducted per pipe for all three pipe samples. This finding then contributed to the body of knowledge by providing statistically-based evidence that the PCAD can produce repeatable and reliable results for laboratory-based leakage characterisation tests.

An analysis of the effective area-slopes and effective area of 3 pipe samples at two different pressure ranges revealed that the effective area-head slope might be pressure-dependent, contrary to the currently available literature.

Additionally, a comparison of the laboratory-derived area-head slopes with FEM equation-based area-head slope values revealed that, except for the 100 mm longitudinal crack, the equations are presently not able to reliably predict the leakage parameters.

Finally, the field tests conducted in a district metered area using the PCAD revealed that for the limited pipes tested, the PCAD was able to conduct pipe condition assessments in real water distribution systems, thus establishing its efficacy in doing so.

In conclusion, this study was able to successfully establish the efficacy of the PCAD in detecting leakage and conducting pipe condition assessments with acceptable reliability and repeatability.

9.2 Recommendations

The following recommendations were drawn from the results and conclusions from this study:

- In this study, the stabilised points were chosen manually, which introduced human-induced variability in the results. It is thus recommended that a more standard and digital method be developed to reduce the variability.
- It was also found that for some leaks such as the circumferential cracks, the longitudinal stress induced by the steel rods had a significant effect. For a standardised and repeatable method of leakage characterisation, it is suggested that a torque wrench be used to secure the steel rods and the torque to be used be standardised to ensure uniformity.
- Due to the inability of the FEM derived equations to reliably predict leak area-head slopes of laboratory manufactured leaks, it is recommended that a study to calibrate the equations be done. In the proposed study, the expected and obtained area-head slope values should be compared and through a regression analysis of a large sample of pipes, the relationship between two will be established.
- The pipe condition assessments in the field revealed that there is a need to develop a method to enable the PCAD to conduct leakage characterisation tests in pipes which cannot be completely isolated.
- Finally, while the study showed that the PCAD could conduct pipe condition assessments, in a few pipes, there is still a need to determine if the PCAD can conduct leakage assessments in an entire DMA and evaluate the results thereof.

REFERENCES

Alkasseh *et al.* (2015) 'Achieving an economic leakage level in Kinta Valley , Malaysia', pp. 31–47.

AWWA (2000) 'AWWA', in *International Water Data Comparisons*. Japan: AWWA, pp. 1–12.

Bartlett (2004) *Pressure Dependant Demands in Student Town Phase 3*. University of Johannesburg.

Brunone, Ferrante and Unbertini (2000) 'Leak Analysis in Pipes Using Transients', *Second Annual Seminar on Comparative Urban Projects*.

Casella and Berger (2002) *Statistical Inference*. 2nd Editio. Florida, USA: Duxbury Thomson Learning. doi: 10.1057/pt.2010.23.

Cassa and van Zyl (2006) 'A Numerical Investigation into the Behaviour of Cracks in uPVC Pipes under Pressure', in *WISA2006 The Water Institute of Southern Africa Biennial Conference and Exhibition*. Durban, South Africa, pp. 1–8. doi: 10.1061/41024(340)65.

Cassa and Van Zyl (2013) 'Predicting the head-leakage slope of cracks in pipes subject to elastic deformations', *Journal of Water Supply: Research and Technology - AQUA*, 62(4), pp. 214–223. doi: 10.2166/aqua.2013.094.

Cassa and Van Zyl (2014) 'Predicting the leakage exponents of elastically deforming cracks in pipes', *Procedia Engineering*. Elsevier B.V., 70, pp. 302–310. doi: 10.1016/j.proeng.2014.02.034.

Cassa, van Zyl and Laubscher (2010) 'A numerical investigation into the effect of pressure on holes and cracks in water supply pipes', *Urban Water Journal*, 7(2), pp. 109–120. doi: 10.1080/15730620903447613.

Chadwick, Morfett and Borthwick (2013) *Hydraulics in Civil and Environmental Engineering*. 5th Editio. New York: Taylor & Francis Group.

Deyi, Van Zyl and Shepherd (2014) 'Applying the FAVAD concept and leakage number to real networks: A case study in Kwadabeka, South Africa', *Procedia Engineering*. Elsevier B.V., 89, pp. 1537–1544. doi: 10.1016/j.proeng.2014.11.450.

Douglas *et al.* (2006) *Fluid Mechanics*. Fifth Edit. Essex, England: Longman imprint.

Erwee (2016) *Automated Mobile Water Leakage Assessment System*. University of Stellenbosch.

Farley (2001) *Leakage Management and Control*.

Farley (2008) *The Manager's Non-Revenue Water Handbook. A Guide to Understanding Water Losses*. 1st edn. Edited by Niels van Dijk, Vivian Raksakulthai. Kuala Lumpur: Ranhill.

Farley (2012) ‘Innovation in Technology for Monitoring, Detecting and Repairing Leaks’, *Techno Focus*, pp. 1–5. doi: 10.1143/JJAP.49.07HC08.

Ferrante (2012) ‘Experimental investigation of the effects of pipe material on the leak law : leak in a steel pipe’, *Journal of Hydraulic Engineering*, 138(8), pp. 736–743. doi: 10.1061/(ASCE)HY.1943-7900.0000578.

Greyvenstein and Van Zyl (2007) ‘An experimental investigation into the pressure - Leakage relationship of some failed water pipes’, *Journal of Water Supply: Research and Technology - AQUA*, 56(2), pp. 117–124. doi: 10.2166/aqua.2007.065.

Hamilton and Charalambous (2013) *Leak Detection: Technology and Implementation*. doi: 10.1088/0953-8984/18/39/020.

Hedden and Cilliers (2014) ‘Parched prospects’, *Institute of security studies*, (September), p. 16.

Hibbeler (2016) *Mechanics of Materials 10th Edition*. Tenth Edit. Edited by Dias. Pearson.

Hicks and Slaton (2013) ‘Determining the Coefficient of Discharge for a Draining Container’, *The Physics Teacher*, 52(1), pp. 43–47. doi: 10.1119/1.4849155.

Hu and Hubble (2007) ‘Factors contributing to the failure of asbestos cement water mains’, *Canadian Journal of Civil Engineering*, 34(5), pp. 608–621. doi: 10.1139/l06-162.

Johnson and Wichern (2007) *Applied Multivariate Statistical Analysis*. 6th Editio. Upper Saddle River, New Jersey 07458: Prentice Hall.

Kabaasha (2017) *REALISTIC MODELLING OF LEAKAGE IN WATER DISTRIBUTION PIPE NETWORKS*. University of Cape Town.

Kanakoudis and Muhammetoglu (2014) ‘Urban water pipe networks management towards non-revenue water reduction: Two case studies from Greece and Turkey’, *Clean - Soil, Air, Water*, pp. 880–892. doi: 10.1002/clen.201300138.

Kayombo (1981) *Pipe Materials in Transmission Mains*. Tampere University of Technology.

Kowalska, Rudawska and Kowalski (2014) ‘Tests on a polyvinyl chloride pipe from an existing water distribution system’, in *WIT Transactions on the Built Environment*, pp. 3–14. doi: 10.2495/UW140011.

Lambert, A. (2002) ‘International report: Water losses management and techniques’, *Water Science and Technology: Water Supply*, 2, pp. 1–20. doi: 10.1177/001789695501300409.

Lambert, A. O. (2002) ‘Water Losses Management and Techniques’, *Water Science and Technology: Water Supply*, 2(4), pp. 1–20. doi: 10.1177/001789695501300409.

Lambert *et al.* (2014) ‘14 Years Experience of using IWA Best Practice Water Balance and Water Loss Performance Indicators in Europe’, *Proceedings of the WaterLoss Conference*

2014, (May), pp. 1–31.

Lambert, Fantozzi and Thornton (2013) 'Practical approaches to modeling leakage and pressure management in distribution systems – progress since 2005', *12th International Conference on Computing and Control for the Water Industry, CCWI2013*, (2011), p. 11.

Li *et al.* (2015) 'A review of methods for burst/leakage detection and location in water distribution systems', *Water Science and Technology: Water Supply*, pp. 429–441. doi: 10.2166/ws.2014.131.

Lopez and van Zyl (2019) 'Pressure-Based Pipe Condition Assessment for Intelligent Water Network Maintenance', in *International Conference on Smart Infrastructure and Construction 2019 (ICSIC)*. ICE Publishing (Cambridge Centre for Smart Infrastructure & Construction), pp. 491–497. doi: 10.1680/icsic.64669.491.

Malde (2015) *An Analysis of Leakage Parameters of Individual Leaks on a Pressure Pipeline through the Development and Application of a Standard Procedure*. University Of Cape Town.

May, J (1994) 'Pressure dependent leakage', *World Water and Environmental Engineering*, p. 1.

May, John (1994) 'Pressure Dependent Leakage', *World Water and Environmental Engineering*, (October 1994).

Mora-Rodríguez *et al.* (2014) 'An overview of leaks and intrusion for different pipe materials and failures', *Urban Water Journal*, 11(1), pp. 1–10. doi: 10.1080/1573062X.2012.739630.

Mukuhlani and Nyamupingidza (2014) 'Water scarcity in communities, coping strategies and mitigation measures: The case of bulawayo', *Journal of Sustainable Development*, 7(1), pp. 144–160. doi: 10.5539/jsd.v7n1p144.

Nsanzubuhoro, van Zyl and Tanyanyiwa (2019) 'A Method For Pressure-Based Leakage Characterization of Pipelines', *Journal of Hydraulic Engineering*, p. 24.

Nsanzubuhoro, van Zyl and Zingoni (2017) 'Predicting the head-area slopes of round leaks in pipes subject to elastic deformations'. doi: 10.1201/9781315641645-94.

Nsanzubuhoro, Van Zyl and Zingoni (2017) 'Predicting the Head-Area Slopes of Circular Holes in Water Pipes', *Procedia Engineering*. Elsevier B.V., 186, pp. 110–116. doi: 10.1016/j.proeng.2017.03.216.

Ogura (1979) 'Experiments about the Relationship between Leakage Quantity and Water Pressure', *Japan Water Works Assosiation*, 572, pp. 38–45.

De Paola *et al.* (2014) 'Experimental investigation on a buried leaking pipe', *Procedia Engineering*, 89, pp. 298–303. doi: 10.1016/j.proeng.2014.11.191.

Pilcher (2003) 'Leak detection practices and techniques: a practical approach', *Water 21* -

Magazine of the International Water Association, December 2, pp. 44–45.

Pilcher (2007) 'Leak Location & Repair Guidance Notes', *Guideline of IWA Water Loss Task Force.*, p. 67. doi: 26 November 2012.

Prohaska (2008) *Investigation of the Discharge Coefficient for Circular Orifices in Riser Pipes*. Clemson University. Available at: http://tigerprints.clemson.edu/all_theses/407.

Puust *et al.* (2010a) 'A review of methods for leakage management in pipe networks', *Urban Water Journal*, 7(1), pp. 25–45. doi: 10.1080/15730621003610878.

Puust *et al.* (2010b) 'A review of methods for leakage management in pipe networks', *Urban Water Journal*. doi: 10.1080/15730621003610878.

Rajani and Kleiner (2001) 'Comprehensive review of structural deterioration of water mains: Physically based models', *Urban Water*, 3(3), pp. 151–164. doi: 10.1016/S1462-0758(01)00032-2.

Richardson (2006) *Civils Technical Manual (PVC)*. Pretoriusstad, Nigel. Available at: http://www.marleypipesystems.co.za/images/pdfdownloads/productbrochures/marley-pvc-civils-technical-manual.pdf.

Schwaller and Van Zyl (2014) 'Implications of the known pressure-response of individual leaks for whole distribution systems', in *Procedia Engineering*. Elsevier B.V., pp. 1513–1517. doi: 10.1016/j.proeng.2014.02.166.

Silva, Mashford and Burn (2011) 'Computer Aided Leak Location and Sizing in Pipe Networks Urban Water Security Research Alliance Technical Report No . 17. Urban Water Security Research Alliance Technical Report NO. 17, 2011(17).de', *urban water security research Alliance technical report NO. 17*, 2011(17).

Srikanth *et al.* (2005) 'Corrosion in a buried pressurised water pipeline', *Engineering Failure Analysis*, 12(4), pp. 634–651. doi: 10.1016/j.engfailanal.2004.02.006.

Tata & Howard (2015) *History of Water Distribution and Treatment - Tata & Howard*. Available at: https://tataandhoward.com/2015/05/history-of-water-distribution-and-treatment/ (Accessed: 21 July 2018).

Thornton and Lambert (2005) 'Progress in practical prediction of pressure: leakage, pressure: burst frequency and pressure: consumption relationships', *... of IWA Special Conference'Leakage*, pp. 1–10. Available at: http://www.leakssuite.com/Research Papers/2005_ThorntonLambert IWA Halifax.pdf.

Thornton and Lambert (2006) 'Managing pressures to reduce new breaks', *Water21*, December, pp. 24–26.

Trow and Farley (no date) 'DEVELOPING A STRATEGY FOR LEAKAGE

MANAGEMENT IN WATER DISTRIBUTION SYSTEMS', 44(0).
Walski (2006) 'A history of water distribution', *Journal / American Water Works Association*, 98(3), pp. 110–121. doi: 10.1016/B978-075067841-4/50004-X.
Yang *et al.* (2011) 'Effects of temperature and hydraulic factors on water supply pipe breakage in seasonally frozen regions', *Conference on Computing and Control for the Water Industry*.
Zheng *et al.* (2011) *Water Loss Reduction*. First Edit. Exton, Pennsylvania: Bentley Institute Press.
van Zyl *et al.* (2013) 'Soil fluidisation outside leaks in water distribution pipes – preliminary observations', *Proceedings of the Institution of Civil Engineers - Water Management*, 166(10), pp. 546–555. doi: 10.1680/wama.11.00119.
van Zyl (2014) *Introduction to Operation and Maintenance of Water Distribution Systems*, *Water Research Commision*.
Van Zyl (2014) 'Theoretical modeling of pressure and leakage in water distribution systems', in *Procedia Engineering*. Elsevier B.V., pp. 273–277. doi: 10.1016/j.proeng.2014.11.187.
van Zyl and Clayton (2007) 'The effect of pressure on leakage in water distribution systems', *Proceedings of the Institution of Civil Engineers - Water Management*, 160(2), pp. 109–114. doi: 10.1680/wama.2007.160.2.109.
Van Zyl, Lambert and Collins (2017) 'Realistic Modeling of Leakage and Intrusion Flows through Leak Openings in Pipes', *Journal of Hydraulic Engineering-ASCE*, 143(9), pp. 3–9. doi: 10.1061/(ASCE)HY.1943-7900.0001346.
Van Zyl and Malde (2017) 'Evaluating the pressure-leakage behaviour of leaks in water pipes', *Journal of Water Supply: Research and Technology - AQUA*, 66(5), pp. 287–299. doi: 10.2166/aqua.2017.136.

APPENDIXES

Appendix A - FlowMetrix Electromagnetic DN25 Flow Meter Calibration Certificate

FLOW metrix

SABS ISO 9001

CERTIFICATE OF CALIBRATION 25mm SAFMAG Certificate : 20140002 Date : 13/01/2014

Calibrated Equipment

Primary Model No. : 025C2HDSSR003W
Primary Serial No. : FMX20000
Secondary Model No. : DCMPU-2 (M.U.T)
Secondary Serial No. : 02115828
Flow Range : 0 - 5 l/s

Configuration

Coil Frequency : 3.125 Hz
ZC Delay : N/A
K Factor : 1.6250
Z Factor : N/A

Environment

Liquid Temperature : 28.7°C
Up / Down Stream ID : 25mm

Quality Control

Operator :
Supervisor :

Results

Run (#)	Time (s)	Reference Total (l)	Reference Rate (l/s)	M.U.T. 1 Total (l)	M.U.T. 1 Error (%)	Reference
1	90	349.75	3.89	349.8	0.01	DN40
2	90	233.18	2.59	232.82	-0.15	DN40
3	90	94.54	1.05	94.3578	-0.19	DN40
4						
5						
6						
7						
8						
9						
10						

At the time of calibration all instrumentation used by the laboratory to measure Volume, Time, Temperature, Length, Weight and Flowmeter Output was traceable to the National Measuring Standards.

DN15	Master Meter Sn #080912013	Flow 0.089 - 1.77 l/s
DN40	Master Meter Sn #091113694	Flow 0.625 - 12.5 l/s
DN150	Master Meter Sn #FMX16181	Flow 9 - 180 l/s
DN300	Master Meter Sn #00023582	Flow 35 - 700 l/s

Uncertainty of measurement is ±0.5%

Operator : ANILC

Page 1 of 1

Safmag House
406 Sydney Road
Congella
Durban

P.O.Box 17143
Congella
South Africa, 4013
Reg. No. CK 1998/11507/23

Tel.: 086 110 6028
Fax : 086 518 8468
Email: enquiries@flowmetrix.co.za
Website: www.flowmetrix.co.za

Appendix B – Primayer PrimeLogger Data Pressure Calibration Certificate

Signal Instrumentation cc
VAT Reg. No. 4115108432 • CK 2008/022066/23
Industrial Instrumentation & Process Control
Calibration • Maintenance • Installation

ilac-MRA
ANAB ACCREDITED CALIBRATION LABORATORY

CALIBRATION CERTIFICATE

Certificate Number:	5407P
Customer:	University of Cape Town
Customer Address:	Civil Engineering Building Rondebosch Cape Town
Calibration of:	Pressure Logger with Display
Make:	Primayer; Primayer
Model:	Primelog Zi-ZDBar; Xap Display
Serial number:	172938; 198019
UUT Resolution :	0.001Bar
Measuring range:	0 to 20 Bar
Condition of UUT:	Used
Location on-site:	Portable

Calibration date:	17/01/2019	Date of issue:	01/2019
Calibration interval (Months):		12	
Recommended recalibration date:		01/2020	
Environmental			
Temperature in °C:	25.9	Relative Humidity in %rh:	40

The measurement results recorded in this certificate were correct at the time of calibration. The subsequent accuracy will depend on factors such as care, handling and frequency of use of the device. It is recommended that recalibration be undertaken at an interval that will ensure that the instrument remains within the desired limits. This calibration certificate may not be reproduced except in full, with prior written approval of the laboratory. The calibration results relate to the above described items only.

ANSI-ASQ National Accreditation Board (ANAB) is a member of the International Laboratory Accreditation Cooperation (ILAC) Mutual Recognition Agreement (MRA). This arrangement allows for the mutual recognition of technical test and calibration data by the member accreditation bodies worldwide. For more information on the arrangement please consult www.ilac.org. The reported expanded uncertainty is based on a standard uncertainty multiplied by a coverage factor of k=2, which provide a confidence level of approximately 95 %, in accordance with the principles defined in the Guide to the Expression of Uncertainty of Measurement , ISO, Geneva, 1993.

Remarks:
The results are an average value automatically calculated from the test results, therefore allow for rounding off when calculating with corrections.

Signature Removed

Calibrated by: J Langenhoven **Technical Signatory:**

Page 1 of 2

Page 1 of 2

Signal Instrumentation cc
VAT Reg. No. 4110188402 • CK 2004/000000/23
Industrial Instrumentation & Process Control
Calibration • Maintenance • Installation

ANAB ACCREDITED CALIBRATION LABORATORY

CALIBRATION CERTIFICATE

Certificate Number: 5407P

Traceability:

Measurement Equipment:	Make	Calibration Due Date:	ID Number:
Digital Pressure Gauge	Additel	11/2019	RS043

The accuracy of all measurements are traceable through National or International Standards to the International System of Units (SI)

Calibration Procedure: CP-001 -

Calibration of: Pressure Logger with Display

Results:	BEFORE ADJUSTMENT		
Reference Value	Indicated Value	Correction	Uncertainty of Measurement (±)
Bar	Bar	Bar	Bar
0.000	0.002	-0.002	0.0093
10.000	10.005	-0.005	0.032
19.999	20.003	-0.004	0.0089

Results:	AFTER ADJUSTMENT	N/A	
Reference Value	Indicated Value	Correction	Uncertainty of Measurement (±)
Bar	Bar	Bar	Bar

The correction must be algebraically added to the Indicated Value to obtain the corrected value.

Page 2 of 2

PO Box 829, Bellville 7535 • Unit 12, Van Riljon Park, 1 Wineland Close, Stikland 7530
Tel: 021 946 1597 • Fax: 021 946 1781 • Cell: 083 270 8578 • E-mail: faan@signalinstrumentation.co.za
Member: S.G. Langenhoven